Evaluation of Performance of In-Use Firefighters' Protective Clothing Using Non-Destructive Tests

A Thesis Submitted to the College of

Graduate Studies and Research

In Partial Fulfilment of the Requirements

For the Degree of Doctor of Philosophy

In the Department of Mechanical Engineering

University of Saskatchewan

Saskatoon

By

Moein Rezazadeh

PERMISSION TO USE

In presenting this dissertation in partial fulfilment of the requirements for a Postgraduate degree from the University of Saskatchewan, I agree that the Libraries of this University may make it freely available for inspection. I further agree that permission for copying of this dissertation in any manner, in whole or in part, for scholarly purposes may be granted by the professor or professors who supervised my dissertation work or, in their absence, by the Head of the Department or the Dean of the College in which my thesis work was done. It is understood that any copying or publication or use of this thesis/dissertation or parts thereof for financial gain shall not be allowed without my written permission. It is also understood that due recognition shall be given to me and to the University of Saskatchewan in any scholarly use which may be made of any material in my dissertation.

Requests for permission to copy or to make other uses of materials in this dissertation in whole or part should be addressed to:

Head of the Department of Mechanical Engineering
University of Saskatchewan
Saskatoon, Saskatchewan S7N 5A9
Canada

OR

Dean
College of Graduate Studies and Research
University of Saskatchewan
107 Administration Place
Saskatoon, Saskatchewan S7N 5A2
Canada

DISCLAIMER

The names of certain commercial products were exclusively used to meet the dissertation and/or exhibition requirements for the degree of Doctor of Philosophy at the University of Saskatchewan. Reference in this dissertation to any specific commercial products, process, or service by trade name, trademark, manufacturer, or otherwise, does not constitute or imply its endorsement, recommendation, or favouring by the University of Saskatchewan. The views and opinions of the author expressed herein do not state or reflect those of the University of Saskatchewan, and shall not be used for advertising or product endorsement purposes.

ABSTRACT

Firefighters' coats and pants, referred to as firefighters' protective clothing in this research, are made of similar fabrics and often include three layers: an outer shell, a moisture barrier, and a thermal liner. Minimum requirements of firefighters' protective clothing performance have been clearly established by various national and international standards for new clothing to ensure the reasonable safety of firefighters. However, there are no clear guidelines on the requirements for continuing performance of firefighters' protective clothing. In general, the protection offered by firefighters' protective clothing is expected to deteriorate over time, but it is still uncertain how destructive different exposures are and how long a piece of firefighters' protective clothing can continue to protect a firefighter to an acceptable level.

Non-destructive techniques are preferable in order to investigate how the performance of protective clothing may change with time since this allows firefighters' protective clothing to return to service after a test. These non-destructive methods, which could be used to monitor the level of deterioration in firefighters' protective clothing performance and to make decisions on retirement of individual pieces of protective clothing, would be extremely useful for fire departments in Canada and other countries.

Thermal exposure is an important factor in ageing of firefighters' protective clothing during firefighting operations. Outer shell and moisture barrier specimens made of common fabrics used in construction of firefighters' protective clothing, and of different colours, were exposed to different levels of thermal exposure simulated using a cone calorimeter in single and multiple stages. Tensile strength of outer shell specimens, and tear strength, water vapour transmission rate, and water penetration pressure of moisture barrier specimens, which are critical aspects of performance of firefighters' protective clothing, were measured. In order to explain the changes in performance after thermal exposure, the temperature profile of specimens during each thermal exposure was recorded. Furthermore, thermogravimetric analysis for each specimen material was carried out and images of the surface of specimens were obtained using scanning electron microscope. The test results demonstrated that tensile strength of outer shell specimens deteriorated faster than other aspects of performance.

Two non-destructive techniques, colour measurement and near infrared spectroscopy, were implemented to correlate tensile strength of outer shell specimens with discoloration and reflectance spectrum. Two types of correlation between tensile strength and colour change were identified among the tested fabrics, depending on the initial fabric colour, which could be a basis to develop numerical models to predict tensile strength of outer shell specimens. Linear predictive equations were developed using a numerical code based on regression analysis, which correlated tensile strength with reflectance of outer shell specimens within the wavelength region of 1500-2500 nm. A three-variable model predicted tensile strength of thermally aged test specimens, the tensile strength of which were 600 N and higher, with a relative error of up to 10%. For test specimens with tensile strength of about 300 N, the relative error was 55%. The difference in error percentage was related to a gap in training data points for the model within the tensile strength range of 300 - 600 N.

ACKNOWLEDGMENTS

I would like to sincerely thank Prof. David Torvi for his trust in me and continuous supervision during my study. His encouragement and financial support to attend conferences is truly appreciated. Mr. David Deutcher and Rick Retzleff were very supportive in set-up and troubleshooting of the equipment in the laboratory. I learned many technical points from them. I would like to specially thank Prof. Scott Noble from Department of Chemical and Biological Engineering for his guidance in infrared spectroscopy and statistical analysis. His wealth of knowledge and strong passion for research were really inspiring. Technical support from Mr. Robert Peace in using scanning electron microscope and Mr. Hans Steinmetz in conducting mechanical strength testing is appreciated.

Mr. Guosheng Liu from Department of Biology and Mr. Louis Roth from Department of Chemical and Biological Engineering were very helpful in coating specimens for scanning electron microscopy and performing tensile strength tests, respectively. Kelley Neale was extremely helpful in preparing documents and paperwork for my study as an international student. Examination of my advisory committee members is acknowledged. I extend my heartfelt appreciation to nice and kind people of Saskatoon for welcoming and accepting me in their community. Socializing with them was a great experience and full of lessons for me.

Generous financial support from Natural Science and Engineering Research Council of Canada (NSERC), Department of Mechanical Engineering, and College of Graduate Studies and Research at the University of Saskatchewan is deeply appreciated. Donation of fabrics by Difco Performance Fabrics (now TenCate Protective Fabrics) and Stedfast Inc. is gratefully acknowledged.

To my three special life gifts from God:

my parents and my wife

TABLE OF CONTENTS

Page

PERMISSION TO USE i
DISCLAIMER ii
ABSTRACT iii
ACKNOWLEDGMENTS v
TABLE OF CONTENTS vii
LIST OF TABLES ix
LIST OF FIGURES xi
LIST OF SYMBOLS xviii
LIST OF ABBREVIATIONS xix
1. INTRODUCTION 1
1.1. Firefighters' protective clothing 1
1.2. Performance requirements for firefighters' protective clothing 3
1.3. Identifying the need for this research 8
1.4. Ageing of firefighters' protective clothing 11
1.5. Potential non-destructive test methods 26
1.6. Scope and objectives of research 35
1.7. Contributions of this research to the literature 37
1.8. Outline of the dissertation 37
2. EXPERIMENTAL APPARATUS AND PROCEDURE 39
2.1. Thermal ageing 39
2.2. Cone Calorimeter 45
2.3. Thermogravimetric analysis (TGA) 48
2.4. Temperature measurement 49
2.5. Tensile strength tests 51
2.6. Tear strength tests 52
2.7. Water vapour permeability tests 53
2.8. Water penetration pressure tests 55
3. OUTER SHELL EXPERIMENTS 57

3.1. Preparation of specimens 57
3.2. Thermogravimetric analysis (TGA) 58
3.3. Temperature measurements 61
3.4. Tensile tests 66
4. MOISTURE BARRIER EXPERIMENTS 78
4.1. Preparation of specimens 80
4.2. Thermogravimetric analysis (TGA) 82
4.3. Temperature measurement 84
4.4. Water vapour permeability test 85
4.5. Water penetration pressure test 89
4.6. Tear strength test 91
5. MULTI-STAGE EXPOSURE EXPERIMENTS 95
5.1. Preparation of specimens 95
5.2. Thermogravimetric analysis 98
5.3. Temperature measurements 101
5.4. Tensile tests 104
5.5. Tear strength 108
5.6. Water vapour permeability test 112
5.7. Water penetration pressure test 114
6. NON-DESTRUCTIVE EXPERIMENTS 117
6.1. Test procedure 119
6.2. Colour measurement 122
6.3. Near infrared spectroscopy 132
7. PREDICTING TENSILE STRENGTH OF OUTER SHELL 144
7.1. Correlation between tensile strength and colour measurement 144
7.2. Correlation between tensile strength and near infrared spectroscopy 151
8. CONCLUSIONS AND FUTURE WORK 174
8.1. Conclusions 174
8.2. Future work 177
REFERENCES 179

LIST OF TABLES

Table — Page

Table 1.1: Evaluation tests of firefighters' protective clothing and required parameters to report according to NFPA 1971 [2] 4

Table 1.2: Tensile strength of new and visibly faded specimens, required time for appearance of visible discoloration [14] 23

Table 1.3: Summary of research on effects of thermal ageing [9] 24

Table 2.1: Thermal environment 1 [56] 40

Table 2.2: Thermal environment 2 [56] 40

Table 2.3: Thermal environment 3 [56] 41

Table 2.4: Thermal environment 4 [56] 41

Table 3.1: Test matrix for outer shell specimens 58

Table 3.2: Temperature of Nomex® IIIA outer shell specimens in different colours after 30 s exposure to a particular heat flux 62

Table 4.1: Thermal exposure duration for each heat flux 82

Table 5.1: Duration of single-stage exposure and the equal number of 30-second stages in multiple-stage exposure to a heat flux of 20 kW/m^2 97

Table 5.2: Maximum temperatures (°C) achieved by different layers of ensemble during exposures to incident heat flux of 20 kW/m^2 (undyed Kevlar®/PBI brown outer shell) 103

Table 5.3: Temperature of brown Kevlar®/PBI outer shell specimens after particular duration of exposure 104

Table 6.1: Mass moisture regain of unexposed yellow Nomex® outer shell specimens 139

Table 7.1: Wavelengths of the most accurate three-variable equation for each type of specimen 161

Table 7.2: Thermal exposure specification and tensile strength of blue, red, dark blue, and yellow Nomex® outer shell specimens for the purpose of interpolation 161

Table 7.3: R^2 and R^2_a for the equations made of 3, 5, 7, and 10 wavelengths 168

Table 7.4: Specifications of the three-variable equations with the highest R^2_a for blue specimens 169

LIST OF FIGURES

Figure Page

Figure 1.1: Three layers of firefighters' protective clothing 2

Figure 1.2: A TPP tester (reprinted from [7] with permission) 5

Figure 1.3: Change in the performance of firefighters' protective clothing with ageing [12] 10

Figure 1.4: Main substitution patterns 13

Figure 1.5: Chemical structure of Nomex® 14

Figure 1.6: Chemical structure of Kevlar® 14

Figure 1.7: Chemical structure of PBI 14

Figure 1.8: Molecular structure of PTFE 15

Figure 1.9: CCHR ratings of Nomex® thermal liner specimens previously exposed to various radiant heat flux exposures using the ASTM F1939 test apparatus [14] 20

Figure 1.10: Tensile strength of Kevlar®/Nomex® outer shell specimens previously exposed to various radiant heat flux exposures using the ASTM F 1939 test apparatus [14] 20

Figure 1.11: Examples of colour fade of 60% Kevlar®/40% Nomex® outer shell specimens after different levels of thermal exposure 31

Figure 1.12: DIA results to correlate discoloration and tensile strength of 60% Kevlar®/40% Nomex® outer shell specimens [14] 32

Figure 2.1: The range of thermal conditions faced by firefighters [65] 42

Figure 2.2: A view of thermal condition classified as "Routine" [14] 42

Figure 2.3: A view of thermal condition classified as "Ordinary" [14] 43

Figure 2.4: A view of thermal condition classified as "Emergency" [14] 43

Figure 2.5: Cone calorimeter 45

Figure 2.6: Conical heater of a cone calorimeter 46

Figure 2.7: Locations of heat flux measurement carried out 25 mm under the conical heater 47

Figure 2.8: Distribution of generated heat flux (35 kW/m^2) 25 mm under the conical heater 47

Figure 2.9: Temperature measurement in the cone calorimeter using thermocouples 50

Figure 2.10: Tensile testing machine 51
Figure 2.11: Specimen marking template 52
Figure 2.12: Position of a specimen in the clamping system in tear strength test 53
Figure 2.13: Water vapour permeability test apparatus 54
Figure 2.14: A schematic view of a test cell of the water vapour permeability test equipment 54
Figure 2.15: A view of a moisture barrier specimen glued to the carrier 55
Figure 2.16: Water penetration pressure test apparatus 56
Figure 3.1: TGA curve for blue outer shell specimens made of Nomex® IIIA 59
Figure 3.2: TGA curve for red outer shell specimens made of Nomex® IIIA 60
Figure 3.3: TGA curve for dark blue outer shell specimens made of Nomex® IIIA 60
Figure 3.4: TGA curve for yellow outer shell specimens made of Nomex® IIIA 61
Figure 3.5: The first 30 s temperature history of the back side of the blue Nomex® IIIA specimens using the infrared thermometer during thermal exposure 63
Figure 3.6: The first 30 s temperature history of back side of the Nomex® IIIA red specimens using the infrared thermometer during thermal exposure 64
Figure 3.7: The first 30 s temperature history of the Nomex® IIIA dark blue specimens using the infrared thermometer during thermal exposure 65
Figure 3.8: The first 30 s temperature history of back side of the Nomex® IIIA yellow specimens using the infrared thermometer during thermal exposure 66
Figure 3.9: Illustration of warp and fill directions in a fabric 67
Figure 3.10: Tensile strength of specimens after exposure to 10 kW/m^2 68
Figure 3.11: Surface of an unexposed Nomex® specimen 69
Figure 3.12: Surface of Nomex®specimen after exposure to 10 kW/m^2 for 600 s 69
Figure 3.13: Surface of Nomex® specimen after exposure to 10 kW/m^2 for 1200 s 69
Figure 3.14: Surface of Nomex®specimen after exposure to 10 kW/m^2 for 2400 s 69
Figure 3.15: Tensile strength of Nomex® specimens after exposure to 20 kW/m^2 70
Figure 3.16: Surface of an unexposed Nomex® specimen 71
Figure 3.17: Surface of Nomex® specimen after exposure to 20 kW/m^2 for 30 s 71
Figure 3.18: Surface of Nomex® specimen after exposure to 20 kW/m^2 for 150 s 71

Figure 3.19: Surface of Nomex® specimen after exposure to 20 kW/m^2 for 300 s 71
Figure 3.20: Tensile strength of Nomex® specimens after exposure to 30 kW/m^2 72
Figure 3.21: Surface of an unexposed Nomex® specimen 73
Figure 3.22: Surface of Nomex® specimen after exposure to 30 kW/m^2 for 15 s 73
Figure 3.23: Surface of Nomex® specimen after exposure to 30 kW/m^2 for 30 s 73
Figure 3.24: Surface of Nomex® specimen after exposure to 30 kW/m^2 for 60 s 73
Figure 3.25: Tensile strength of specimens after exposure to 40 kW/m^2 74
Figure 3.26: Surface of an unexposed Nomex® specimen 74
Figure 3.27: Surface of Nomex® specimen after exposure to 40 kW/m^2 for 10 s 74
Figure 3.28: Surface of Nomex® specimen after exposure to 40 kW/m^2 for 20 s 75
Figure 3.29: Surface of Nomex® specimen after exposure to 40 kW/m^2 for 30 s 75
Figure 3.30: Average tensile strength of Nomex® specimens after thermal exposure to particular heat flux for specific duration 77
Figure 4.1: Layers of firefighters' protective clothing 78
Figure 4.2: Transmitted heat flux through Crusader®790 outer shell when the copper calorimeter is in direct contact with the fabric and when there is a 3.2 mm (1/8 in.) spacer between them 81
Figure 4.3: TGA curve for membrane ePTFE side of Stedair® 4000 moisture barrier specimens 83
Figure 4.4: TGA curve for substrate (Nomex®) side of moisture barrier specimens 84
Figure 4.5: Temperature history of the back side of Stedair® 4000 moisture barrier specimens during thermal exposure 85
Figure 4.6: Water Vapour Transmission Rate (WVTR) of moisture barrier specimens 86
Figure 4.7: The polymeric layer of a membrane of an unexposed specimen 87
Figure 4.8: The polymeric layer of a membrane of a specimen exposed to 10 kW/m^2 for 120 s 87
Figure 4.9: ePTFE fibres in the membrane of the unexposed moisture barrier specimen 88
Figure 4.10: ePTFE fibres in the membrane of the specimen exposed to 10 kW/m^2 for 120 s 88

Figure 4.11: ePTFE fibres in the membrane of the specimen exposed to 10 kW/m^2 for 300 s 88
Figure 4.12: ePTFE fibres in the membrane of the specimen exposed to 15 kW/m^2 for 60 s 88
Figure 4.13: Surface of specimen after exposure to 20 kW/m^2 for 300 s 89
Figure 4.14: Required pressure for water penetration for moisture barrier specimens 90
Figure 4.15: Tear strength of moisture barrier specimens after thermal exposure 93
Figure 5.1: TGA curve for brown Kevlar®/PBI outer shell fabrics 99
Figure 5.2: TGA curve for black Kevlar®/PBI outer shell fabrics 99
Figure 5.3: TGA curve for membrane side of Stedair®3000 moisture barrier specimen 100
Figure 5.4: TGA curve for substrate side of moisture barrier specimen 101
Figure 5.5: Temperature history of front and back sides of outer shell and moisture barrier layers of specimens during exposure to 20 kW/m^2 for three consecutive stages ... 102
Figure 5.6: Tensile strength of brown Kevlar®/PBI outer shell fabric along fill direction 106
Figure 5.7: Tensile strength of brown Kevlar®/PBI outer shell fabric along warp direction 106
Figure 5.8: Tensile strength of black Kevlar®/PBI outer shell fabric along fill direction 107
Figure 5.9: Tensile strength of black Kevlar®/PBI outer shell fabric along warp direction 107
Figure 5.10: Tensile strength of brown and black Kevlar®/PBI outer shell specimens as percent of initial tensile strength after single exposure for particular duration 108
Figure 5.11: Tear strength of Stedair® 3000 moisture barrier fabrics along fill direction after single-stage exposure to 20 kW/m^2 110
Figure 5.12: Tear strength of Stedair® 3000 moisture barrier fabrics along warp direction after single-stage exposure to 20 kW/m^2 110
Figure 5.13: Tear strength of Stedair® 3000 moisture barrier fabrics along fill direction after multi-stage exposure to 20 kW/m^2 111
Figure 5.14: Tear strength of Stedair® 3000 moisture barrier fabrics along warp direction after multi-stage exposure to 20 kW/m^2 111
Figure 5.15: Average tear strength of Stedair® 3000 moisture barrier specimens after single and multi-stage exposures as percentage of tear strength for an unexposed specimen 112

Figure 5.16: WVTR of Stedair® 4000 specimens after single-stage and multi-stage exposures 114
Figure 5.17: Required pressure for water penetration in Stedair® 4000 after single-stage and multi-stage exposures 115
Figure 6.1: The RGB colour system [14] 120
Figure 6.2: Conversion of discoloration of specimens to a representative colour 120
Figure 6.3: Interrogation area and regions of interest for colour measurement 121
Figure 6.4: The trend of discoloration in Nomex® outer shell fabrics of different colour 124
Figure 6.5: Colour change in Nomex® fabrics of different colours after exposure to 10kW/m^2 for particular duration 125
Figure 6.6: Colour change in blue Nomex® specimens 126
Figure 6.7: Colour change in red Nomex® specimens 127
Figure 6.8: Colour change in dark blue Nomex® specimens 128
Figure 6.9: Colour change in yellow Nomex® specimens 128
Figure 6.10: Colour change in brown Kevlar®/PBI specimens after single-stage and multi-stage exposures 129
Figure 6.11: Colour change in black Kevlar®/PBI specimens after single-stage and multi-stage exposures 130
Figure 6.12: Colour difference in regions 1 (central area) and 2 (whole area) for brown specimens 131
Figure 6.13: Colour difference in regions 1 (central area) and 2 (whole area) for black specimens 132
Figure 6.14: Reflectance spectrum of unexposed Nomex® specimens of different colours 133
Figure 6.15: Reflectance spectrum for blue Nomex® specimens after thermal exposure to 10 kW/m^2 134
Figure 6.16: Reflectance spectrum for blue Nomex® specimens after thermal exposure to 20 kW/m^2 135
Figure 6.17: Reflectance spectrum for blue Nomex® specimens after thermal exposure to 30 kW/m^2 136

Figure 6.18: Reflectance spectrum for blue Nomex® specimens after thermal exposure to 40 kW/m^2 136
Figure 6.19: Repeatability of reflectance spectrum of specimens after different levels of thermal exposure 137
Figure 6.20: Effect of moisture on reflectance spectrum of yellow Nomex® unexposed specimens 139
Figure 6.21: Reflectance spectrum for brown Kevlar®/PBI specimens after thermal exposure to 20 kW/m^2 140
Figure 6.22: Reflectance spectrum for black Kevlar®/PBI specimens after thermal exposure to 20 kW/m^2 141
Figure 6.23: Effect of single-stage and multi-stage exposures on reflectance spectrum of black Kevlar®/PBI specimens 142
Figure 7.1: Correlation of tensile strength with colour difference for blue Nomex® specimens 146
Figure 7.2: Correlation of tensile strength with colour difference for dark blue Nomex® specimens 146
Figure 7.3: Correlation of tensile strength with colour difference for black Kevlar®/PBI specimens 147
Figure 7.4: The first type of colour change and its correlation with tensile strength 147
Figure 7.5: Correlation of tensile strength with colour difference for red Nomex® specimens 149
Figure 7.6: Correlation of tensile strength with colour difference for yellow Nomex® specimens 149
Figure 7.7: Correlation of tensile strength with colour difference for brown Kevlar®/PBI specimens 150
Figure 7.8: The second type of colour change and its correlation with tensile strength 150
Figure 7.9: Range of adjusted R^2 values in equations made of a particular number of variables for blue Nomex® specimens 154
Figure 7.10: Range of adjusted R^2 values in equations made of a particular number of variables for red Nomex® specimens 155

Figure 7.11: Range of adjusted R^2 values in equations made of a particular number of variables for dark blue Nomex® specimens 156
Figure 7.12: Range of adjusted R^2 values in equations made of a particular number of variables for yellow Nomex® specimens 157
Figure 7.13: Range of adjusted R^2 values in equations made of a particular number of variables for brown Kevlar®/PBI specimens 158
Figure 7.14: Range of adjusted R^2 values in equations made of a particular number of variables for black Kevlar®/PBI specimens 159
Figure 7.15: Accuracy of the three -variable model for blue Nomex® specimens to predict tensile strength of interpolating points 162
Figure 7.16: Accuracy of the three-variable model for red Nomex® specimens to predict tensile strength of interpolating points 163
Figure 7.17: Accuracy of the three-variable model for dark blue Nomex® specimens to predict tensile strength of interpolating points 164
Figure 7.18: Accuracy of the three-variable model for yellow Nomex® specimens to predict tensile strength of interpolating points 165
Figure 7.19: The three-variable model for brown Kevlar®/PBI specimens 166
Figure 7.20: The three-variable model for black Kevlar®/PBI specimens 166
Figure 7.21: Replication of data points by the best equations made of 3, 5, 7, and 10 wavelengths for blue specimens 168
Figure 7.22: The three-variable model based on wavelengths in region 1500 – 1900 nm 170
Figure 7.23: The three-variable model based on wavelengths in region 1900 – 2500 nm 170
Figure 7.24: The three-variable model based on selective wavelengths 171

LIST OF SYMBOLS

English Letters

B_e	Magnitude of blue component of colour of an exposed specimen
B_u	Magnitude of blue component of colour of an unexposed specimen
G_e	Magnitude of green component of colour of an exposed specimen
G_u	Magnitude of green component of colour of an unexposed specimen
m	Number of observations of a dependent variable
n	Number of independent variables
p	Total number of coefficients of independent variables
R_e	Magnitude of red component of colour of an exposed specimen
R_u	Magnitude of red component of colour of an unexposed specimen
R^2	Coefficient of determination
R^2_a	Adjusted coefficient of determination
t_{12}	Required time for a copper calorimeter to undergo temperature rise of 12°C
t_{24}	Required time for a copper calorimeter to undergo temperature rise of 24°C
X	An independent variable
Y	A dependent variable
$\hat{Y}$	Predicted value of a dependent variable
$\bar{Y}$	Mean of real values of a dependent variable

Greek Letters

α	A coefficient of an independent variable
ΔColour	Colour difference from the colour of an unexposed specimen
Δt_n	Duration of the n^{th} stage of the exposure
Δt_{total}	Total duration
ε	Deviation of a predicted response value from a real value

LIST OF ABBREVIATIONS

CRE	Constant-Rate-of-Extension
CCHR	Conductive and Compressive Heat Resistance
DIA	Digital Image Analysis
ePTFE	expanded Polytetrafluoroethylene
FTIR	Fourier Transform Infrared
PBI	Polybenzimidazole
SCBA	Self Contained Breathing Apparatus
SEM	Scanning Electron Microscope
RGB	Red-Green-Blue
TGA	Thermogravimetric Analysis
THL	Total Heat Loss
TPP	Thermal Protective Performance
WVTR	Water Vapour Transmission Rate

1. INTRODUCTION[1]

1.1. Firefighters' protective clothing

Fires have always been a major source of damage all over the world. On average, 59,936 fires occurred in Canada annually from 1993 to 2002, which caused 374 deaths, 3072 injuries, and $1.2 billion in property losses per year [1]. When fires occur, firefighting has always been considered as an important way to decrease the level of damage. The type of firefighting which is involved in buildings, aircraft interiors, vehicles, vessels, and generally enclosed structures is called structural firefighting [2]. Firefighting to deal with fire that occurs in vegetation and prairie is considered as wildland firefighting [3]. This research concentrates on elements of protective clothing used in structural and wildland firefighting.

To protect firefighters and enable them to work efficiently under severe conditions, they are equipped with firefighters' protective clothing. Firefighters' protective clothing plays an important role in mitigating firefighters' injuries. Firefighters' protective clothing is a general term which includes pants, coats, hoods, helmets, gloves, boots and self-contained breathing apparatus. In this dissertation, the term firefighters' protective clothing will be used to refer to coats and pants since they are the focus of this research. Firefighters' protective clothing should protect firefighters from the impact of flame and heat and prevent the penetration of water and other external liquids towards the body. It should be strong enough not to tear easily when it is in contact with sharp and abrasive surfaces and when subjected to friction involved in some movements like crawling. Ease of mobility and flexibility during firefighting operation, and high visibility in hazy atmospheres and both day and night time are other important specifications of firefighters' protective clothing. Furthermore, the clothing should help to regulate some physiological reactions of the body like perspiration and high heart rate in hot environments and during hard work. Not all these specifications can be completely met by only one layer of firefighters' protective clothing. Multi-layer structure of firefighters' protective clothing also provides supplementary insulation by tiny air spaces between layers and subsequently, more protection without any extra weight or cost associated with fabrics.

[1] A portion of this chapter has been published in Fire Technology [9].

The moisture and heat flow to a firefighters' body is restricted by firefighters' protective clothing. Similarly, the dissipation of heat generated by physiological body functions such as metabolism and perspiration is limited. So, highly insulating firefighters' protective clothing poses some problems for heat and moisture removal from the body, which may lead to an increase in body temperature, steam burns, heat stress and in severe conditions, death [4]. Also, higher heat protection may necessitate thicker layers of fabrics, which makes the clothing heavier and consequently, limits the agility of firefighters. Therefore, there is a trade-off between protection of the firefighter's body from thermal exposure and heat removal from their body.

Firefighters' protective clothing is typically composed of three layers, the outer shell, the moisture barrier, and the thermal liner (Figure 1.1). The outer shell is the outermost layer and the first line of defence. Its role is protection against heat, flame, cuts, and abrasion. The moisture barrier is the middle layer and prevents external liquids such as water and chemicals, bloodborne pathogens, and viral agents from penetrating into the body. Some types of moisture barriers contain small pores which prevent passage of liquid drops, but allow vapour diffusion and decrease the risk of steam burns to some extent. The thermal liner is the innermost layer and acts as an insulating layer. It plays a major role in thermal protection and protects firefighters from heat or cold. The slippery surface of thermal liner in contact with the skin provides firefighters with ease of donning and doffing, and assists in agility and mobility during firefighting operations. Some types of thermal liners have the additional advantage of wicking away perspiration.

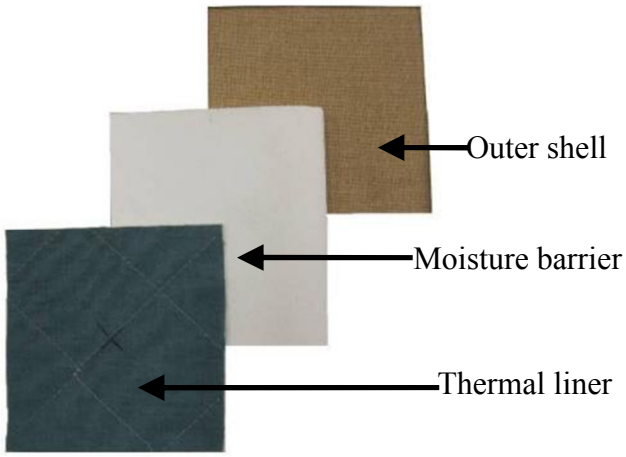

Figure 1.1: Three layers of firefighters' protective clothing

1.2. Performance requirements for firefighters' protective clothing

The standards for protective clothing for new structural firefighting (e.g., NFPA 1971 [2] and CGSB-155.1 [5]), describe the minimum requirements for new firefighters' protective clothing and the test methods to evaluate these requirements. All required tests in NFPA 1971 to evaluate firefighters' protective clothing and the reported properties in the tests are summarized in Table 1.1. However, there is no quantitative standard and test for in-use firefighters' protective clothing. Similar test procedures to NFPA 1971 will be used to assess the changes in characteristic parameters of used firefighters' protective clothing in this dissertation.

In terms of thermal performance, new firefighters' protective clothing is tested for flame resistance, thermal shrinkage resistance, Thermal Protective Performance (TPP), Thermal Heat Loss (THL), and Conductive and Compressive Heat Resistance (CCHR). The flame resistance test is applicable to all layers of firefighters' protective clothing. In the flame resistance test, a specimen is exposed vertically above a methane flame, the height of which is 38 mm, for 12 s. Then, the flame source is removed and afterflame time is recorded. Afterflame time is the time for which the specimen continues to burn with flame. Char length, the length of visible damage along the fabric edge, is also measured. For all new fabrics, afterflame time should not exceed 2 s on average and no evidence of melting or dripping should be observed during exposure to flame. Also, the char length should not be longer than 100 mm on average.

The thermal shrinkage resistance test is applicable to all layers of firefighters' protective clothing. Specimens are heated inside an oven, the temperature of which is kept at 260°C, for 5 min. Then, the specimen is checked for any evidence of melting or dripping. The specimen width and length are measured to calculate the average percentage of change in both dimensions. The maximum allowable percentage of shrinkage in any direction is 10%.

Table 1.1: Evaluation tests of firefighters' protective clothing and required parameters to report according to NFPA 1971 [2]

Test	Property to be reported	Application			
		Composite specimen	Outer shell	Moisture barrier	Thermal liner
Flame resistance	Afterflame time & char length		*	*	*
Heat and thermal shrinkage resistance	Percent change in width and length		*	*	*
Thermal Protective Performance (TPP)	Product of exposure energy heat flux and estimated time to second-degree burn	*			
Total Heat Loss (THL)	Average total heat loss, intrinsic thermal resistance, intrinsic evaporative resistance	*			
Conductive and Compressive Heat Resistance (CCHR)	Required time for the test sensor to achieve a temperature rise of 24°C	*			
Tear resistance	Tear resistance		*	*	*
Cleaning shrinkage resistance	Percent change in width and length		*	*	*
Breaking strength	Required force to break the specimen		*		
Water absorption resistance	The percent of absorbed water		*		
Water penetration resistance	Appearance of any water			*	
Liquid penetration resistance	Appearance of any liquid			*	
Viral penetration resistance	Appearance of any broth			*	
Light degradation resistance	Appearance of any water			*	
Whole garment liquid penetration	A diagram indicating the locations of any liquid leakage	Whole garment			

Figure 1.2 illustrates an NFPA 1971 standard TPP tester. In the TPP test, a specimen is composed of all layers of firefighters' protective clothing. The specimen is exposed to a heat flux of 84 kW/m^2 (roughly 2 cal/(cm^2·s)). A sensor is placed at the back of the specimen. It measures transferred energy from the heat source to the back of the specimen. Temperature rise detected by the sensor is compared with benchmark data [6] to estimate required time for a second degree burn to human skin. TPP value is defined as the total incident heat energy on the specimen per unit surface area at the point of second degree burn and is calculated by multiplication of the incident heat flux and the estimated required time for second degree burn. The minimum TPP value for new firefighters' protective clothing is 35 cal/cm^2. However, higher TPP values do not mean better overall protection for firefighters. Even though firefighters' protective clothing should insulate the body from external heat (implied by higher TPP value), it should allow dissipation of metabolic heat from the interior of the garment to the outside environment.

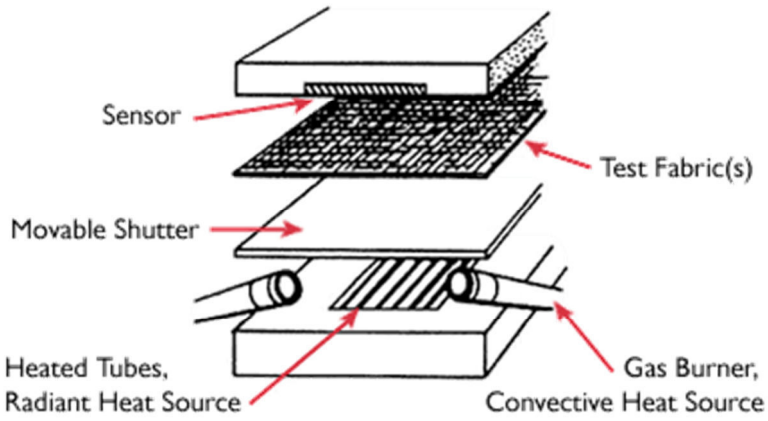

Figure 1.2: A TPP tester (reprinted from [7] with permission)

Heat stress is an important issue in industries, especially in which workers are required to wear semi-permeable or impermeable protective clothing. Firefighters usually work in hot and humid environments and sometimes are involved in hard physical work, which can increase the body core temperature. To reduce the heat accumulation in the body and consequently temperature rise, the body attempts to mitigate this temperature increase through physiological reactions such as sweating. Since some firefighters' protective clothing is impermeable to water and some chemical liquids, the Total Heat Loss (THL) test is included in the NFPA 1971 standard to measure the loss of heat to outside the clothing by diffusion of water vapour and

conduction of heat through the three layers of firefighters' protective clothing. Total heat loss value is in fact an indicator of the capability of the firefighters' protective clothing in heat stress reduction.

A specimen consisting of the three layers of the firefighters' protective clothing is placed on a hot test plate and air flows over the specimen and the test plate. The temperature of air flow and the test plate is kept constant during the experiment. Conductive (dry) heat loss is measured by the required energy to maintain the test plate temperature constant. The evaporative (wet) heat loss is measured similarly, but the test plate is uniformly wetted with water before the test. A new composite specimen of firefighters' protective clothing should have minimum total heat loss of 205 kW/m^2.

Firefighters' protective clothing, especially in shoulder and knee areas, can come in contact with hot surfaces due to crawling and other activities during firefighting. The Conductive and Compressive Heat Resistance (CCHR) test is performed on a specimen composed of three layers of firefighters' protective clothing to evaluate this aspect of performance. The composite specimen is placed on a hot surface maintained at 280°C under a pressure of 140 g/cm^2 (2 psi) for the shoulder area specimens and 562 g/cm^2 (8 psi) for the knee area specimens. In a similar procedure to TPP test, a sensor is placed at the back of the specimen. The required time for a temperature rise of 24°C relative to initial temperature is recorded as the CCHR rating. For a new composite specimen, the CCHR rating should be higher than 25 s.

Mechanical strength of all of layers of firefighters' protective clothing is tested by measuring tear resistance. In the tear resistance test, a specimen is slit in the centre and is pulled by jaws of a tensile testing machine. The required force to continue the tear is recorded. The minimum tear strength of an outer shell fabric should be 100 N. The minimum requirement for moisture barrier and thermal liner fabrics is 22 N. All layers of firefighters' protective clothing should also be tested for cleaning shrinkage resistance. Specimens are washed for five cycles using a specific washing and drying procedure. The percentage of change in each dimension should not exceed 5%.

Some tests are only applicable to one specific layer of firefighters' protective clothing. Water absorption resistance and breaking strength tests are only applicable to the outer shell layer. In the water absorption resistance test, a specimen is placed in an embroidery hoop and a 500 mL volume of distilled water is sprayed onto the specimen. The water absorption percentage is

calculated and should not be more than 30% for a new outer shell. The breaking strength of an outer shell specimen is measured using a tensile testing machine. A new outer shell specimen shall have a minimum breaking strength of 623 N.

Water, liquid, and viral penetration, and degradation resistance tests are only conducted for the moisture barrier layer. In the resistance to water penetration test, a moisture barrier specimen is placed between two clamping cylinders and hydraulic pressure is applied to the underside of the specimen. For new specimens, no evidence of water shall appear on the other side of the specimen before the pressure reaches 172 kPa. In addition, specimens are checked against five liquids: aqueous film-forming foam, battery acid, fire-resistant hydraulic fluid, surrogate gasoline fuel, and swimming pool chlorinating chemical. In the resistance to liquid penetration test, a specimen acts as a partition in front of the hazardous liquid in a horizontal cylindrical test cell. The test takes 60 min. in total. In the first 5 min. of the test, the liquid pressure is the same as ambient pressure. Then, the liquid pressure is increased to 13.8 kPa gauge for 1 min. For the remaining 54 min. of the test, the liquid pressure is kept at ambient pressure. During the test, no visible penetration of the liquid should be observed on the specimen surface in the viewing side of the test cell. Using the same equipment and pressure/time sequence, moisture barrier specimens are monitored for resistance to viral penetration. Instead of specified liquids, as in the liquid penetration resistance test, the test cell is filled with bacteriophage nutrient broth (Phi-X). The broth closely simulates blood-borne pathogens' size, morphology, and stability. A new moisture barrier should be impermeable to broth during the test.

In the light degradation resistance test, a moisture barrier specimen is exposed to simulated daylight radiation using a xenon arc lamp and appropriate filters. The specimen is aged in a test chamber under specified temperature and relative humidity for 40 hr. After 4 hr of conditioning in a dark environment, it is exposed to a pressure of 13.8 kPa (2 psi) under a column of water for 1 min. No water should appear on the surface of the specimen.

Resistance to liquid penetration is so important that in addition to tests on individual layers of firefighters' protective clothing, the complete set of firefighters' protective clothing is also tested. The purpose of a liquid penetration test on the whole garment is detection of leakage or absorption of liquid on the whole ensemble, especially around seams, zippers, and areas which are in close contact with gloves, boots, hoods, and respiratory protective equipment. The whole firefighters' protective clothing is worn on a mannequin already covered by a liquid-absorptive

garment. Five nozzles are positioned on the top and the bottom of the mannequin. The mannequin is exposed to sprayed water from the nozzles in four orientations for 5 min. each. At the end of the test, the firefighters' protective clothing is removed from the mannequin and is inspected for any evidence of liquid penetration on the liquid-absorptive garment and individual layers of the specimen. The location of leakage is identified on a diagram of the mannequin. No evidence of wetting should be observed during inspection.

1.3. Identifying the need for this research

As was discussed, this specialized clothing should meet a number of performance requirements in thermal protection, mechanical strength, and liquid penetration resistance and the minimum level of each aspect of performance is established clearly by standards such as NFPA 1971 [2] and CGSB-155.1 [5]. Although these aspects of performance may change differently after exposure to various external factors, performance of firefighters' protective clothing gradually deteriorates in general. Therefore, firefighters' protective clothing reaches its retirement age when its performance falls below a critical level. This critical level is not clear and in some cases may not be even visible to the naked eye.

Useful life (service life) can be defined as the period of time during which the firefighters' protective clothing provides acceptable protection. The useful life of firefighters' protective clothing depends on a number of factors including the type of materials from which it is constructed, the number, duration, and intensity of destructive exposures which the clothing has faced, the amount of abrasion and wear, and the maintenance and storage procedures used [8,9]. Based on the history of fire protective clothing, remaining useful life varies from item of clothing to item of clothing. Consequently each item of firefighters' protective clothing is expected to have a different retirement age.

A number of associations and manufacturers have developed standards or guidelines for determining the end of the useful life of protective clothing. NFPA 1851 [10], one existing standard for the selection, care, and maintenance of structural firefighters' protective clothing, states that clothing shall be retired not later than ten years after its manufacture date. In addition, NFPA 1851 mandates fire departments to discard a piece of protective clothing if it is so damaged or contaminated that the repair or decontamination is not cost effective. In the case of contamination by CBRN terrorism agents (chemicals, biological agents, and radiological

particulates), firefighters' protective clothing must be retired immediately regardless of physical appearance or repair cost. The standard suggests a typical guideline for retirement age based on a matrix that defines the reasonable repair cost of firefighters' protective clothing as a percentage of replacement cost for each year of service life up to ten years. If the repair cost of firefighters' protective clothing is estimated to be higher than the specified cost in this matrix, it should be replaced with a new piece of firefighters' protective clothing.

Some manufacturers suggest a normal useful life of three to five years for firefighters' protective clothing, which may decrease to two to three years in an active fire department. Manufacturers suggest that the useful life is seldom more than seven years [11]. However, providing a definitive number of years of useful life for firefighters' protective clothing is problematic and not reliable. In general, the useful life of fire protective clothing varies from member to member and fire department to fire department. It is because of the fact that the role of firefighters in comparison with their colleagues' role in fire operation can be significantly different. The severity and number of firefighting operations performed in fire departments are also different. Different firefighters, even in the same department, have different roles in firefighting and their protective clothing is exposed to different conditions over the same period. Therefore, firefighters usually don fire protective clothing, the exposure, usage, and maintenance history of which is unlikely to be similar to other members' fire protective clothing. In addition, fire departments in different areas may encounter different types, sizes, and frequency of fire. For example, a fire department in a large metropolitan area may not be comparable with a fire department in a rural area in terms of number and size of fires and type of firefighting operations.

Some types of damage to firefighters' protective clothing like tears, fading, and brittleness are quite apparent. They can be detected quite easily by careful investigation of the surface. But the level of damage to the firefighters' protective clothing may not be completely reflected by visible degradation. It may degrade below the minimum accepted level of performance before emergence of any visual cues (Figure 1.3). Slater [12] implied that performance of textiles may reach an unacceptable level without appearance of visual indications. He defined two levels in degradation of fabrics, a functional level and a visual level. The functional level is the limit below which the fabric becomes functionally unacceptable. The visual level is the point at which visual indicators of deterioration like colour fade or tears become visible to the naked eye.

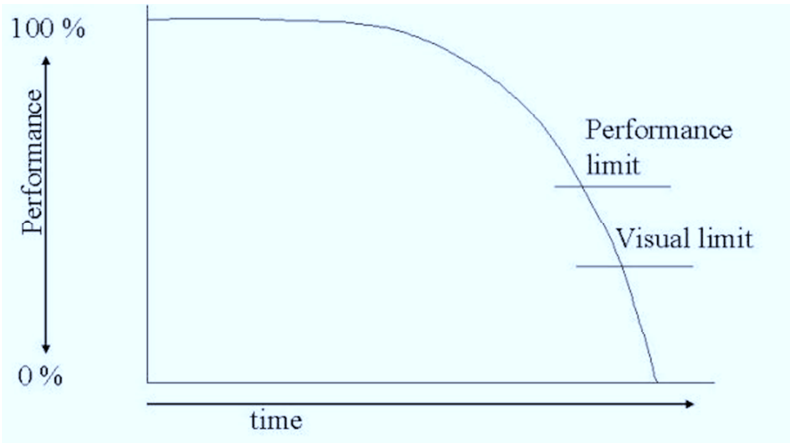

Figure 1.3: Change in the performance of firefighters' protective clothing with ageing [12]

Slater [12] stated that the functional level does not usually coincide with the visible level. In some specialized clothing such as firefighters' protective clothing, this issue could bring about severe consequences. If degradation past the functional level occurred before the visible level was reached for a piece of protective clothing, the wearer could be in danger. Davis et al. [13], who investigated the performance of two outer shell fabrics after exposure to ultraviolet radiation, could not determine if there was significant deterioration in mechanical strength of exposed specimens just by pulling on the fabrics by hand. Visual observation also did not reveal significant deterioration since the specimens were just slightly darker after exposure. However, measured values of tensile and tear strength of these fabrics were lower than the values for the fabrics when new. Hence, discoloration and manual inspection for physical damage (rips, tears, cuts, seam integrity, broken stitches) and thermal damage (charring, burn holes) do not necessarily indicate an unacceptable level of deterioration [13,14,15]. On the other hand, some aspects of the performance of fabrics may still be acceptable even after discoloration.

Torvi and Hadjisophocleous [8] conducted a comprehensive review of research into firefighters' protective clothing. They pointed to a survey carried out by the Underwriters Laboratories of Canada's (ULC) Committee on Research for the Fire Services showing durability and appropriate retirement age of firefighters' protective clothing to be issues of major concern for fire departments in Canada. Although this survey dates back to 1996, a practical method to determine the retirement age of firefighters' protective clothing has not yet been discussed in the literature. In addition, a review on developments and needs in materials used for personal protective equipment identified a concern about the performance of materials during

their entire service life [16]. Limitations of the NFPA 1851 standard and subsequently, a need to develop an improved guideline for retirement of firefighters' protective clothing was recently addressed by Nazare et al. [17].

As was discussed in section 1.2, the standards on protective ensembles for structural firefighting, such as NFPA 1971 [2], describe the minimum requirements for new protective clothing and the test methods to evaluate them. Virtually, all the test methods in these standards are destructive. Hence, measuring the performance of in-use firefighters' protective clothing without destroying a piece of clothing is almost impossible. Performing the destructive tests on a limited number of pieces of protective clothing as a representative of all clothing in a fire department cannot completely assess the level of damage to individual piece of clothing. Owing to the fact that firefighters in the same department have different roles in firefighting and their protective clothing is exposed to different conditions, the use and maintenance histories of individual pieces of clothing may be different over the same period. This sampling procedure may also be too expensive for some departments. Ensuring that protective clothing continues to provide an acceptable level of protection over its entire service life is critical to firefighters' safety. Therefore, there is a need to develop and improve non-destructive methods for evaluating the condition of in-use firefighters' protective clothing.

1.4.Ageing of firefighters' protective clothing

In gerontology, the science of the medical aspects of ageing, ageing is defined as the accumulation of all changes in a system with the passage of time [18]. These changes are irreversible and usually cause decline or loss of functionality. However, some features may improve as a result of ageing [19]. Such a definition for ageing can be generalized to textiles. The major destructive consequence of ageing in firefighters' protective clothing is degradation.

The performance of each layer of firefighters' protective clothing has a significant influence on the level of protection provided. In general, the protection offered by firefighters' protective clothing is expected to deteriorate over time. But it is still uncertain how destructive different exposures are and how long a piece of firefighters' protective clothing can continue to protect a firefighter to an acceptable level.

In the textile area, degradation is defined as weakening and loss of those properties that are necessary for the satisfactory performance due to the changes occurring as a result of the ageing

process [20]. It should be noted that degradation is not only exclusive to the time after employing the firefighters' protective clothing in fire departments. Some types of degradation during the production of fabrics, dyeing, finishing processes and storage occur before the end user starts using the protective clothing.

A number of factors influence the ageing and subsequently degradation of firefighters' protective clothing, including [9]:

- the type of material used to manufacture the clothing;
- the nature of firefighting operations, including resulting exposures to high temperatures and heat fluxes, and ultraviolet radiation;
- wear and abrasion to the clothing; and
- the specific maintenance procedures used.

The relative importance of the above individual factors may vary from department to department and by the type of firefighting operations. An extensive review on previous research was conducted into the effects of each of the above factors on the ageing and degradation of firefighters' protective clothing [9]. As the effect of thermal ageing is the focus of this research, the literature review section in this thesis will concentrate on previous work in this specific area.

To develop the methods to assess the amount of damage to the firefighters' protective clothing, it is necessary to know the influence of these factors on the performance of the garments. Knowing the relative effect of these factors on specific aspects of performance of firefighters' protective clothing helps in understanding what aspects of the garment's performance deteriorate dramatically and after exposure to which conditions. Consequently, exposures and aspects of garment performance which should be emphasized in the experiments are determined. Then, the range of these exposures in the parametric map of the test matrix based on the conditions in the firefighting environment is set.

A major factor influencing degradation is the type and weight of the textile from which each layer of firefighters' protective clothing is constructed. Different types and weights of fabrics will undergo different amount of degradation after the same use and exposures to high temperatures and heat fluxes, ultraviolet radiation. Abrasion will also affect different fabrics in different ways. In the past few decades, a variety of materials for use in firefighters' protective

clothing have been developed. Nomex®[1], Kevlar®, and PBI (Polybenzimidazole) are the backbone of various flame resistant fabric blends and may be used in construction of all layers of firefighters' protective clothing. The beneficial property of these fabrics is that instead of melting or dripping or igniting, they char when exposed to elevated temperatures. In addition, they decompose at much higher temperatures than other fabrics. They are, also, inherently flame resistant which means that the flame resistance does not diminish during the life of the fibre.

Poly(phenyleneisophthal-amide) has a structure in the form of a long chain polyamide with the amide linkages (-CO-NH-) of which more than 85% are connected directly to two aromatic rings [21]. It is available in two different chemical structures: *meta* and *para* oriented phenylene forms. The two forms differ in the position of amide groups in the phenylene group. Meta and para are part of chemistry nomenclature, which define the relative position of substituents (atoms or group of atoms) other than hydrogen in relation to each other on an aromatic hydrocarbon (Figure 1.4). In the meta position, the atoms are in positions 1 and 3 in relation to each other (corresponding to R and meta in Figure 1.4), while in the para position, the atoms are in the opposite positions (corresponding to R and para in Figure 1.4).

Nomex® and Kevlar® are two registered trademarks for a family of polyamide (aramid) fibres. They have a wide range of applications in industry. Nomex® is a name for poly(meta-phenyleneisophthal-amide) (Figure 1.5), whereas Kevlar® represents poly(para-phenyleneisophthal-amide) (Figure 1.6) which is similar to a rod-like molecular structure.

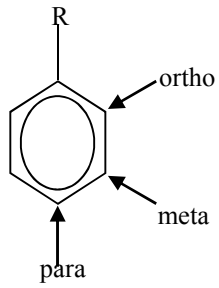

Figure 1.4: Main substitution patterns

[1] Certain commercial products are identified in this dissertation in order to adequately specify the results of research. In no case does such identification imply recommendation or endorsement by the authors, nor does it imply that the product or material identified is the best available for the research purpose.

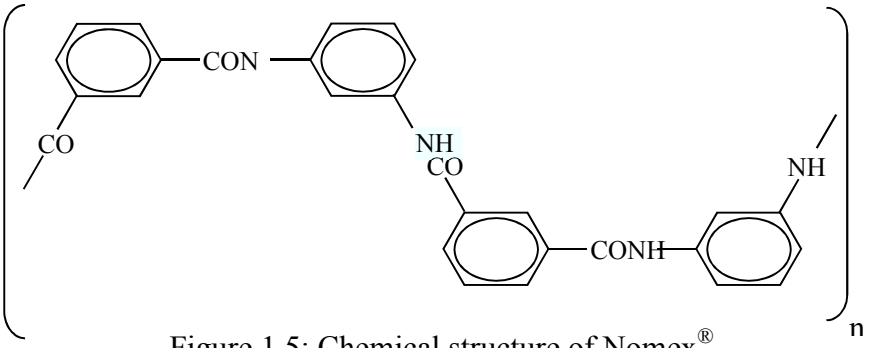

Figure 1.5: Chemical structure of Nomex®

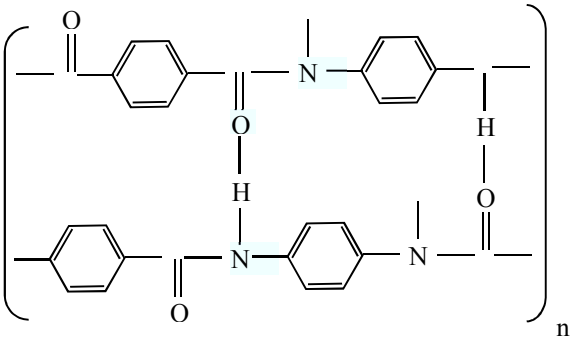

Figure 1.6: Chemical structure of Kevlar®

PBI is an abbreviation for polybenzimidazole which is an aromatic polymer and a synthetic fibre with a high thermal stability and a high chemical resistance. PBI (Figure 1.7) is a long-chain aromatic polymer with molecular formula of -$(C_{20}N_4H_{12})_n$- [21]. PBI fibres, like Nomex® and Kevlar®, do not melt or drip and retain the strength, integrity, and flexibility after exposure to flame. In addition, PBI has a high chemical resistance and textile-like performance which makes it appropriate for construction of outer shell of firefighters' protective clothing.

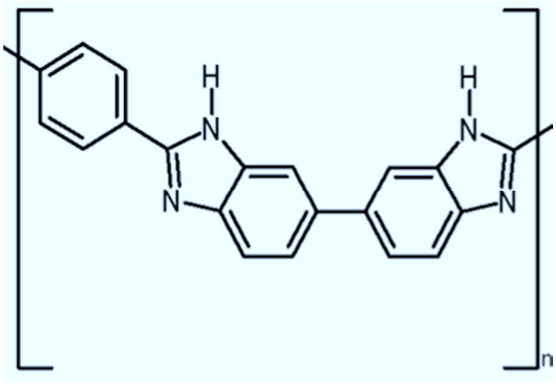

Figure 1.7: Chemical structure of PBI

Polytetrafluorethylene (PTFE) is a common material in construction of moisture barriers. The PTFE film is laminated to a substrate (a support fabric). The substrate is usually made of Nomex®. There are some micropores on the surface of the moisture barrier film which are big enough to allow water vapour generated by perspiration to pass through the fabric, but small enough to prevent water and other external liquids from penetrating through the fabric. The breathability of the moisture barrier reduces heat stress during intense activity. Like other polymers, the PTFE molecule is composed of a chain of carbon atoms surrounded by fluorine atoms. Carbon and fluorine form a very strong bond and the fluorine atoms protect the weak carbon chain. The chemical formula of PTFE is $(C_2F_4)_n$ and its molecular structure is shown in Figure 1.8.

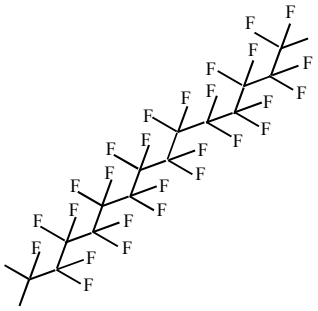

Figure 1.8: Molecular structure of PTFE

Firefighters are often exposed to high temperatures and heat fluxes during firefighting operations. These exposures can provide sufficient energy for chain scission and escape of volatile degradation products [22]. Much of the research that has been conducted into ageing of firefighters' protective clothing has been concerned with the effects of thermal ageing. The intensity of incident heat flux or temperature, duration of exposure, and frequency of exposure have all been shown to be influential factors in determining the effects of thermal exposures.

Jain and Vijayan [23] considered the number and depth of the microgrooves on the fibres of meta-aramid specimens after thermal exposure. It was found that they were a function of both temperature and duration of thermal exposure. Results indicated that the severity of thermal deterioration on a specimen surface that was exposed to 300°C for 400 hr. was higher than that of a surface exposed to 400°C for 2.25 hr.

Iyer et al. [24,25] examined the effects of thermal exposures on para-aramid specimens. Specimens of para-aramid were aged in a series of isothermal tests in a furnace using a variety of temperatures from 150°C to 550°C (the fabric's decomposition temperature), for cumulative durations ranging from 0.5 to 7000 hr. in one to 12 stages. After each stage of exposure, the specimens' surface structure was studied, and tensile strength and weight loss were measured.

In the early stages of ageing, alterations in the form of peel-off and grooves were observed on the surface of specimens by scanning electron microscopy. Holes (loss of material) and protrusion of material appeared later in the ageing process. These morphological changes were accompanied with weight loss and a decrease in tensile strength of the specimens, which indicated a good correlation between these properties. The study revealed that the structure and properties of specimens changed in a similar manner after each thermal exposure, but the magnitude of changes varied with both temperature and cumulative duration of exposure. The changes in the specimens observed at higher temperatures and shorter durations were similar to the changes observed at lower temperatures and longer durations.

Iyer and Vijayan [26] studied the effects of multi-stage isothermal exposures on thermal degradation of para-aramid fibres in terms of structural characteristics such as surface change, weight loss, and crystallinity and mechanical properties such as tensile strength. The specimens made of para-aramid fibre were exposed to temperatures of 250, 300, 400, and 500°C in a furnace for duration ranging from 0.5 to 120 hr. In the multi-stage process, there was at least a 45 min. gap between the two stages of exposure while the specimen was cooled with air. X-ray diffraction pattern, weight, and tensile strength were measured before and after the completion of the multi-stage exposure. It was found that three factors were influential in a multi-stage thermal exposure: exposure temperature, total duration of an n-stage exposure (Δt_{total}), and duration of each stage of the exposure (Δt_n). Total exposure duration is the sum of the exposure durations for all n stages, which is given by:

$$\Delta t_{total} = \Delta t_1 + \Delta t_2 + \Delta t_3 + \ldots + \Delta t_n \tag{1.1}$$

The results revealed that the three aforementioned factors were acting in unison. The higher the temperature, total duration, and number of stages of multi-stage thermal exposure, the more severe the thermal degradation was. Within the range of temperature studied and for the same

total exposure duration, the effect of multi-stage isothermal exposure on deterioration and decomposition of para-aramid fibres was less severe than that of single-stage exposure.

An et al. [27] investigated the effects of thermal ageing on the performance of chemical protective clothing. The performance parameters that were studied included the change in mass per unit area, tensile and tear strength, bending flexibility, and chemical permeation resistance. Thermal ageing was done in two forms, convective and conductive heat exposures. In the convective method, the specimens were placed inside an oven with forced circulation at 94°C (200°F) for four hr. In the conductive method, the specimens were placed on a metal plate maintained at 94°C (200°F), for 5 min. The performance of fabrics that were aged using both methods was nearly the same.

The mass per unit area did not change noticeably for fabrics undergoing both thermal ageing methods. On average, the tensile and tear strength decreased by 10% to 20% of the original value. However, the bending flexibility increased indicating a positive contribution to firefighter agility inside the ensemble if the ensemble is intact enough to protect the wearer. The reduction of mechanical strength and bending stiffness were attributed to having a softer material with lower crystallinity after thermal ageing. Resistance to penetration of the particular chemical agents examined in the research was enhanced since chemical resistance parameters, including permeation breakthrough time and steady state permeation rate, improved after the exposures. Although the results cannot be generalized to other chemical agents, reduction of number and size of micropores in the material by heat induced material flow were given as reasons for the results.

Day et al. [22] examined the effects of thermal exposure on the mechanical and thermal protective properties of some types of fabrics used in firefighters' protective clothing. Specimens from outer shell and moisture barrier materials were selected. The fabrics were placed in an oven at temperatures ranging from 150 to 250°C for periods of 5 min. to 7 days. The effect of thermal exposure on thermal shrinkage and weight loss was dependent on the fabric type. For example, Nomex® specimens underwent a negligible amount of thermal shrinkage (1%) and weight loss (less than 5%). However, tear strength of Nomex® specimens decreased by approximately 20%. Although all outer shell specimens suffered significant reduction in tear strength, the tear strength of most of the moisture barrier specimens increased after thermal exposure, which was attributed to crosslinking reactions. However, the flame resistance properties, including charred

length and afterflame time, as well as Thermal Protective Performance (TPP) rating did not change considerably.

Vogelpohl [36] examined pieces of actual firefighters' protective clothing which had been in service for periods ranging from one year to more than five years. The history of used clothing was described in terms of service age, average number of calls that the fire department responded to per year, and the main maintenance procedures employed. She assessed specimens of twenty pieces of used firefighters' protective clothing along with new specimens of the same type of material to determine the level of reduction in thermal protection and mechanical properties as a consequence of thermal ageing. Three different types of inherently flame resistant fabrics were used for the outer shell of this clothing: 100% Nomex®, 40% PBI/60% Kevlar®, 50% PBI/50% Kevlar®, and 40% Nomex®/60% Kevlar®.

Flame resistance and TPP rating were measured, along with water absorption and penetration resistance, and mechanical properties. The outer shell and thermal liner of all the firefighters' protective clothing passed the thermal protection tests included in the 1991 edition of the NFPA 1971 standard for new structural firefighters' protective clothing [2]. The results showed an increase in flame resistance for used specimens in comparison with the new specimens. TPP values of the used clothing were higher than those of new clothing composed of the same materials, which was attributed to the increased thickness of the used clothing. It was thought that the used fabric contained more air spaces, which increased the TPP value.

The outer shell of all used fabrics absorbed more than 10% water, while new specimens did not absorb an appreciable amount of water. In addition, the moisture barrier of most specimens failed the water penetration test and a reduction in tensile strength for used protective fabrics was observed. Mechanical properties, including tensile and tear strength of the outer shell, decreased on average by 40% and 10%, respectively. However, on average, tear strength of the moisture barrier and the thermal liner of all tested firefighters' protective clothing increased by 40% and 20%, respectively. This increase in the tear strength of the moisture barrier of in-use/retired firefighters' protective clothing is in agreement with Day et al.'s measurements in which moisture barriers made of three different materials were artificially aged by thermal exposures [14].

Vogelpohl's research showed that the TPP value of these pieces of firefighters' protective clothing did not decrease. However, the deterioration in flame resistance of inner layers,

mechanical strength of the outer shell and water resistance of the outer shell and the moisture barrier of the used clothing was significant. In spite of decrease in the flame resistance and mechanical properties, most of the used firefighters' protective clothing could still pass the requirements in the 1991 version of NFPA 1971 for these properties.

Thorpe [14] also performed tests to evaluate the expected performance of in-use firefighters' protective clothing. He thermally exposed specimens consisted of an outer shell, a moisture barrier, and a thermal liner. He carried out tests on Nomex® thermal liner before and after thermal exposures to measure Conductive and Compressive Heat Resistance (CCHR), tensile and tear strength, and water penetration resistance. The specimens were exposed to radiant heat flux values of 5 to 30 kW/m^2 for a variety of times, ranging from 30 to 3600 s, using the radiant panel apparatus described in ASTM F1939 [28]. Thorpe found that CCHR rating of the specimen increased when it was exposed to higher heat flux values or longer exposure durations (Figure 1.9). The increase in CCHR rating was attributed to more entrapped air pockets inside the fabric weaves which became stiff after the thermal exposure.

On the other hand, tensile strength of the Kevlar®/Nomex® outer shell of the specimens decreased at higher heat flux values or longer exposure durations (Figure 1.10). The tensile strength of some specimens was still higher than the minimum value specified in NFPA 1971 [2] for new firefighters' protective clothing (623 N) after the thermal exposure. Results of the water penetration test, which is applicable to the moisture barrier layer, showed that specimens without visible holes or tears were impermeable to the specified amount of water placed on their surface. This test method is similar to the procedure in NFPA 1851 [10]. Inasmuch as the results of these water penetration tests in the current form are pass or failure, rather than a specific measurement, they cannot be used to develop a detailed understanding of deterioration in the moisture barrier's resistance to water penetration after thermal exposures. Such an understanding could be provided by expressing the results in terms of the water pressure necessary for penetration to occur.

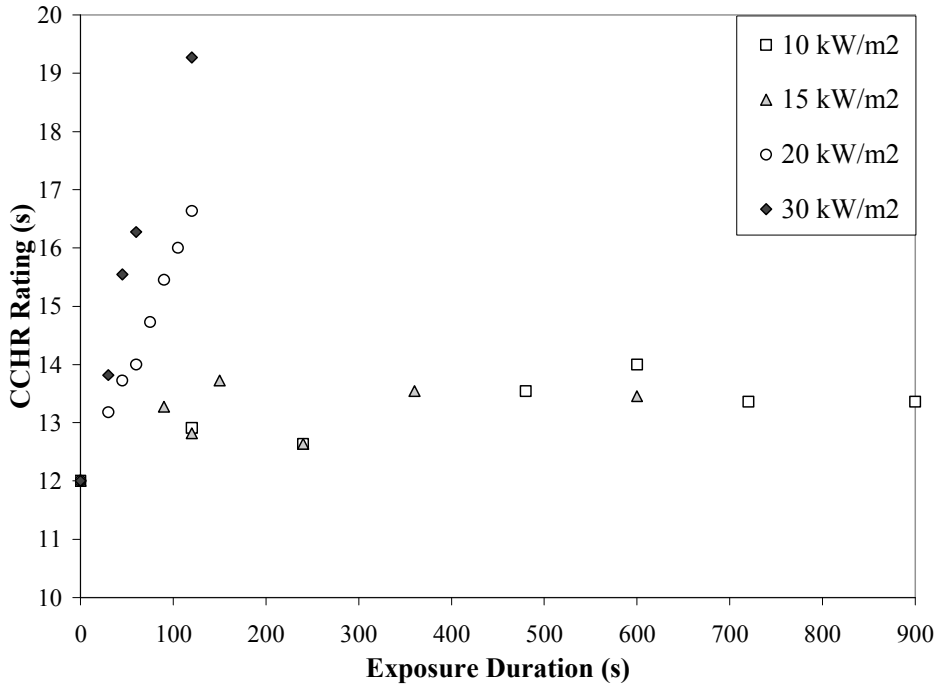

Figure 1.9: CCHR ratings of Nomex® thermal liner specimens previously exposed to various radiant heat flux exposures using the ASTM F1939 test apparatus [14]

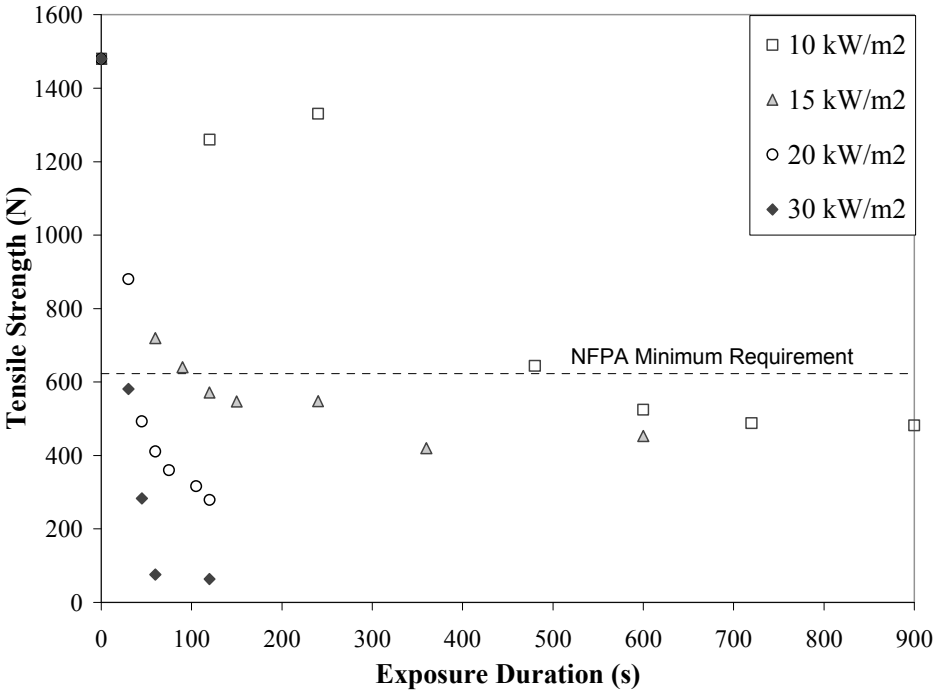

Figure 1.10: Tensile strength of Kevlar®/Nomex® outer shell specimens previously exposed to various radiant heat flux exposures using the ASTM F 1939 test apparatus [14]

Rossi et al. [15] studied the effects of thermal ageing on thermal protection and mechanical properties of six different combinations of fabrics used to form the three layers in firefighters' protective clothing in two stages. In the first stage, the thermal protection criteria were defined as the times required for a copper calorimeter covered with the specimen to undergo temperature rises of 12°C and 24°C (t_{12} and t_{24} respectively) when exposed to a specified heat flux. Also, the length of time required for colour change in the outer layer of the specimen to be observed by the naked eye was recorded as the discoloration time.

The following procedure was used in the first stage of research:

- the new specimens were exposed to a radiant heat flux of 40 kW/m^2 or a primarily convective heat flux of 80 kW/m^2 for a duration long enough to measure t_{24},
- t_{12}, t_{24}, and discoloration time were determined for each specimen,
- the same specimens were conditioned at 20°C and 65% relative humidity for 24 hours,
- the specimens were exposed to the same heat flux values for a second time, and
- both t_{12} and t_{24} were measured again.

For the 40 kW/m^2 exposure, the test method specified in ISO 6942 [29] was utilized, which uses six silicon carbide heating rods as the heat source. The Meker burner, described by EN367 [30], was employed as the heat source for the primarily convective 80 kW/m^2 exposure.

The results showed that both t_{12} and t_{24} decreased in the second exposure compared to the first exposure. The decrease in these values was generally larger for specimens subjected to higher heat fluxes. t_{12} and t_{24} decreased by 7% and 6% respectively after the second exposure to the 40 kW/m^2 heat flux and they decreased by 19% and 14% after the second exposure to the 80 kW/m^2 heat flux. The higher level of decrease in t_{12} and t_{24} after the 80 kW/m^2 exposure was attributed to the higher temperatures reached in the layers of the specimens and subsequently, the more severe damage that occurred to the specimen.

One of the specimens which had been completely charred after the first exposure to the heat source had a slightly larger value of t_{24} for the second exposure to the heat source. This increase in t_{24} may demonstrate how charring can produce an extra insulating layer. This observation is consistent with the observations of Vogelpohl [36] and Thorpe [14] indicating that a char layer can have a slight positive effect on thermal protection properties. However, in practice the charred fabric usually becomes so brittle that the fabric cannot be expected to remain intact.

In the second stage of the research, Rossi et al. measured tensile and tear strength of the outer layer of the specimens when there was visible discoloration of the specimens. The following procedure was used in the second stage of research:

- the new specimens were exposed to the same heat flux as in the first stage, but for a duration equal to the discoloration time measured in the first stage, and
- the tensile and tear strength of specimens were measured after this thermal exposure and compared with the tensile and tear strength of new specimens.

The results showed three types of behaviour for the six tested specimens. Three specimens had almost the same tensile strength after the thermal exposure as new specimens indicating that mechanical strength of the outer shell was preserved at least up to the discoloration point. Two specimens showed loss of strength before discoloration became visible to the naked eye. Since no structural change was observed in the specimen by a scanning electron microscope (SEM), the deterioration of mechanical strength during the thermal exposure for these specimens was attributed to the break of polymer chains.

The remaining specimen exhibited a type of behaviour between the first and second types of behaviour described above. There was no significant loss of strength after exposure to a radiant heat flux of 40 kW/m^2 until discoloration, but when the specimen exposure took one second longer than the discoloration time, it lost about 50% of its tensile strength. For this specimen, the discoloration point was almost coincident with the sharp reduction in tensile strength when it was exposed to heat flux of 40 kW/m^2. When this specimen was exposed to a primarily convective heat flux of 80 kW/m^2, it experienced about 40% decrease of tensile strength exactly at the discoloration point. Rossi et al. found that the effect of thermal ageing on tear strength was similar to the tensile strength.

Most of the specimens in this research were still able to pass the requirements for new firefighters' protective clothing in EN 469 [31] after thermal ageing. This standard defines the functional level (lower limit) for tensile strength as 450 N. Table 1.2 shows tensile strength of specimens when they were new and when visible discoloration in the second stage occurred.

Table 1.2: Tensile strength of new and visibly faded specimens, required time for appearance of visible discoloration [14]

Specimen	Tensile strength of new specimens (N)	40 kW/m^2		80 kW/m^2	
		discoloration time (s)	Tensile strength after discoloration (N)	discoloration time (s)	Tensile strength after discoloration (N)
1	2095 ± 61	10	1263 ± 67	5	850 ± 48
2	2292 ± 144	10	2047 ± 234	2	2037 ± 151
3	1180 ± 17	6	1163 ± 6	1.5	1163 ± 15
4	1323 ± 49	7	1223 ± 81	3	798 ± 168
5	1157 ± 14	6	1180 ± 17	1.5	1147 ± 12
6	1586 ± 13	9	1557 ± 35	2.5	1573 ± 21

Table 1.3 shows a summary of the work on effects of thermal ageing [9]. In summary, research has shown that flame resistance and mechanical properties of fabrics deteriorate more severely through thermal exposure than other aspects of performance [9]. Such a loss in mechanical strength is more noticeable during the early stages of exposure. But deficiency in flame resistance properties was significant after long period of using firefighters' protective clothing. Dirt and contaminates may be flammable, which could affect flame resistance if these accumulate within a fabric.

Table 1.3: Summary of research on effects of thermal ageing [9]

Investigator(s)	Thermal ageing method	Duration of thermal ageing	Parameters studied	Key results
Jain and Vijayan [32]	Exposure to 200-400 °C in a furnace	0.5-2000 hr. (1 stage)	- X-ray diffraction pattern - Weight loss - Tensile strength - Microstructural features	- Decrease in X-ray crystallinity and tensile strength, and increase in weight loss and damage to surface of fibres depend on both temperature and duration of thermal exposure
Iyer et al. [26,33,34]	Exposure to 150-550 °C in a furnace	0.5-7000 hr. (1-12 stages)	- X-ray diffraction pattern - Weight loss - Tensile strength - Microstructural features	- Decrease in X-ray crystallinity and tensile strength, and increase in weight loss and damage to surface of fibres depend on duration of each stage in a multiple stage exposure
An et al. [35]	Two methods: - convective exposure at 94°C in an oven - conductive exposure at 94°C on a metal plate	- 4 hr. - 5 min.	- Mass per unit area - Tensile and tear strength - Bending flexibility - Chemical permeation resistance	- Changes in performance of fabrics aged using both methods were nearly the same - Reduction of number and size of micropores in the material by heat induced material flow was key reason for observed changes in properties
Day et al. [22]	Exposure to 150 - 250°C in an oven	5 min. to 7 days	- Thermal shrinkage - Weight loss - Char length - Afterflame time - TPP value - Tear strength	- Changes in thermal shrinkage and weight loss depended on fabric type - Char length, afterflame time, and TPP rating changed only slightly - Tear strength of outer shell specimens decreased, while tear strength of moisture barrier specimens increased

Table 1.3 (Continued): Summary of research on effects of thermal ageing

Vogelpohl [36]	Evaluated used firefighters' protective clothing	1 – 5^{+} years in service	- Afterflame time - Char length - TPP rating - Water absorption and Penetration resistance - Tensile strength - Tear strength	- Tear strength of used outer shell specimens lower than for new specimens; tear strength of used moisture barrier and thermal liner specimens higher than for new specimens - Tensile strength of used specimens lower than for new specimens - Afterflame time, char length, and TPP rating of used clothing were higher than for new clothing; - Moisture barrier of most used specimens failed NFPA 1971 requirements for new clothing - Outer shell of used clothing absorbed more water than new clothing
Thorpe [14]	Exposure to 5 - 30 kW/m^2 using radiant panel	30 - 3600 s.	- CCHR rating - Tensile strength - Tear strength - Water penetration resistance	- Increase in CCHR rating, decrease in tensile strength, and decrease in water penetration resistance depend on both heat flux and duration
Rossi et al. [15]	Two exposures to 40 kW/m^2 (quartz tubes) or 80 kW/m^2 (Meker burner)	17 - 33 s	- Required time for 12 or 24 °C temperature rise of a test sensor (t_{12} or t_{24}) - Tensile and tear strength	- Decrease in t_{12} and t_{24} during second exposure - discoloration may not necessarily indicate point at which there is significant decrease in mechanical strength of the specimens

1.5. Potential non-destructive test methods

A non-destructive test technique is a type of examination in which the quality of a specimen for further operation is assessed without affecting its future performance. Many non-destructive test techniques change the specimen permanently. However, they are still classified as non-destructive tests since the performance of the specimen is not changed and it can continue working. For instance, acoustic emission used for detecting microcracks alters the structure of the material, but not to the point where the performance of the material is affected. These techniques are being used extensively in many areas of engineering to evaluate in-use condition and as a predictive tool to estimate remaining service life [37].

In these techniques, some properties of the material serve as the indicators of performance deterioration. If those properties can be measured, the level of material deterioration may be determined and can help to estimate the remaining life time of the material. Two major issues should be discussed before choosing a non-destructive method. The first issue is to identify the physical properties of the specimen which deteriorate with use, or the nature of the flaws which will appear in the specimen gradually during service time. The second issue is what physical process the non-destructive method is based on. These two issues will determine whether the non-destructive method is applicable to the test specimen or not [37].

In the standard on care and maintenance of protective ensembles for structural firefighting, NFPA 1851 [10], some non-destructive test methods have been proposed for evaluation and inspection of in-service firefighters' protective clothing. In the first test method, the inner layer, which includes both the moisture barrier and thermal liner, is evaluated by using a light source. The criterion of evaluation is the amount of light passing through the liner. Brighter areas may indicate the material deficiency in insulating layers. However, this method depends on the inspector's judgement, which is subjective. In the second test method, which is also applicable to the inner layer, a cup of a water-alcohol mixture is poured on the moisture barrier side of the inner layer and the other side of the inner layer is visually inspected for leakage. In the third test method, the substrate of the moisture barrier is exposed to water pressure of 6.9 kPa (1 psi) and water leakage on the other side is determined visually.

Torvi and Hadjisophocleous [38] discussed development of a management system to keep a written record of use, care, and maintenance of firefighters' protective clothing. Such a

management system would assist in making a decision as to the proper time to retire an article of firefighters' protective clothing. In collaboration with a research committee, they proposed some guidelines which could be used in conjunction with visual inspections and records of service provided by the management system to assist the fire departments with determination of retirement age of firefighters' protective clothing. They suggested that some methods which are employed in other areas of engineering might be applicable to estimation of remaining life of firefighters' protective clothing.

Some non-destructive tests which have been used in various applications and can be applicable to firefighters' protective clothing to assess the level of damage are discussed in the following sections:

1.5.1. Raman spectroscopy

Galiotis [39] suggested Raman spectroscopy as a non-destructive method to measure stress and strain in high performance fibres like para-aramids. He stated that any disorder on the surface of the fibres as a result of mechanical force or thermal exposure appears as a 'disorder-indicator' band or frequency shift in the Raman spectra of the fibres. Therefore, Raman peaks and their position can indicate changes in high performance fibres at the microscopic scale.

Washer et al. [40] stated that Raman spectrum characteristics such as position, bandwidth, and relative intensity of peaks can vary depending on environmental agents such as thermal and ultra violet exposures. Since each Raman peak is related to a specific vibrational mode in the polymer, any defects can change the vibrational modes and consequently the Raman spectrum characteristics. Therefore, the characteristics of a Raman spectrum can be employed as a diagnostic tool to identify the level of deterioration in the material properties. Washer et al. [40] examined a series of new and thermally aged strand specimens of Kevlar® using an incident laser of various wavelengths and power levels. The results showed that the average peak intensity of aged specimens decreased in comparison with that of unaged specimens, but the average bandwidth of peaks in the Raman spectrum of aged specimens increased in comparison with that of unaged specimens. The peak position of the Raman spectrum did not change for aged and unaged specimens.

Thorpe [14] developed some non-destructive methods to establish a quantitative measurement of degradation. He implemented Raman spectroscopy to correlate degradation to

tensile strength of the outer shell. Using Raman spectroscopy to count the photons did not yield consistent results because of high fluorescence and a poor signal to noise ratio. This poor signal to noise ratio occurred at shorter wavelengths of incident light such as the 514 nm laser. Washer et al. [40] made a similar comment. It was thought that using an incident light of longer wavelength might enhance the resolution. In a different method, Raman spectroscopy was employed by Thorpe [14] to determine the luminescence of the fabric. However, different shapes of Raman luminescence spectra and variable location of the peaks of the curves for different locations on the same specimen implied a lack of repeatability of this method, which was attributed to an inconsistency in the dyeing process and specific colour of the fabric used in his study.

1.5.2. X-ray diffraction

Iyer and Vijayan [23] studied the effects of multi-stage isothermal exposures on thermal degradation of Kevlar® fibres in terms of structural characteristics such as surface change, weight loss, and crystallinity and mechanical properties such as tensile strength. X-ray diffraction pattern, weight, and tensile strength were measured before and after the completion of the multi-stage exposure. X-ray diffraction results demonstrated that there seems to be a clear correlation between crystallinity and some physical properties of the fabric such as weight loss and tensile strength.

Jain and Vijayan [29] investigated the effect of thermal ageing on the properties of Nomex® fibres using the X-ray diffraction method. They exposed meta-aramid specimens to temperatures of 200, 300, 350 and 400ºC for durations between 0.5 and 2000 hours. Before the test and at different stages of the thermal exposure, the specimens were examined to consider changes in crystallinity, surface damage, and mechanical strength.

The X-ray diffraction method was employed to assess the change in crystallinity since the diffraction intensity is an indicator of the specimen crystallinity. The diffraction intensity was defined as the area under the X-ray diffraction pattern. The test results showed a reduction in diffraction intensity with an increase in exposure duration. As exposure duration increased, a limit of zero crystallinity was reached where no sharp peak of reflected radiation in the X-ray diffraction pattern was detectable. The results showed that the reduction of crystallinity was accelerated at higher temperatures and that for a specific exposure temperature, crystallinity

decreased with exposure time. Mechanical properties of meta-aramid fibre such as tensile strength and strain were examined by analyzing the load-extension curve for different combinations of temperature and exposure time. Tensile strength and strain at the fracture point decreased with increasing temperature or duration of thermal ageing.

Iyer et al. [30, 31] carried out similar research on another common fabric in construction of firefighters' protective clothing, Kevlar®. They correlated some features of an X-ray diffraction pattern such as position and half width of reflection peaks and integrated intensity of the diffraction profile, with the temperature and duration of exposure. With an increase in temperature and duration of exposure and in a general fashion, the intensity reduced, the position of peaks shifted toward lower angles, and the peaks broadened after sharpening in the early stage of exposure. Based on the relative changes of parameters during thermal exposures, tensile strength and crystallinity were found to be the most sensitive parameters. Therefore, thermal decomposition can be considered as a progressive process in which a relationship between tensile strength and crystallinity of the specimen may be developed through X-ray diffraction analysis.

In a similar effort, Arrieta et al. [41] studied the effect of thermal ageing on crystallinity of outer shell specimens made of a 60% Kevlar®/40% PBI fabric. This study can be helpful to link mechanical strength with crystallinity of specimens after thermal ageing. Specimens were thermally aged at temperatures of 190, 220, 275, 320°C inside an electric oven for durations from 1 hr to 15 days. Specimen crystallinity was determined using two methods: X-ray diffraction and Raman spectroscopy. Two trends of change in crystallinity of thermally aged specimens were observed. In the first trend, specimen crystallinity calculated using X-ray diffraction eventually increased by 20% after thermal ageing. In the second trend, disappearance of Raman spectral lines was attributed to decrease in crystallinity of thermally aged specimens. This difference in variations in crystallinity was related to different orders of crystallites which were highlighted in each technique.

1.5.3. Liquid penetration

Bray and Stull [42] conducted a feasibility study on employing a liquid penetrant as a simple non-destructive method in detection of cracks, holes, and any loss of integrity in chemical/biological protective clothing. Eight common fabrics used in construction of

chemical/biological protective clothing were abraded. The fabrics were then assessed by several liquid penetrants with different characteristics. The fluorescent penetrants with high visibility made nearly all the defects in the polytetrafluoroethylene/meta-aramid laminate visible in the form of luminous halos. The fatigued specimens were also tested for chemical permeation and viral penetration. In most cases, observation of halos was consistent with the failure of the fabrics in chemical permeation and viral penetration tests.

1.5.4. Active Thermography

Gralewicz and Wiecek [43] evaluated the use of active thermography as a non-destructive technique to detect defects in fire protective fabrics. They cut out circles from the five layers between the second and the sixth out of 16 layers of para-aramid fabric. The diameter of the circles ranged from 2 to 22 mm and represented defects in successive layers of a specimen. The layers were bound together under high temperature and pressure and formed the specimen. The specimen was placed between a lamp as the source of excitation energy and an infrared camera was used to analyze the temperature distribution within the specimen. The results showed that defects of diameter smaller than 8 mm between the second and third layers and the third and fourth layers were not detected by the system. Also, the minimum diameter of detected defects between the fourth and fifth layers and the fifth and sixth layer increased to 11.1 and 19 mm, respectively. This technique works based on the difference in thermal properties between the defect and the base material. Therefore, it may not be helpful in detecting the defects in early stages of degradation since the defect size would be too small to be identified and the thermal properties may not have changed considerably.

1.5.5. Colour measurement

Thorpe [14] also studied the use of Digital Image Analysis (DIA) and colorimetry. Both tests were used to measure the discoloration of the fabric during the thermal exposure. Discoloration, or colour difference, in both methods was defined as the colour difference between a new and exposed specimen, measured using two distinct colour measurement systems, RGB and CIE L*a*b colour space. The results were used to correlate the colour fade and tensile strength of outer shell specimens made of 60% Kevlar®/40% Nomex® fabric which was brown in colour. As the fabric was exposed to a high heat flux using the RPP tester, the dye first came out of the fabric, which increased the colour difference (Figure 1.11). The colour difference then decreased

as thermal decomposition began and the colour of the exposed area started to turn dark brown. During latter parts of the exposure, the colour difference again increased as the exposed area changed to dark brown and then black. This type of figure may be helpful in prediction of tensile strength of in-use firefighters' protective clothing.

The scatter of the data and the schematic correlation of tensile strength with colour change are shown in Figure 1.12. One problem with using DIA for this specific fabric is the nature of the colour changes as the dye is removed and the fabric undergoes thermal degradation (Figure 1.11). For example, a specific value of colour difference corresponds with two or three values of tensile strength (Figure 1.12). Developing a collection of baseline figures for a variety of fabrics with different colours, considering the sensitivity of the results to deposition of contaminants in the fabric, and determining the required level of resolution of specimen image were identified by Thorpe as some of the issues which need to be investigated before making broad practical use of these methods.

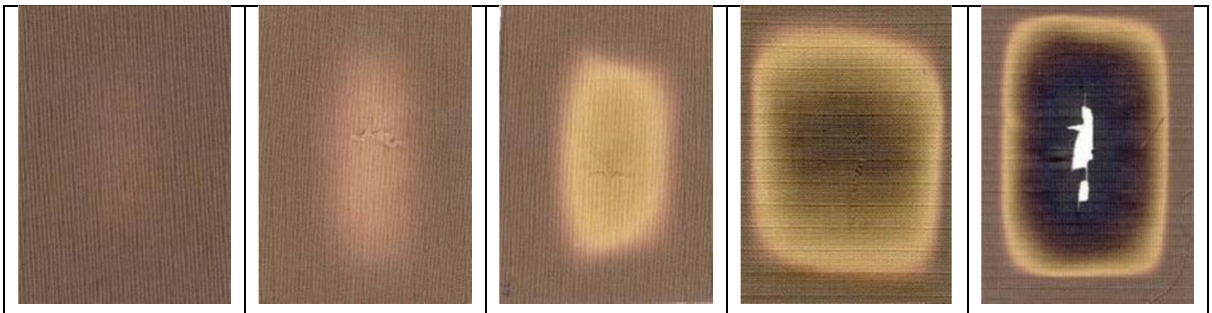

new	10 kW/m^2 for 240 s	10 kW/m^2 for 600 s	20 kW/m^2 for 75 s	30 kW/m^2 for 120 s

Figure 1.11: Examples of colour fade of 60% Kevlar®/40% Nomex® outer shell specimens after different levels of thermal exposure

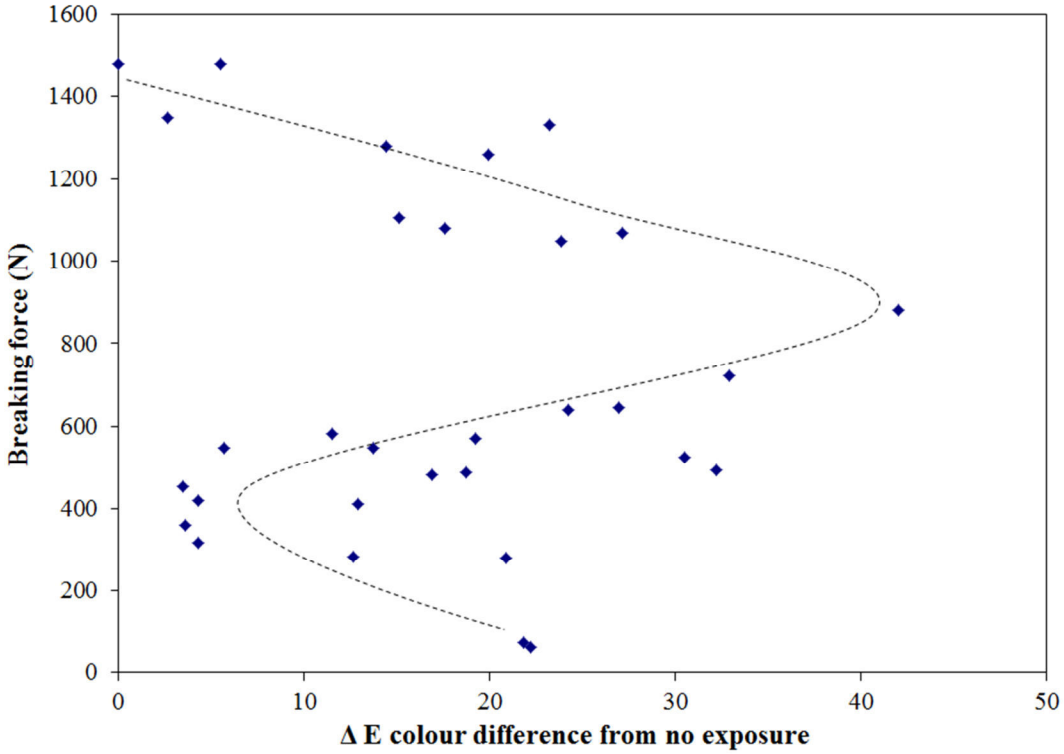

Figure 1.12: DIA results to correlate discoloration and tensile strength of 60% Kevlar®/40% Nomex® outer shell specimens [14]

1.5.6. Infrared spectroscopy

Infrared spectroscopy can be used for identification of compounds and investigation of material composition. Change in peak intensities in the transmission spectrum can also be used to study degradation in materials. In dispersive spectroscopy, a grating or prism separates the infrared light into individual frequencies and the amount of energy reflected/absorbed/transmitted through a specimen is measured. Then, the final result will be a spectrum which is a plot of reflectance/absorbance/transmittance versus frequency. In Fourier Transform Infrared (FTIR) spectroscopy, the desired parameter at all frequencies as a signal is measured simultaneously rather than individually. Therefore, the signal has information about all frequencies. It is decoded using a Fourier transformation, the well-known mathematical technique. Obviously, FTIR spectroscopy is much quicker than conventional IR spectroscopy to acquire a spectrum [44].

Davis et al. [13] found that after sufficient exposure of fabrics, containing PBI, Nomex®, and Kevlar®, to ultraviolet radiation the intensity of some peaks decreased and some new peaks emerged due to formation of new species. They used FTIR within the wavelength region of 5500-12500 nm to explain degradation of the specimen coating and relative resistance of different species to ultraviolet radiation. However, they reported that one source of uncertainty is overlapping of peaks of several species.

Similarly, FTIR spectroscopy within wavelength regions of 2800-3400 nm and 5500-6200 nm was implemented for interpretation of changes in mechanical properties of PBI, Nomex®, and Kevlar® by Nazare et al. [17]. Specimens were aged by means of exposure to ultraviolet radiation and hot and humid environment to simulate routine firefighting operations and storage rooms. Infrared spectra of aged specimens were analyzed and compared with the spectrum of unexposed specimens. It was shown that the change in the characteristic peaks' intensity and broadening indicates alteration in chemical composition of specimens, which was consistent with the deterioration in tear and tensile strength of aged specimens.

On the contrary, Arrieta et al. [45] revealed that thermal degradation of a blend of 60% Kevlar®/40% PBI could not be detected in absorption peaks of the infrared spectra within the wavelength region of 2500-20000 nm using FTIR. Specimens were thermally aged at a temperature range of 190 to 320°C inside an oven. Depending on the magnitude of ageing temperature, the ageing duration was selected from less than an hour at 320°C to 2 weeks at 190°C. Even though the tensile strength of specimens decreased noticeably after certain level of ageing, the variation of the absorption peaks was subtle. They concluded that formation of new chemical groups in this particular fabric after thermal aging could not be distinguished by infrared spectroscopy.

Dispersive infrared spectroscopy was also employed by Gu et al. [46] in a research study on degradation of an epoxy coating system due to ultraviolet radiation exposure. Two groups of epoxy specimens were aged in the laboratory and field separately. Quantification of chemical degradation of the epoxy specimens using absorbance ratio in the infrared spectrum (within a wavelength region of 190-820 nm) showed that mechanisms of degradation were similar in both groups of specimens. Peaks at different wavelengths in the infrared spectrum were used to indicate different molecular bonds in the molecular structure. Decreases in peak intensities

signified chain scission and mass loss. New bands in the spectrum were used to indicate formation of new products.

Cai and Yu [47] analyzed the volatiles produced during thermal degradation of Kevlar® and Nomex® specimens using FTIR spectroscopy in the wavelength region of 2500-25000 nm. The absorbance spectra of volatiles were recorded at different temperatures. Absorption peaks were assigned to different compounds. At different temperatures, peaks began to appear or disappear, which was attributed to identification of new groups or decomposition of compounds.

Infrared spectroscopy has also been used in various other areas of science. Researchers in the field of heritage conservation [48,49] worked on new and aged silks to monitor the condition of organic artefacts. They aged silk specimens under heat, light, and humidity and compared the absorption spectra of specimens. Since there was a slight difference among the spectra of new and aged specimens except in the water absorption band, they correlated tensile strength of specimens to the change in the intensity of water absorption peak.

Resistance to wrinkle in cotton fabrics can be improved by the use of a resin in finishing. An optimal amount of resin is required to be chemically bonded to the fabric. This amount is important in gaining the appropriate level of durable press. Ghosh et al. [50] implemented dispersive IR spectroscopy within the wavelength region of 1100-2500 nm to determine the amount of durable press resin in cotton fabrics. Based on the change in absorbance spectra, they picked three wavelengths and developed a model to predict the amount of fixed resin on cotton fabrics. The results of this model were in good agreement with conventional techniques.

Evaluation of wood properties using infrared spectroscopy has been of interest among many researchers. Mora [51] implemented infrared spectroscopy to assess wood properties in forest trees. Wood disks from 20 forest trees were selected as specimens and infrared spectra of specimens in the range of 1100-2500 nm were recorded. Statistical models based on regression methods were developed to predict density of wood specimens. Similarly, Kludt [52] gathered infrared spectra of three specific wood specimens in the wavelength region of 1000-2500 nm using an FTIR spectrometer. He correlated moduli of rupture and elasticity to absorbance spectra of specimens using statistical regression techniques. Kelley [53] filed a patent describing a method of predicting compression strength of decayed wood. He correlated mechanical strength of wood with the change in infrared spectra of specimens within the region of 400-1150 nm using multivariate statistical techniques. This correlation was found useful in prediction of

reliability of wood structures exposed to decaying microorganisms. Hendrick et al. [54] worked on prediction of stiffness and tensile strength of woods using dispersive IR spectroscopy over the wavelength range 350-2500 nm. They found that prediction of desired parameters using a shorter spectra range of 950-1850 nm was almost as accurate as the prediction over the full range of 350-2500 nm, which can be used in developing small and inexpensive instruments.

1.6.Scope and objectives of research

This research focuses on degradation due to thermal exposures since thermal exposure is considered as a routine and important ageing factor in fire services. As will be discussed in section 2.1.1, the range of thermal exposure selected for this study represents ordinary firefighting operations. There are two reasons for selecting this intensity of thermal exposure. First, the damage to the garment under what will be described as routine conditions is difficult to be assessed critically and accurately by the naked eye. Second, the damage to the garment under what will be described as emergency conditions could be high enough to be observed by the naked eye without the need to use non-destructive test methods. Specimens for this research are selected from common fabrics used in construction of firefighters' protective clothing. Then, the performance of thermally aged specimens made of firefighters' protective fabrics is evaluated by destructive and non-destructive test methods. Finally, statistical models are used to correlate the results of the two groups of tests.

In summary, the main objectives of this research are outlined as follows:

- To evaluate the effect of thermal exposure on critical aspects of performance of firefighters' protective clothing;
- to evaluate the effect of multi-stage thermal exposures on critical aspects of performance as compared to single stage thermal exposures of the same total duration;
- to develop non-destructive techniques in order to predict aspects of performance of firefighters' protective clothing after thermal exposure.

In order to develop methods to estimate the useful life of firefighters' protective clothing, the main factors that affect ageing and degradation of these clothing were identified, along with vulnerable aspects of performance to severe and fast deterioration. Based on previous research summarized in Table 1.3, it was determined that flame resistance (such as afterflame time) and

thermal protection (such as TPP values) properties of outer shell layer of firefighters' protective clothing did not deteriorate as severely and sharply as mechanical strength. For outer shell specimens, mechanical strength is a major aspect of performance since this layer acts as the first line of defence and should protect the inner layers. Breaking (tensile) strength is measured as an indicator of this aspect of performance in this research. In addition, the literature review indicated that there have not been many previous studies on the performance of the moisture barrier layer of firefighters' protective clothing after thermal exposure. The performance of the moisture barrier is evaluated by resistance to water penetration and water vapour permeability owing to the fact that the main duties of the moisture barrier are keeping the firefighter dry and reducing heat stress.

The focus of this research is the outer shell and moisture barrier layers of firefighters' protective clothing. The thermal liner is the innermost layer of firefighters' protective clothing and is protected by other two layers, the outer shell and moisture barrier. It sustains the least level of thermal energy and reaches the lowest temperature among the layers of the garment during thermal exposure. Hence, it is expected that the thermal liner receives less severe damage than the two outer layers. In fact, it is expected that the thermal liner would only receive severe damage if the two outer layers were already damaged. So, no tests of thermal liner by itself were included in this research. Therefore, the first objective of this research is the assessment of the effect of thermal exposure on the tensile strength of outer shell and resistance to water vapour permeability and water penetration of moisture barrier layers of firefighters' protective clothing.

In most studies reported in the literature, the level of damage to firefighters' protective fabrics is estimated by using simulated long-term exposures to harmful conditions. These simulations may not completely determine the level of damage to firefighters' protective clothing in real applications in fire departments, because firefighters wear their protective clothing repeatedly over its service life. Hence, the second objective of this research is to evaluate the effect of multi-stage thermal exposures on critical aspects of performance as compared to single stage thermal exposures of the same total duration.

In order to choose an appropriate non-destructive technique for evaluation of in-use firefighters' protective clothing, several factors were considered. These factors were cost and time effectiveness, simplicity, ability to do in situ measurement, and potential for future commercialization. After preliminary tests, colour measurement and infrared spectroscopy were

selected. The outer shell is the outermost layer of firefighters' protective clothing and is the first line of protection against thermal and other exposures. The outer shell can be separated from the inner layers, but the two inner layers are sewn together. Therefore, it is easier to separate and inspect the outer shell than the other two layers of firefighters' protective clothing in practice. As the third objective of this research, non-destructive techniques are used to predict tensile strength of outer shell test specimens after thermal exposure.

1.7. Contributions of this research to the literature

The contributions of this research are outlined as follow:

- Determining the effects of single-stage thermal ageing on the resistance to water penetration and water vapour permeability of moisture barrier specimens made of Nomex® for substrate and ePTFE for the membrane using constant heat flux thermal ageing;
- Evaluating the effect of single-stage thermal ageing on the tensile strength of outer shell specimens made of Nomex® and a blend of 60% Kevlar® /40% PBI;
- Comparing the effect of multi-stage and single-stage thermal exposures on the tensile strength of outer shell specimens and water vapour permeability and water penetration pressure of moisture barriers;
- Refining a non-destructive method to predict the tensile strength of outer shell fabrics using colour measurement; and
- Demonstrating that NIR spectroscopy is a potential non-destructive technique to predict tensile strength of outer shell specimens and how a device that utilizes only a few wavelengths may be used to do this.

1.8. Outline of the dissertation

Chapter one is an introduction to this research and contains a review of studies in different fields available in the literature. Objectives and contributions of this research to the literature are also specified. The experimental procedure and apparatus used in this research are explained in chapter two. Results of experiments on outer shell and moisture barrier layers are discussed in chapters three and four. The effects of single-stage and multi-stage thermal exposures on

performance of firefighters' protective clothing are examined in chapter five. Evaluation of firefighters' protective clothing using non-destructive techniques is described in chapter six. Predictions of tensile strength of outer shell layers using non-destructive techniques are explained in chapter seven. Conclusions and future work are discussed in chapter eight.

2. EXPERIMENTAL APPARATUS AND PROCEDURE

2.1. Thermal ageing

Simulation has been applied in a variety of fields such as industry, business, economy, and social sciences. Simulation is a technique to create a model representing a real or imaginary system as practically as possible. In simulation, some details of the systems and consequently, their effects are neglected to simplify the model. The behaviour of the system can be understood and analysed by running experiments using the designed model since implementing the system in order to carry out the experiments can be very costly, time consuming or even impossible. The quality of the analysis depends on how closely different facets of the system are reflected in the model [55].

As was discussed in the first chapter, ageing of firefighters' protective clothing is caused by a number of factors. Exposure to high temperature and intense heat flux are critical factors since they are often present in firefighting operations. To assess the effect of thermal ageing on firefighters' protective clothing during its service life, specimens of firefighters' protective clothing should be exposed to conditions which simulate those on the fire ground. Conditions on the fire ground depend on various factors such as surroundings, origin of ignition, type and layout of combustible materials on the fire scene, and ventilation. Intensity, exposure duration, and frequency of exposure are considered the main parameters in simulation of thermal ageing. This chapter discusses how these parameters were selected to simulate thermal ageing in this research.

2.1.1. Intensity of thermal ageing

Structural firefighting protective clothing provides a high level of protection for firefighters. Many researchers have applied a practical and simple method to quantify the thermal environment based on the temperature and heat flux. The National Institute of Standards and Technology (NIST) summed up researchers' work on thermal environments for firefighting, which are categorized into either three or four thermal classes [56]. Each thermal class is described by a range of surrounding air temperature, heat flux, and duration which firefighters are expected to be able to work safely within that class (Tables 2.1-2.4).

Table 2.1: Thermal environment 1 [56]

Research group (Year)	Thermal environment title	Temperature range	Heat flux range (kW/m^2)	Duration of safe work
USFA FEMA (1992) [57]	-	-	-	-
IAFF (Based on Abeles, 1985) [58]	Class 1	< 40 °C	< 0.5	< 30 min
Foster & Roberts (1995) [59]	Routine	< 100 °C	< 1.0	25 min
Coletta (1976) [60]	-	-	-	-
Abbott (1976) [61]	-	-	-	-

Table 2.2: Thermal environment 2 [56]

Research group (Year)	Thermal environment title	Temperature Range (°C)	Heat flux range (kW/m^2)	Duration of safe work
USFA FEMA (1992) [57]	Routine	20 - 60	1.0 to 2.1	-
IAFF (Based on Abeles, 1985) [58]	Class 2	40 - 95	0.5 to 1.0	15 min
Foster & Roberts (1995) [59]	Hazardous	100 - 160	1.0 to 4.0	10 min
Coletta (1976) [60]	Routine	< 60	0.4 to 1.25	-
Abbott (1976) [61]	Routine	< 70	0.5 to 1.7	-

Table 2.3: Thermal environment 3 [56]

Research group (Year)	Thermal environment title	Temperature range	Heat flux range (kW/m^2)	Duration of safe work
USFA FEMA (1992) [57]	Ordinary	60 - 300	2.1 to 25	10 to 20 min
IAFF (Based on Abeles, 1985) [58]	Class 3	95 - 250	1.0 to 1.75	5 min
Foster & Roberts (1995) [59]	Extreme	160 - 235	4.0 to 10.0	-
Coletta (1976) [60]	Hazardous	60 - 300	1.25 to 8.3	-
Abbott (1976) [61]	Ordinary	70 - 300	1.7 to 12.5	-

Table 2.4: Thermal environment 4 [56]

Research group (Year)	Thermal environment title	Temperature range (°C)	Heat flux range (kW/m^2)	Duration of safe work
USFA FEMA (1992) [57]	Emergency	300 - 1000	25 to 125	15 to 30 s
IAFF (Based on Abeles, 1985) [58]	Class 4	260 - 815	1.75 to 42	< 10 s
Foster & Roberts (1995) [59]	Critical	235 - 1000	10 to 100	briefly
Coletta (1976) [60]	Emergency	300 - 1000	8.3 to 105	briefly
Abbott (1976) [61]	Emergency	300 - 1100	12.5 to 208	briefly

Based on the set of thermal environment titles given in Tables 2.1-2.4, which was first suggested by Simms and Hinckley [62] and has been used in many scientific papers [57, 63, 64, 65, 66], firefighting environments are categorized into three regions: routine, ordinary, and emergency. Figures 2.1-2.4 illustrate these regions. It should be noted that depending on the heat flux and temperature at the location where firefighters are working, a particular fire may be classified in any of these groups. In Figures 2.2-2.4, heat flux was measured using sensors located 4 m from the wall and 1.75 m above the ground in front of the window.

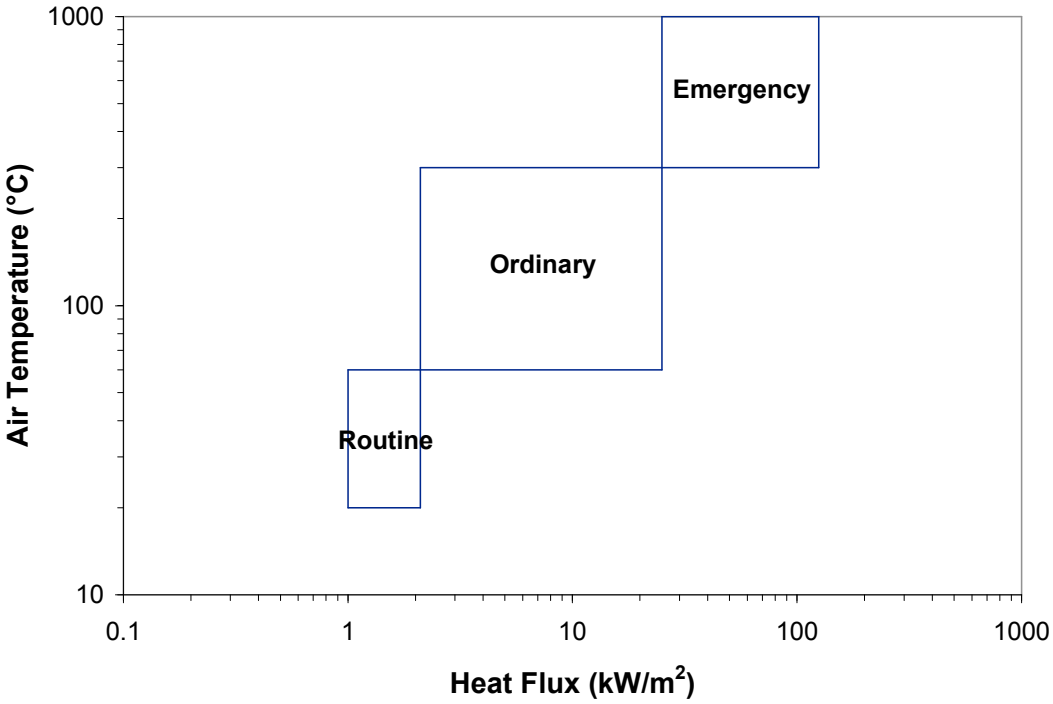

Figure 2.1: The range of thermal conditions faced by firefighters [65]

Figure 2.2: A view of thermal condition classified as “Routine” [14]

Figure 2.3: A view of thermal condition classified as “Ordinary” [14]

Figure 2.4: A view of thermal condition classified as “Emergency” [14]

In Figure 2.1, the routine condition describes a level of thermal exposure which could be received in front of a fireplace or experienced by firefighters at the very early stages of fire growth or in arrival at the fire scene. Figure 2.2 could be an example of this condition. The heat flux in the field fire test shown in Figures 2.2 to 2.4 escalated as the burning area of the exterior face of the house increased [14]. This increased the area of the flames and hence the area that emitted thermal radiation to the heat flux gauges on the tripod. The escalation of a fire depends on the fire spread within the house. As a result of increase in the burn area and perhaps flame area, the emitted thermal energy increased. A more serious fire falls into ordinary condition

(Figure 2.3). The ordinary condition may be experienced by firefighters in this later stage of fire growth, and or when the firefighter is at a short distance from a more severe fire. The fire in the emergency group is fierce and occurs when a firefighter is in a room near flashover conditions (Figure 2.4). The level of damage to the garment in this condition is often to such an extent that major repairs are required or even the garment must be retired. Hence, the damage to the garment under emergency condition could be high enough to be observed by the naked eye without the need to use non-destructive test methods. In brief, intensity of thermal exposure in these experiments is set to represent ordinary and early stage of emergency conditions, which could cause various levels of damage over a reasonable duration of exposure.

2.1.2. Frequency and duration of thermal ageing

Firefighters respond to a variety of emergencies. As reflected in the National Fire Incident Reporting System (NFIRS) 2004 data [67], only 8.2% of runs by firefighters in U.S.A. involved fire suppression. On the other hand, firefighters are supposed to wear their Self Contained Breathing Apparatus (SCBAs) during the entire firefighting operation, from arrival until departure of the fire scene. A working firefighter deploys the air inside the SCBA tank in approximately 15 min. [68]. This indicates that first-line firefighters should back off during firefighting operation to refill their SCBA tank. Tables 2.1-2.4 indicate safe work time for firefighters. Safe work time even under exposure to low heat fluxes is not suggested longer than 30 min. In summary, low frequency of thermal exposure, the need to refill SCBA tanks on the fire scene, and safety of firefighters emphasize the necessity for simulation of thermal ageing by multi-stage exposures. Depending on the intensity of the thermal environment, the exposure duration in each stage can be selected appropriately based on information in Tables 2.1-2.4.

Firefighters may try aggressive tactics in extinguishing fires and therefore, they are sometimes exposed to more intense thermal environment. However, in general, firefighters spend most of their time in working under relatively low temperatures and heat fluxes. In a study of City of Montreal Fire Departments in 1993-1994 [68], it was found that only 66% of the personnel acted as a first-line combat firefighter. 10% of personnel who were officially called firefighters were not exposed to fire at all. First-line and second-line combat firefighters spent 1924 min./year on fire scenes on average. However, the study showed a broad exposure time to fire among them in different fire departments. Firefighters in the 10 busiest departments were

exposed to fire for 3244 min./year on average in 62 fire incidents, while firefighters in the 10 quietest departments worked under fire exposure for 906 min./year on average in 19 fire incidents. In brief, total fire exposure time depends strongly on the location of fire departments even in one specific city and role of the particular role of individual firefighters.

2.2. Cone Calorimeter

The cone calorimeter is a very useful apparatus in small-scale fire testing (Figure 2.5). It can record information such as ignition time, mass loss, combustion products, and heat release rate when specimens are exposed to different heat fluxes. These parameters are important in understanding the burning behaviour of many materials and increasing fire safety in different environments.

Figure 2.5: Cone calorimeter

A small but very important part of this apparatus is a coil wound in the form of a truncated cone, which is called a conical heater (Figure 2.6). It is such an essential part that the name of the entire apparatus originated from its shape. The conical heater generates radiative heat fluxes to ignite specimens. Fumes coming off the specimen are collected using an exhaust hood and ventilation system above the conical heater.

The maximum heat flux that can be generated in the cone calorimeter is 100 kW/m^2. The diameter of the conical heater is 16 mm. The conical heater can be positioned horizontally or vertically to be suitable for two testing layouts. The conical heater temperature can be set to provide a given incident heat flux. An air-cooled shutter under the conical heater protects specimens from heating before starting the test and gives an operator additional time to check measurement devices. This is especially important for materials which have a very small mass such as fabrics or ignite easily.

Figure 2.6: Conical heater of a cone calorimeter

The cone colorimeter can generate a relatively uniform heat flux over the surface of specimens. Thomas Ingold[3] marked the area under the conical heater using a 2.5 cm by 2.5 cm grid and placed a Schmidt-Boelter heatflux gauge (GTW-10-32-485A, Medtherm, Huntsville, AL) at the corner of each square in the grid at a distance of 25 mm below the conical heater to measure the heat flux distribution. The heat flux was measured to be 35 kW/m^2 at the central point (0,0). Figure 2.8 shows the variation of heat flux over the grid. Point (0,0) specifies the center of the conical heater. A central and elliptical part of the specimen surface, the diameters of which are 10 cm by 9 cm, receives a heat flux which is approximately 90% of the value of the nominal heat flux by the conical heater. This elliptical part is big enough to surround specimens for different tests (8.5 cm by 5.8 cm for exposed part of specimens for tensile testing) in this research when they were exposed to the conical heater for thermal ageing.

[3] Undergraduate research assistant at the University of Saskatchewan

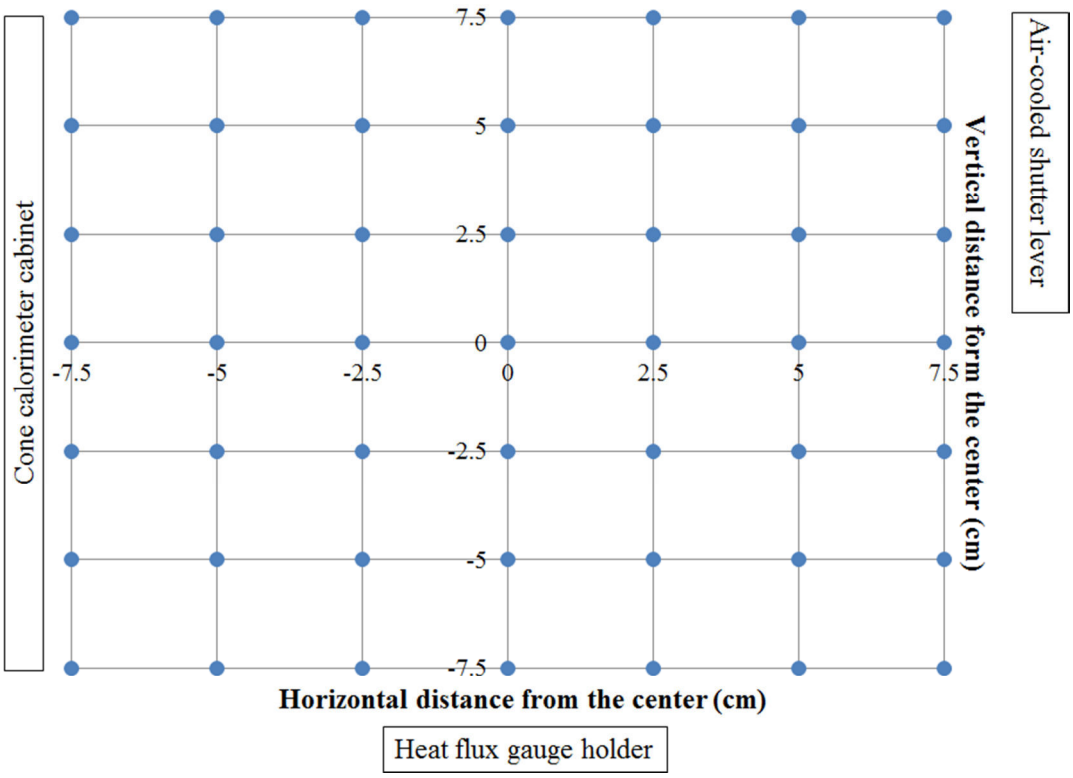

Figure 2.7: Locations of heat flux measurement carried out 25 mm under the conical heater

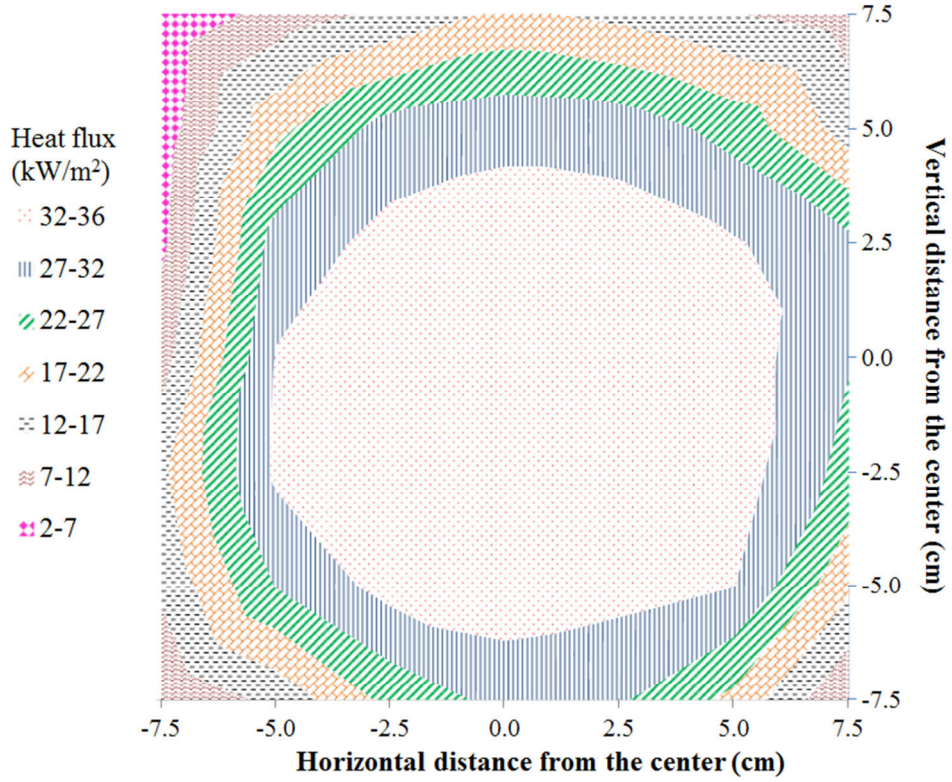

Figure 2.8: Distribution of generated heat flux (35 kW/m^2) 25 mm under the conical heater

When protective clothing is worn by a firefighter, the outer shell layer is directly exposed to fire and the thermal liner layer is in contact with the firefighter's body. Each surface of these cone test specimens has a different boundary condition, while in an isothermal ageing inside an oven, both sides of an individual specimen will experience similar boundary conditions. So, thermal ageing of multi-layer specimens using a constant heat flux might better represent the exposure of a piece of firefighters' protective clothing during firefighting services. In isothermal ageing, specimens are hung in an oven, the temperature of which is set at a specific value. Oven recovery time after placing specimens inside and closing the door could be a concern especially for a short period of exposure. That is why the conical heater is used for thermal ageing of specimens to generate a certain heat flux in this thesis research.

Thermal ageing of all specimens in this research was done in a similar manner. Specimens were cut to specific sizes from fabrics depending on the testing requirement and were conditioned for 24 hr at 22±2°C and 65±2% relative humidity in a chamber based on NFPA 1971standard [2]. This condition can be easily created by placing a beaker which contains 39.5 g of table salt dissolved in 100 mL of tap water after 24 hr. The procedure to provide this specific condition is similar to the procedure in ASTM E 104 standard [69]. A peripheral margin of the specimen was covered with metal bars to constrain the exposed area to the central part of the specimen. Specimens were thermally exposed within 5 min. after removal from the conditioning chamber [2]. The exposed area of the specimen was used as the interrogation area for non-destructive techniques described in chapter 6.

For calibration, the heat flux was measured 25 mm below the center of the heater by a Schmidt-Boelter heat flux gauge (GTW-10-32-485A, Medtherm, Huntsville, AL) cooled by a water flow. After removing the heat flux gauge, the specimen was placed on a stand 25 mm below the conical heater of the cone calorimeter for various exposure durations.

2.3. Thermogravimetric analysis (TGA)

Thermogravimetric Analysis (TGA) is a test method which exposes the specimen to a controlled temperature program in a controlled environment. The different parts of TGA equipment are a sensitive balance, a specimen holder, and a furnace, inside of which a purge gas flows. The purge gas can provide an inert or reactive atmosphere for tested specimens. The purge gas flow can be selected based on the application of the material in the real world. It also

removes decomposition products from the specimen compartment. To create an inert atmosphere, nitrogen or argon is usually used, while air is often used for combustion and oxidation studies.

During the test, the mass of the specimen is recorded as a function of temperature or time and is plotted at the end of the experiment as output. The mass loss curve is usually accompanied by a derivative mass loss curve which simplifies interpretation of results. The derivative mass loss curve highlights the points where mass loss rate is noticeable. TGA can characterize materials in order to determine degradation temperature, moisture and volatile composition, lifetime, and decomposition kinetics.

From the TGA curves, several points can be understood [70]. Any decrease in the weight indicates evaporation or release of volatiles from specimens. This may imply decomposition of specimen material. An increase in the weight may indicate formation of new species as a result of a chemical reaction with the purging gas in the atmosphere. In addition, the thermal stability of specimens is pinpointed by the temperature at which weight change begins due to decomposition and chemical change. However, TGA cannot determine which components were lost at a specific temperature.

In this research, the temperature history of different layers of firefighters' protective clothing during thermal exposure was measured. TGA helped to explain the changes in the properties of the fabrics after thermal exposure. TGA experiments in this research were conducted using a TA Instruments Q500 (New Castle, DE) in air and nitrogen atmospheres. The heating rate and final temperature were set at 20°C/min. and 800°C in all experiments. The mass of individual specimens was in the range of 8-12 mg and the specimens were placed in high temperature 100 μL platinum crucibles.

2.4. Temperature measurement

Type K thermocouples (Omega, Laval, QC) were used for temperature measurements in chapters 4 and 5. Thermocouple wires with diameter of 0.25 mm (36 AWG-GG-K-36-SLE) were spot welded to each other to form a bead. The beads were sewn to the centre point of the front and back sides of each layer of a specimen to measure the temperature. An infrared thermometer (Cyclops 300AF, Minolta/Land, Dronfield, UK) was also employed to measure the temperature of the centre point of the back side of specimens in chapter 3 and was mounted on a tripod. The

thermocouples and infrared thermometer were connected to a data acquisition system (HP Agilent 34970A, Santa Clara, CA) which can record the temperature approximately every 0.2 s.

Specimens were cut to 10 cm by 10 cm (4 in. by 4 in.) from the individual fabrics and were conditioned in a chamber at 22±2°C and 65±2% relative humidity for 24 hours. The specimens were mounted on a specimen holder. The specimen holder is the same as in ASTM F 2700 [71]. This specimen holder is 152.4 mm by 152.4 mm (6 in. by 6 in.), with a 50.8 mm by 50.8 mm (2 in. by 2 in.) hole in the centre through which the specimen is exposed to the conical heater. The specimen holder was placed on a stand, the height of which was adjustable. The height of the stand was set such that the distance between the bottom of the conical heater and the surface of the specimen was 25 mm. Figure 2.9 shows the test set-up for temperature measurement.

The heat flux value was measured 25 mm below the centre of the conical heater by a Schmidt-Boelter heat flux gauge (GTW-10-32-485A, Medtherm, Huntsville, AL) cooled by a water flow. The conical heater temperature was set to provide a desired incident heat flux. When the conical heater reached the steady-state condition and generated this incident heat flux, the heat flux sensor was removed from its place. Then, the air-cooled shutter was closed to obstruct the conical heater. The stand and the specimen holder were placed under the conical heater for thermal ageing. The specific heat flux and duration of thermal ageing for each set of experiments will be discussed in the next chapters. After the opening the shutter, the specimen was exposed to the incident heat flux. In the multi-stage exposures (chapter 5), the shutter was closed at the end of each stage. After the specimen cooled down, the shutter was reopened for the next stage of exposure.

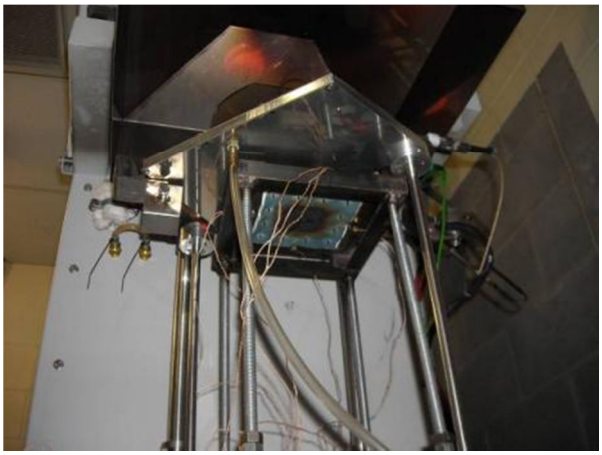

Figure 2.9: Temperature measurement in the cone calorimeter using thermocouples

2.5. Tensile strength tests

Tensile strength of the outer shell specimens was measured according to NFPA 1971 [2]. Based on the NFPA standard, the tensile test should be conducted according to the test procedure in ASTM D 5034 [72]. The tensile testing machine was an Instron 1122 with load capacity of 5 kN (Figure 2.10). The machine was a Constant-Rate-of-Extension (CRE) type, which operated at 200 mm/min rather than 300 mm/min as specified in ASTM D 5034 [72] because of a limitation in the choice of speed on the tensile testing machine. The face of the jaws was coated with an anti-slip coating. The jaw dimension was 25 mm (1 in.) perpendicular to the direction of the application of the force by 37.5 mm (1.5 in.) parallel to the direction of the application of the force. The clamping system was pneumatic and air pressure was set at 75 psi (517 kPa).

It is worth mentioning that the dimension of the testing machine's jaws influences the measured values. Slippage of the specimen in the jaws is a common problem in this test method. In addition, damage to the specimens by the jaws and stress concentration near the jaws can cause the breakage of the specimen to occur near the jaws. These issues are characteristics of this type of test method, which increases the uncertainty of test results [72]. This could be a reason why relatively high variation is observed in the test results, as will be discussed in later chapters.

Figure 2.10: Tensile testing machine

2.6. Tear strength tests

Tear strength tests were performed according to NFPA 1971 in the fill direction of moisture barrier specimens. As the standard states, the tear test should be conducted according to the ASTM D5587 [73] test procedure. Specimens were cut to 15 cm by 10 cm (6 in. by 4 in.). A peripheral margin of the specimen was covered with metal bars to constrain the exposed area to the central part of the specimen. In the test method, a pre-test cut is created at the smallest base of the marked trapezoid in the form of a slot with the width of 1.5 mm and length of 15 mm (Figure 2.11). The oblique sides of the marked trapezoid are edged with testing machine clamps jaw and the specimen area inside the marked trapezoid is left folded and loose (Figure 2.12).

The jaw face was 50 mm by 75 mm. The shorter side was parallel with the direction of force application (clamp movement). In order to prevent or reduce slippage of the specimen, a piece of sand paper was glued to each of the jaw faces. The same equipment used for tensile tests of outer shell specimens (section 2.4) was employed in performing tear tests. The clamping system was pneumatic and air pressure was set at 75 psi (517 kPa). The clamps speed was set at 300 mm/min. The highest peak point was recorded as tear strength of a specimen.

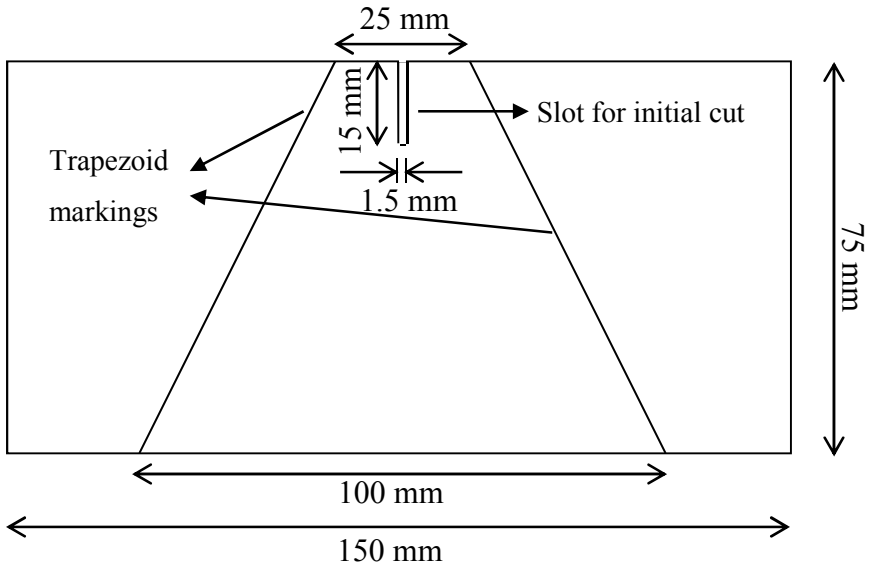

Figure 2.11: Specimen marking template

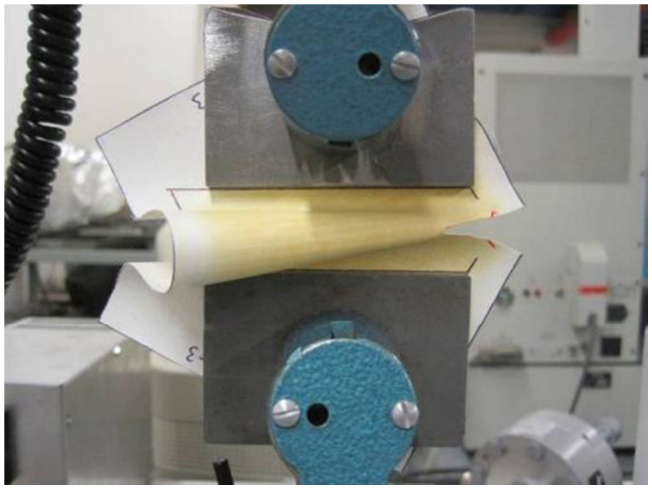

Figure 2.12: Position of a specimen in the clamping system in tear strength test

2.7. Water vapour permeability tests

The Total Heat Loss (THL) test is included in the NFPA 1971 standard to measure the loss of heat to outside the clothing by diffusion of water vapour and conduction of heat through the three layers of firefighters' protective clothing. The test set-up is relatively complicated and costly since the test is carried out in a controlled atmosphere chamber, and different sensors to monitor input power, temperature, relative humidity, and air velocity are required. Other test methods can also be used in measuring the water vapour transmission and are applicable to one layer of firefighters' protective clothing [74]. Owing to the fact that the moisture barrier has a greater impact than outer shell and thermal liner on the total heat loss through firefighters' protective clothing, only the moisture barrier was tested in this research project.

The apparatus used to determine water vapour permeability of the moisture barrier was a Permatran-W Model 101K (Figure 2.13). This apparatus complies with ASTM D 6701 [75]. It works based on water vapour absorption by a dry gas stream. In brief, the system has six cells and each cell consists of two chambers. The bottom of the upper chamber is covered with a guard film and the chamber is filled with distilled water. Dry nitrogen, which is used as a carrier gas, is delivered to the lower chamber. A specimen is located between the two chambers. Water vapour permeates through both the guard film and the specimen and is absorbed by the nitrogen. A sensor measures the relative humidity of nitrogen when it leaves the chamber. Then, the amount of moisture and consequently the transmission rate is calculated. Figure 2.14 illustrates a schematic view of one cell of the equipment.

Figure 2.13: Water vapour permeability test apparatus

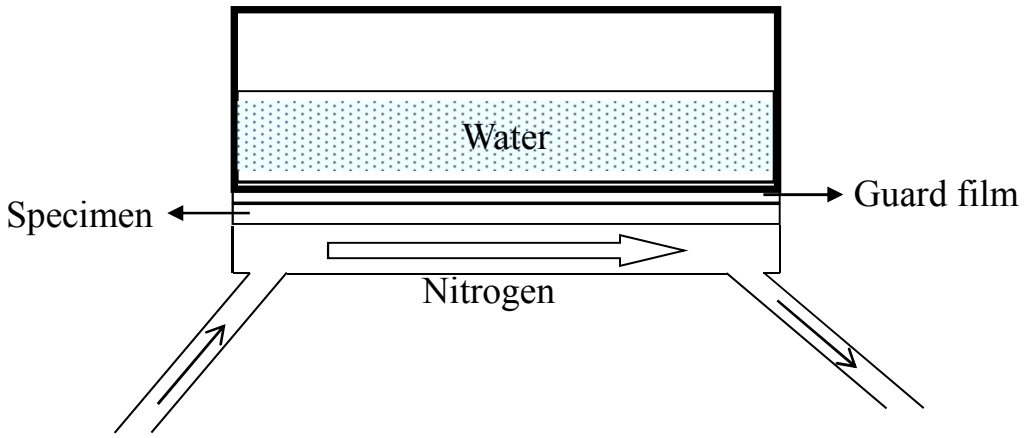

Figure 2.14: A schematic view of a test cell of the water vapour permeability test equipment

Specimens were cut to 17.8 cm by 17.8 cm (7 in. by 7 in.). After thermal exposures, which were conducted using the procedure described in section 2.2, specimens were glued and fit to a specimen carrier (Figure 2.15). The shape of the specimen carrier allows six tests to be run simultaneously. Each test was carried out in an individual cell. Therefore, the test was repeated six times independently and the presented results are the average values. Temperature and relative humidity in the cells were set to 23°C and 60%, respectively.

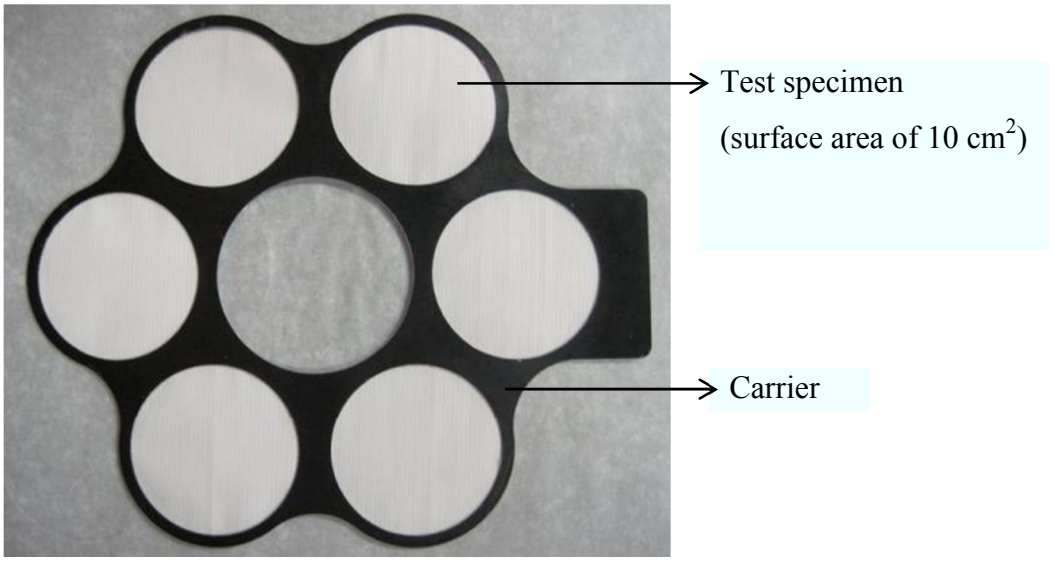

Figure 2.15: A view of a moisture barrier specimen glued to the carrier

In order to measure the water vapour permeability of the specimen only, this test was performed with no specimen between the two chambers first and the Water Vapour Transmission Rate (WVTR) through the guard film only was measured. In the following tests, a specimen was mounted between the two chambers (i.e., under the guard film) and vapour transmission rate was measured. The vapour transmission of the specimen was calculated by subtracting the two transmission rates.

2.8. Water penetration pressure tests

The NFPA 1971 standard requires that the resistance to water penetration of moisture barrier specimens be tested in accordance with the Federal Test Method Standard No. 191A [76]. The standard uses a motor-driven tester to apply hydraulic pressure. Specimens were cut to 8.9 cm by 8.9 cm (3.5 in. by 3.5 in.). A peripheral margin of the specimen was covered with metal bars to constrain the exposed area to the central part of the specimen. This exposed area, 7.6 cm by 7.6 cm (3 in. by 3 in.) underwent the water penetration pressure test. Each test was repeated three times independently and the presented results are the average values.

A test cell quite similar to the apparatus defined by the standard was used to measure the water penetration pressure of the specimens after thermal exposure. The apparatus consisted of two plexiglass cylindrical parts which hold the specimen firmly in between (Figure 2.16). Both

cylindrical parts have a concentric circular opening 3.15 cm in diameter. However, the opening diameter in the test cell used in this research was 5.7 cm. The lower cylinder was filled with water.

Water pressure was increased using a hand pump of a Druck DPI 605 (Burlington, VT) pressure calibrator at a rate of 10.8 kPa/min. (1.6 psi/min.). In a darkened room and using a lamp light, the upper (substrate) side of the specimen was observed carefully for appearance of water. This pressure increase and surface observation were repeated until water drops eventually appeared on the specimen. The corresponding hydrostatic pressure was recorded as the water penetration pressure in pounds per square inch.

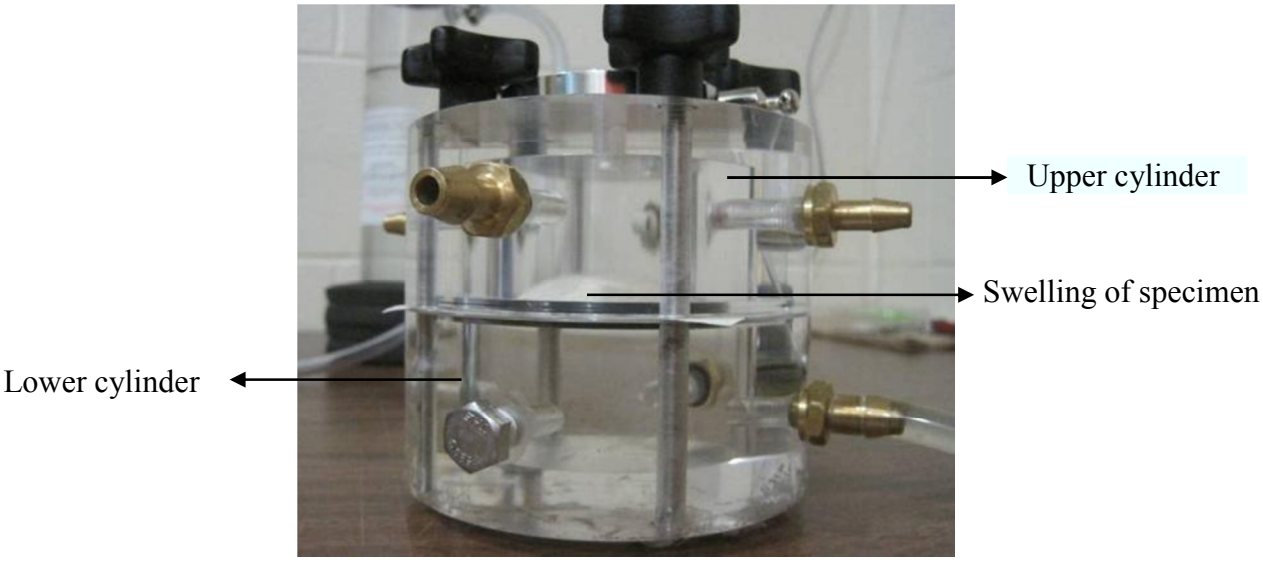

Figure 2.16: Water penetration pressure test apparatus

3. OUTER SHELL EXPERIMENTS

The outer shell may be considered the most important layer of firefighters' protective clothing, as it is the first line of defence against flame, heat, abrasion, tear, cut, and water absorption and protects the inner layers. Most outer shell fabrics are available in different colours. Dying enhances visibility and appearance of firefighters. There are a variety of outer shell fabrics in the market and they all must pass the minimum requirements in standards. However, various factors such as working weight (summation of dry weight and moisture regain), durability (to high temperature, flame, ultraviolet radiation, laundering), mechanical strength, water repellency, ease of movement, and price determine the selection of outer shell fabric [77]. Fire departments put different levels of emphasis on these factors based on the frequency and type (fire suppression, rescue, vehicle accidents, EMS) of operations, humidity and temperature of local climate, fire attack procedure, design, and budget to choose the most suitable outer shell fabric.

It was discussed in section 1.6 that tensile strength is the aspect of performance of the outer shell layer of firefighters' protective clothing, which is the emphasis of this research. This chapter focuses on the tensile testing of outer shell specimens. TGA curves, temperature profiles, and SEM images of specimens will be used to explain these test results. A brief conclusion and relation between this chapter and the next chapters will be presented.

3.1. Preparation of specimens

Nomex® and Kevlar® have been in the market for almost 40 years and are widely used in industry including protective clothing. They are used in construction of all layers of firefighters' protective clothing. There is often a trade-off among different physical properties of most materials. For example, Kevlar® is stronger but less flexible than Nomex®. So, outer shells are usually made of a blend of fabrics to enhance the general performance and improve the quality of the blended fabric.

The specimen used in this series of tests was a single layer of outer shell fabric, Nomex® IIIA made of Type 462 Nomex® fibres with a surface weight of 203 g/m^2 in plain weave. Type 462 Nomex® is a blend of approximately 93% Nomex®, 5% Kevlar®, and 2% static dissipative fibre and is used for different types of thermal protective apparel including wildland firefighting [78].

The fibre is dye mergeable and therefore, the manufactured fabric is available in different colours. Test specimens were selected from four colours: blue, red, dark blue, and yellow. Various colours of outer shell specimens were chosen in order to evaluate colour measurement technique described in more detail in section 7.1.

In section 2.1.1, it was discussed that the heat fluxes chosen in this research simulates the ordinary and early stage of emergency conditions. This range of condition can cause a level of damage which may be difficult to be detected by manual inspection and to make a decision on further usage of a piece of firefighters' protective clothing. In addition, heat fluxes in this range have been used as standard values to conduct performance tests in different codes [79]. Accordingly, heat fluxes of 10, 20, 30, and 40 kW/m^2 were selected. Specimens were exposed to each heat flux for specific durations (Table 3.1). The higher the heat flux was, the shorter the duration of exposure was selected.

Table 3.1: Test matrix for outer shell specimens

Incident heat flux (kW/m^2)	Exposure duration (s)
10	600, 1200, 2400
20	30, 150, 300
30	15, 30, 60
40	10, 20, 30

One specimen from each colour was cut to 15.1 cm by 10.2 cm (6 in. by 4 in.) from the fabrics and was aged according to the procedure described in section 2.2. Despite differences in their colours, the specimens were cut from fabrics with the same composition (section 3.2). Therefore, when discussing the effects of thermal exposure on the performance of this particular material, average values of test results of the four fabrics are provided. A peripheral margin of the specimen was covered with metal bars to constrain the exposed area (8.5 cm by 5.8 cm) to the central part of the specimen. The exposed area of the specimen, 8.5 cm by 5.8 cm, was used as the interrogation area for non-destructive techniques described in chapter 6.

3.2. Thermogravimetric analysis (TGA)

TGA was conducted for specimen materials of all colours used in the outer shell experiments. Figures 3.1-3.4 show TGA curves for Nomex® IIIA at a heating rate of 20°C/min in

air environment. The mass loss curves in Figures 3.1-3.4 are similar, which may indicate that dyes used in different colours of the studied fabrics have similar chemical composition. So the colour of fabrics does not affect degradation of the outer shell specimens made of the single fabrics used in this research. In the early stages of the test, mass loss is observed as a result of moisture release. At about 300°C, the dye began to come out, which was accompanied by a small weight loss (2-3%). At approximately 400°C, the weight loss rate increased sharply. Around 600°C, the mass loss rate changed considerably, which could indicate complete decomposition of the specimen. By reaching 600°C, the specimen lost almost 75% of its initial weight.

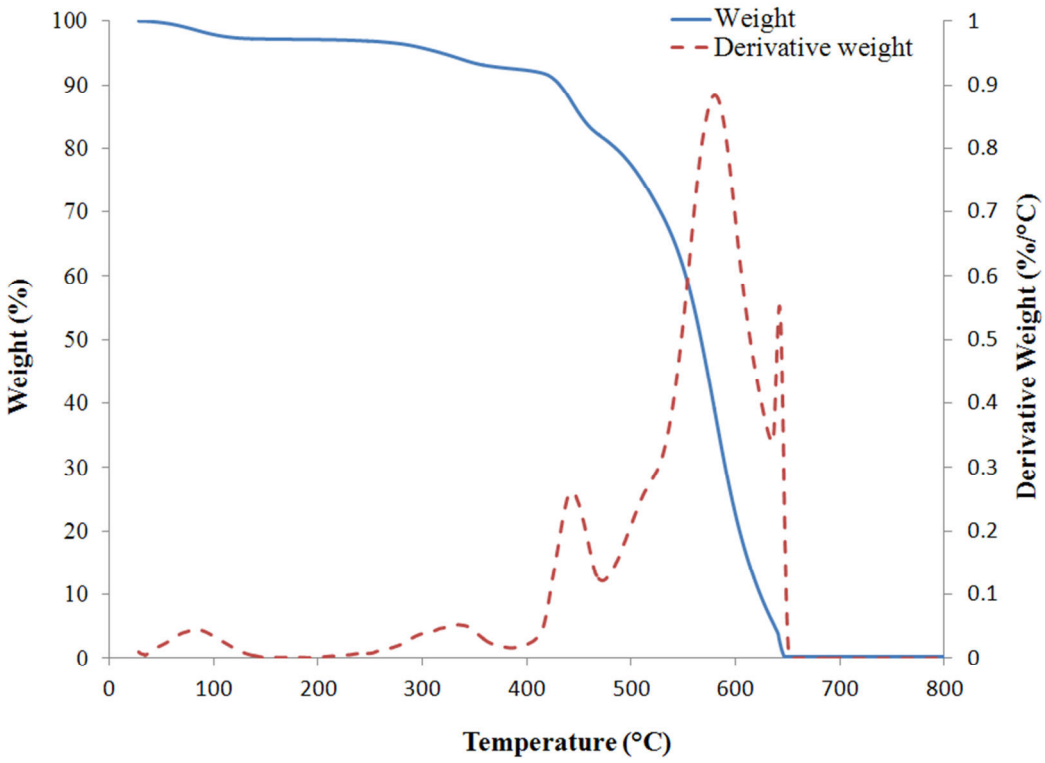

Figure 3.1: TGA curve for blue outer shell specimens made of Nomex® IIIA

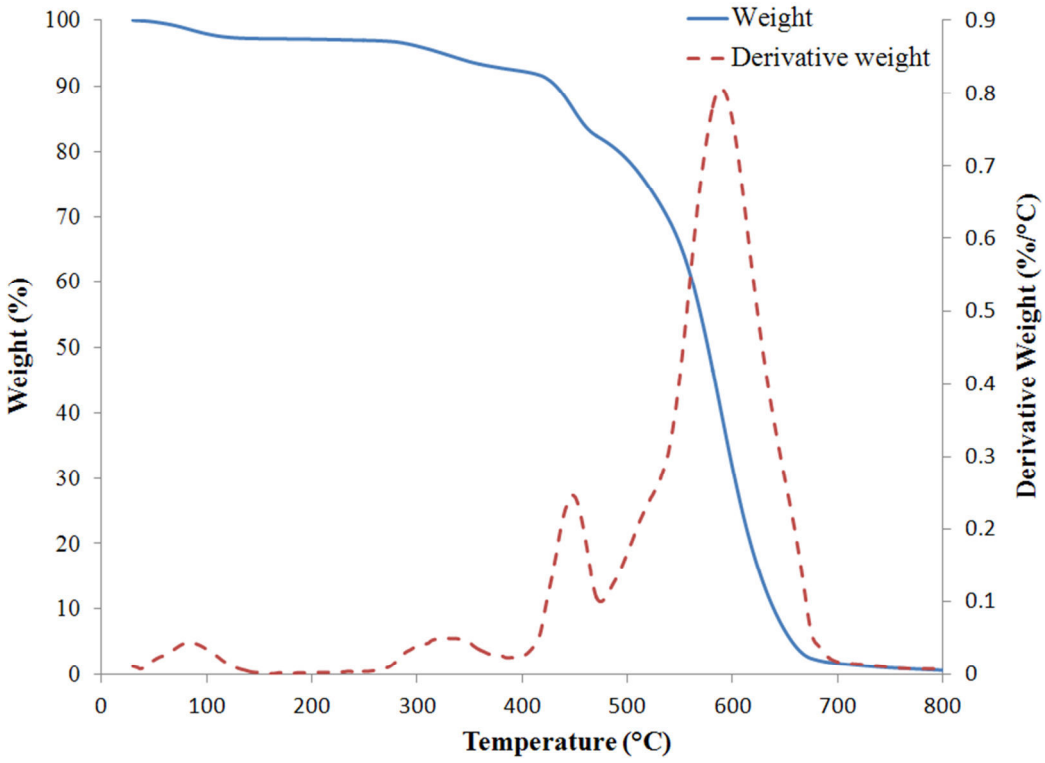

Figure 3.2: TGA curve for red outer shell specimens made of Nomex® IIIA

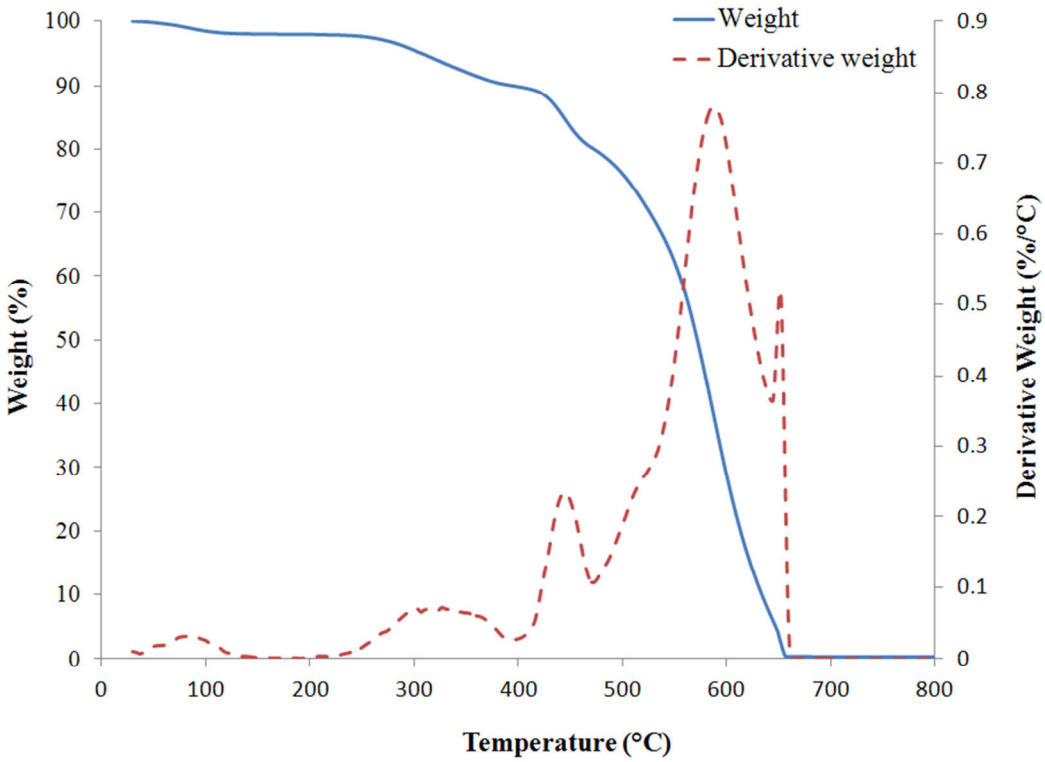

Figure 3.3: TGA curve for dark blue outer shell specimens made of Nomex® IIIA

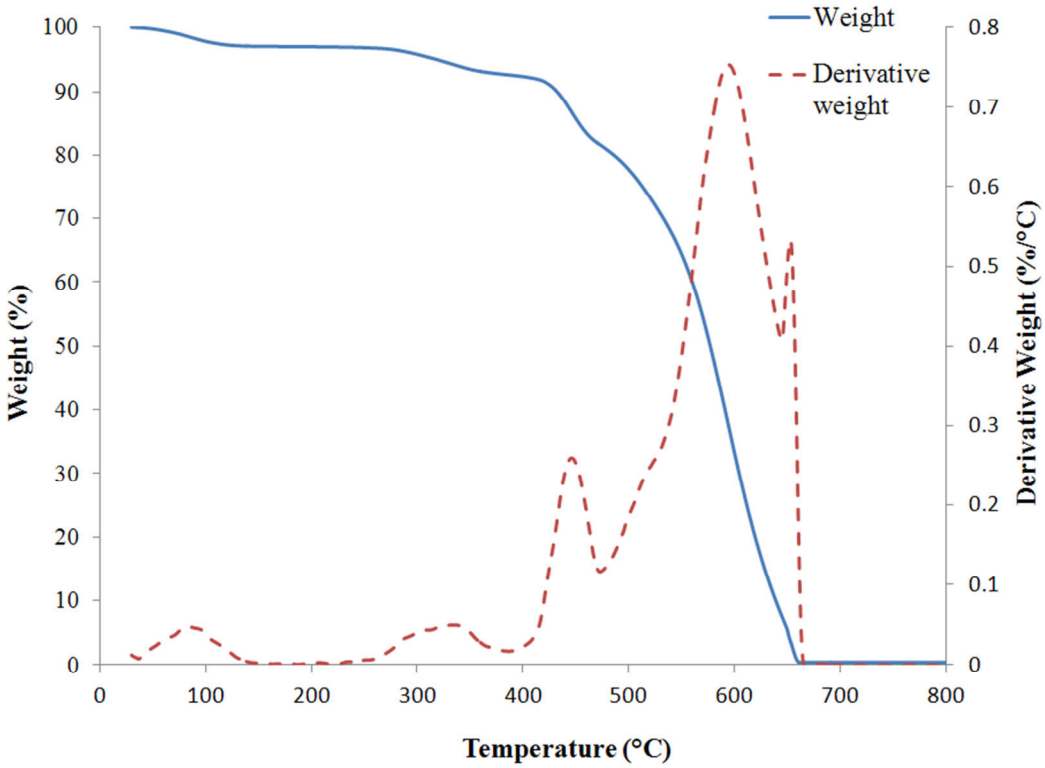

Figure 3.4: TGA curve for yellow outer shell specimens made of Nomex® IIIA

3.3. Temperature measurements

During thermal ageing of specimens, the temperature of the back side of specimens was measured using the infrared thermometer. Specimens were exposed to particular heat fluxes for three durations according to Table 3.1. The histories of average temperature of the specimens for the first 30 s of the thermal exposure to a particular heat flux are shown in Figures 3.5-3.8. Although the shutter was closed at the beginning of the experiment, limited heat transfer occurred to the specimen through the shutter. This is the reason why the specimen temperature might be up to 10°C higher than the lab temperature at the beginning of the experiment. The figures show that all specimens, regardless of their colour, reached almost the same temperature for a particular thermal exposure (Table 3.2). This is expected since specimens were made of fabrics of similar composition and comparable surface weight (section 3.1). The required time for all specimens to reach a steady-state temperature was found to be around 25 s. Therefore, for any exposure taken longer than 25 s, the specimen temperature remained quite constant.

Table 3.2: Temperature of Nomex® IIIA outer shell specimens in different colours after 30 s exposure to a particular heat flux

Thermal exposure		Temperature of specimens (°C)			
Heat flux (kW/m^2)	Duration (s)	Blue	Red	Dark blue	Yellow
10	600	213	223	224	221
	1200	214	221	224	219
	2400	222	225	223	224
20	30	315	311	313	315
	150	312	312	315	316
	300	317	314	316	316
30	30	382	379	386	381
	60	382	376	385	378
40	30	359	348	351	337

It was also observed that specimens reached higher temperature values in exposure to $30kW/m^2$ than exposure to $40kW/m^2$. Nomex® like other firefighters' protective fabrics does not burn with flame and only chars during thermal exposure. Formation of char on the front side of the specimen in exposure to $40kW/m^2$ was faster than for $30kW/m^2$, which can act as an insulating layer and protect the back side to some extent. Appendix A shows the pictures of outer shell specimens after the thermal exposures listed in Table 3.1. In addition, the carbonization process in Nomex® is endothermic and absorbs thermal energy [80]. Furthermore, volatiles are released in the form of smoke during charring of the specimen. The formation of smoke especially at the early stages of thermal exposure between the specimen surface and the conical heater can partly hinder the absorption of thermal radiation by the specimen material, which decreases temperature of the specimen.

Thermogravimetric experiments are conducted in a controlled environment and may not accurately simulate the real conditions in thermal ageing experiments. However, TGA results can indicate the range of temperatures over which changes occur. Based on TGA results, it is expected to observe considerable change in performance of outer shell specimens after reaching 300°C. This temperature was achieved after exposure to heat fluxes of 20 kW/m^2 and higher.

Therefore, it may be the reason why deterioration in tensile strength of outer shell specimens was observed after thermal exposure to heat fluxes of 20 kW/m^2 and higher (section 3.4).

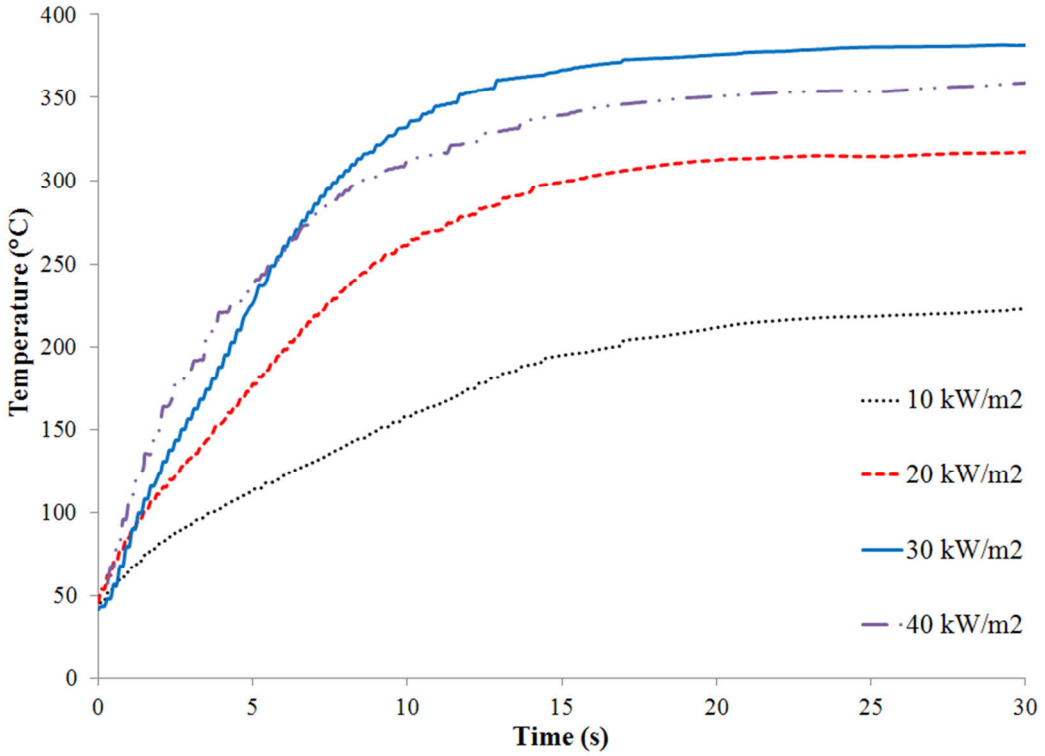

Figure 3.5: The first 30 s temperature history of the back side of the blue Nomex® IIIA specimens using the infrared thermometer during thermal exposure

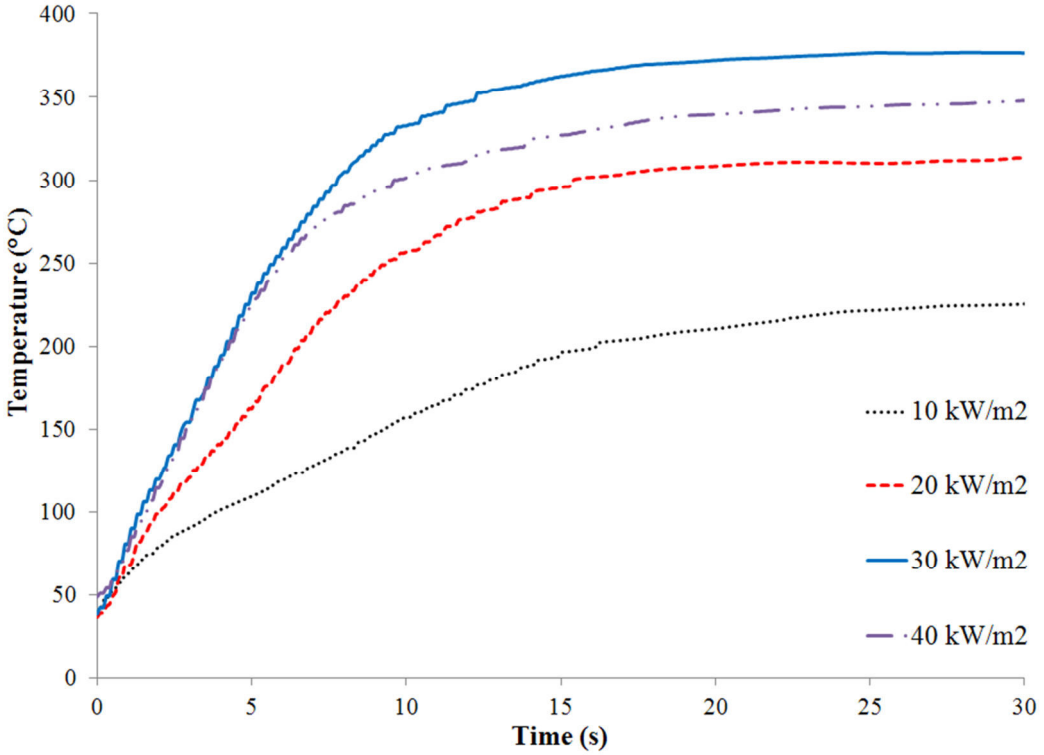

Figure 3.6: The first 30 s temperature history of back side of the Nomex® IIIA red specimens using the infrared thermometer during thermal exposure

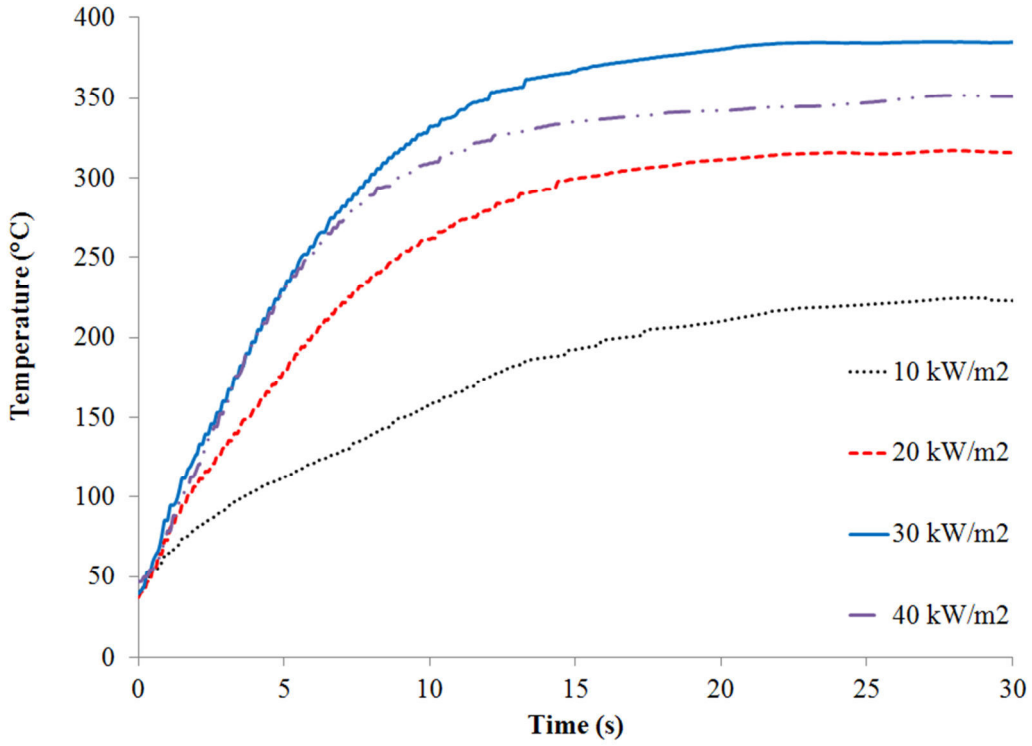

Figure 3.7: The first 30 s temperature history of the Nomex® IIIA dark blue specimens using the infrared thermometer during thermal exposure

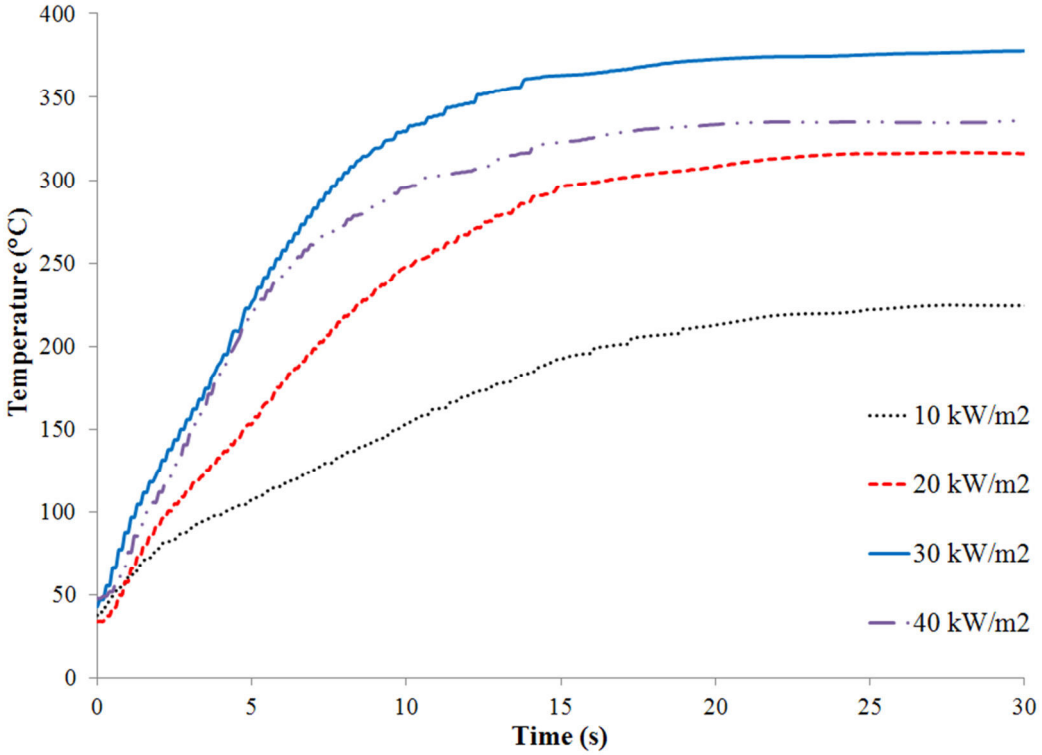

Figure 3.8: The first 30 s temperature history of back side of the Nomex® IIIA yellow specimens using the infrared thermometer during thermal exposure

3.4. Tensile tests

Firefighters are involved in everyday activities like crawling and hose handling, which result in abrasion to their protective clothing. Fabrics are subjected to forces of different magnitudes and directions when they are in contact with surfaces on the fire ground, and the equipment that they carry. Among all layers of firefighters' protective clothing, the outer shell should have the primary resistance against wear, tears, and cuts, as it is the outermost layer and directly in contact with abrasive and sharp surfaces. High mechanical strength translates into fewer repairs, less replacement cost, and longer wear life of outer shell and consequently, the entire firefighters' protective clothing.

Outer shell strength changes as a result of exposure to different factors such as heat in everyday operations. An outer shell fabric which is initially strong enough to pass minimum standard requirements may lose its integrity over time. Tensile strength is an indication of mechanical strength and was used in this research to evaluate the strength of outer shell

specimens after thermal ageing. In a case study conducted by the author among a group of mechanical engineering students, it was found that people may be able to exert roughly 70 N to pull a fabric from edges by hands. So, manual inspection may not reveal loss of strength in firefighters' protective clothing if there is no visual evidence of tear or rupture in yarns.

In textile engineering, a fibre is constructed from thousands of strands collected into a group. The fibres which are threaded along the length and the width of a fabric are called warp and fill, respectively. The terms warp and fill are also used for pointing out the direction of fibres in a fabric. Figure 3.9 illustrates warp and fill directions. Mechanical strength of a fabric is directly proportional with the number of fibres per unit length and strength of fibres in any directions can change accordingly. Normally, fill fibres are as strong as warp fibres [81]. But, for the Nomex® IIIA fabric used in this research, the tensile strength in the fill direction is weaker. Since standard requirements for mechanical strength of new fabrics are the same for both directions of a fabric, tensile strength of specimens was measured only in the weaker fill direction.

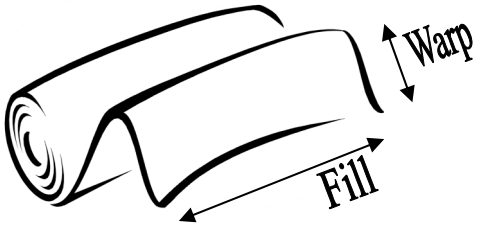

Figure 3.9: Illustration of warp and fill directions in a fabric

Tensile tests were conducted for thermally aged specimens based on the procedure described in section 2.5. Since specimens of different colours are made of a single fabric and similar weave, the tensile strength should not be affected by the colour of the specimen. Figures 3.10, 3.15, 3.20, and 3.25 illustrate the tensile strength of specimens of different colours after exposure to a particular heat flux. Labels next to data points in the figures show the average value of tensile strength of four tested specimens. NFPA 1971 requires a minimum tensile strength of 623 N in any direction for new outer shell fabrics of structural firefighters' protective clothing. This minimum value is represented by a dotted line in the figures in order to indicate the effect of thermal exposure on the tensile strength of specimens in comparison with the standard requirement. These fabrics have a lower surface weight than most outer shell fabrics, and are

typically used for protective coveralls for wildland firefighting and other applications. Therefore, a minimum tensile strength of 623 N may not be applicable for these fabrics.

Figure 3.10 shows the tensile strength of outer shell specimens after exposure to 10 kW/m^2 for durations of 600, 1200, and 2400 s. It is observed in the figure that tensile strength of specimens did not change or changed only slightly after these thermal exposures. This is expected since the specimens reached a maximum temperature of 220°C in an exposure to 10 kW/m^2 (Figures 3.5-3.8). According to TGA curves (Figures 3.1-3.4), this level of temperature is not expected to cause significant degradation in the fabric. Specimens were also observed using a scanning electron microscope. Figures 3.12-3.15 compare the surface of an unexposed specimen with specimens after exposure to 10 kW/m^2 for specific durations using a scanning electron microscope. These figures suggest no evidence of noticeable damage to fibres after this level of thermal exposure.

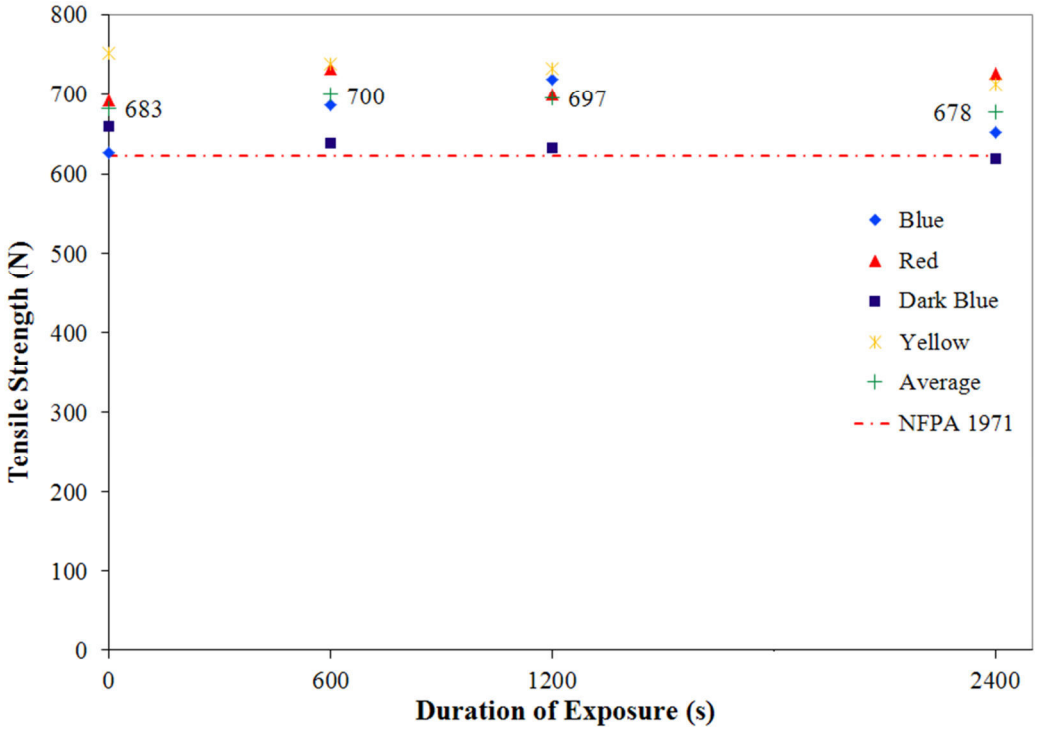

Figure 3.10: Tensile strength of specimens after exposure to 10 kW/m^2

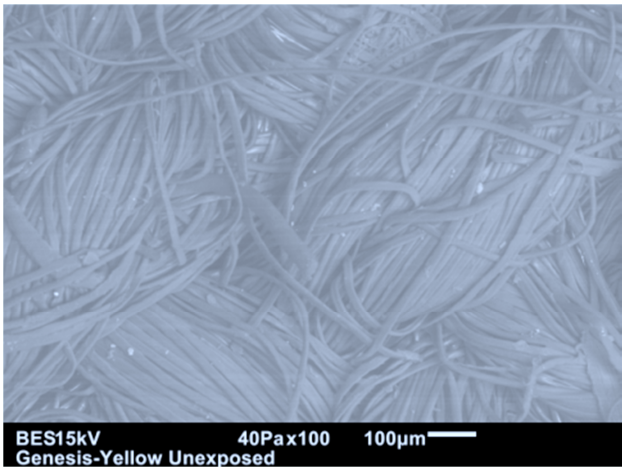

Figure 3.11: Surface of an unexposed Nomex® specimen

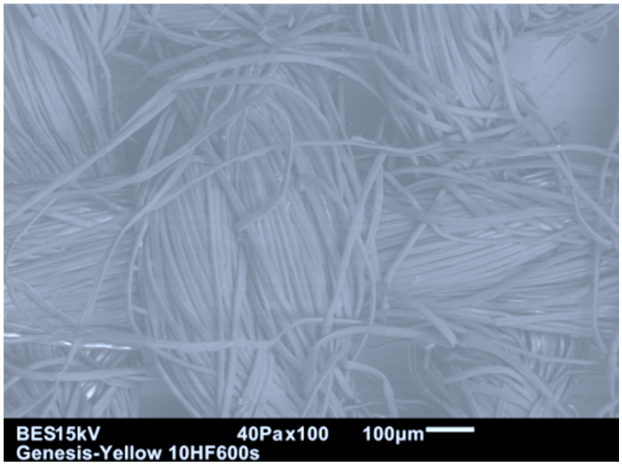

Figure 3.12: Surface of Nomex® specimen after exposure to 10 kW/m^2 for 600 s

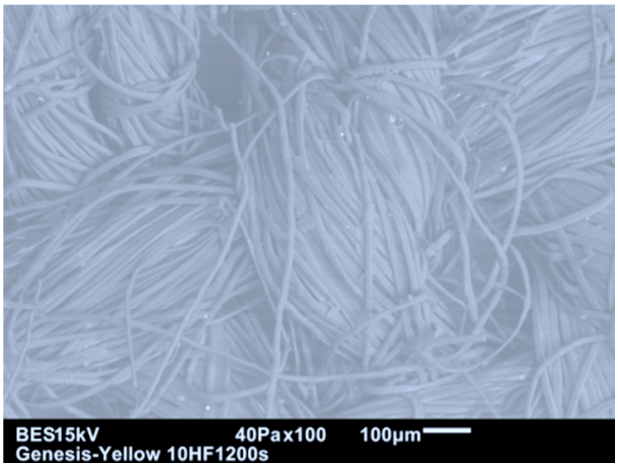

Figure 3.13: Surface of Nomex® specimen after exposure to 10 kW/m^2 for 1200 s

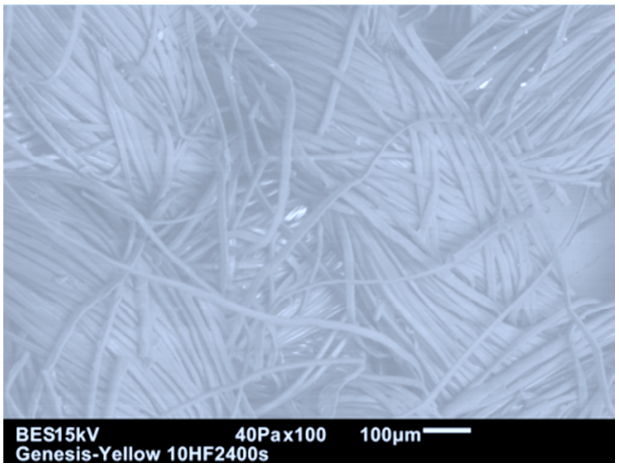

Figure 3.14: Surface of Nomex® specimen after exposure to 10 kW/m^2 for 2400 s

Figure 3.15 presents the tensile strength of specimens after exposure to 20 kW/m^2 for durations of 30, 150, and 300 s. The figure indicates that there is about 5% increase in tensile strength of specimens after a 30 s exposure to 20 kW/m^2. Even though this increase might be because of uncertainty in results, the nominal increase may be related to crosslinking reactions. Longer exposures to 20 kW/m^2 caused a decrease in the strength of specimens. On average, the strength of specimens after 150 s and 300 s decreased by 7% and 17%, respectively.

Temperature measurement results (Figures 3.5-3.8) show that specimens reached around 300°C during exposure to 20 kW/m^2. Around this temperature, slight weight loss (approximately 2-3%) occurs according to TGA curves (Figures 3.1-3.4). Discoloration of specimens

(Appendix A) indicates significant colour change after 150 s and longer exposure to 20 kW/m^2. This evidence points to dye removal from the specimen fabric. In addition to dye removal, it is known that factors such as oxidation, chain fracture, crosslinking and disorientation influence the change in mechanical strength in Nomex®. Oxidation, chain fracture, and disorientation decrease tensile strength of specimens. But, crosslinking can increase tensile strength. Just as an example, thermally aged specimens inside an oven at 250°C after only one min. lost 30-35% of their initial strength [82]. Figures 3.17-3.20 show the surface of specimens under an SEM. The fibres' width and appearance seem quite similar to those in an unexposed specimen even though exposure to 20 kW/m^2 for 300s (Figure 3.19) reduced tensile strength by almost 20% of initial strength. This decrease does not indicate significant deterioration in the specimen fabric, which may be the reason why no obvious change in SEM images was observed.

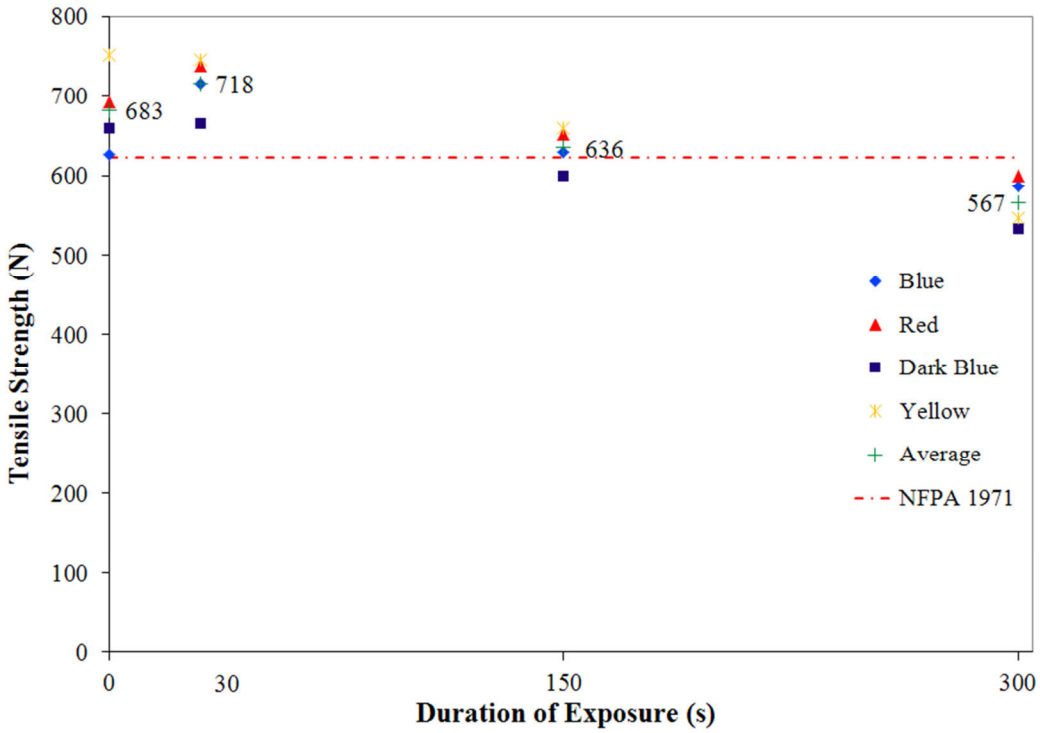

Figure 3.15: Tensile strength of Nomex® specimens after exposure to 20 kW/m^2

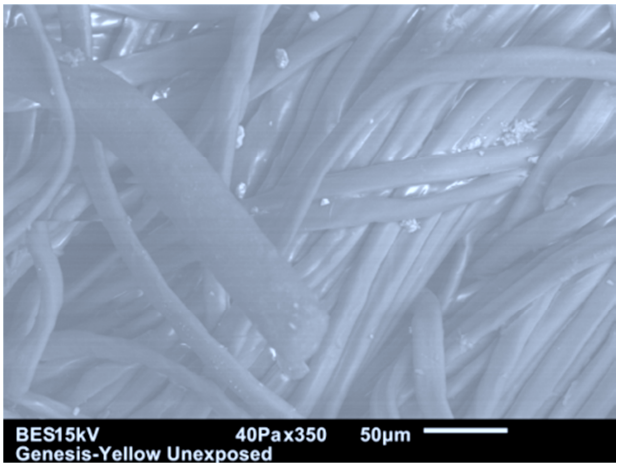

Figure 3.16: Surface of an unexposed Nomex® specimen

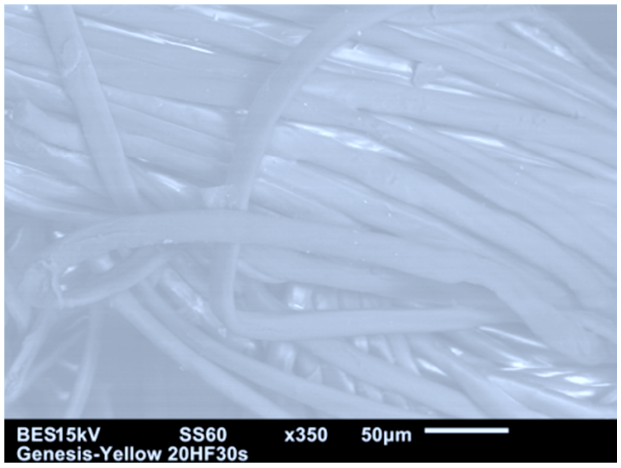

Figure 3.17: Surface of Nomex® specimen after exposure to 20 kW/m^2 for 30 s

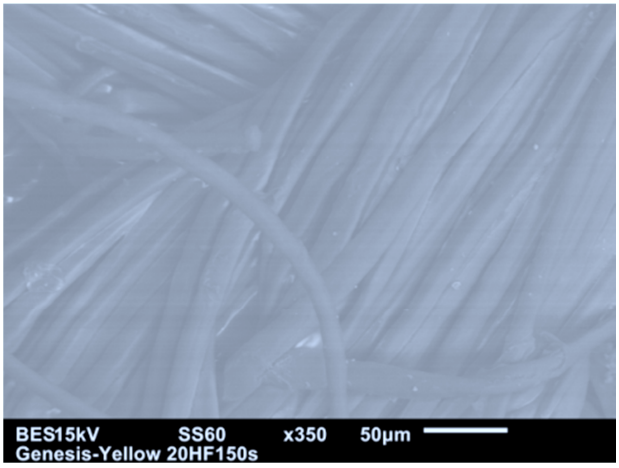

Figure 3.18: Surface of Nomex® specimen after exposure to 20 kW/m^2 for 150 s

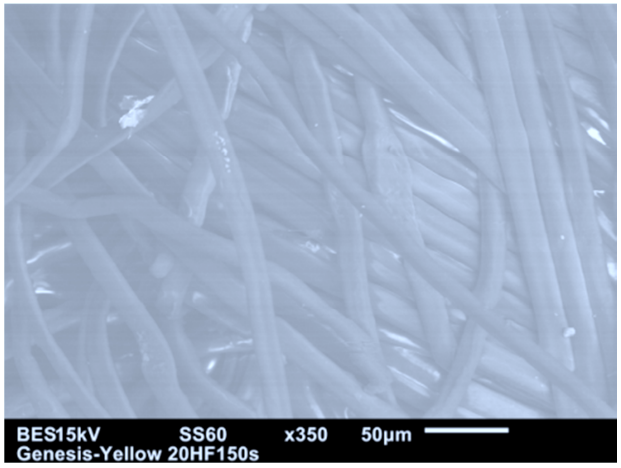

Figure 3.19: Surface of Nomex® specimen after exposure to 20 kW/m^2 for 300 s

Tensile strength of specimens after exposure to 30 kW/m^2 for particular durations is shown in Figure 3.20. The figure shows that 15 s of exposure is long enough to reduce the tensile strength to below the NFPA 1971 standard requirement for new outer shell fabrics. Longer exposures were so detrimental that tensile strength of specimens dropped to 40% and 36% of the strength of an unexposed specimen after 30 s and 60 s, respectively. Temperature measurements indicated that specimens reached approximately 380°C during exposure to 30 kW/m^2 (Figures 3.5-3.8), which is around the onset of decomposition of the specimen material based on TGA graphs (Figures 3.1-3.4). It is worth noting that the temperature of the back side of the specimen was measured using the infrared thermometer, which is lower than the temperature of the front side

of the specimen to some degree. So, the front side of the specimen may get more degradation than expected based only on temperature measurement by the infrared thermometer. In addition, the infrared thermometer measured the average temperature of a series of points on the surface of the back side of the specimen. So, the maximum temperature on the back side of the specimen could be higher to a certain degree. Inspection of surface of specimens using SEM (Figures 3.21-3.24) shows that fibres yarns eventually got thinner and branched into fibres as a result of heat exposure (e.g., circled region in Figure 3.23). This branching is accompanied by carbonization and gradual charring of the fibres, which makes the specimen weaker.

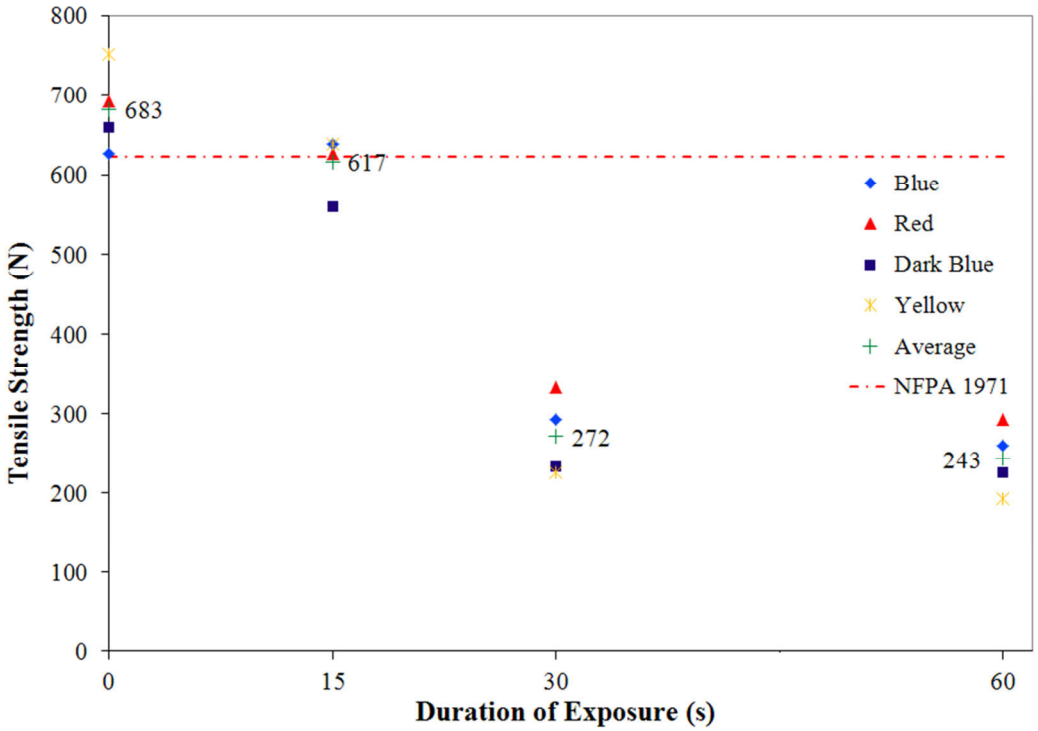

Figure 3.20: Tensile strength of Nomex® specimens after exposure to 30 kW/m^2

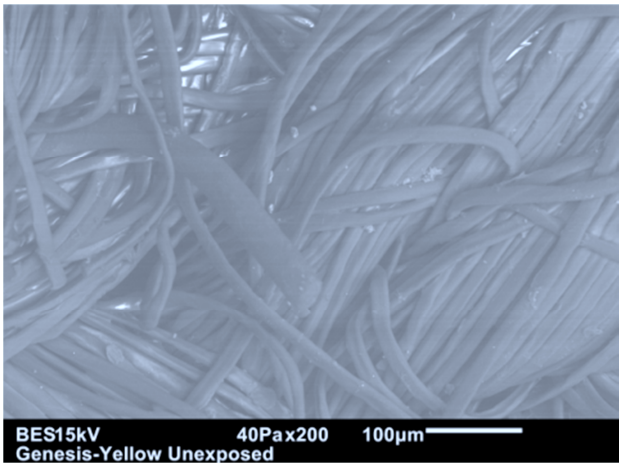

Figure 3.21: Surface of an unexposed Nomex® specimen

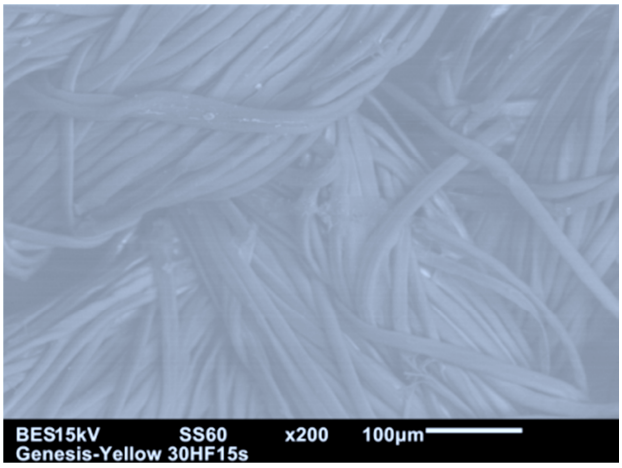

Figure 3.22: Surface of Nomex® specimen after exposure to 30 kW/m^2 for 15 s

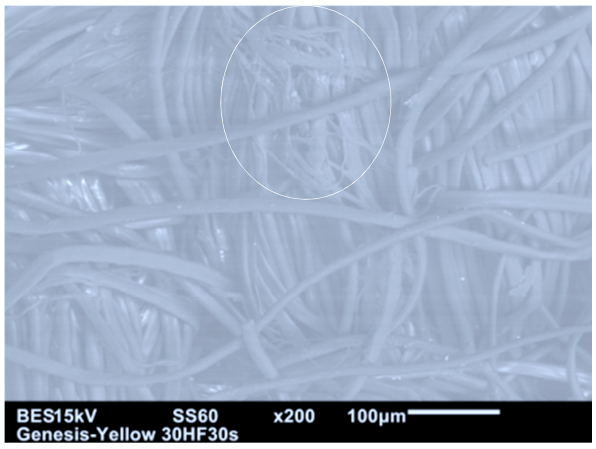

Figure 3.23: Surface of Nomex® specimen after exposure to 30 kW/m^2 for 30 s

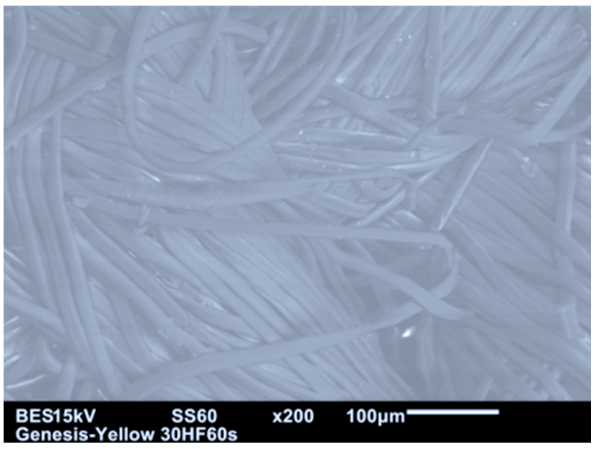

Figure 3.24: Surface of Nomex® specimen after exposure to 30 kW/m^2 for 60 s

Test results in Figure 3.25 show that tensile strength of specimens dropped sharply under more severe thermal exposure (40 kW/m^2). After only 10 s of exposure to 40 kW/m^2, the tensile strength of the specimen decreased by 65%. 20 s and 30 s exposures reduced tensile strength of specimens by as much as 90%. During thermal exposure, specimens underwent thermal decomposition and volatile compounds were released as fumes. During the carbonization process and thermal decomposition, fibres swell, char, and form a mass (Figures 3.26-3.29). Such a mass covers the space among fibres and reduces heat transfer to the unexposed side of the specimen.

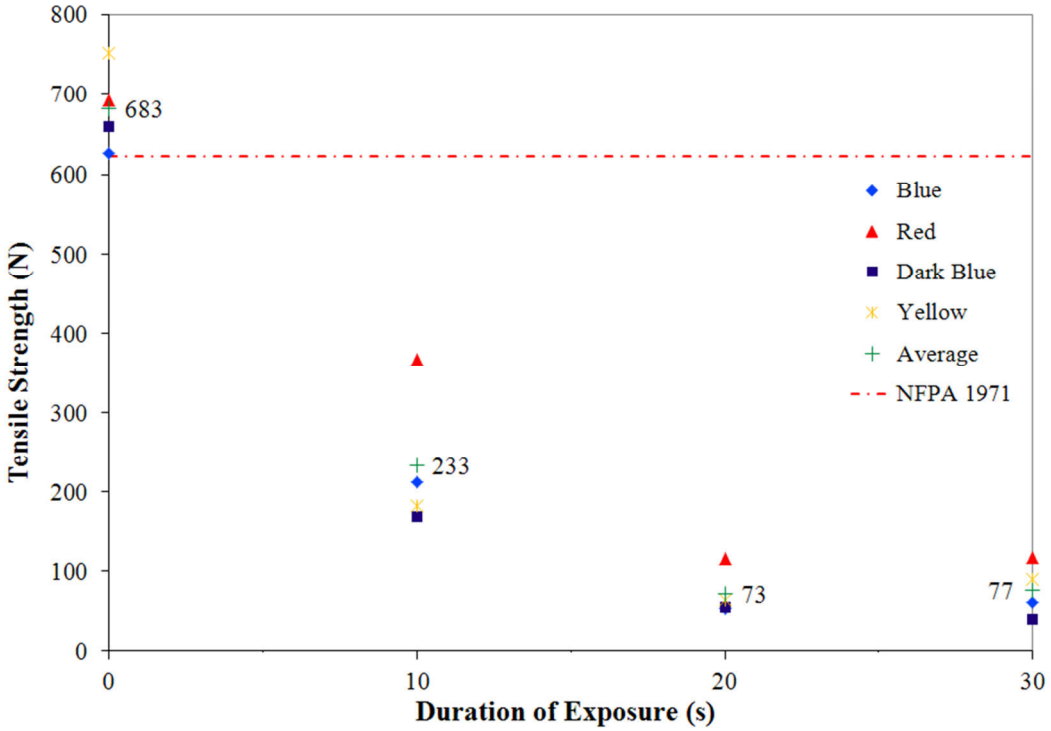

Figure 3.25: Tensile strength of specimens after exposure to 40 kW/m^2

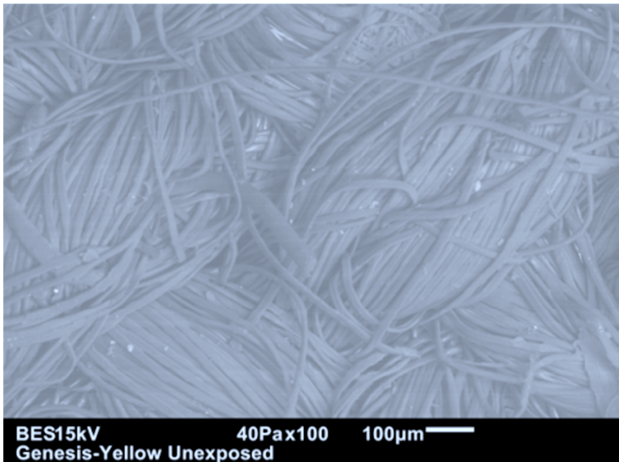

Figure 3.26: Surface of an unexposed Nomex® specimen

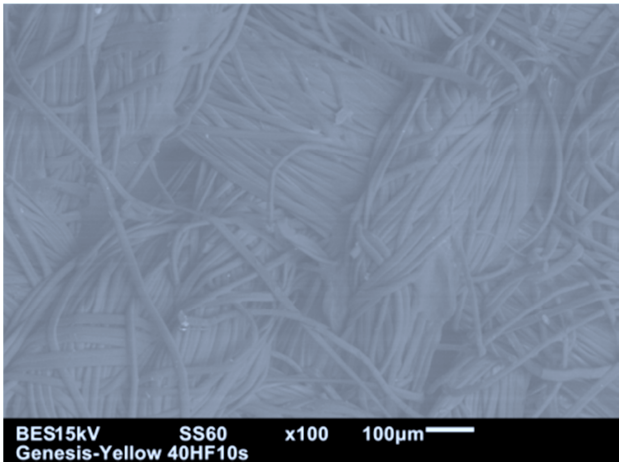

Figure 3.27: Surface of Nomex® specimen after exposure to 40 kW/m^2 for 10 s

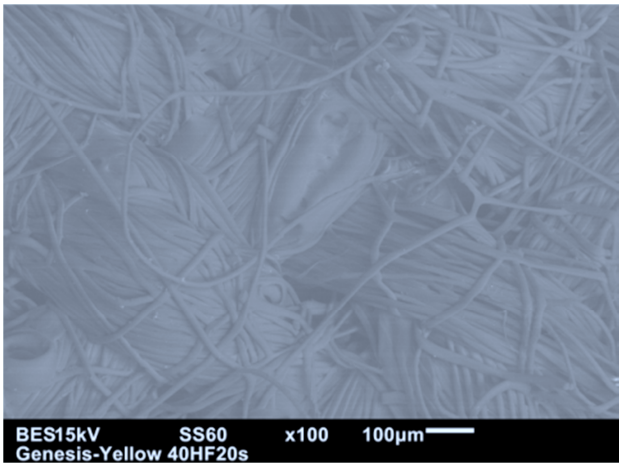

Figure 3.28: Surface of Nomex® specimen after exposure to 40 kW/m^2 for 20 s

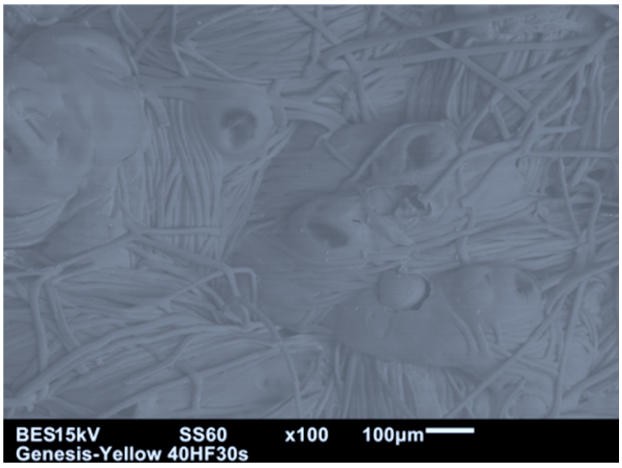

Figure 3.29: Surface of Nomex® specimen after exposure to 40 kW/m^2 for 30 s

Figure 3.30 shows the average tensile strength of the four colours of specimens after various levels of thermal exposure. Bars on the columns in the figure indicate standard error of the mean for four independent tests. It is equal to the standard deviation divided by the square root of the sample size (number of independent tests). The bias error reported by the manufacturers of the test equipment used in this research was negligible in comparison with the random error. In this case, the uncertainty is basically similar to the standard error of the mean. The difference is that the uncertainty is calculated by multiplying the standard error of the mean and the t-value in Student's t-distribution. Because of limitations in amount of fabrics to cut test specimens and equipment time to conduct tests, the number of replicated independent tests was less than five tests mentioned in the NFPA standard [2]. The number of independent tests is given in all sections that discuss the test results (sections 3.4, 4.1, 4.4, 4.5, 4.6, 5.4, 5.5, 5.6, and 5.7). The higher t-value associated with the low number of independent tests increases uncertainty and may not represent fluctuations in the test results properly. Therefore, it was decided to present the standard error of the mean for the purpose of statistical analysis of experiments rather than the uncertainty. However, uncertainty can be easily estimated by multiplying the standard error of the mean by the t-value for a certain number of tests.

Based on test results in the figure, a longer duration of exposure to similar intensity of heat flux reduces tensile strength of specimens. The downward trend in tensile strength varies depending on the intensity of thermal exposure. In exposure to 10 kW/m^2, increasing exposure

duration from 600 s to 2400 s reduced the tensile strength by 5%. Even after 2400 s (40 min) of exposure, the tensile strength of specimens still met the NFPA 1971 requirement for new outer shells. The rate of change in tensile strength of specimens increased in exposure to 20 kW/m^2, as tensile strength was reduced by around 20% by changing exposure duration from 30 s to 300 s. At higher intensities, the downward trend of tensile strength in the early stage of thermal exposure was much stronger than in later stages. In exposure to 30 kW/m^2, tensile strength reduced by 55% when duration of exposure increased from 15 s to 30 s. Continuing the exposure for an additional 30 s reduced tensile strength by only 10%. 10 s of exposure to 40 kW/m^2 decreased the tensile strength of specimen by 65%. Longer exposure for 20 s decreased the tensile strength by 70%. However, an additional 10 s exposure did not affect the tensile strength of the specimen.

Both intensity and duration of thermal exposure influence the tensile strength of specimens. Tensile strength of a specimen after exposure to 20 kW/m^2 for 30 s was comparable with the strength value after exposure to 10 kW/m^2 for 600 s. Exposure to 20 kW/m^2 for 150 s caused approximately the same level of damage to specimens as exposure to 30 kW/m^2 for 15 s. 60 s exposure to 30 kW/m^2 seems to be equivalent to 10 s exposure to 40 kW/m^2 in terms of effects on the tensile strength of specimens.

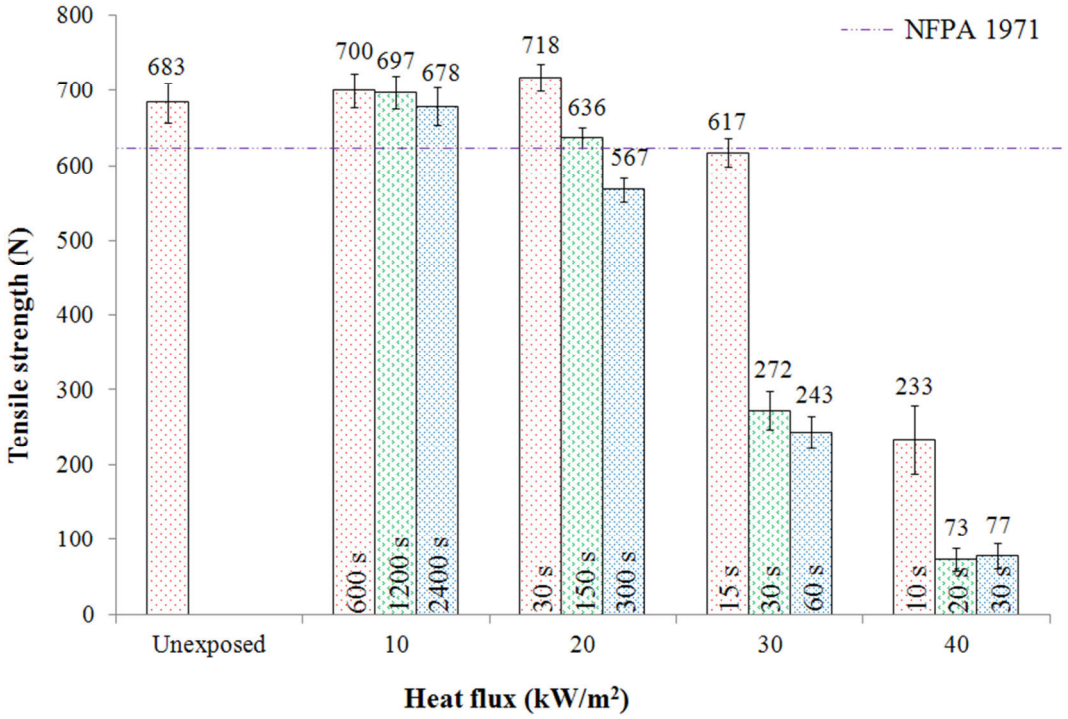

Figure 3.30: Average tensile strength of Nomex® specimens after thermal exposure to particular heat flux for specific duration

Outer shell specimens of different colours were selected for tensile testing in this chapter. The trend of change in Figure 3.30 reflects that the selected test matrix for thermal ageing described in Table 3.1 created different levels of deterioration in tensile strength of the outer shell fabric. The variety of colours and different levels of deterioration in mechanical strength assist in evaluating the capability of non-destructive techniques for prediction of tensile strength of outer shell specimens in chapters 6 and 7.

Except for low levels of thermal ageing (exposure to 10kW/m^2 for 600 s and 1200 s and 20 kW/m^2 for 30 s), tensile strength of specimens reduced after thermal ageing. This decrease was dependent on intensity and duration of thermal exposure. Temperature measurements and TGA results were used in explaining deterioration in mechanical strength of the specimen fabric.

4. MOISTURE BARRIER EXPERIMENTS

The moisture barrier is the second layer of firefighters' protective clothing and is surrounded by the outer shell and thermal liner layers. Since it is enclosed by other layers, the moisture barrier is not normally seen or touched, which makes careful and regular inspection of moisture barriers difficult. The moisture barrier plays an important role in dissipation of metabolic heat, maintenance of thermal equilibrium, and mitigation of the risk of heat exhaustion and scalding injury. The moisture barrier reduces body temperature and prevents steam burns to skin and heat stress injuries by allowing the perspiration to escape outward. In addition, it prevents external liquids including water, some common chemicals, viral agents, and bloodborne pathogens from penetrating into the body during firefighting operations. Figure 4.1 illustrates the role of moisture barrier.

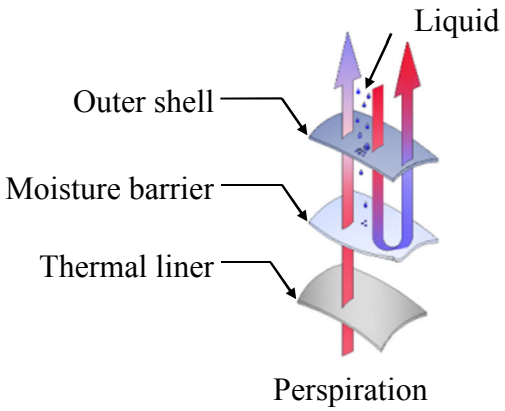

Figure 4.1: Layers of firefighters' protective clothing

If liquids penetrated into inner layers of firefighters' protective clothing, they would occupy the air spaces in the thermal liner layer and increase the thermal conductivity of the insulative material. Just as an example, the thermal conductivity of water is approximately 0.58 W/(m·K), while the thermal conductivity of air is around 0.024 W/(m·K). In addition, a dry piece of protective clothing is lighter than a wet one. Finally, liquid penetration can cause scald burn on the wearer' skin. Scald burn is caused by any type of hot liquids such as hot water present in the fire ground. Exposure to hot liquids especially when the protective clothing is compressed to the body transfers significant heat to skin, which results in scald burn injury [83].

During firefighting operations, the heart rate of firefighters is very high. Accumulation of metabolic heat in the body aggravates the cardiac workload. In fact, more firefighters die of sudden cardiac death (53% of firefighter deaths) than from burns (10%) [84]. Therefore, the performance of the moisture barrier has a significant influence on firefighters' safety. In addition, the moisture barrier is the most easily damaged layer of firefighters' protective clothing. It is also difficult to be inspected visually since it cannot be separated from the thermal liner. All these considerations necessitate more work on the performance of moisture barriers, as little information on the change in liquid penetration and vapour permeation of moisture barrier fabrics after thermal ageing is available in the literature.

One type of moisture barrier is composed of a continuous monolithic polymer layer with no pores. These moisture barriers are non-permeable to water vapour and are known as non-breathable. The use of this type of moisture barrier was strictly limited in the U.S. and Canadian markets after release of a new edition of NFPA 1971 in 2000 since this document mandated thermal heat loss and breathability requirements for new firefighters' protective clothing [85]. The next edition of NFPA 1971 in 2007 placed more emphasis on this requirement and increased the minimum thermal heat loss from 135 to 205 W/m^2 in the Total Heat Loss test (Table 1.1). The second type of moisture barriers has micropores which permit transport of water vapour through the barrier. It allows the body perspiration to escape from the clothing outward. However, the pores are small enough to prevent passage of water and other liquids from outside toward the wearer's body. The third type known as bi-component moisture barriers is a combination of the first two types. A monolithic hydrophilic polymer is laminated on the moisture barrier. This continuous layer reduces the water vapour permeability rate, but it is counteracted partly by the hydrophilic nature of the polymeric layer.

The moisture barrier membrane is a delicate thin film. So, it is bonded to a face fabric (substrate) for protection and durability. The substrate could be a woven or non-woven fabric. To better protect the membrane film, which degrades at a lower temperature than the other layers of the ensemble, the moisture barrier is placed between outer shell and thermal liner layers in such a way that the substrate faces the outer shell layer and the membrane film is in contact with the thermal liner layer. Contamination of the membrane film by skin oil, perspiration, and dirt makes the pores smaller and acts as a hydrophilic agent which wets the membrane film. This reduces

the permeability of water vapour and breathability of moisture barrier. To address this issue, the membrane film is laminated with an oleophobic layer which is resistant to oil.

The focus of this chapter is performance of the moisture barrier after thermal ageing. Water Vapour Transmission Rate (WVTR), water penetration pressure, and tear strength of thermally aged moisture barrier specimens are measured. The procedure for carrying out the tests and the tests results will be discussed and interpreted using TGA curves, temperature history, and SEM images of specimens. The connection between this chapter and the rest of this research will be considered at the end.

4.1. Preparation of specimens

The specimens in this part of research were from a single layer of moisture barrier fabric, Stedair® 4000 with a surface weight of 170 g/m^2. The fabric consists of a bi-component membrane laminated on a substrate. The membrane is comprised of an ePTFE (expanded Polytetrafluoroethylene) film in combination with a continuous hydrophilic and oliophoebic polymer layer. The substrate is constructed of a woven Nomex® with 2% carbon fibres.

In order to approximate the level of heat flux that moisture barriers receive on the fire ground, a series of tests were conducted. An outer shell specimen made of Crusader® 790 (60%Kevlar®/40%Nomex® T462) with a surface weight of 265 g/m^2 was exposed to heat fluxes of 10, 20, and 30 kW/m^2 which represent the ordinary and very early stage of emergency conditions. Using the same procedure same as outlined in section 2.3, the outer shell specimen was cut and mounted on the specimen holder. A copper calorimeter sensor was placed behind the outer shell specimen to measure the transmitted heat flux in two orientations. In the first orientation, the sensor was in contact with the outer shell specimen. In order to consider the interlayer space between outer shell and moisture barrier layers in firefighters' protective clothing, a 3.2 mm (1/8")-thick aluminum spacer was positioned between the outer shell specimen and the copper calorimeter in the second orientation. Three tests were conducted for each heat flux and each orientation. The error bars in Figure 4.2 indicate the standard error of the mean for three independent tests.

Figure 4.2 shows the average of transmitted heat flux through the outer shell specimen. It illustrates that almost 50% of the incident heat flux passed through the outer shell specimen and reached the heat flux gauge. In the case of a 3.2 mm gap between the outer shell specimen and

the heat flux gauge, about 35% of the incident radiation reached the heat flux gauge, which indicates the added insulation by air gaps in firefighters' protective clothing. These values can approximate the level of heat flux that a moisture barrier receives under ordinary and early stage of emergency conditions. Based on these results, heat fluxes for thermal ageing of moisture barrier specimens were selected as 50% of heat fluxes used for ageing of outer shell fabrics in Table 3.1. To maintain consistency, duration of thermal exposure was the same as duration of thermal exposure for outer shell experiments in Table 3.1. Furthermore, one moisture barrier specimen was exposed to 20 kW/m^2 for 5 min. in order to investigate the effect of an extreme thermal exposure. Table 4.1 shows the test matrix for moisture barrier specimens

Thermal ageing of moisture barrier specimens was done in a similar manner to the procedure outlined in section 2.2. The only difference was that the specimen was mounted on top of the 3.2-mm (1/8 in.) spacer and a Kaowool insulating block. This block was the same as the insulating block of the copper calorimeter sensor used in the tests to measure heat flux.

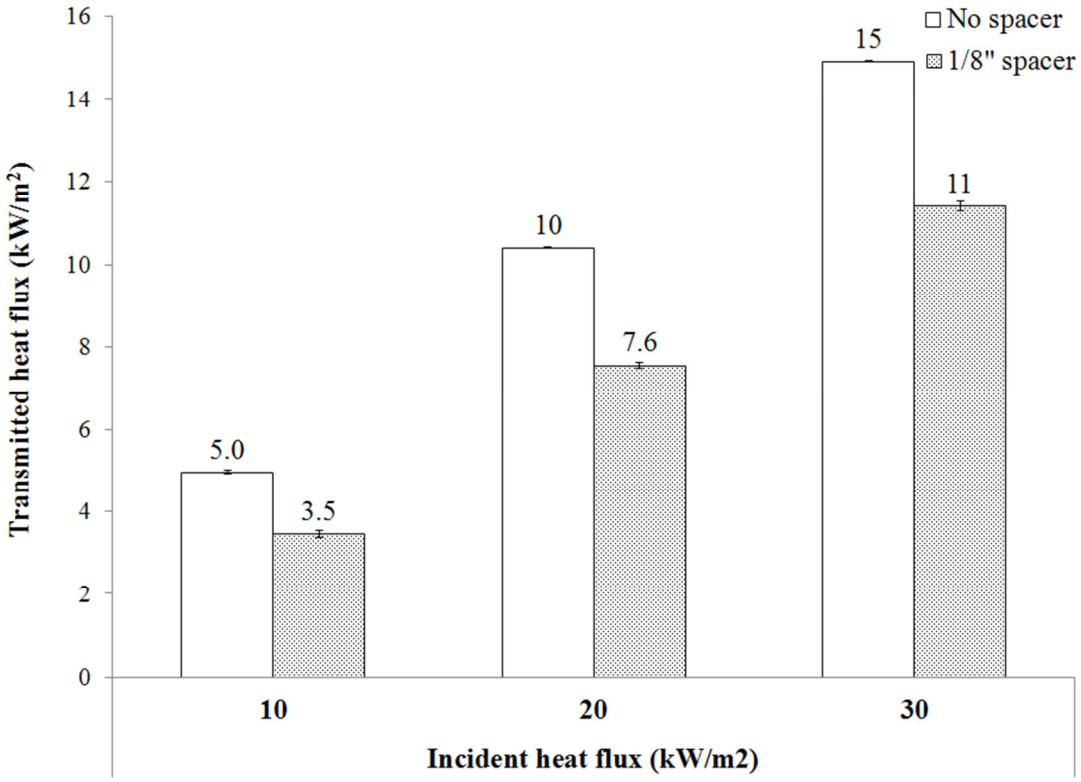

Figure 4.2: Transmitted heat flux through Crusader®790 outer shell when the copper calorimeter is in direct contact with the fabric and when there is a 3.2 mm (1/8 in.) spacer between them

Table 4.1: Thermal exposure duration for each heat flux

Incident heat flux (kW/m^2)	Exposure duration (s)
5	600, 1200, 2400
10	30, 60, 90, 120, 150, 300
15	15, 30, 60
20	300

Inasmuch as the main roles of the moisture barrier layer are prevention of liquids penetration and heat stress reduction by permeability to perspiration (water vapour), water penetration pressure and Water Vapour Transmission Rate (WVTR) were measured for the specimens. Furthermore, tear strength of moisture barrier specimens, as an indication of mechanical strength, was recorded. The tests were carried out on unexposed and thermally aged specimens. The temperature of the specimens was also measured using an infrared thermometer according to the procedure outlined in section 2.4. Thermogravimetric analysis was also conducted for both substrate and membrane of moisture barrier material.

4.2. Thermogravimetric analysis (TGA)

Thermogravimetric Analysis (TGA) was conducted for both the membrane and the substrate of the moisture barrier fabric specimen. Figures 4.3-4.4 show TGA curves for membrane and substrate fabrics, respectively. According to Figure 4.3, the membrane starts losing weight and decomposing slowly at 220°C. After reaching 300°C, the weight loss increased sharply. The specimen had lost 50% of weight when the temperature reached 400°C. A sharp peak in the weight loss trend was observed around 500°C. The specimen was completely decomposed by around 570°C.

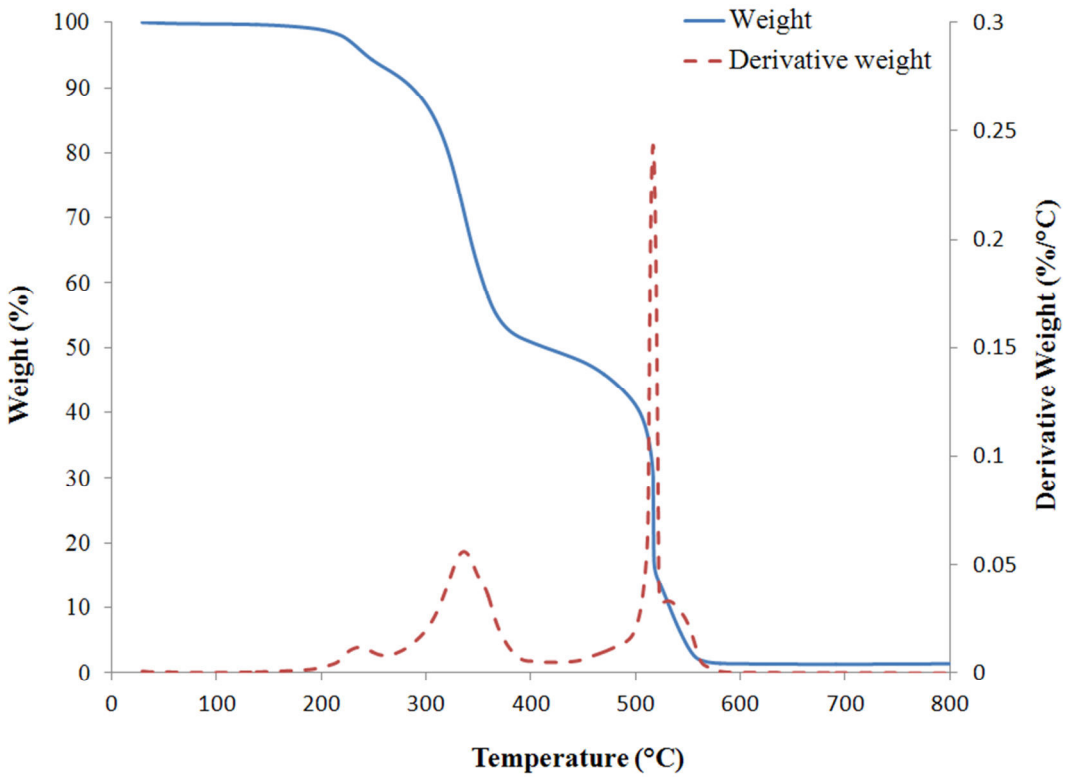

Figure 4.3: TGA curve for membrane ePTFE side of Stedair® 4000 moisture barrier specimens

Figure 4.4 illustrates the weight loss trend of Nomex®, which was used as the substrate of moisture barrier specimens and is not exactly the same as Nomex fabric used in outer shell specimens. At the beginning of TGA experiment, 2-3% of weight loss is observed as a result of moisture release. The first peak of weight loss occurred at around 300°C, when the specimen weight decreased by roughly 10%. The second peak of weight loss occurred when the specimen temperature reached 450°C. By around 650°C, the specimen material was completely decomposed.

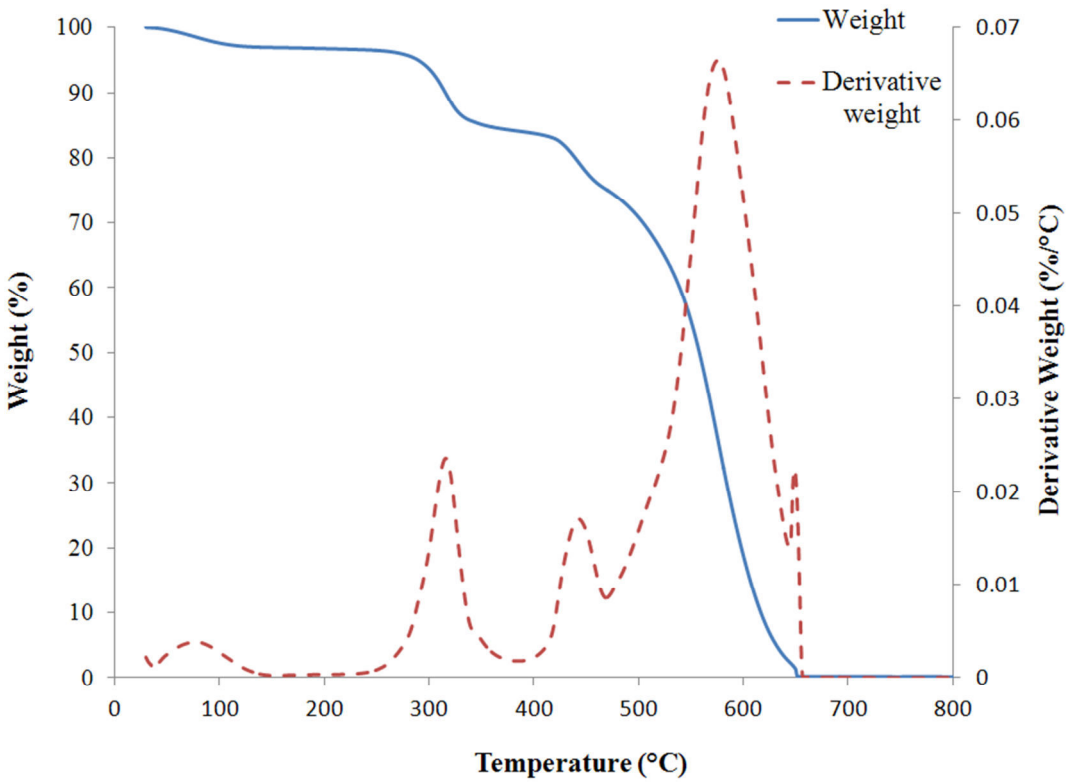

Figure 4.4: TGA curve for substrate (Nomex®) side of moisture barrier specimens

4.3. Temperature measurement

In this section, the temperature history of the specimen during thermal exposure is compared with the TGA curve in order to explain the changes in the properties of the fabrics after thermal exposure. Temperature histories of moisture barrier specimens during exposure to different heat fluxes are shown in Figure 4.5. The temperature was recorded for the maximum duration of exposure for each heat flux shown in Table 4.1. Comparison of temperature measurements in Figure 4.5 with the key temperatures in the TGA curves (Figures 4.3-4.4) indicates that specimens in the selected test matrix underwent different levels of degradation.

In exposure to 5 kW/m^2, moisture barrier specimens reached 190°C. Based on TGA curves in Figures 4.3-4.4, significant weight loss as a result of decomposition of specimen material was not observed before specimens reached 200°C. The specimen's temperature approached 260°C after 300 s thermal exposure to 10 kW/m^2. This temperature is high enough for onset of decomposition in both substrate and membrane of moisture barrier specimens. The specimen temperature reached 280°C after a one min exposure to 15 kW/m^2. Similarly, this temperature is

high enough for decomposition of specimen material. After a 5 min exposure to 20 kW/m^2, the specimen temperature was recorded as 385°C. At this temperature, substrate and membrane of specimens lost 15% and 50% of initial weight based on TGA curves.

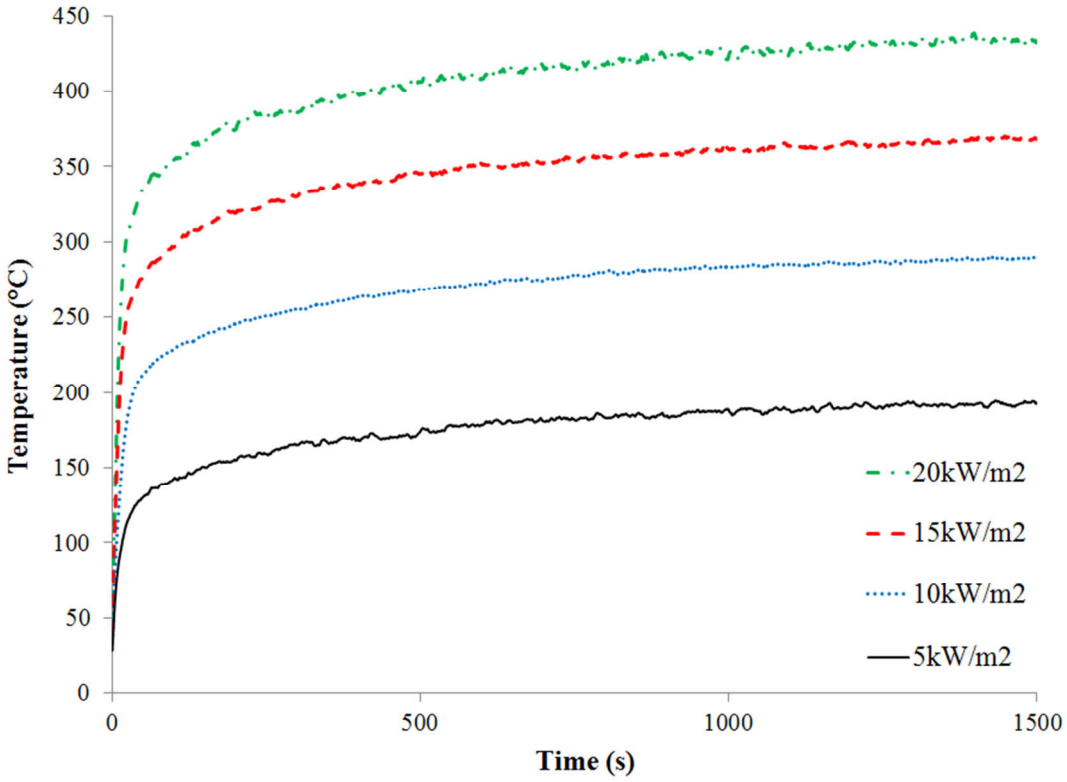

Figure 4.5: Temperature history of the back side of Stedair® 4000 moisture barrier specimens during thermal exposure

4.4. Water vapour permeability test

Experiments were carried out on moisture barrier fabrics after thermal exposures based on the procedure outlined in section 2.7 and Table 4.1. Figure 4.6 shows the average values of water vapour transmission rate for moisture barrier specimens after exposure to a certain heat flux for a particular duration. Data labels in the figure present the numerical value of each column. The bars indicate the standard error of the mean for 6 independent tests. Generally speaking, WVTR increased slightly after thermal exposure. However, the extent of increase was dependent on the intensity and duration of thermal exposure. Exposure to 5 kW/m^2 for 2400 s and exposure to 10 kW/m^2 for 30 s both increased the WVTR by 5%. In exposure to 5 kW/m^2, the specimen

temperature reached less than 200°C which is not intense enough for substantial degradation of the specimen material (Figure 4.5). It may be why major changes in WVTR after exposure to 5 kW/m^2 were not observed. 30-s to 300-s exposures to 10 kW/m^2 increased WVTR by 5% to 15%. A more intense thermal exposure, 20 kW/m^2 for 300 s, increased WVTR dramatically by 3 times as compared to that of an unexposed specimen.

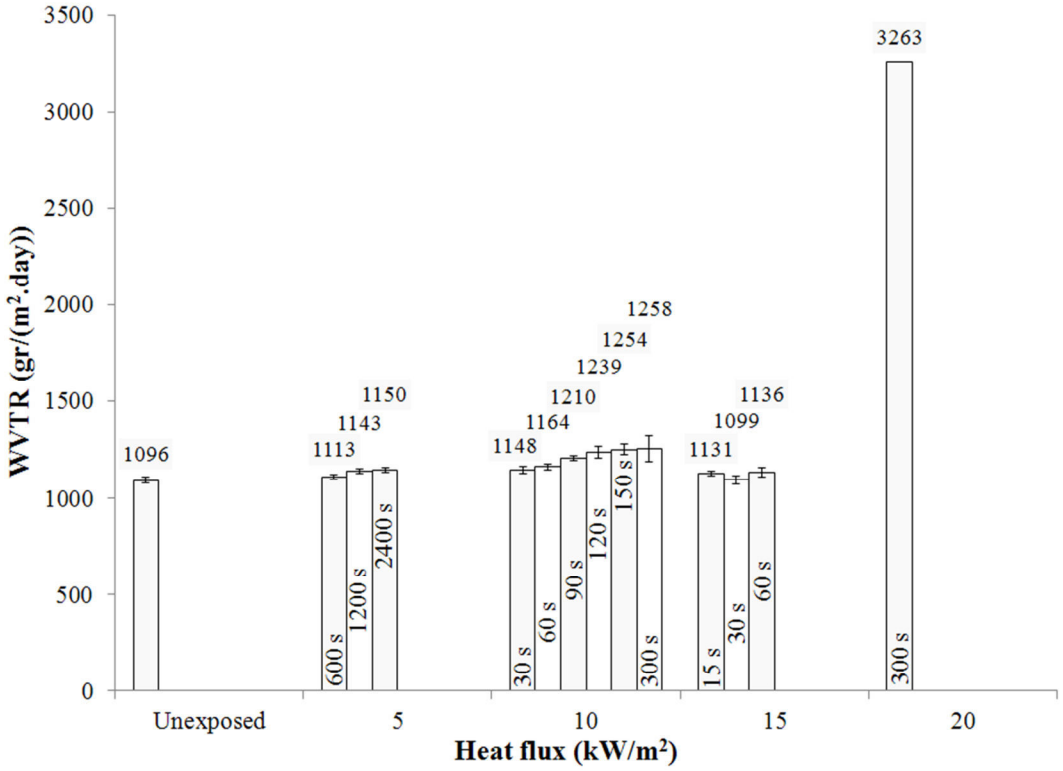

Figure 4.6: Water Vapour Transmission Rate (WVTR) of moisture barrier specimens

The figure shows that specimens may be less permeable to water vapour after exposure to 15 kW/m^2 than 10 kW/m^2 for similar durations (30 s and 60 s). Specimens after exposure to 15 kW/m^2 for 30 s have the same level of water vapour permeability as an unexposed specimen, but exposure to 10 kW/m^2 for 30 s increased WVTR by 5%. These observations may imply that there are two different mechanisms, which work in opposite directions. Investigating the form of fibres on the surface of specimens using SEM may help to reveal these mechanisms. Since the moisture barrier membrane is covered with a thin and continuous layer of oliophoebic polymer, the form of ePTFE fibres cannot be observed under SEM. In order to peel off the continuous

polymeric layer, the membrane was torn off the substrate. As a result of this pulling off, the continuous polymeric layer was partly taken off the membrane, so the complete layer could not be observed using SEM.

The polymeric layer decreases the WVTR, as it covers the micropores. So, the WVTR depends on both of the size of the pores and the cracks on the polymeric layer. The effects of thermal exposures on these two factors determine how the WVTR of specimens changed. Figures 4.7-4.8 illustrate the polymeric layer fibres in an unexposed specimen and in a specimen after exposure to 10 kW/m^2 for 120 s, respectively. Thermal exposures cause cracks and holes in the polymeric layer and clusters are formed on the layer. Hence, the effects of thermal exposures on the polymeric layer increase the WVTR through the moisture barrier specimen.

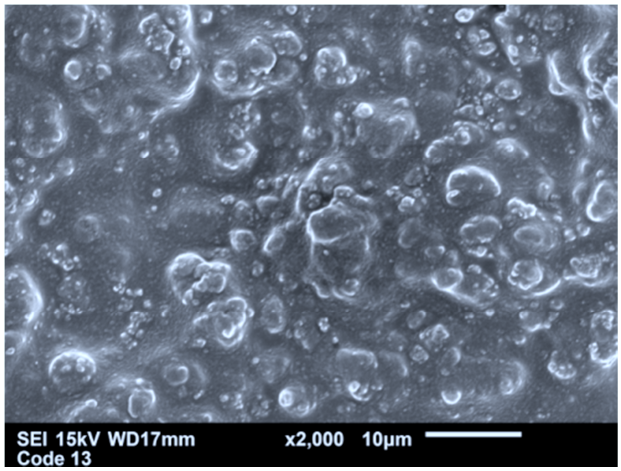

Figure 4.7: The polymeric layer of a membrane of an unexposed specimen

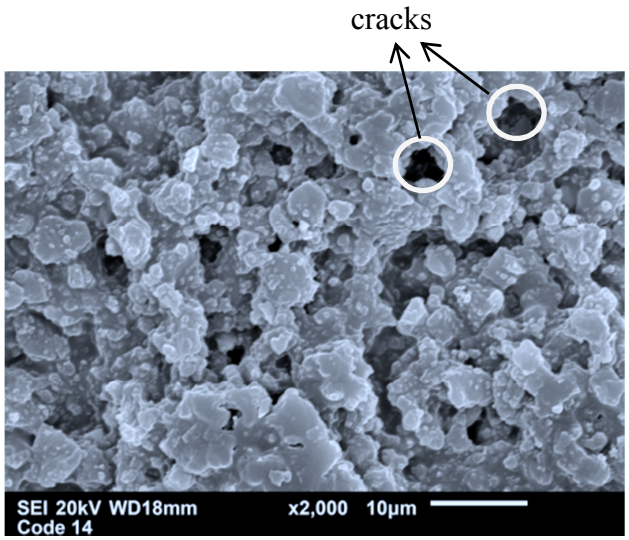

Figure 4.8: The polymeric layer of a membrane of a specimen exposed to 10 kW/m^2 for 120 s

Figures 4.9-4.12 illustrate the effect of thermal exposure on the size of the micropores. It is observed that the size of the micropores decreased after thermal exposure. Images for all thermally aged specimens are available in Appendix B. Smaller micropores are translated into smaller pathways for water vapour to permeate through the moisture barrier fabric. Therefore, thermal exposure can reduce the WVTR as a result of tighter pores.

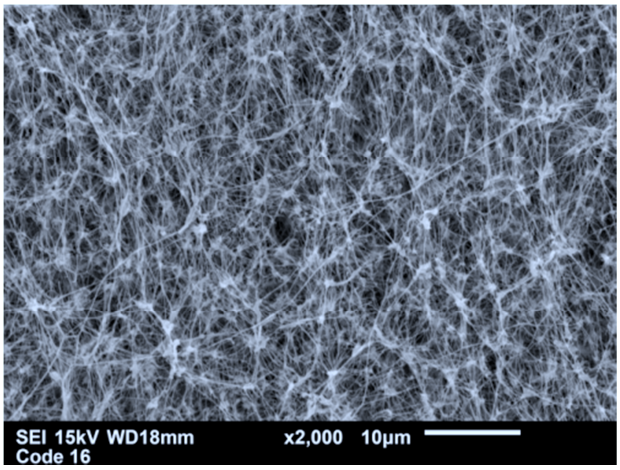

Figure 4.9: ePTFE fibres in the membrane of the unexposed moisture barrier specimen

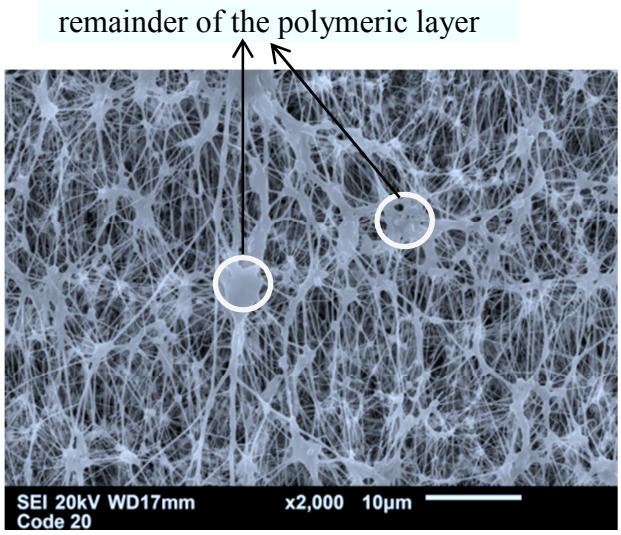

Figure 4.10: ePTFE fibres in the membrane of the specimen exposed to 10 kW/m^2 for 120 s

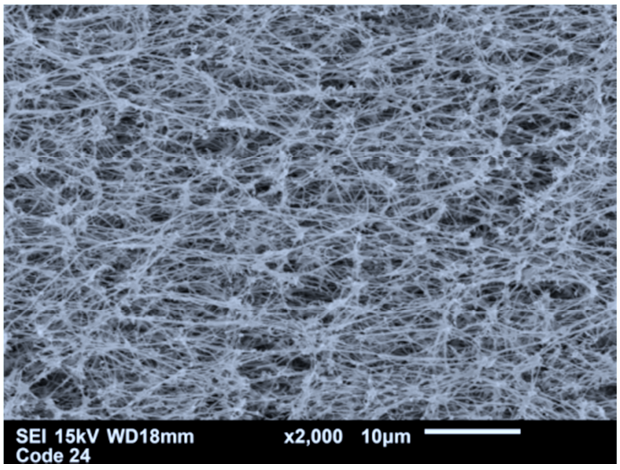

Figure 4.11: ePTFE fibres in the membrane of the specimen exposed to 10 kW/m^2 for 300 s

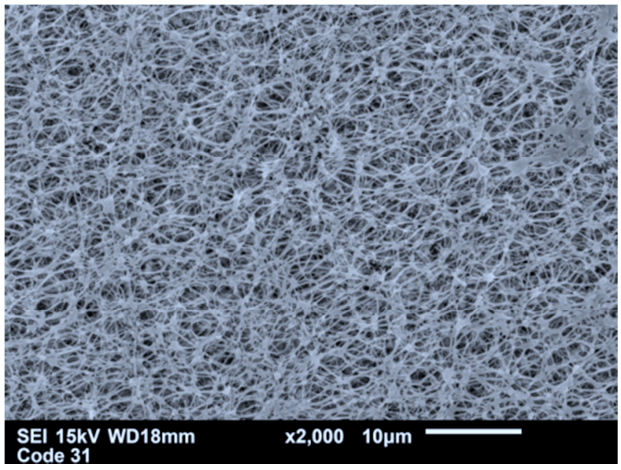

Figure 4.12: ePTFE fibres in the membrane of the specimen exposed to 15 kW/m^2 for 60 s

A trade-off between the formation of cracks in the polymeric layer and smaller pore size of ePTFE fibres after thermal exposure (to 5, 10, and 15 kW/m^2) may explain the changes in the WVTR. After exposure to 20 kW/m^2 for 300 s, WVTR increased three-fold. Figure 4.13 explains this significant change. In the figure, ePTFE fibres are completely disintegrated. In addition, fissures and large holes are observed in the polymeric layer. These alterations in the structure of the specimen increased WVTR notably.

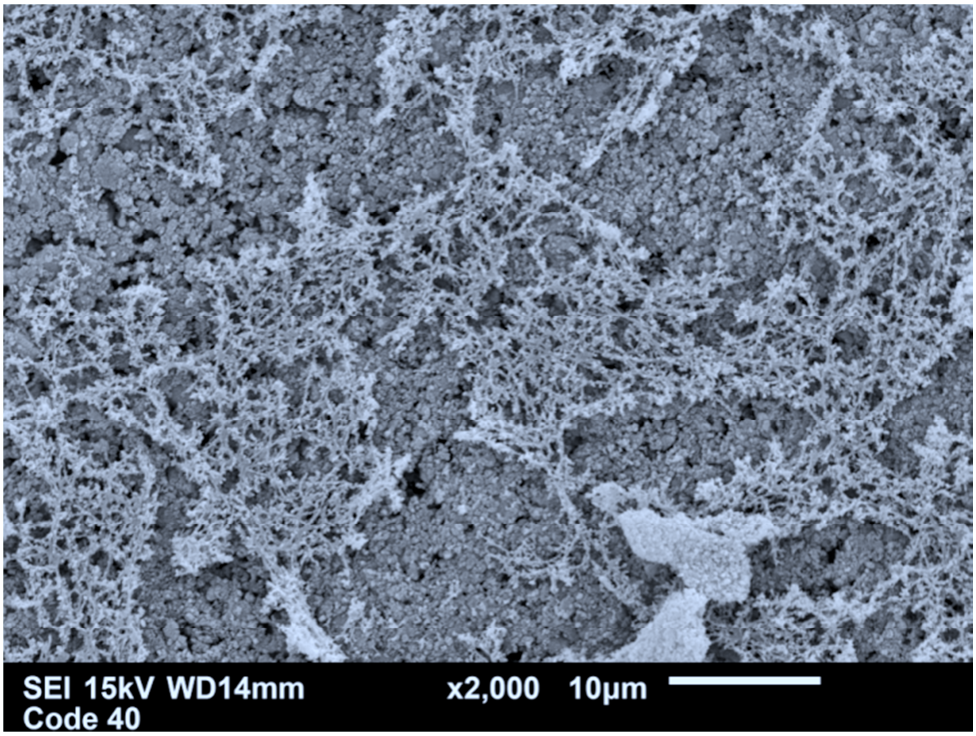

Figure 4.13: Surface of specimen after exposure to 20 kW/m^2 for 300 s

4.5. Water penetration pressure test

Experiments were carried out on moisture barrier fabrics after thermal exposure based on section 2.8 and Table 4.1. Figure 4.14 shows the average values of penetration pressure for moisture barrier specimens after exposure to a certain heat flux for a particular duration. Data labels in the figure present the numerical value of each column. The bars indicate standard error of the mean for three independent tests. The figure shows that in general the required pressure for penetration of water decreased after thermal exposure. An exposure to 10 kW/m^2 for 600 s decreased the penetration pressure by 20%. Longer exposures to 10 kW/m^2 for 1200 s and 2400 s reduced the penetration pressure by approximately 30% and 35%, respectively. During exposure to 10 kW/m^2, specimens reached around 190°C. Weight loss was not observed for the specimen materials in TGA curves (Figures 4.3-4.4). Reduction of penetration pressure could be related to appearance of cracks and holes (Figures 4.7 and 4.8) in the polymeric layer of membrane of specimens after long exposure to relatively low levels of heat flux.

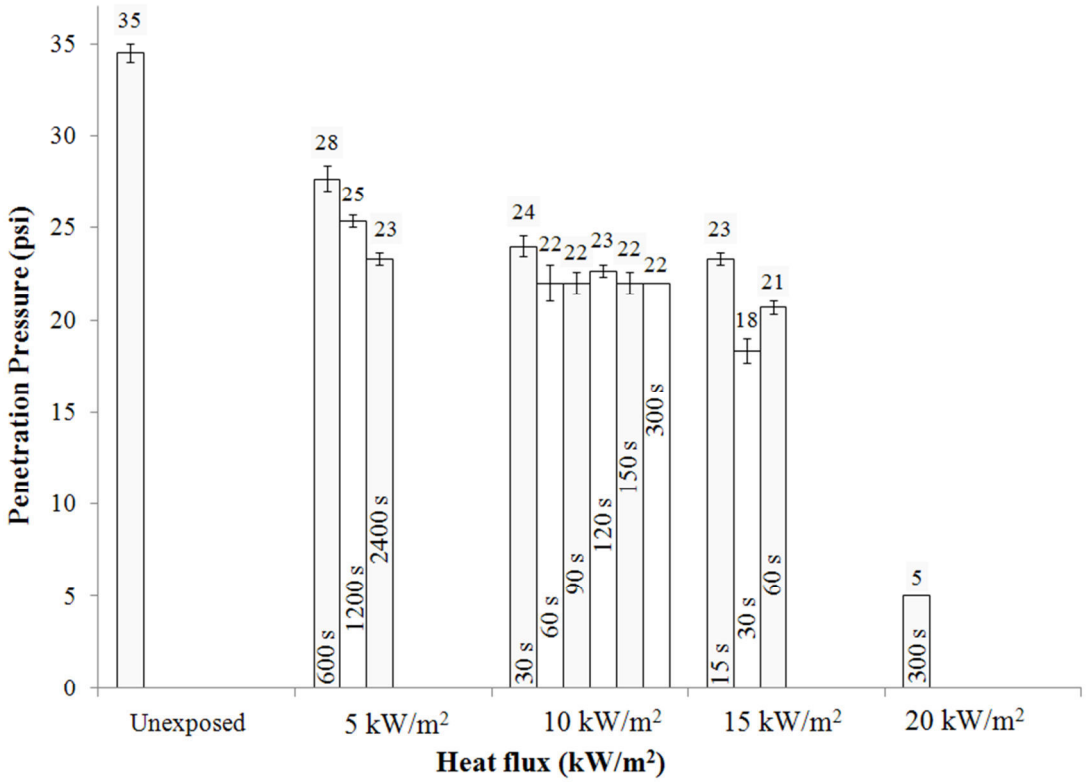

Figure 4.14: Required pressure for water penetration for moisture barrier specimens

Even though exposure to 10 kW/m^2 for 30 s and 15 kW/m^2 for 15 s decreased the penetration pressure to 70% of the value for an unexposed specimen, longer durations of exposure did not decrease the penetration pressure significantly. The specimens reached temperatures in the range of 200°C to 280°C during exposure to 10 and 15 kW/m^2 for durations in the test matrix (Table 4.1). This range of temperature is below 300°C when TGA curves indicated a weight loss of around 10% for the membrane of the moisture barrier specimen. This may justify why relatively short (up to 300 s) durations of exposure to 10 and 15 kW/m^2 did not make a noticeable difference in water penetration pressure of thermally aged specimens. Exposure to the highest intensity (20 kW/m^2) increased the membrane temperature to about 400°C which is high enough for significant weight loss and consequently, degradation of performance. The penetration pressure of the specimen decreased to 5 psi (34.5 kPa), which can be attributed to disintegration of specimen fabric and substantial strength loss after the thermal exposure (Figure 4.13). It is expected to observe an overall decreasing trend for the required water penetration pressure, which is related to intensity and duration of thermal exposure.

The minimum required pressure for penetration of water in new moisture barrier fabrics is 25 psi (172 kPa) according to NFPA 1971 standard [2]. Since the size of the available test cell for this experiments was not the same as the standard test cell, the results of this experiment may differ to some extent from the results for an experiment based on the standard test cell. Therefore, it is difficult to draw a firm conclusion at which thermal exposure decreased the water penetration pressure to less than the minimum requirement specified in NFPA 1971.

4.6. Tear strength test

Experiments were repeated three times for each specimen based on procedure in section 2.6. Figure 4.15 shows the average values for tear strength of moisture barrier specimens after exposure to a certain heat flux for particular duration. Data labels in the figure present numerical value of average tear strength. The bars indicate the standard error of the mean for three independent tests.

The figure reflects two trends in tear strength of specimens after thermal exposure. The first trend observed after relatively low intensity or short duration of thermal exposure is an increase in the tear strength of specimens. It seems that the first trend is dominant after low to moderate thermal exposures causing early stages of degradation in a specimen fabric. The second trend is a decrease in tear strength after more intense thermal exposure. This could be related to commencement of major decomposition of a specimen fabric. A membrane is a thin delicate film and is laminated to a support fabric (substrate) to increase mechanical strength of moisture barrier. So, tear strength of moisture barrier specimens depend on mechanical strength of both constituents.

After exposure to 5 kW/m^2 for 600 s to 2400 s, tear strengths of specimens changed by maximum ±5% of the value for an unexposed specimen. Temperature measurement (Figure 4.5) showed that the maximum temperature of specimens during thermal exposure to 5, 10, and 15 kW/m^2 was not high enough to cause major decomposition (Figures 4-3-4.4) in moisture barrier fabrics. The specimens reached temperatures in the range of 200°C to 280°C during exposure to 5, 10, and 15 kW/m^2 for durations in the test matrix (Table 4.1). This range of temperature is below 300°C when TGA curves (Figures 4.3 and 4.4) indicated a weight loss around 10% for the substrate and membrane of the moisture barrier specimen. After exposures to 10 kW/m^2, tear strength of specimens increased with duration of exposure. The tear strength

increased by roughly 5% to 50% after exposure to 10 kW/m^2 for 30 s and 300 s, respectively. The rise in tear strength was not uniform though. While tear strength of a specimen increased by 15% after a 150-s exposure, it increased by approximately 50% after a 300-s exposure. Such a jump in tear strength of specimen was also observed after exposure to 15 kW/m^2 for 30 s. Tear strength of a specimen increased by 5% after exposure to 15 kW/m^2 for 15 s whereas it rose by 30% after 30 s of exposure to the same heat flux. Furthermore, the abrupt rise in tear strength of specimens exposed to 15 kW/m^2 was observed after shorter exposures than those specimens exposed to 10 kW/m^2. The sharp increase in tear strength might be because of activation of a mechanism (crosslinking) in degradation of specimen fabric. A certain level of energy might be required to trigger this mechanism. It may be why the steep increase in tear strength of specimens was observed earlier in more intense thermal exposure.

Crosslinking is a major mechanism in chemical changes of polymers. One polymer chain is connected with an adjacent one by creation of a bond. Crosslinking usually occurs after chain stripping. It is especially important in char formation, which creates a high molecular weight and consequently less volatilized structure. Dipolar, hydrogen, or van der Waals forces facilitate the link between the neighbouring chains. The link is called a crosslink, which influences the physical properties of the polymer. Crosslinking increases char formation. As a result of crosslinking, the polymer becomes stronger, stiffer, and more brittle (less ductile). Crosslinking may increase mechanical strength of the polymer, while other chemical mechanisms such as chain scission decrease it [86]. The increase in tear strength of moisture barrier specimens has been reported in other studies and has been attributed to crosslinking [22].

Further degradation as a result of more intense or longer thermal exposure can affect other mechanisms of decomposition such as chain scission. In exposure to 20 kW/m^2, specimens reach approximately 400°C which is high enough for major decomposition in both substrate and membrane of the specimen according to Figures 4.3-4.5. This could be the reason why a 55% loss in tear strength of the specimen was measured after exposure to 20 kW/m^2 for 300 s.

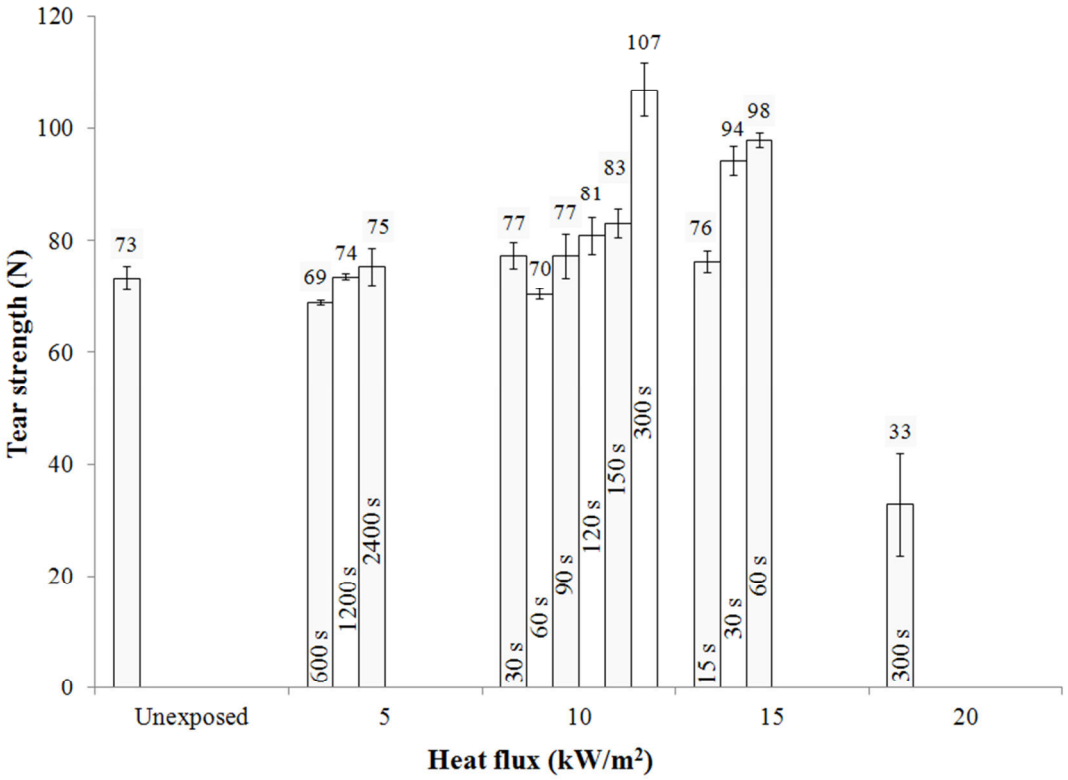

Figure 4.15: Tear strength of moisture barrier specimens after thermal exposure

This chapter focused on the change in some aspects of performance of moisture barrier specimens made of an ePTFE-based fabric. The aspects of interest were WVTR, water penetration pressure, and tear strength of specimens. The experiments revealed that WVTR did not decrease after selected thermal exposure, which is actually advantageous in performance of firefighters' protective clothing. A decrease in WVTR can reduce thermal comfort, and increase the risk of heat stress and steam burns. Water penetration pressure decreased by 40% after exposures to 10 and 15 kW/m^2. However, it might be almost 20% less than the minimum standard requirement (25 psi) for new moisture barrier fabrics. The water penetration pressure dropped by 85% only after an intense exposure to 20 kW/m^2 for 300 s. Tear strength increased after thermal exposure selected for this research except for an intense exposure to 20kW/m^2 for 300 s. Based on the changes in WVTR, water penetration pressure, and tear strength of the moisture barrier fabric exposed to specific thermal exposures in this research, water penetration pressure for thermally aged moisture barrier specimens deteriorates faster and more severely in

the range of thermal exposures considered here, and should receive more attention in future research.

Among the aspects of performance studied in this research, water penetration pressure demands more attention since it had the largest decrease after the thermal exposures selected for this research. However, it did not decrease further and reached a steady value after longer exposures to 10 and 15 kW/m^2. These exposures represent ordinary and early stage of emergency conditions on the fire ground (incident heat fluxes of 20 and 30 kW/m^2 on the outer shell layer of firefighters' protective clothing. Based on experiments in Chapter 3, tensile strength of specimens decreased faster and more severely under these conditions. For instance, the tensile strength of the outer shell specimen decreased by 60% after a 30 s exposure to 30 kW/m^2 which is equivalent to an exposure to 15 kW/m^2 for moisture barrier specimens. Comparison of changes in the water penetration pressure of the moisture barrier fabric with the change in the tensile strength of the outer shell fabric indicates that mechanical strength of outer shell is demanding the most attention in this research.

5. MULTI-STAGE EXPOSURE EXPERIMENTS[4]

It was discussed in section 1.5.2 that if a thermal exposure occurs in multiple stages rather than a single stage, the number of stages can influence the rate of change in performance of firefighters' protective clothing. In practice, firefighters wear their protective clothing repeatedly over its service life. They also need to leave the fire scene to refill their breathing apparatus almost every half an hour. On the one hand, single-stage exposures may not simulate thermal ageing of firefighters' protective clothing closely. Therefore, there is a need to compare the effect of multi-stage and single-stage thermal exposures in this research project [87]. In this chapter, specimens will be exposed to multi-stage exposure and tensile strength of outer shell fabrics and tear strength, penetration pressure, and water vapour permeability of moisture barrier fabrics will be measured and discussed.

5.1. Preparation of specimens

Two groups of tests were carried out in order to investigate the effect of multi-stage thermal exposure on firefighters' protective clothing. In the first group, specimens were composed of three layers of a firefighters' protective clothing. Fabrics which are used in construction of three layers of firefighters' protective clothing were cut to similar dimensions. They were placed on top of each other as a bundle and were thermally exposed to the conical heater in a single stage and then in multiple stages. In the second group of tests, experiments in Chapter 4 were repeated for the same moisture barrier specimens after being thermally exposed in multiple stages.

In the first part and in order to simulate three layers of firefighters' protective clothing in the experiments, specimens consisted of an outer shell, a moisture barrier, and a thermal liner. The orientation of the three layers of the specimen was the same as in firefighters' protective clothing. The outer shell fabric was exposed to the conical heater. The moisture barrier was placed in such a way that its substrate was in contact with the outer shell and its membrane was in contact with the thermal liner. The thermal liner's face cloth was on the unexposed side of the specimen.

[4] A portion of this chapter has been published in ASTM Special Technical Publication, 1544 STP [87].

Four protective fabrics used in construction of the three layers of firefighters' protective clothing were considered in this work: Guardian® 750, Guardian® 790, Stedair® 3000, and XE-289. Guardian® 750 and Guardian® 790 are a blend of 60% Kevlar® and 40% PBI with a surface weight of 255 and 268 g/m^2, respectively and are used as outer shell fabric for firefighters' protective clothing. The Guardian® 750 outer shell was undyed and therefore was the natural light brown colour of these fibres and will be called the brown Kevlar®/PBI outer shell in the rest of this thesis. The Guardian® 790 was a piece-dyed fabric (i.e., the fabric was dyed after being woven), and was black in colour and therefore, it will be called the black Kevlar®/PBI outer shell in this thesis. Two colours for outer shell fabrics will assist in evaluating the effect of colour on the capacity of the non-destructive techniques to predict the tensile strength of outer shell specimens in chapters 6 and 7. Stedair® 3000 is an ePTFE (Expanded Polytetrafluoroethylene) based moisture barrier laminated to Nomex® E89™. The surface weight of the fabric is 180 g/m^2. Stedair® 3000 is heavier than Stedair® 4000 used in chapter 4 and ensembles with this moisture barrier have a higher TPP rating and lower THL than ensembles containing a Stedair® 4000 moisture barrier. XE-289 is a three-layer fabric with a surface weight of 244 g/m^2 and is used as a thermal liner in firefighters' protective clothing and is made of Nomex® E89™. This thermal liner consists of two nonwoven layers and a dyed aramid face cloth.

Thermal ageing of specimens was conducted in a similar manner to the procedure in section 2.2. Two different sets of specimens were thermally aged using single and multiple exposures. A heat flux of 20 kW/m^2 was selected for the purpose of thermal ageing of specimens, as it represents the ordinary range of conditions in Table 3.1. It is also very similar to the 21 kW/m^2 heat flux that is used in several standards for flame resistant clothing [79]. Specimens for thermal ageing were cut to 15.2 cm by 10.2 cm (6 in. by 4 in.) from the aforementioned fabrics of each layer. Ensembles with both outer shell fabrics were tested. A peripheral margin of the specimen was covered with metal bars to constrain the exposed area to the central part of the specimen. The exposed area of the specimen, 8.5 cm by 5.8 cm, was used as the interrogation area later in chapter 6.

Specimens were then thermally aged using exposures to a heat flux level of 20 kW/m^2 in two ways. The first group of specimens underwent a single exposure, while the second group was exposed multiple times. Specimens in the first group experienced a single exposure for durations of 15, 30, 45, 60, 90, 120, and 150 s. Specimens in the second group were exposed to 2, 3, 4, and

5 stages of 30 s thermal exposures. After each exposure, specimens were cooled down to approximately the laboratory temperature for 5 min., and then exposed to the conical heater for the next exposure of 30 s. Hence, these specimens underwent total thermal exposures of 60, 90, 120, and 150 s. This allowed the effects on the fabric performance of single and multiple thermal exposures of the same total duration to be compared. Photographs of the specimens after single and multiple exposures are shown in the Appendix C. Table 5.1 shows the test matrix of experiments for multi-stage thermal exposure. A single thermal exposure for 300 s and correspondingly 10 stages of thermal exposure were conducted for black specimens only.

Table 5.1: Duration of single-stage exposure and the equal number of 30-second stages in multiple-stage exposure to a heat flux of 20 kW/m^2

Total duration of exposure (s)	30	60	90	120	150	300
Number of 30-second stages	1	2	3	4	5	10

In the second group of tests, a single layer of moisture barrier was used as a specimen since the moisture barrier layers of the first group of the specimens were already used for tear strength tests. Extra moisture barrier specimens were required to investigate the effect of multi-stage exposure on water penetration pressure and water vapour transmission rate of a moisture barrier fabric and compare them with the corresponding parameters after single-stage exposure. The moisture barrier fabric, Stedair® 4000, was the same fabric used in experiments in chapter 4. Earlier in this section, it was discussed that a heat flux of 20 kW/m^2 was selected for the thermal ageing of outer shell specimens. Based on heat flux measurement in section 4.1, an incident heat flux of 20 kW/m^2 was translated into a heat flux of 10 kW/m^2 for moisture barrier specimens. Therefore, heat flux of 10 kW/m^2 was chosen to investigate the effect of multi-stage exposures on performance of moisture barrier specimens. Thermal ageing of moisture barrier specimens were conducted the same as procedure in section 2.2. Single-stage and multiple stages of 30 s exposures to heat flux of 10 kW/m^2 were performed for durations in Table 5.1. An air blower was used to accelerate the cooling of specimens. So, a 5 min. gap between consecutive stages of exposure was enough for the specimens to reach lab temperature. Then, water penetration, and water vapour permeability tests were run for the exposed specimens.

5.2. Thermogravimetric analysis

In a similar fashion to section 2.3, thermogravimetric analysis of the specimen fabrics was performed to point out critical temperatures in degradation trend of fabric materials. The only difference is that TGA was conducted in nitrogen environment only for the brown and black Kevlar®/PBI outer shell fabrics in this section. The presence of oxygen speeds up chemical reactions. Comparing TGA curves in nitrogen and air environments for Nomex® and Kevlar® shows that the weight loss peaks in both environments would occur at similar range of temperatures [78,80] even though the remaining combustion process will be different.

Figures 5.1-5.2 illustrate TGA curves for brown and black Kevlar®/PBI fabrics, respectively. The mass loss curves for both fabrics are similar. It is expected since the fabrics are made of the same fibres. Similar to section 3.2, colour of fabrics did not have a significant effect on the weight loss trend since TGA curves are similar for both brown and black Kevlar®/PBI fabrics. At the early stages of experiments at a temperature range of 70°C to 100°C, the weight loss is because of moisture release from the specimen. The curves showed that the specimen contained around 7% moisture, which is in agreement with manufacturers' data [78]. The specimen weight remained constant until it reached a temperature about 200°C. Within the temperature range of 300°C to 550°C, the specimen weight decreased gradually. By reaching 550°C, the specimen lost 15% of initial weight. At this temperature, a sharp decrease in weight occurred. A similar trend for the weight loss was observed for the black outer shell fabric.

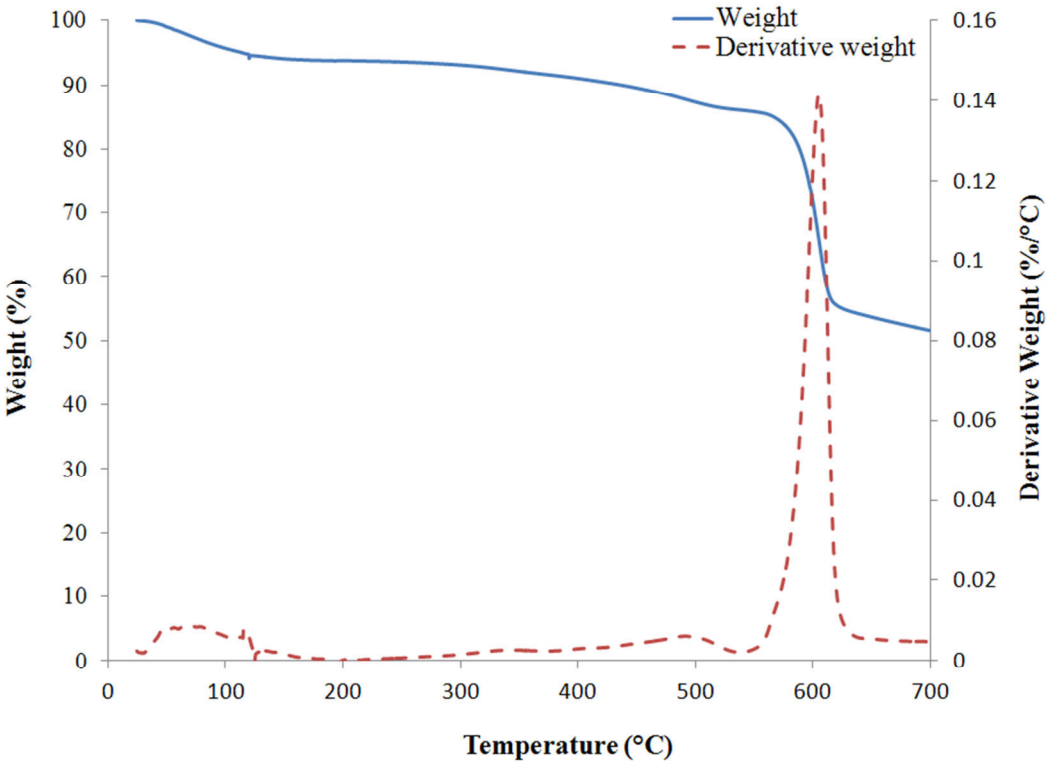

Figure 5.1: TGA curve for brown Kevlar®/PBI outer shell fabrics

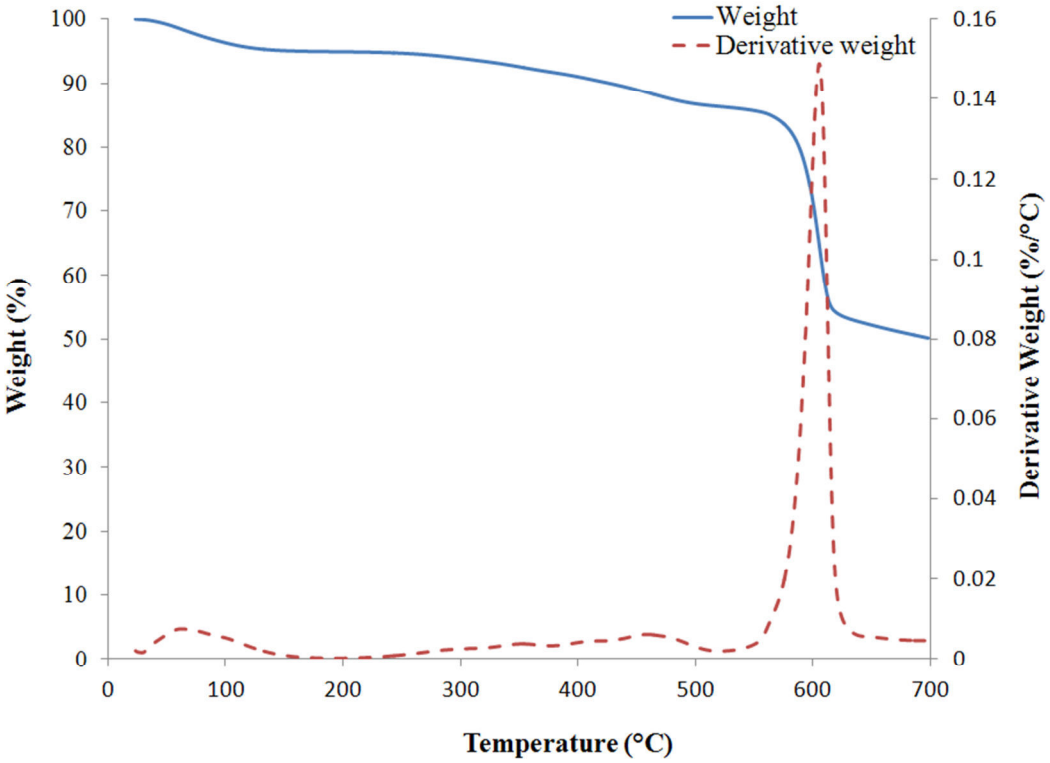

Figure 5.2: TGA curve for black Kevlar®/PBI outer shell fabrics

The TGA curve for the membrane side of moisture barrier specimens is plotted in Figure 5.3. The weight loss trend is very similar to the one for Stedair® 4000 fabric used in chapter 4 since the membrane is made of ePTFE in both fabrics. The same as Figure 4.3, the membrane started decomposing slowly at 220°C. The weight loss trend was stronger after the specimen reached 300°C. The specimen had lost 50% of weight when the temperature increased to 400°C. A sharp peak in the weight loss trend was observed around 500°C and the specimen decomposed completely by about 600°C.

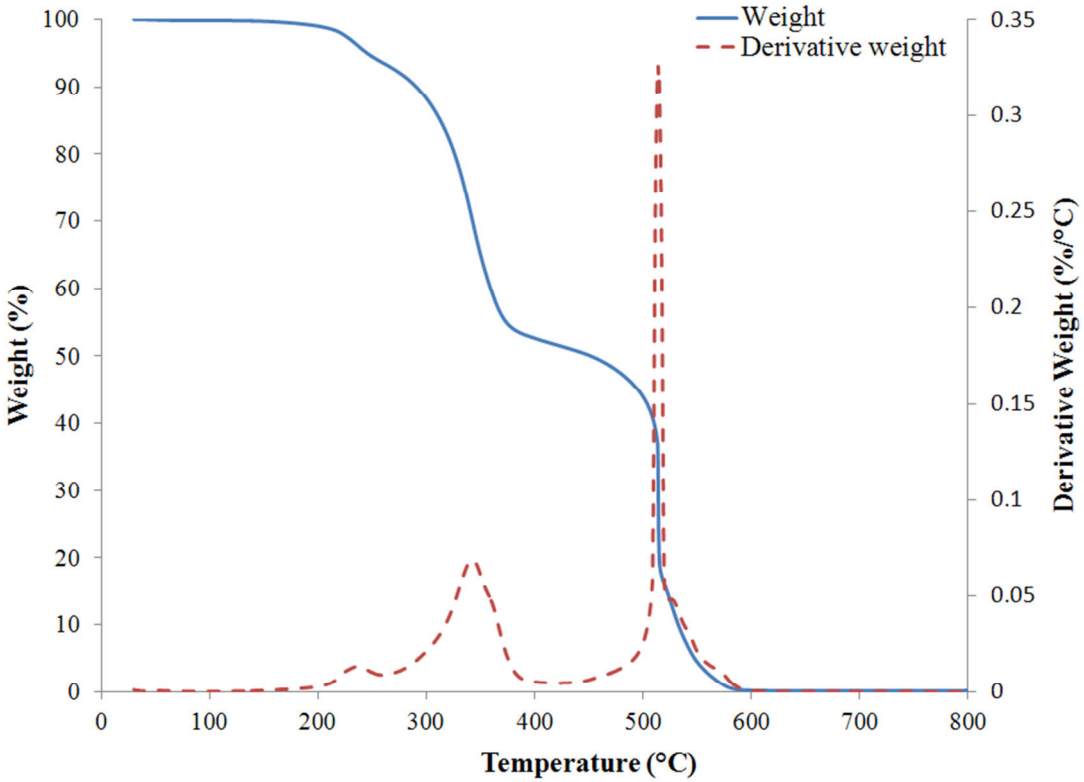

Figure 5.3: TGA curve for membrane side of Stedair®3000 moisture barrier specimen

Figure 5.4 illustrates the weight loss trend for Nomex® E89™ used as a substrate in the moisture barrier specimens. At the beginning of the experiment, 2-3% weight loss occurred as a result of moisture release. The first peak of weight loss occurred around 280°C and the specimen weight decreased by roughly 20% when it reached 330°C. One minor peak at 420°C and one sharp peak at 480°C occurred and the by the time the temperature reached around 600°C, the specimen decomposed completely.

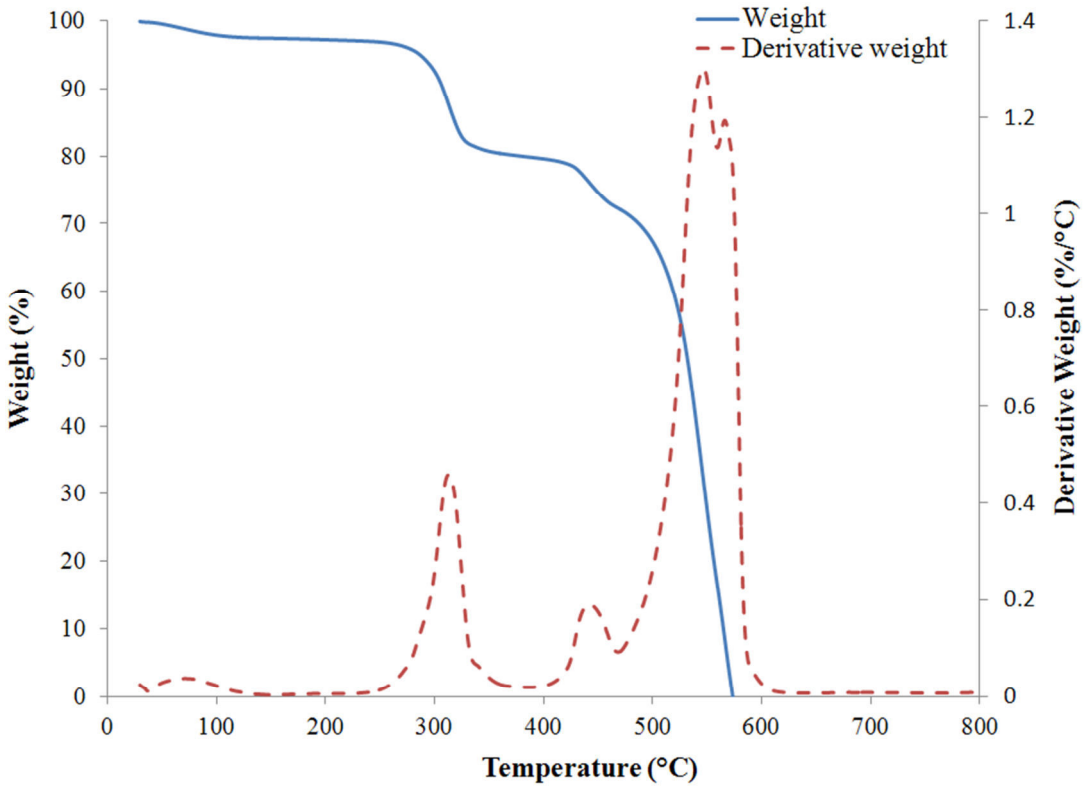

Figure 5.4: TGA curve for substrate side of moisture barrier specimen

5.3. Temperature measurements

In order to interpret the changes in the performance of the fabrics evaluated, temperatures of different layers of ensembles with the undyed brown Kevlar®/PBI outer shell were measured during exposures to incident heat fluxes of 20 kW/m^2 using the same procedure in section 2.2. It is expected that temperature profile of black outer shell specimens would be similar to the brown Kevlar®/PBI specimens since both fabrics are made of the same fibres with similar surface weight and only different in colour. In addition, similarity between TGA curves for both fabrics in Figures 5.1-5.2 indicates this point.

Specimens were exposed to the conical heater in three stages in each test. Individual tests were repeated two times. Figure 5.5 depicts the temperature profiles of front and back sides of individual layers for the three stages of exposure. As this research project is focused on the performance of the outer two layers, the temperature history of the thermal liner is not included in the figure. Stages of exposure to heat flux of 20 kW/m^2 were selected to be 6 min. to assure reaching steady-state temperature. After each stage of exposure, approximately 40 min. was

required for the specimen to cool down and reach the laboratory temperature. Although the shutter was closed, limited heat transfer occurred to the specimen through the shutter. This is the reason why the specimen was not at room temperature at the beginning of the experiment or at the end of each stage of thermal exposure.

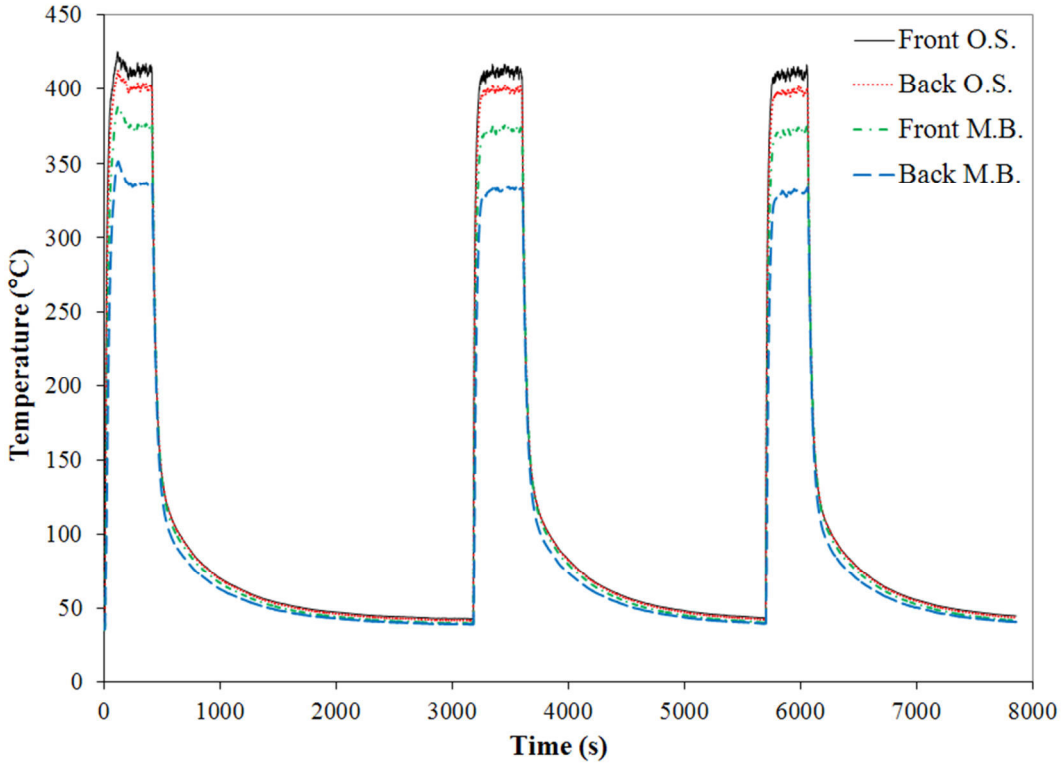

Figure 5.5: Temperature history of front and back sides of outer shell and moisture barrier layers of specimens during exposure to 20 kW/m^2 for three consecutive stages

The averages of the values for the maximum temperature measured during each stage of exposure to heat flux of 20 kW/m^2 are presented in Table 5.2. The maximum temperature of the outer shell is approximately 420°C which is in the temperature range that degradation of the outer shell material is expected to occur based on TGA results (Figure 5.1). The effect of the thermal exposure on the specimen in the first stage of exposure is different from that in the second and third exposures. First, a small temperature drop is observed in the first exposure before reaching steady-state condition. This may indicate that the specimen has undergone some

thermal degradation at this temperature. As a result of the drop, the temperature of the specimen decreases about 10°C.

Table 5.2: Maximum temperatures (°C) achieved by different layers of ensemble during exposures to incident heat flux of 20 kW/m^2 (undyed Kevlar®/PBI brown outer shell)

Layer & orientation of the specimen \ No. of stage of exposure			1	2	3
Outer Shell	Front side	No. 1	420	414	412
		No. 2	417	411	416
	Back side	No. 1	413	405	403
		No. 2	410	403	405
Moisture Barrier	Front side	No. 1	380	362	361
		No. 2	381	366	371
	Back side	No. 1	351	329	327
		No. 2	338	324	325

The maximum temperature of the moisture barrier also decreased in subsequent exposures. This may indicate degradation of the moisture barrier. Temperature measurement in Table 5.2 shows that the substrate and membrane of moisture barrier specimens reached 380°C and 345°C during thermal exposure, respectively. These temperatures are beyond the temperatures that significant decomposition of substrate and membrane fabrics began (Figures 5.3-5.4).

It might be beneficial to interpretation of changes in the mechanical strength of specimens after particular duration of exposure if it was known which temperature a specimen reached at the end of each exposure. Table 5.3 specifies the temperature of specimens after various duration of exposure. The information in this table is extracted from Figure 5.5. Temperature measurements show that specimen layers reached their maximum temperature after almost 120 s. After 120 s, temperature of specimen dropped gradually, as it was described earlier in this section. The outer shell layer of the specimen reached 270°C after only 15 s, which is high enough for commencement of degradation.

Table 5.3: Temperature of brown Kevlar®/PBI outer shell specimens after particular duration of exposure

Duration of exposure (s) / Temperature (°C)		15	30	45	60	90	120	150	300
Outer Shell	Front side	270	352	387	397	414	420	418	413
	Back side	236	329	367	384	402	410	406	401
Moisture Barrier	Front side	159	266	324	349	379	387	382	376
	Back side	102	207	268	305	341	351	343	337

5.4. Tensile tests

All three layers of specimens were cut to 15.1 cm by 10.2 cm (6 in. by 4 in.) from the aforementioned fabrics of each layer for thermal ageing. Ensembles with both brown and black Kevlar®/PBI outer shell fabrics were tested. A peripheral margin of the specimen was covered with metal bars to constrain the exposed area (8.5 cm by 5.8 cm) to the central part of the specimen.

Since mechanical strength of fabrics differ in warp and fill directions, specimen layers were cut from both directions of two brown and black Kevlar®/PBI outer shell fabrics. For each individual thermal exposure condition (duration and number of exposure combination), four specimens were prepared: two specimens from the warp direction and two specimens from the fill direction. After the thermal exposures, the tensile strength of the outer shell of the thermally aged specimens was measured based on procedure in section 2.5. NFPA 1971 mandates a minimum value of 623 N for the tensile strength of the outer shell layer of new firefighters' protective clothing in any direction. This requirement is shown in Figures 5.7-5.10, which include the tensile testing results. In the figures, a duration of 0 indicates an unexposed outer shell fabric.

Figures 5.7-5.10 depict the tensile strength of the brown and black Kevlar®/PBI outer shell fabrics in fill and warp directions after single-stage and multi-stage exposures. Multi-stage exposures are in fact multiple 30-s exposures performed consecutively. In order to display the rate of reduction in tensile strength more clearly, Figure 5.10 illustrates the tensile strength of specimens of both brown and black Kevlar®/PBI outer shell fabrics after single-stage exposure for the certain duration in both fill and warp directions as a percentage of tensile strength of the

unexposed fabric. Figure 5.10 implies that rate of reduction in tensile strength of specimens is the same for both warp and fill directions.

The figure shows that the tensile strength of both colours of outer shell fabrics decreased by around 15% from the value for new fabrics after only 15 s of exposure to 20 kW/m^2. Temperature of specimens after 15 s was high enough for some levels of degradation in specimens based on TGA curves in Figures 5.1-5.2 and Table 5.3. After 30 s of exposure, the specimens lost 40% of initial tensile strength and the tensile strength of both outer shell fabrics did not meet the NFPA 1971 standard requirement for a new outer shell fabric. The tensile strength continued to decrease after subsequent exposures. After exposure for 150 s, tensile strength of brown and black Kevlar®/PBI specimens was reduced by 55% and 65%, respectively. The incremental decrease after the subsequent exposures was much less than the initial decrease after the first 30 s exposure.

Figures 5.7-5.10 also compare the decreases in tensile strength for single and multiple exposures of the same total duration for both outer shell fabrics. For both fabrics a given total duration of thermal exposure produces a smaller reduction in tensile strength of the outer shell fabrics if the exposure is done in several stages rather than one stage. This result can be explained in terms of the higher maximum temperature that the outer shell fabrics reach in a single exposure of a given total duration than in multiple 30 s exposures that produce the same total duration of exposure. For example, temperature measurements shown in Table 5.3 would indicate that the brown outer shell fabric should reach a maximum temperature of approximately 415°C at the end of a 90 s exposure to 20 kW/m^2, while if the 90 s total duration exposure was done in three 30 s stages, the fabric should reach a temperature of approximately 350°C at the end of each 30 s stage. This difference in maximum temperature would mean that the fabric should undergo more thermal degradation in the single 90 s exposure than in three 30 s thermal exposures.

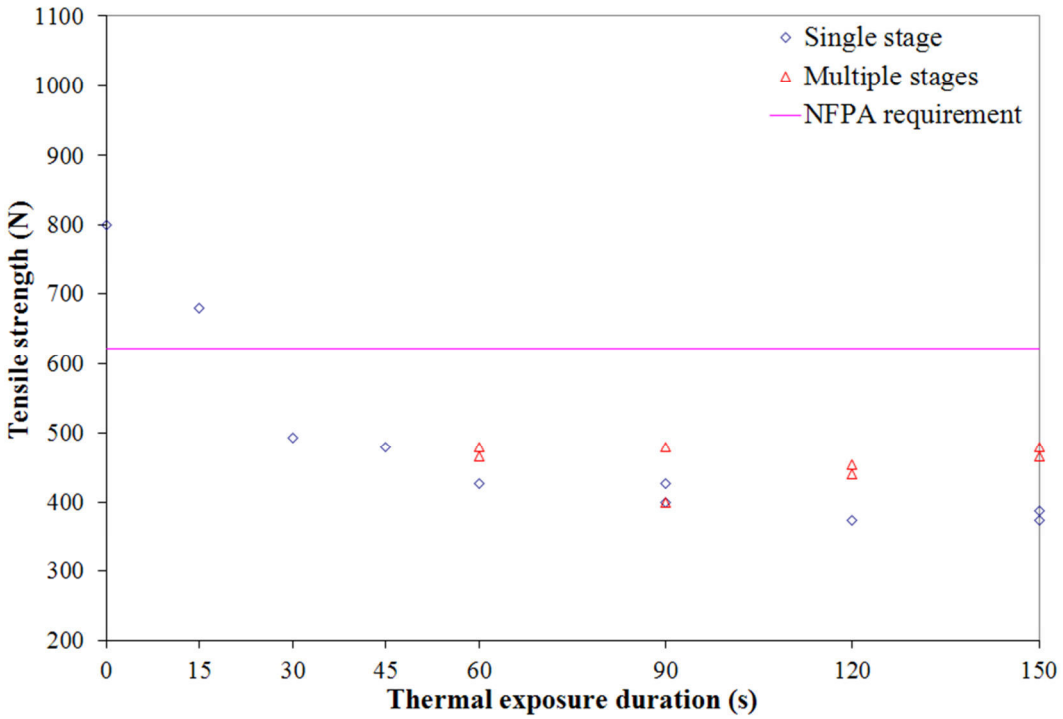

Figure 5.6: Tensile strength of brown Kevlar®/PBI outer shell fabric along fill direction

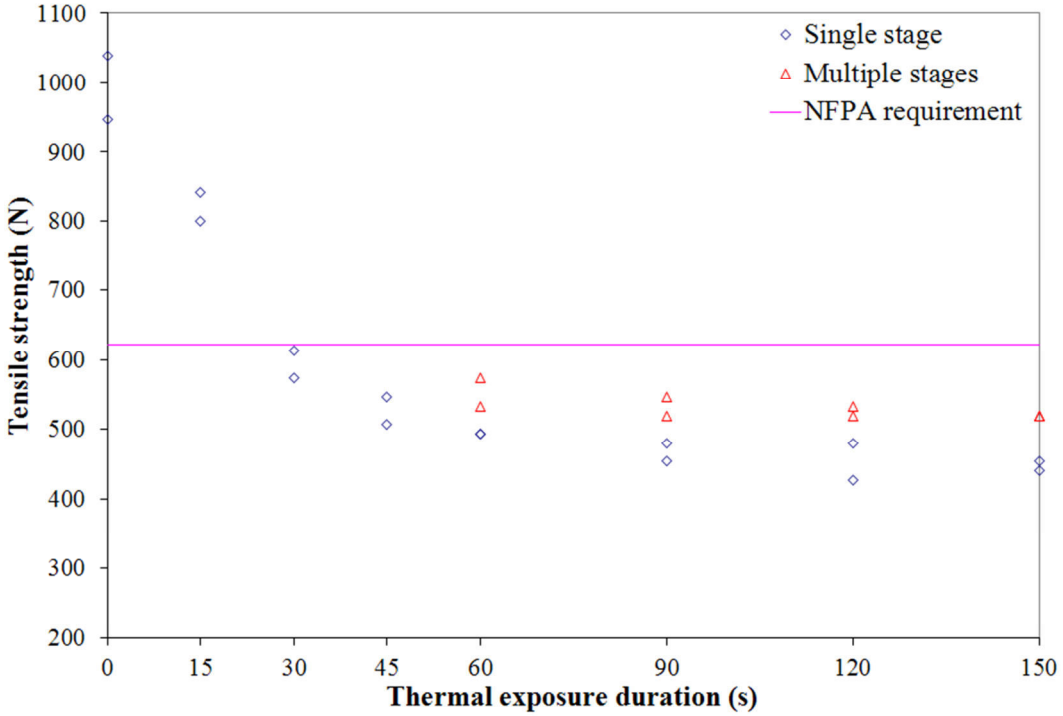

Figure 5.7: Tensile strength of brown Kevlar®/PBI outer shell fabric along warp direction

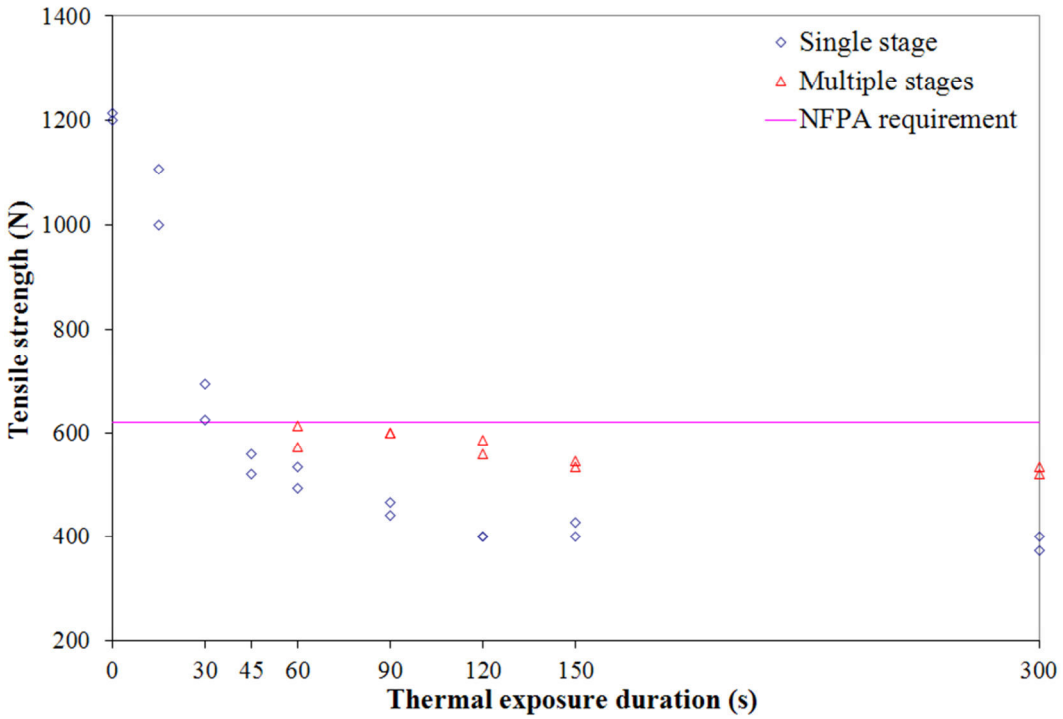

Figure 5.8: Tensile strength of black Kevlar®/PBI outer shell fabric along fill direction

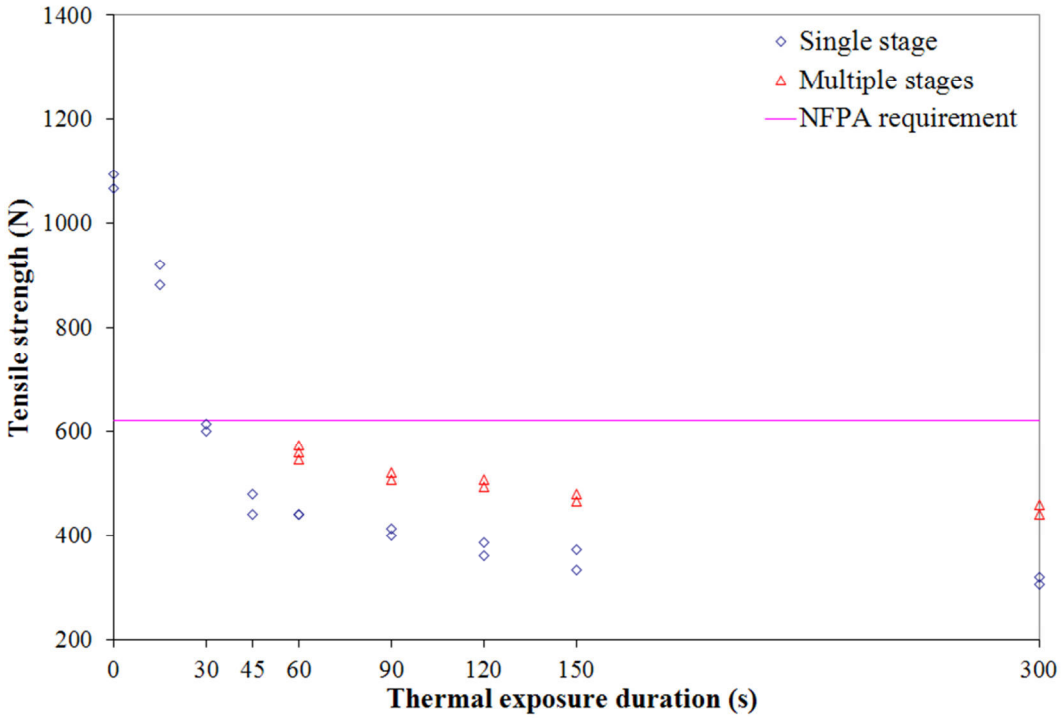

Figure 5.9: Tensile strength of black Kevlar®/PBI outer shell fabric along warp direction

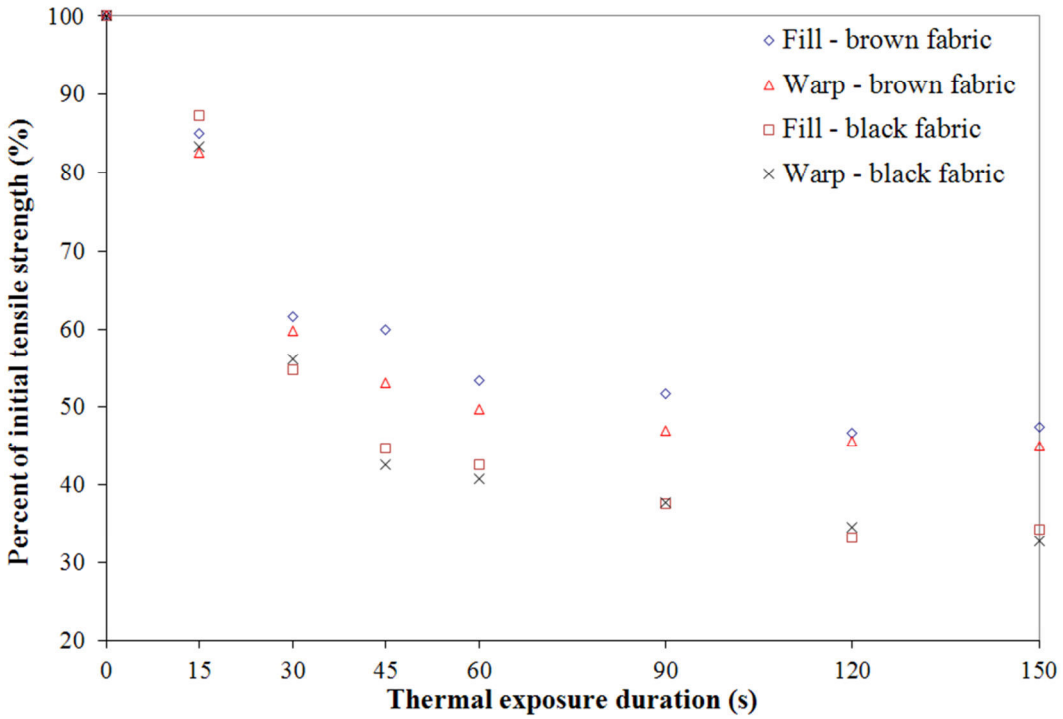

Figure 5.10: Tensile strength of brown and black Kevlar®/PBI outer shell specimens as percent of initial tensile strength after single exposure for particular duration

5.5. Tear strength

In the first group of tests, specimens included three layers of firefighters' protective clothing. Tear strength tests were conducted on the moisture barrier layer of thermally exposed ensembles. The test procedure is the same as the one described in section 2.6. Similar to outer shell specimens, moisture barrier specimens were tested in both fill and warp directions. In single-stage exposure, the ensemble specimens were exposed to 20 kW/m^2 for 30, 60, 90, 120, and 150 s. In multi-stage exposure, the specimens were exposed to 2, 3, 4, and 5 stages of 30 s. Since brown and black Kevlar®/PBI outer shell fabrics are made of basically the same material, it is expected that moisture barriers received the same level of thermal exposure regardless of the type of the outer shell fabric. So, the tear strength of moisture barrier layers in two sets of specimens should be comparable.

Two moisture barrier specimens were thermally aged in an ensemble, the outer shell of which was brown Kevlar®/PBI fabric. The other two moisture barrier specimens were thermally aged in an ensemble with the black Kevlar®/PBI outer shell. Brown and black set in the legends

of Figures 5.12-5.15 specify which ensemble the moisture barrier specimen was selected from. Data labels next to data points in the figure show the numerical value of the average of tear strength of four specimens tested independently. The minimum requirement determined by NFPA 1971 standard for tear strength of new moisture barrier fabrics is 22 N and was specified in the figures for the sake of comparison.

Figures 5.12-5.13 depict tear strength of moisture barrier specimens along the fill and warp directions after single-stage exposure of the whole specimen to 20 kW/m^2. Within the first 45 s of thermal exposure, the average value of tear strength of specimens in both directions changed slightly (around 10%). Temperature measurement of the fabric (Table 5.3) shows that the substrate and the membrane of the specimen reached about 325°C and 270°C after 45 s of thermal exposure. Based on TGA curves in Figures 5.3-5.4, some levels of degradation could occur in both substrate and membrane of the specimen, which may cause loss in tear strength. This effect may be compensated by crosslinking reactions. Measurement uncertainty can also explain this change to some extent.

After 60 s of exposure, a downward trend was observed in tear strength in both directions. The temperatures of the substrate and membrane reached their maximum values (380°C and 340°C, respectively) eventually, and as a result of longer exposure and higher absorbed thermal energy, specimens might undergo more severe degradation. This can explain the loss in tear strength. Tear strength of specimens was reduced by approximately 75% after 150 s exposure in both directions. However, it was still above the minimum requirement (22 N) for tear strength of new moisture barrier fabric, which is set by NFPA 1971.

Figures 5.14-5.15 show the same information as Figures 5.12-5.13 but for multi-stage thermal exposures. Figures 5.12-5.13 imply that a 30 s exposure did not affect tear strength of specimens noticeably. Table 5.3 shows that substrate and membrane of specimens reached 266°C and 207°C, respectively. The corresponding temperatures in TGA curves for substrate and membrane of specimens (Figures 5.3-5.4) demonstrates that the level of degradation should be minimal. Even though specimens were exposed multiple times, they reached basically a relatively low temperature which was not high enough for severe degradation, and consequently significant reduction of tear strength. After five stages of exposure, tear strength of specimens in both directions increased by roughly 10%, which could be a result of crosslinking reactions in addition to the effect of measurement uncertainty.

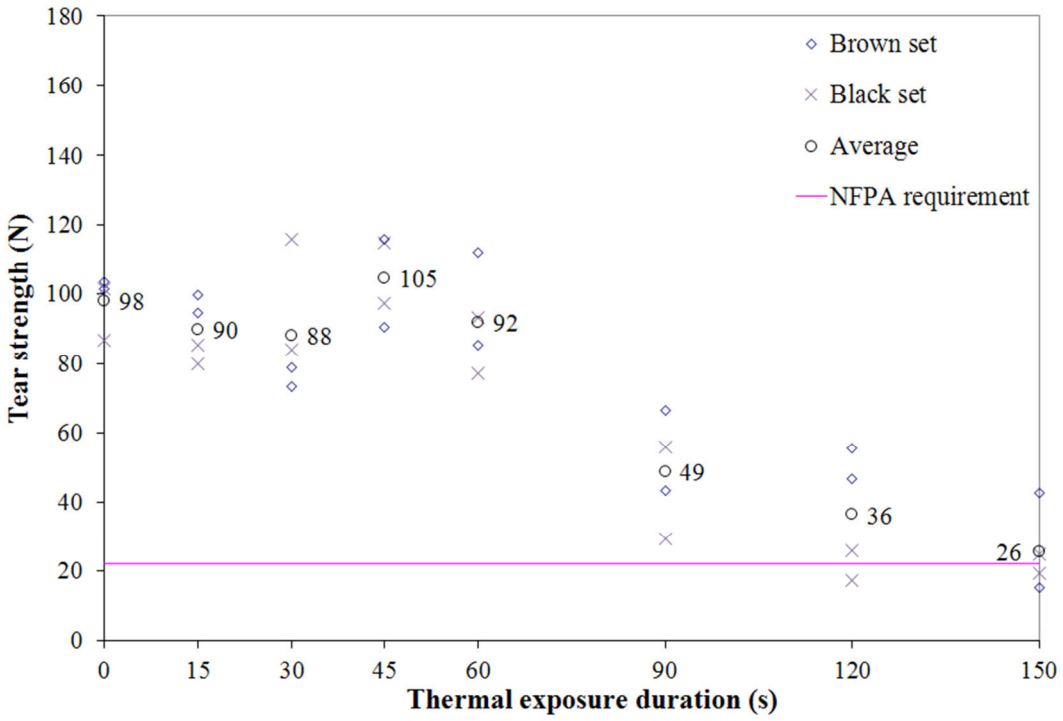

Figure 5.11: Tear strength of Stedair® 3000 moisture barrier fabrics along fill direction after single-stage exposure to 20 kW/m^2

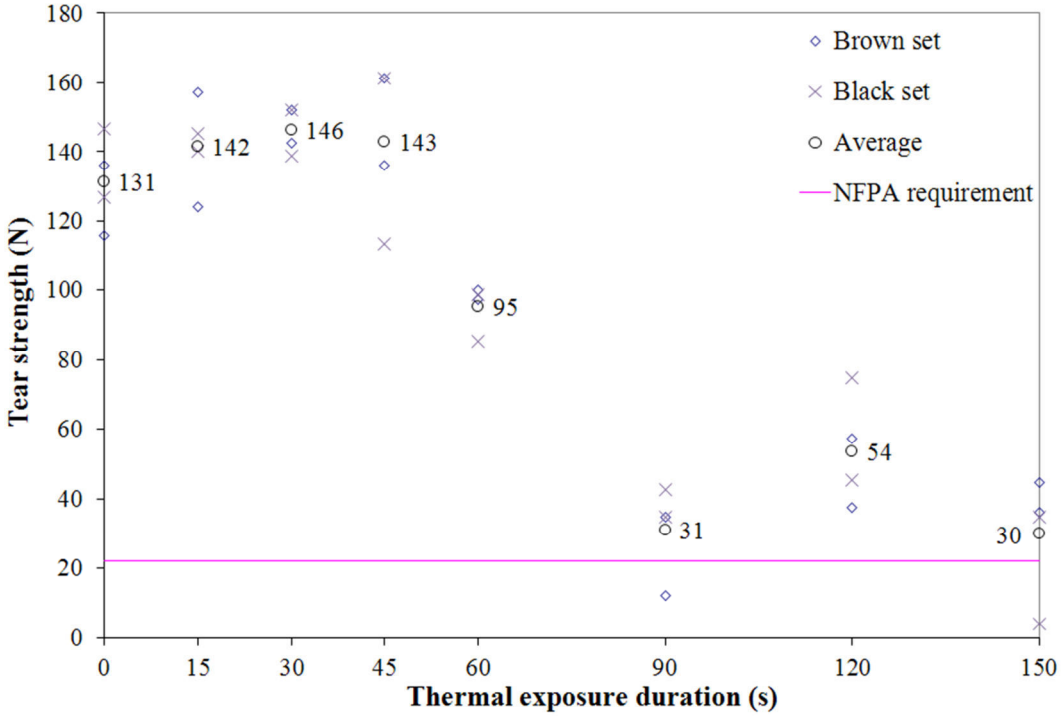

Figure 5.12: Tear strength of Stedair® 3000 moisture barrier fabrics along warp direction after single-stage exposure to 20 kW/m^2

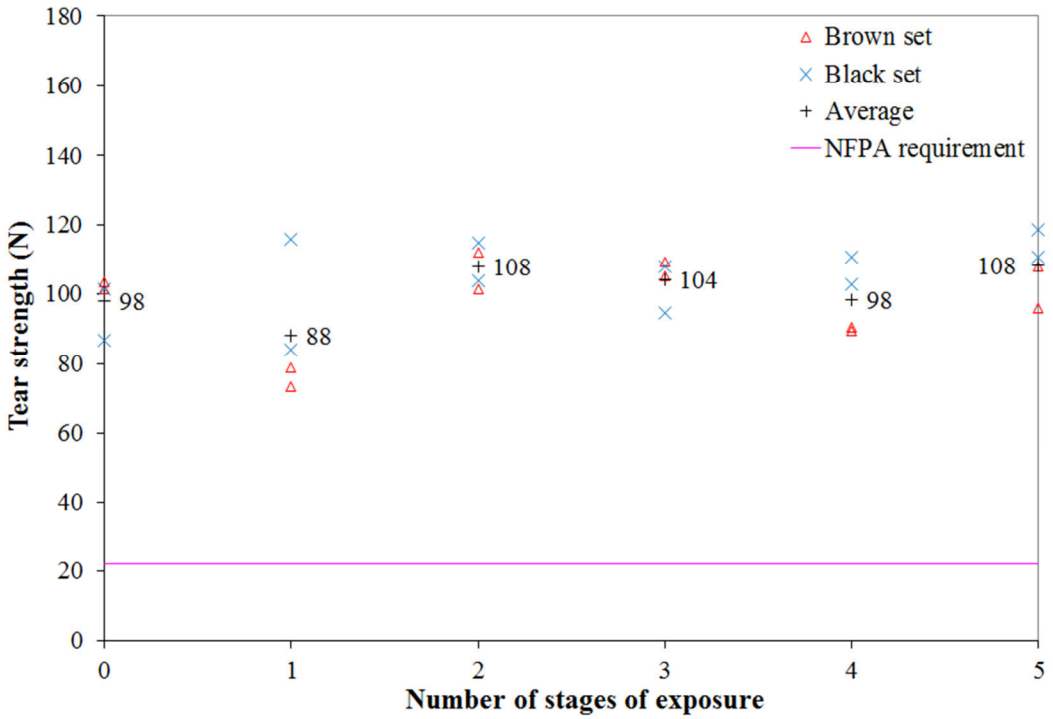

Figure 5.13: Tear strength of Stedair® 3000 moisture barrier fabrics along fill direction after multi-stage exposure to 20 kW/m^2

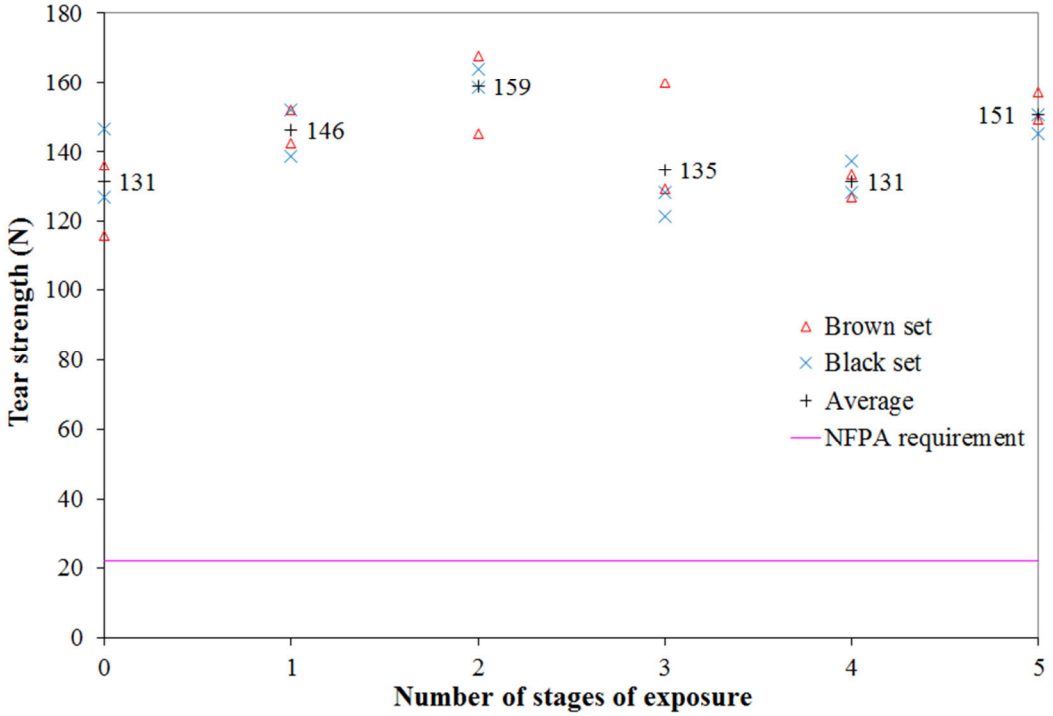

Figure 5.14: Tear strength of Stedair® 3000 moisture barrier fabrics along warp direction after multi-stage exposure to 20 kW/m^2

Figure 5.15 compares tear strength of specimens after single-stage and multi-stage exposures for both warp and fill directions. It shows tear strength of specimens by percentage of the value for an unexposed specimen. Multi-stage exposures had a minor effect on tear strength of specimens since each 30 s stage of exposure to heat flux of 20 kW/m^2 was not long enough for significant degradation of specimen fabric. Even after five stages of exposure, tear strength of specimens was still in the vicinity of the tear strength of unexposed specimens. If the length of each stage of exposure had been longer, significant change might have been observed. Specimens lost 80% of initial strength after 150 s of a single-stage exposure. The trend of change in tear strength is not similar for both directions, which may be due to the nonwoven structure of the substrate in the moisture barrier specimens.

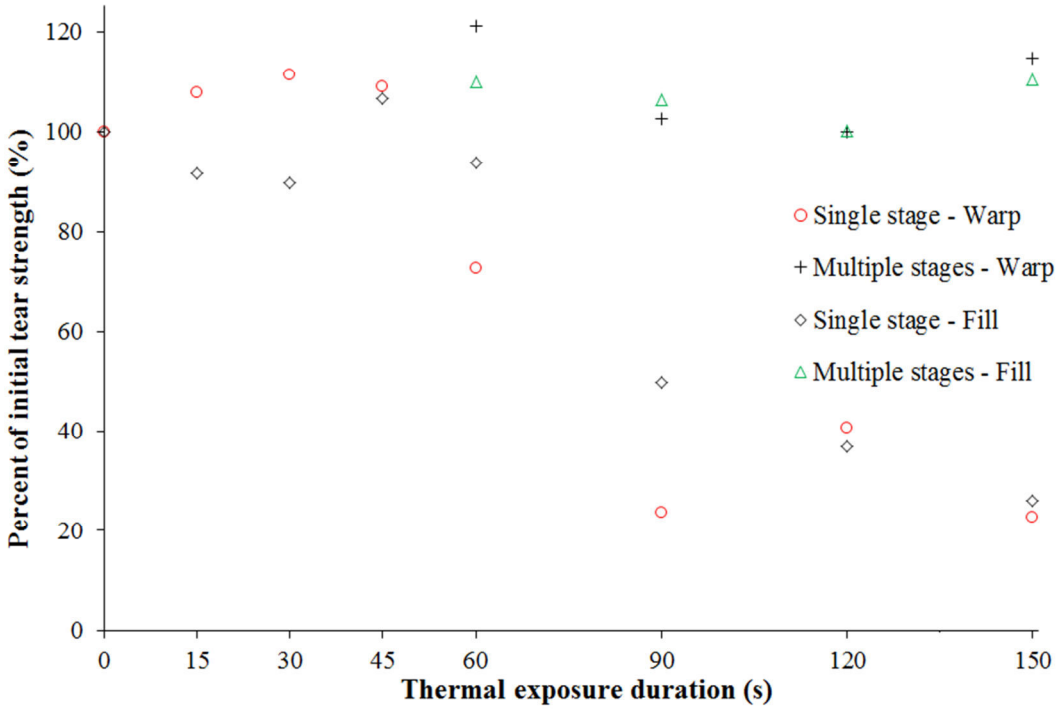

Figure 5.15: Average tear strength of Stedair® 3000 moisture barrier specimens after single and multi-stage exposures as percentage of tear strength for an unexposed specimen

5.6. Water vapour permeability test

Water Vapour Permeability Rate (WVTR) of Stedair® 4000 moisture barrier specimens were carried out using the same procedure as section 4.4 and 2.7. WVTR of thermally exposed

specimens is shown as a function of duration of a single-stage thermal exposure in Figure 4.6. Figure 5.16 presents corresponding values for specimens thermally exposed in multiple stages. Experiments were repeated on three specimens independently and the average values of WVTR are specified by data labels on top of each column. The bars represent standard error of the mean of the three independent tests.

Specimens reached 190°C after 30 s exposure to 10 kW/m^2, as was shown in Figure 4.5. This temperature was not high enough to cause significant degradation in the specimen material. Under repetitive 30 s exposures to 10 kW/m^2, minor degradation may occur in specimens. This level of damage to the specimen material did not make a substantial change in WVTR of moisture barrier specimens. Even after five stages of 30 s exposure, less than a 5% change in WVTR was observed.

Figure 5.16 also compares WVTR of specimens after single-stage and multi-stage exposures. The figure shows that the difference between WVTR of specimens increases with total duration of exposure. The discrepancy between WVTR of specimens after single-stage and multi-stage exposures increased from 5% for 60 s exposure (two stages) to 10% for 150 s exposure (five stages). Even though it was not a significant change, it may indicate that the effect of multi-stage exposure would be more significant for longer and more frequent exposures. However, a wider range of duration and number of stages is required to support this conclusion.

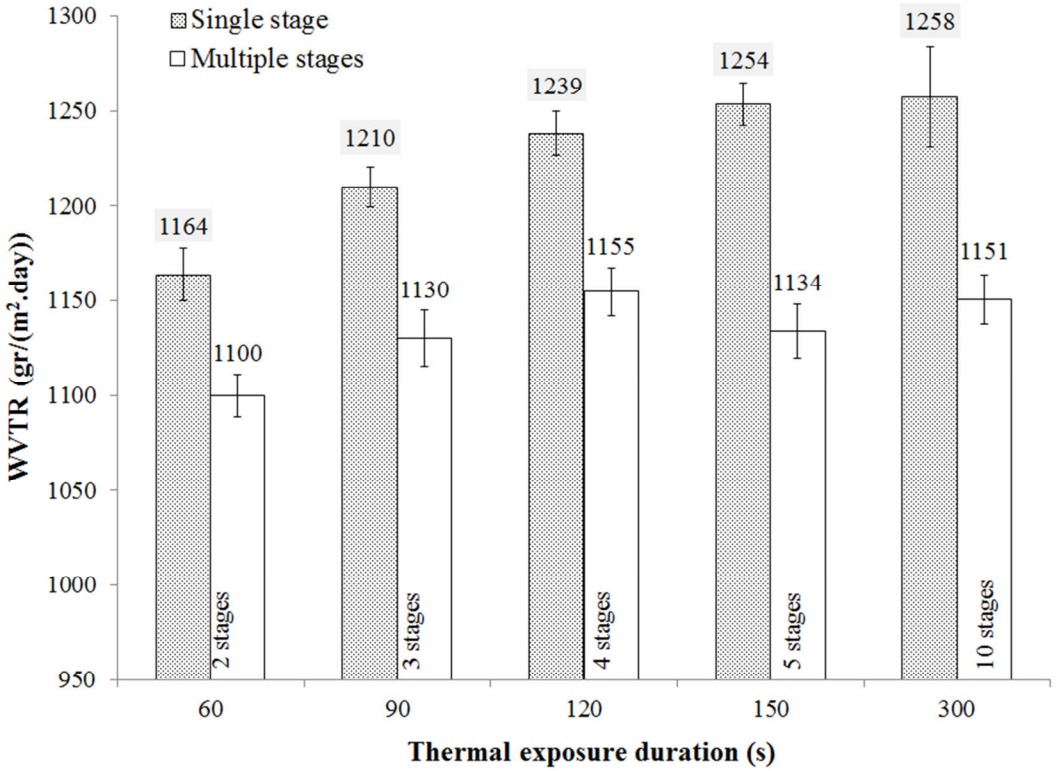

Figure 5.16: WVTR of Stedair® 4000 specimens after single-stage and multi-stage exposures

5.7. Water penetration pressure test

Water penetration tests were carried out using the same procedure as described in section 2.8. Figure 4.14 depict the required pressure for water penetration in single layer Stedair® 4000 moisture barrier specimens exposed to 10 kW/m^2 for the durations listed in Table 5.1. Figure 5.17 illustrates these values along with the values for the same fabric after multi-stage exposure. Data labels present average values of penetration pressure for three independent tests on thermally exposed specimens. The bars represent standard error of the mean of the three independent tests. Similar to results for WVTR, almost no change was observed in penetration pressure of specimens that underwent multi-stage thermal exposures. Similarly, it can be attributed to the low temperature of specimens after 30 s exposure (Figure 4.5), which was not enough for major degradation in specimens and consequently change the water penetration pressure.

Furthermore, the figure shows that water penetration pressure for specimens after multi-stage exposure is on average 5-10% higher than after single-stage exposure. Similar to section 5.6, the

results indicate minor change in water penetration pressure after multi-stage exposure. This can originate from lower degradation in specimens after multi-stage exposure. This is due to the lower temperatures reached in each stage of multi-stage exposure.

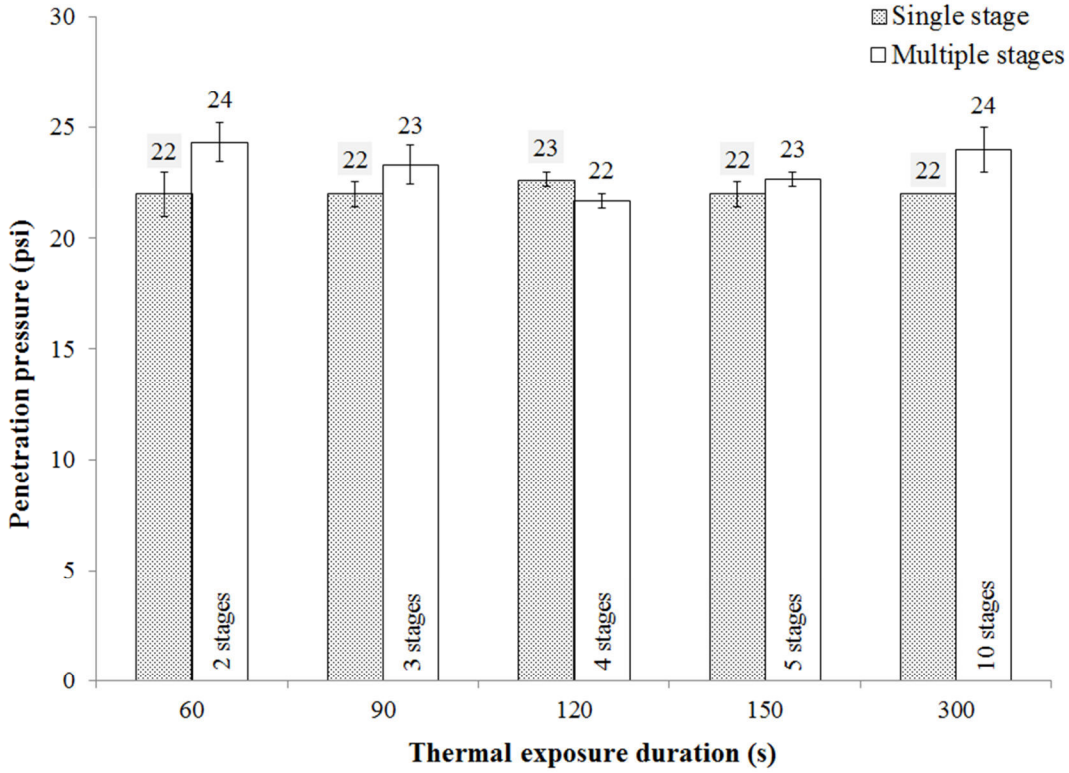

Figure 5.17: Required pressure for water penetration in Stedair® 4000 after single-stage and multi-stage exposures

In summary, the effects of multi-stage exposures on outer shell and moisture barrier specimens were studied in this chapter. It was found that the levels of deterioration in tensile strength of outer shell specimens and tear strength, WVTR, and water penetration pressure of moisture barrier specimens after multi-stage exposures were less than after a single-stage exposure for the same total duration. This was attributed to lower level of degradation in specimens after multi-stage exposure since specimens reached a lower temperature at the end of each stage than at the end of single-stage exposure. A wider test matrix which includes more exposures of different intensities and durations is required to draw more definitive conclusion on the effect of multi-stage thermal exposure. Since firefighters' protective clothing is worn many

times over the entire service life, multi-stage thermal exposure should be taken into account in order to evaluate the level of damage in firefighters' protective clothing. The test results in this chapter will be used in the remainder of the thesis to provide an opportunity to evaluate the ability of two non-destructive techniques to predict tensile strength of two outer shell specimens with different colours and materials in addition to the specimens described in chapter 3. In addition, the effect of dye used in outer shell specimens on the ability of these non-destructive techniques to predict tensile strength will be considered in chapter 7 using the test results in this chapter.

6. NON-DESTRUCTIVE EXPERIMENTS

In section 1.5, it was explained that non-destructive techniques include a broad variety of test methods. They are implemented to assess performance of an in-use system while causing either no, or marginal, damage. These methods are economical and save time and can reduce the possibility of costly accidents and catastrophes. In non-destructive techniques, specific properties of a material, or in general, any signal parameter which changes as a result of damage in the material or flaw in the system, are evaluated on a quantitative or qualitative basis. Then, deviation from the initial value of the signal parameters in a healthy system is linked to the change in desired aspect of performance of the system.

In order to choose appropriate non-destructive techniques for evaluation of in-use firefighters' protective clothing, a feasibility study was conducted and concentrated on several factors. These factors were availability of equipment, cost and time effectiveness, simplicity, and potential for future commercialization. Common fabrics used in making firefighters' protective clothing are highly resistant to electricity. So, non-destructive techniques based on electrical conductivity or magnetic permeability cannot be used for this application. These fabrics are also highly crystalline to possess strong mechanical strength. X-ray diffraction can be used in assessment of crystallinity and was initially considered as a promising test method. However, the high cost involved with X-ray diffraction, even for a series of preliminary tests prevented further examination of this method. After an extensive literature review and a series of feasibility tests, two non-destructive techniques were selected. Colour measurement and infrared spectroscopy met almost all the selection criteria discussed above.

Colour fastness is defined as the resistance of the textile colour to fading or removal during manufacturing, textile processes, service, storage, or ageing by destructive agents [88]. The depth of the dye in the fibre, binding forces between the dye and fibre, and the type of detrimental exposures are key factors in analysis of colour fastness or discoloration. Depending on the particular kind of dye-fibre combination, physical and/or chemical forces bind the dye to the fibres. Physical forces such as hydrogen bonding, van der Waals, and ionic forces bind the dye to the fibres and then, in certain cases, chemical forces such as covalent bonds between the functional groups within the fibre and the dye contribute to their linkage [88]. In addition, it is known that considerable loss in mechanical strength of aramids, a common type of outer shell

material, occurs at temperatures lower than 400°C as a result of subtle changes such as oxidation, chain fracture, crosslinking and disorientation [82]. Hence, any level of discoloration may be translated into partial loss of mechanical strength. Thorpe [14] found potential in this technique for prediction of tensile strength of outer shell fabrics. The objective of this part of the current research is to further examine this technique by testing the ability of the method to predict tensile strength for fabrics of a larger variety of colours and after a wider range of degradation.

Infrared spectroscopy is a method of spectroscopy which uses the infrared portion of the electromagnetic spectrum [44]. Similar to other techniques of spectroscopy, it is used for identification of compounds and investigation of material composition. Infrared radiation is a section of the electromagnetic spectrum with wavelengths from approximately 0.78 to 1000 μm. It spans the range of frequencies from the red end of the visible light at high frequencies to the microwave region at low frequencies. The infrared region is commonly divided into three parts: near IR (wavelength range of 0.78–2.5 μm), mid IR (wavelength range of 2.5–50 μm), and far IR (wavelength range of 50–1,000 μm). The most frequently used region in infrared spectroscopy is the mid IR region. The far IR region is usually used for analysis of heavy molecules and requires the use of specialized optical devices.

Near IR spectroscopy is vastly used in food science, agriculture, pharmacy, and chemistry. It is usually employed in process control applications and analysis is faster because of higher imaging speed and minimal and simple sample preparation. Similar to other techniques of spectroscopy, it is used for identification of compounds and investigation of material composition. A beam of infrared light with known wavelength is divided into two; one beam is used as the reference beam and the other beam is incident on the specimen and passes through the specimen. The transmitted beam and reference beam are examined to measure the amount of absorbed energy by the sample at that wavelength.

By changing the wavelength, the absorbed and also, transmitted spectra are defined for the sample as a function of wavelength. This will provide some information about the sample structure, the types of molecular bonds, and functional groups which are present in the molecule. The infrared transmitted spectrum of a substance is like a photograph of the molecules of the substance. By commencement of degradation in materials, volatile products leave the molecule and the original molecule is decomposed to some lighter molecules. This structural change in the molecule alters the wavelength range of absorbed energy bands and consequently, the value and

location of peaks in percent absorbance-wavelength graph. The chemical structures of Nomex® and Kevlar®, which were used in this research, are composed of functional groups such as –CH, –OH, and –NH (Figures 1.5-1.6). Change in these functional groups can affect aspects of performance of protective fabrics including mechanical strength. The absorption bands related to these functional groups are within the NIR region and therefore, they can be identified effectively using reflectance spectrum recorded by NIR spectroscopy [52]. The objective of this part of research was to determine whether NIR spectroscopy can be used to predict tensile strength of two outer shell fabrics of different colours, and to determine which specific wavelengths in the NIR spectra can be used to determine when changes in the tensile strength of the fabric have occurred.

6.1. Test procedure

The outer shell can be easily inspected since it is the outermost layer of firefighters' protective clothing. It is the first line of defence and may be damaged more severely than other inner layers even though it is more resilient than the other layers. In addition, if the deterioration of the outer shell were correlated with the critical aspects of performance of inner layers such as water vapour permeability of the moisture barrier, inspection of outer shell might be sufficient for the overall inspection of the firefighters' protective clothing. Based on test results presented in chapter 3-5, it was found that the change in tensile strength of outer shell within the test matrix and tested fabrics was more significant than the changes in aspects of performance of moisture barrier specimens considered in this research. So, non-destructive tests in this research project were conducted using only outer shell specimens. The specifications of the fabrics used in this research were provided in sections 3.1, 4.1, and 5.1.

6.1.1. Colour measurement

Before running tensile strength tests, the outer shell surface colour was evaluated using a commercial office scanner (Epson Perfection V30, Markham, Canada) and a MATLAB® code. The code was written originally by Thorpe [14]. It was revised by the author to perform statistical analysis and produce output results in Microsoft® Excel format. The colour was measured in the Red-Green-Blue (RGB) system. In the RGB system, colour is defined in three dimensions in terms of magnitudes of red, green, and blue components of the colour. The (0,0,0)

point describes black and white is defined by (1,1,1). Figure 6.1 illustrates the RGB colour system.

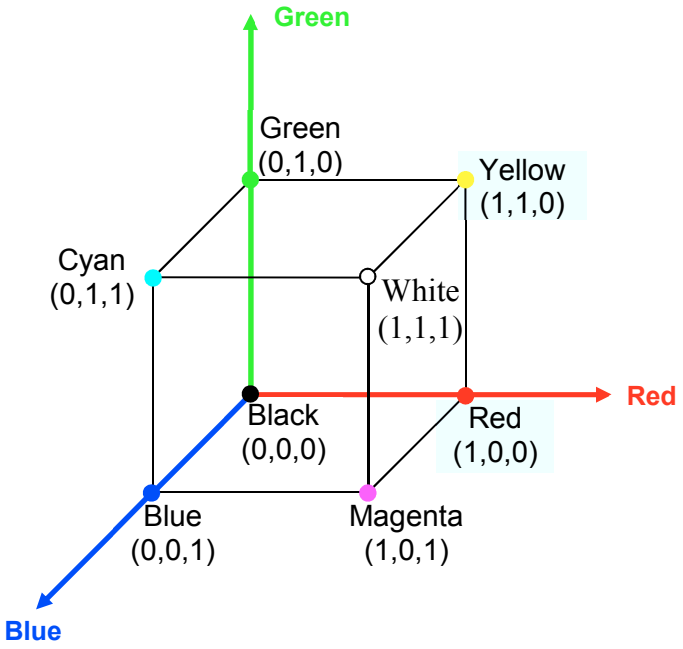

Figure 6.1: The RGB colour system [14]

The exposed area of the front side of the outer shell specimen was scanned with 24-bit colour and 300 dpi resolution as a bitmap file using the Epson scan software (v3.50). The scanner was set at true colour. The code read the image file and stored the colour as an m×n×3 matrix. The m and n values indicate the location within the interrogation area, while the third component of the matrix indicates which of the three colours in the RGB system is measured. The average value of each m×n submatrix represents the magnitude of each colour component (Figure 6.2) for the area of interest. Subsequently, the colour of the thermally aged outer shell fabric was compared with that of the unexposed outer shell fabric.

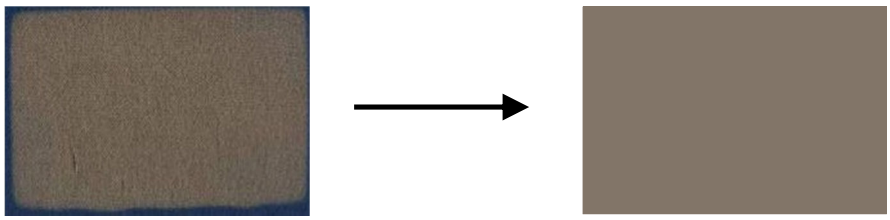

Figure 6.2: Conversion of discoloration of specimens to a representative colour

Colour difference was calculated based on Equation 6.1 [14] for the whole interrogation area (region 1 in Figure 6.3) as well as a central part of the interrogated area (region 2 in Figure 6.3):

$$\Delta Colour = \sqrt{(R_e - R_u)^2 + (G_e - G_u)^2 + (B_e - B_u)^2} \tag{6.1}$$

where R, G, and B denotes magnitudes of colour components, Red, Green, and Blue, respectively. Subscripts e and u signify exposed and unexposed condition, respectively.

A comparison of colour difference based on central area (region 1) and whole area (region 2) was made to examine the uniformity of discoloration of the specimen over the entire exposed area (Figure 6.3). From a practical point of view, this information can help when developing evaluation procedures for fabrics.

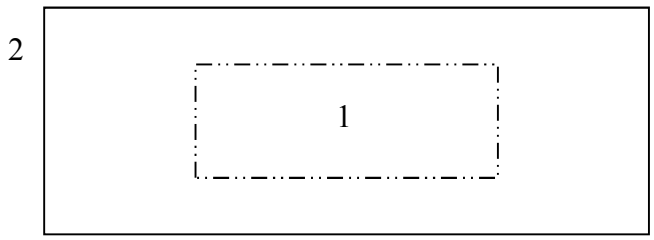

Figure 6.3: Interrogation area and regions of interest for colour measurement

6.1.2. NIR spectroscopy

In NIR spectroscopy, a beam of infrared light with known wavelength is shone on the specimen. If the beam frequency is equal to the frequency of any type of vibrational motions of molecules in chemical bonds of the specimen, the beam can be absorbed at varying intensities. The radiation that is not absorbed is either transmitted through, or reflected off, the specimen.

Diffuse reflectance NIR spectroscopy is implemented for rough surface solids such as cloth [44]. Reflectance is defined as the ratio of the intensity of the reflected light from the specimen to the intensity of the light reflected from a background or a reference material. Reflected radiation off the specimen in all directions is collected and measured by the spectrophotometer detector. By changing the wavelength, the reflected spectrum is acquired as a function of wavelength. Since the diffuse reflectance is a result of the incident radiation penetration into the specimen, the reflectance spectrum provides similar information about the

specimen structure as the transmission or absorption spectra, such as the types and strength of molecular bonds and functional groups which are present in the molecule. This is a valuable spectroscopic indicator.

Specimens were conditioned for 24 hours at 22±2°C and 65±2% relative humidity in a conditioning chamber and were tested within 5 min. after removal from conditioning chamber. The specimens were secured inside the compartment of a UV-Vis-NIR spectrophotometer (Varian, Cary 5G Palo Alto, CA) such a way that the front side of outer shell specimens were exposed to the equipment's light source. A 100% baseline was recorded using a reference disk (SRS-50), the absolute reflectance of which was known. The light source was blocked and a zero line was recorded. The emitted light is shone through a port which is a circle of 16 mm diameter. The surface of a specimen which covers the port is exposed to the emitted light. The reflectance spectra of unexposed and thermally aged outer shell specimens were recorded in the range of 250 - 2500 nm with a scan rate of 600 nm/min and intervals of 1 nm. The slit height and beam mode were set at "reduced" and "double", respectively. The software for the equipment was set to automatically correct the baseline to consider deviation from zero reflectance and modify all the recorded spectra. The reflectance spectrum was recorded at three distinct points on the exposed area. The average of three reflectance values was used. The interrogation area was the exposed area, 8.5 cm by 5.8 cm, of specimens prepared for tensile testing.

6.2. Colour measurement

In section 3.1, it was explained that the thermally exposed area restricted by metal bars (8.5 cm by 5.8 cm) was used as the interrogation area for the purpose of colour measurement. Discoloration of specimens after thermal ageing was quantified using equation 6.1. It is important to note that discoloration was assessed on the basis of initial colour of the new fabric from which specimens were made. There is no single origin for colour measurement of specimens with different colours. This is why colour change values between specimens of two different colours may vary substantially.

A general trend in discoloration of all specimens with different colours was observed. Figure 6.4 illustrates this trend qualitatively using the images of the exposed area of Nomex® specimens after selected thermal exposures. During exposure to relatively low heat fluxes (e.g., 10 kW/m^2), dye began to come out of the fabrics gradually (Figure 6.4a). Eventually, all the dye

was gone and the natural colour (brown) of fabrics was revealed during exposure to moderate heat fluxes (e.g., 20 kW/m^2) (Figure 6.4b). Exposure to higher heat fluxes (e.g., 30 and 40 kW/m^2) charred the specimen surface (Figure 6.4c). The char rate increased with exposure duration (Figure 6.4d) and the exposed area was completely black for longer exposures. Appendix A shows a complete set of images of specimens with different colours after all exposures in Table 3.1.

Figure 6.5 shows the early part of the trend quantitatively. In this part, the dye began to come out of the fabric. Therefore, the colour change increased. The rate of increase depends on how far the natural colour of the fabric is from the initial dyed colour in the colour measurement system, which is the RGB system in this research. Figures 6.6 to 6.9 show the trend of colour change for blue, red, dark blue, and yellow specimens after various levels of thermal exposure conducted according to the procedure outlined in section 3.1. In Figure 6.6, discoloration in exposure to 10 kW/m^2 was the lowest among blue specimens. Significant discoloration was caused after long exposures to this relatively low intensity of heat flux. It may be explained by Figures 3.5-3.8. Specimens reached a maximum temperature of 220°C during exposure to 10 kW/m^2, which is the starting point for degradation and dye removal. As a result of blue dye erosion, the specimen turned to a brown colour which is the natural colour of Nomex®. As a result of more intense thermal exposure and consequently higher temperatures, dye came out of the specimen completely. Exposure to 20 kW/m^2 for only 30 s increased colour difference to almost two times higher than that for an exposure to 10 kW/m^2 for 2400 s.

However, the discoloration trend was reversed after more intense thermal exposure. Generally speaking, more intense and longer exposures to 20, 30, and 40 kW/m^2 decreased the numerical value of the colour difference. The decrease in the value of the colour difference can be explained by formation of char after thermal exposure. As the colour of the specimen surface was turning to black, the colour value in the RGB system got closer to the initial dyed colour (blue in this case). This is why such a decrease in colour value is observed in the figure. The colour measurement value tended to a specific value after severe thermal exposures, which may indicate complete charring of the specimen. Figures 6.4c and 6.4d show charring of specimens after different levels of thermal exposure.

a) After exposure to 10kW/m^2 for 2400s	b) After exposure to 20kW/m^2 for 30s	c) After exposure to 30kW/m^2 for 30s	d) After exposure to 40kW/m^2 for 30s

Figure 6.4: The trend of discoloration in Nomex® outer shell fabrics of different colour

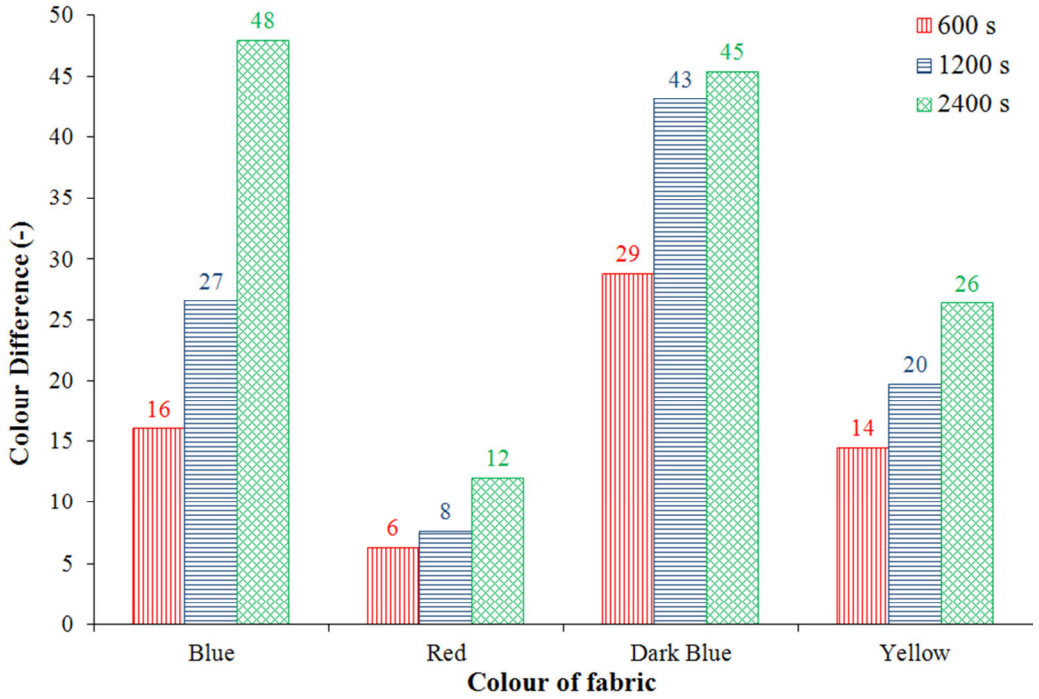

Figure 6.5: Colour change in Nomex® fabrics of different colours after exposure to 10kW/m^2 for particular duration

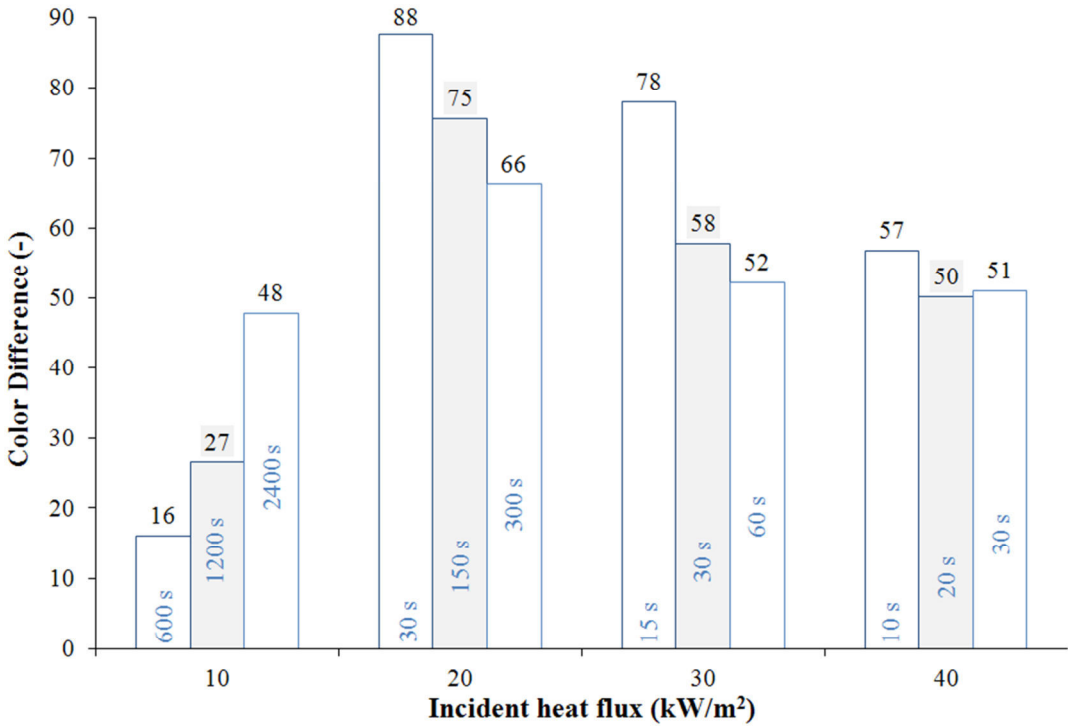

Figure 6.6: Colour change in blue Nomex® specimens

Figure 6.7 presents the same information for red specimens. In the same way as blue specimens, specimen colour changed slightly in exposure to 10 kW/m^2. In general, the colour difference increased after more severe thermal exposures. Char formation on the surface of specimens after complete dye removal increased the colour difference as well.

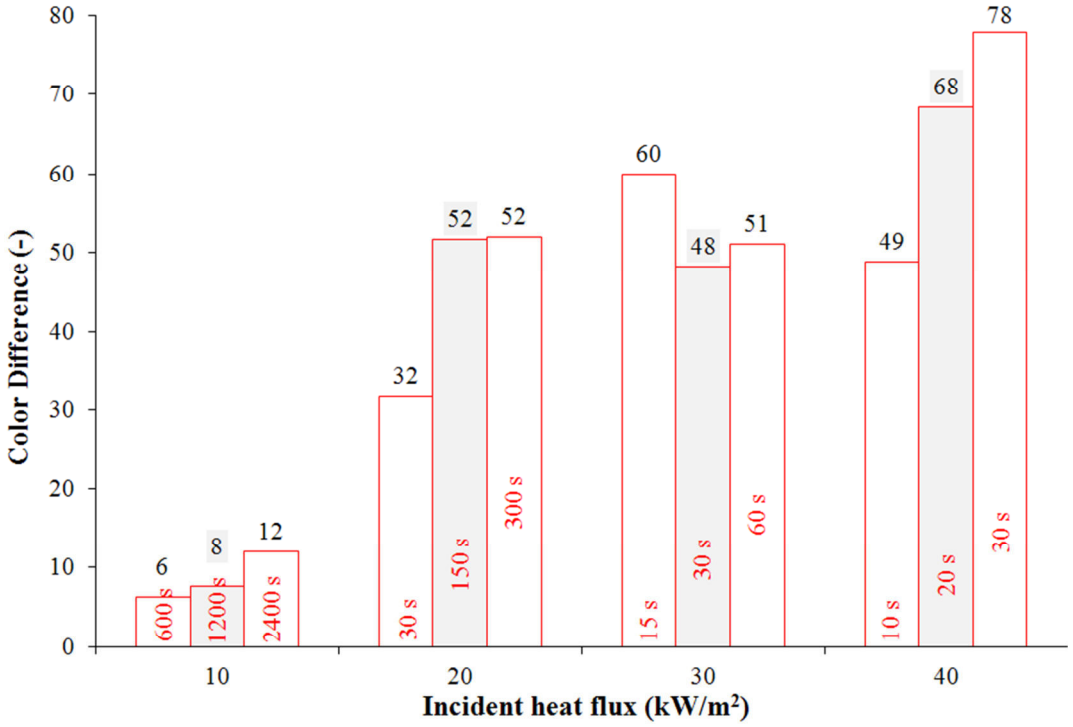

Figure 6.7: Colour change in red Nomex® specimens

Figure 6.8 depicts the colour change for dark blue specimens. The trend in colour change is very similar to the one for blue specimens (Figure 6.8). As dark blue is closer to black, the colour change value after the most intense thermal exposure (15) is smaller than corresponding value for blue specimens (50). Discoloration of yellow specimens is illustrated in Figure 6.9. The trend in colour change is similar to the one for red specimens. Yellow is the brightest colour among the tested specimens and is the furthest colour from black. This explains the highest value of colour change for the charred yellow specimens after exposure to 40 kW/m^2 for 30 s.

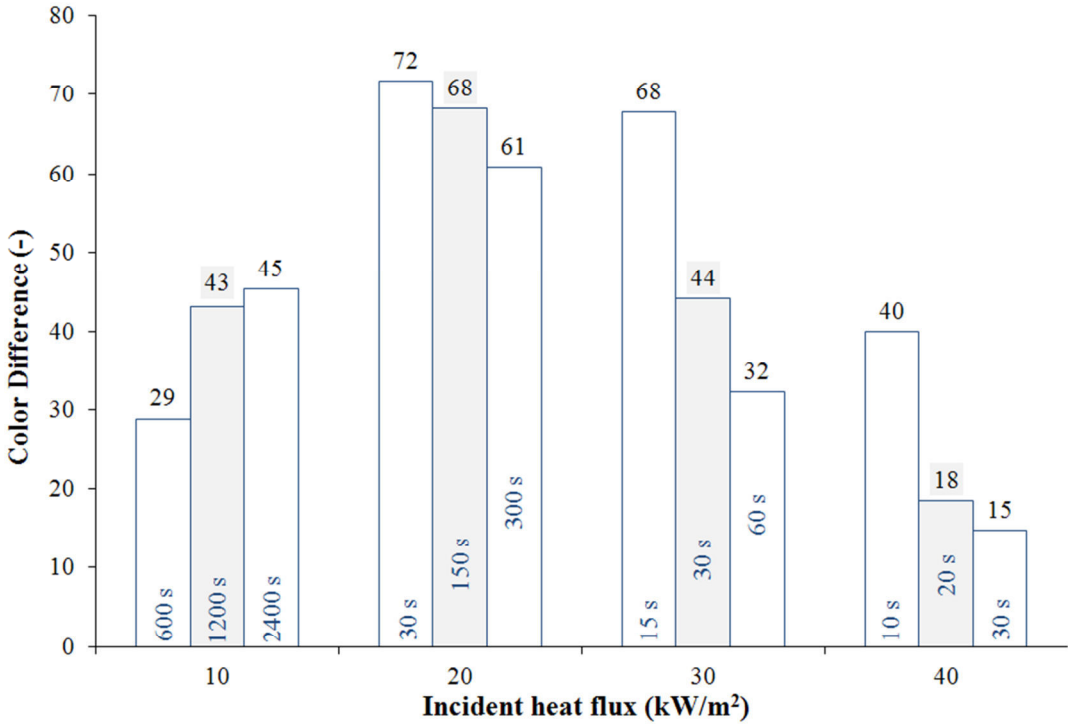

Figure 6.8: Colour change in dark blue Nomex® specimens

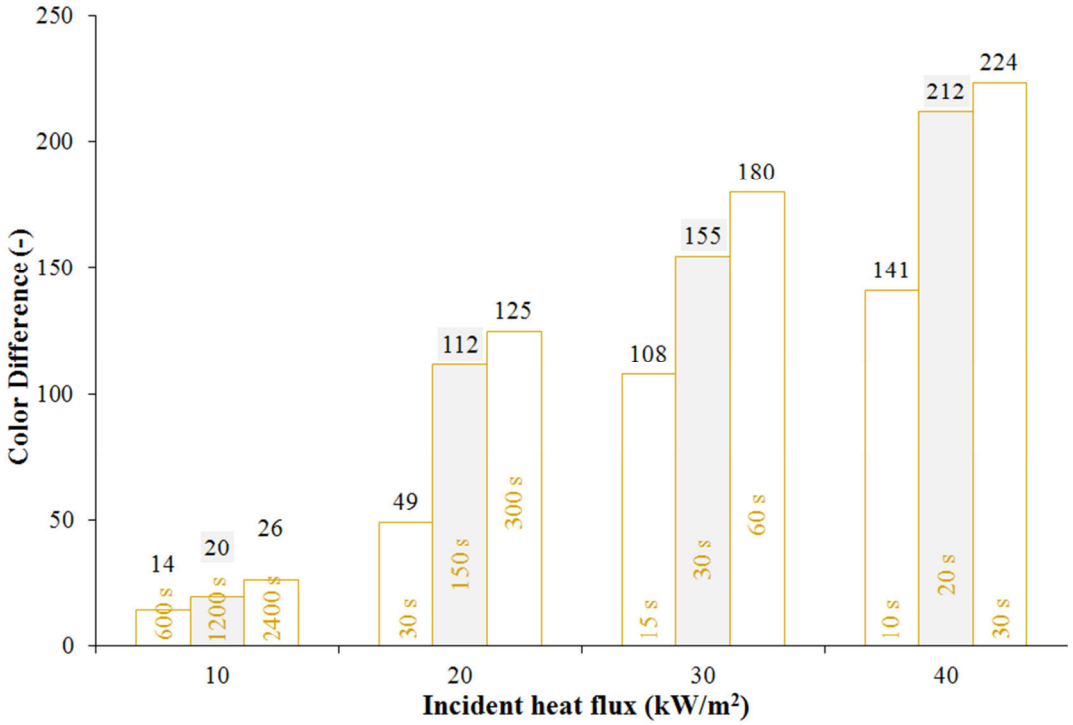

Figure 6.9: Colour change in yellow Nomex® specimens

The thermally aged specimens discussed in section 5.1 were also tested to consider the effect of multi-stage ageing on discoloration of specimens. Brown specimens were undyed specimens of the natural colour of the fabric, while black specimens were dyed. It was discussed in chapter 5 that multi-stage exposures cause less severe damage than single-stage exposures. So, it is expected to observe a similar difference in discoloration of specimens after two different forms of exposure.

Figure 6.10 shows the effect of two types of thermal exposure to 20 kW/m^2 on discoloration of brown specimens. Since there is no dye in brown specimens, the colour changed from brown to black and colour difference increased with exposure duration. In multi-stage exposures, specimens reached lower temperature in each stage of exposure in comparison with single-stage exposure for the same total duration (Figures 3.5-3.8). Accordingly, discoloration after multi-stage thermal exposure was less severe than single-stage exposure.

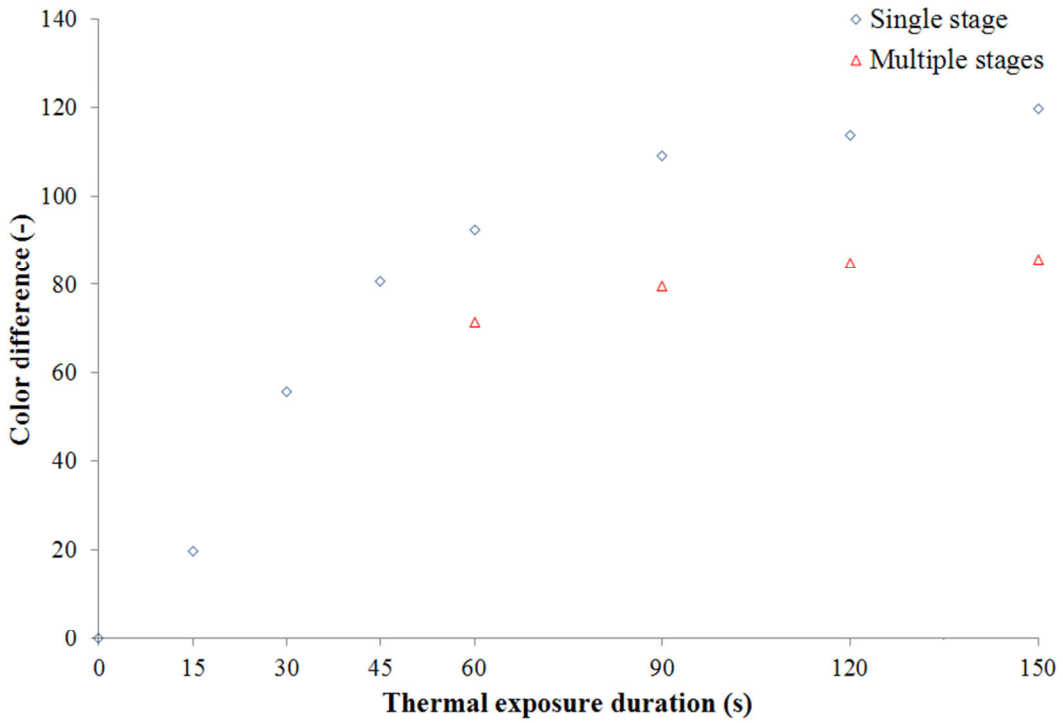

Figure 6.10: Colour change in brown Kevlar®/PBI specimens after single-stage and multi-stage exposures

Discoloration of black specimens after single-stage and multi-stage exposures is illustrated in Figure 6.11. Contrary to brown specimens, there are two trends of discoloration in black specimens after thermal exposure, which is similar to the trends of colour change observed for blue and dark blue specimens. The figure shows that after 30 s of thermal exposure to 20 kW/m^2, the colour difference reached its maximum value, which indicates complete removal of dye. By this length of exposure, the specimen colour changed from its initial colour, black, to the natural colour of fabric, brown. As a result of longer exposure, specimens charred and turned black gradually. Since the initial colour of specimen was black, the colour difference decreased with duration of exposure. However, it approached a specific value, as the specimen charred completely. Furthermore, colour difference for specimens after multi-stage exposures was higher than after single-stage exposure for the same total duration. This is supported by lower amount of charring in specimens after multi-stage exposure.

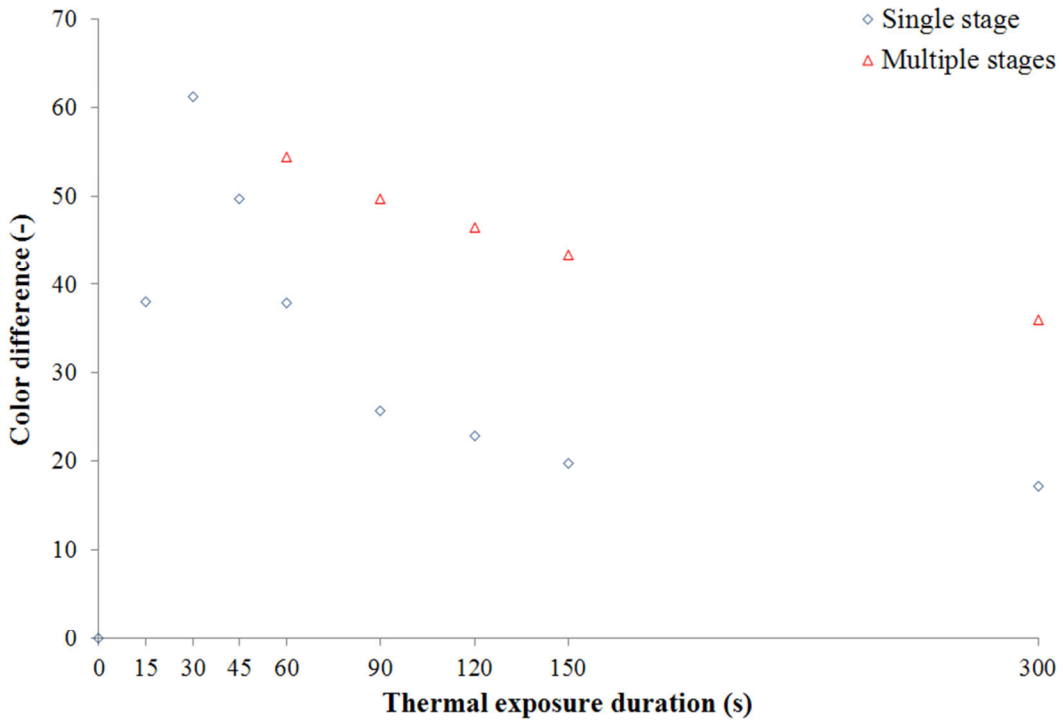

Figure 6.11: Colour change in black Kevlar®/PBI specimens after single-stage and multi-stage exposures

A question arises about the uniformity of discoloration over the exposed area of specimens after thermal exposure. In other words, how sensitive colour measurement is to the size of interrogation area. In order to answer this question, region 1, the area of which is one-quarter of the exposed area, and region 2, the whole exposed area, were selected as the interrogation area for colour measurement. Figures 6.12 and 6.13 compare the colour difference in regions 1 and 2 for brown and black specimens, respectively. In both figures, the colour difference value is almost the same in both regions. In Figure 6.12, the colour difference measured in the central area of the brown specimens is a bit higher than the value in the whole area, while there is an opposite difference between these values for black specimens in Figure 6.13. Brown specimens were not dyed and so, higher colour difference value means higher degradation and damage. On the contrary, black specimens were dyed and therefore, a lower colour difference (after dye removal) translates into higher degradation and damage. This observation may be supported by the fact that central area receives a bit higher rate of energy flux and subsequently thermal energy than the whole area (Figure 2.8).

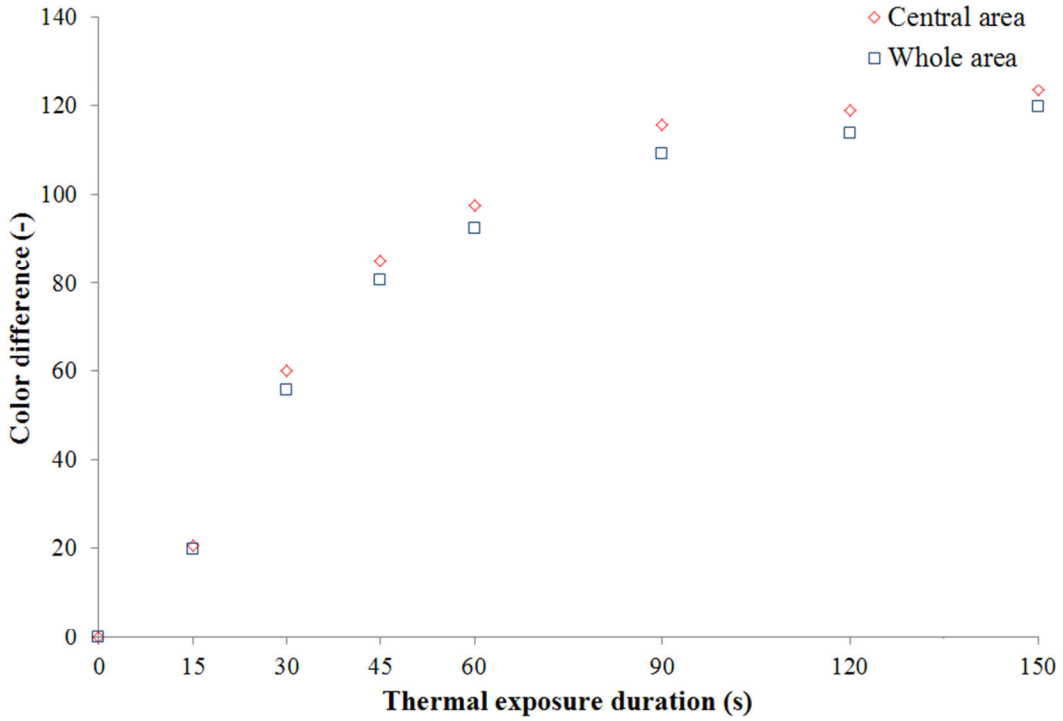

Figure 6.12: Colour difference in regions 1 (central area) and 2 (whole area) for brown specimens

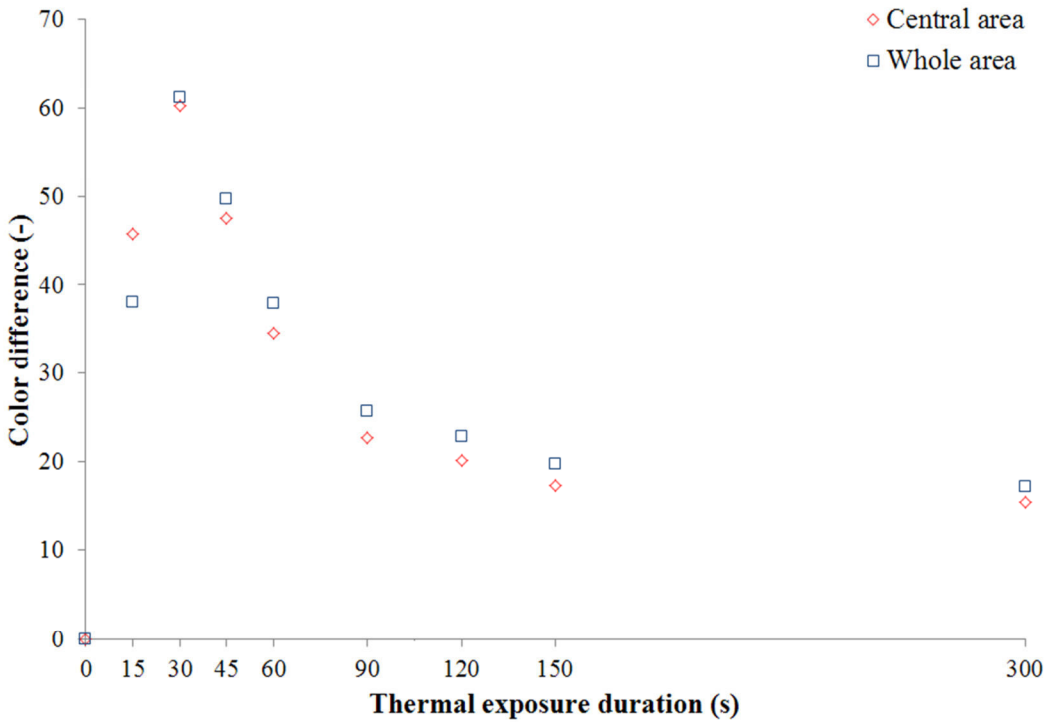

Figure 6.13: Colour difference in regions 1 (central area) and 2 (whole area) for black specimens

6.3.Near infrared spectroscopy

In a similar manner to colour measurement, two groups of outer shell specimens were tested using NIR spectroscopy. The first group of specimens had been thermally aged in a single stage according to the procedure described in section 2.2. They were each a single layer of Nomex® outer shell specimens of different colours. The second group of specimens were Kevlar®/PBI outer shell fabrics brown and black, which had been aged in single-stage and multi-stage exposures based on procedure in 5.1.

Diffuse reflectance spectra of specimens were recorded using the UV-Vis-NIR spectrometer. The equipment span (input full scale) is 250 – 2500 nm. In order to consider probable effects of thermal ageing on ultra violet and visible regions, the reflectance spectrum was recorded within the full range. Figure 6.14 illustrates the reflectance spectrum for unexposed specimens in different colours within the full range. Even though there is a difference among the reflectance spectra for different colours within the full spectrum, it is distinct within the visible range (380 – 750 nm). A literature review on wavelength bands in the near infrared region concluded that the wavelength region lower than 1486 nm is sensitive to colour change [89]. In order to minimize

the effect of colour in analysis, the reflectance spectrum is only evaluated and illustrated within the range of 1500 – 2500 nm in the next figures.

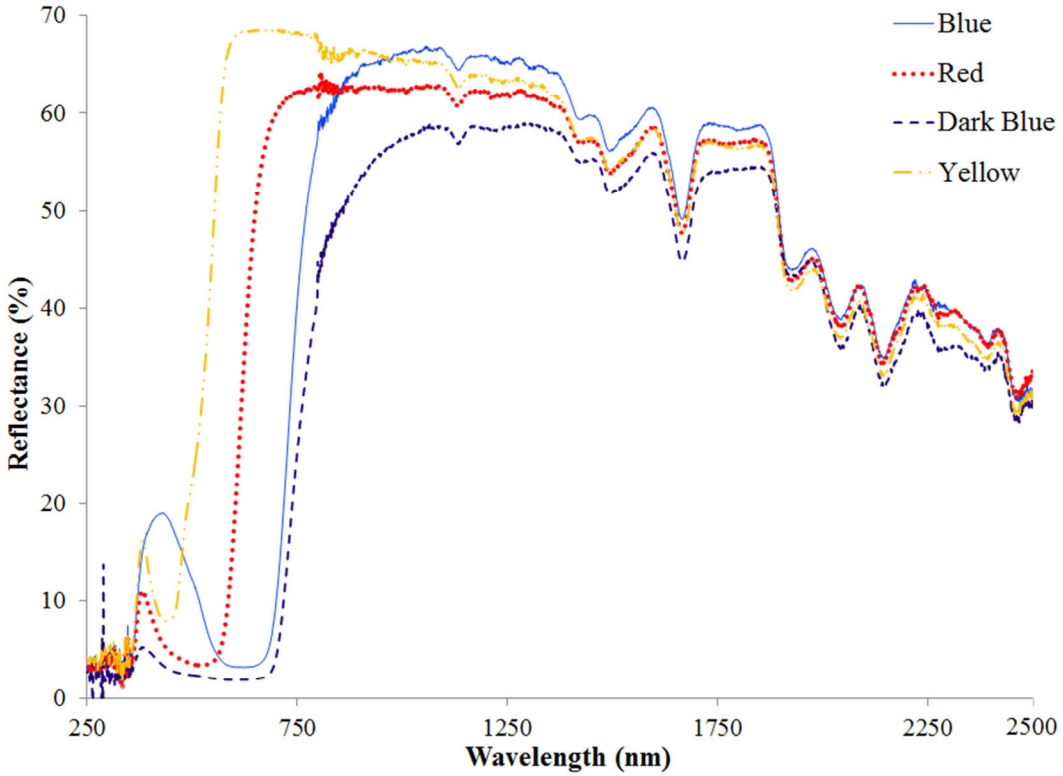

Figure 6.14: Reflectance spectrum of unexposed Nomex® specimens of different colours

Figures 6.15 to 6.18 depict the reflectance spectrum of blue specimens after certain durations of thermal exposure to 10, 20, 30, and 40 kW/m^2, respectively. The reflectance spectrum for unexposed specimens was added to figures to perceive the effect of different levels of thermal exposure on the reflectance spectra. The change in reflectance spectrum after thermal exposure is similar for specimens of different colour. Appendix D shows the reflectance spectra after thermal exposure for specimens in red, dark blue, and yellow. Since the change in reflectance spectrum after different levels of thermal exposure is the focus of this section, only reflectance spectra of blue specimens are considered in this section.

Figure 6.15 shows that reflectance spectra of the specimen after thermal exposure to 10 kW/m^2 decreased slightly in comparison with that of an unexposed specimen. Longer durations (1200 s and 2400 s) of exposure changed reflectance by less than 5%. This may

indicate that specimens did not undergo severe degradation. It is supported by maximum temperature (around 220°C) of specimens during thermal exposure (Figure 3.1), which was not high enough to cause severe degradation based on TGA curves.

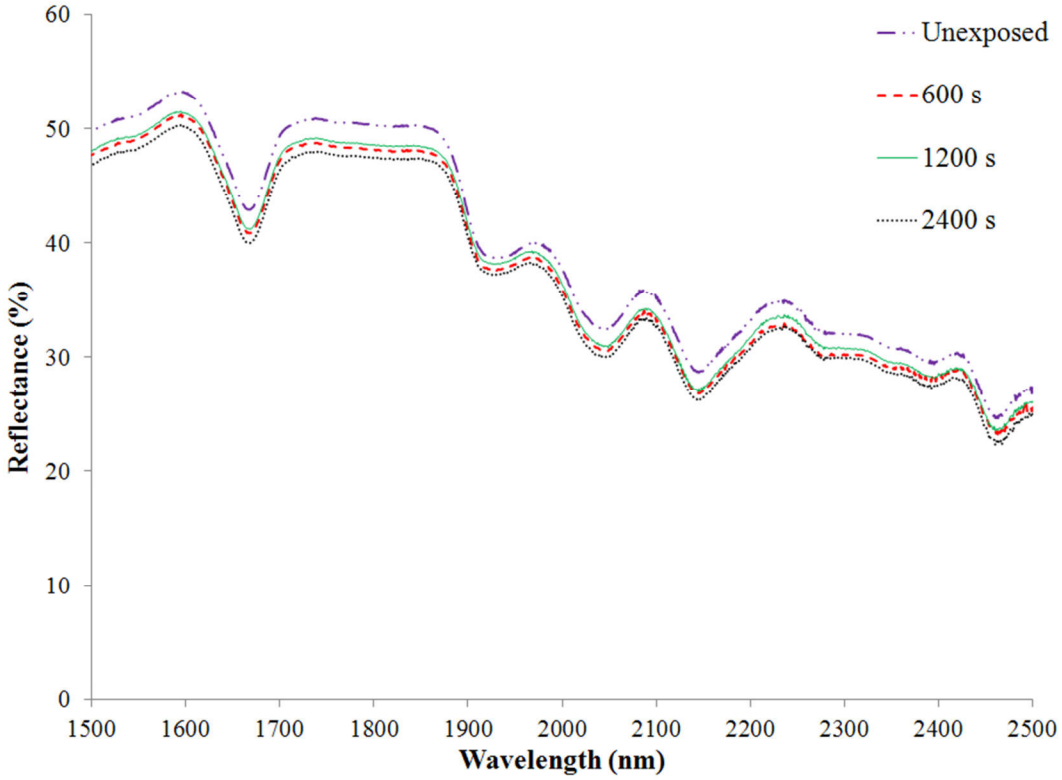

Figure 6.15: Reflectance spectrum for blue Nomex® specimens after thermal exposure to 10 kW/m^2

Similarly, reflectance decreased by less than 5% after exposure to 20 kW/m^2 as is shown in Figure 6.16. In exposures to 20 kW/m^2, specimens reached a maximum temperature of around 320°C which corresponds to minor degradation of the fabric material. Minor degradation and discoloration can affect surface morphology and optical properties like refractive index, which influence reflective and scattering properties of the specimen surface [89]. Exposures to 30 kW/m^2, especially for relatively long duration (60 s), decreased reflectance of specimens, as illustrated in Figure 6.17. The major change in reflectance after longer durations of exposure occurred within 1500 – 2000 nm. This wavelength region is dominated by vibrations of –CH and –OH functional groups [89] which are present in the structure of the fabrics. Figure 6.18 shows a

significant decrease in reflectance of specimens after exposure to 40 kW/m^2. This decrease was up to 50% for some wavelengths in the region of 1500 – 2000 nm after 30-s exposure. This significant decrease was explained by the fact that specimens underwent severe degradation after exposure to 40 kW/m^2. Therefore, major changes in chemical structure of specimen fabrics took place, which led into substantial change in the reflectance spectrum of specimens.

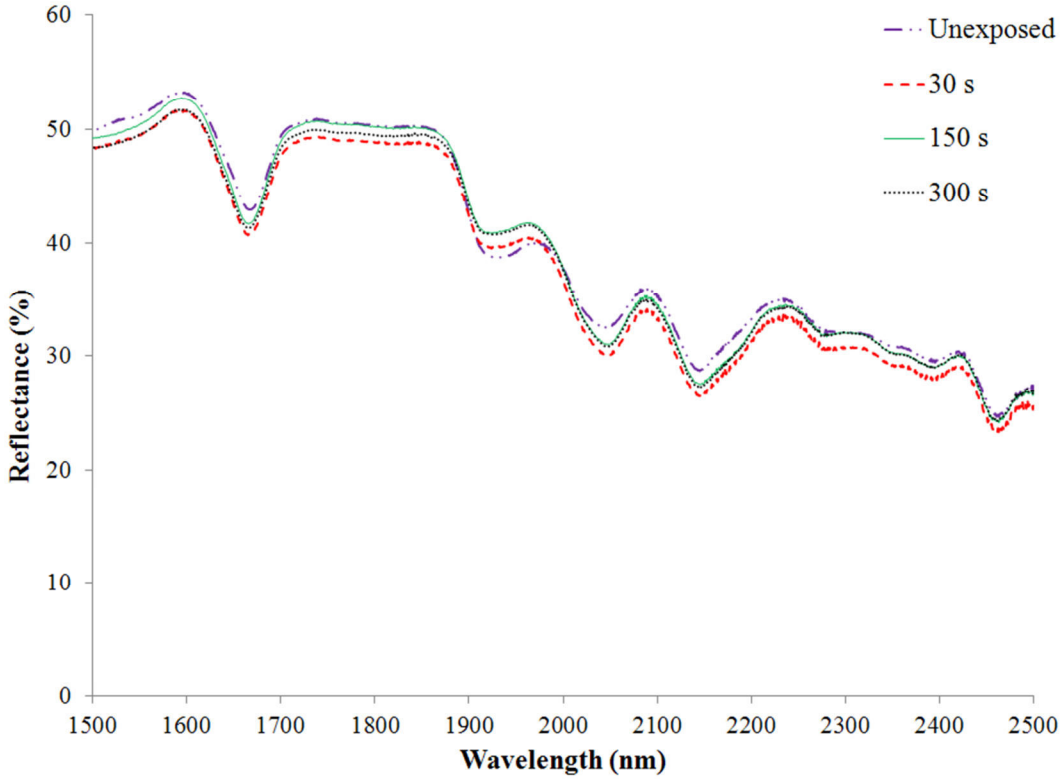

Figure 6.16: Reflectance spectrum for blue Nomex® specimens after thermal exposure to 20 kW/m^2

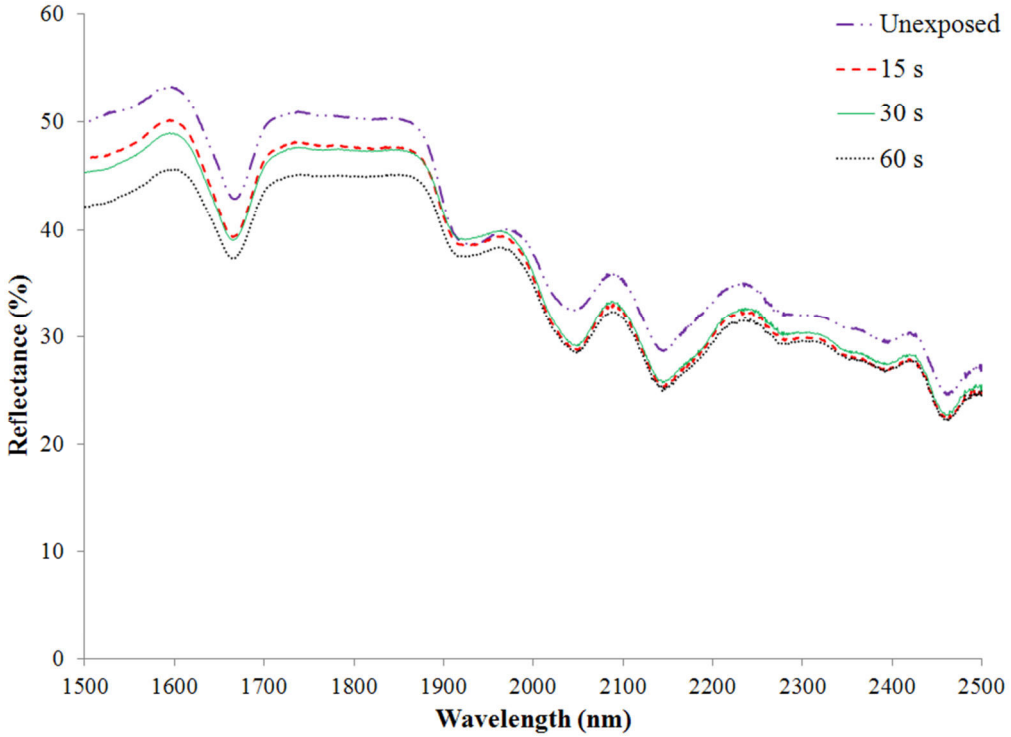

Figure 6.17: Reflectance spectrum for blue Nomex® specimens after thermal exposure to 30 kW/m^2

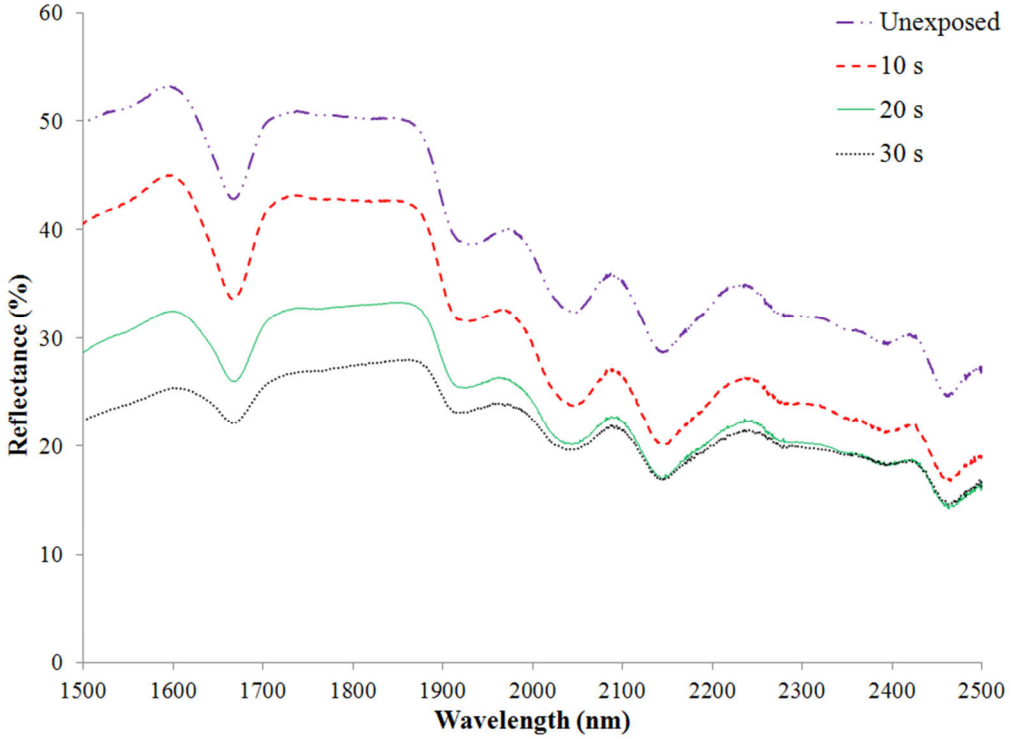

Figure 6.18: Reflectance spectrum for blue Nomex® specimens after thermal exposure to 40 kW/m^2

The repeatability of reflectance spectrum of specimens after different levels of thermal exposure was investigated, as depicted in Figure 6.19. The figure compares reflectance spectra at two locations on the unexposed dark blue specimens, blue specimens after exposure to 20 kW/m^2 for 300 s, and red specimens after exposure to 40 kW/m^2 for 30 s within the full wavelength region of the spectrophotometer. For the sake of clarity only two examples of the reflectance spectra are included, although three spectra were recorded. The figure shows that the reflectance spectrum is repeatable to a great extent (less than 2%) within the exposed area of specimens in different colours. This level of repeatability can indicate precise measurement over a uniformly thermally exposed surface of fabric and uniformity of physical and chemical changes over the exposed area of specimens.

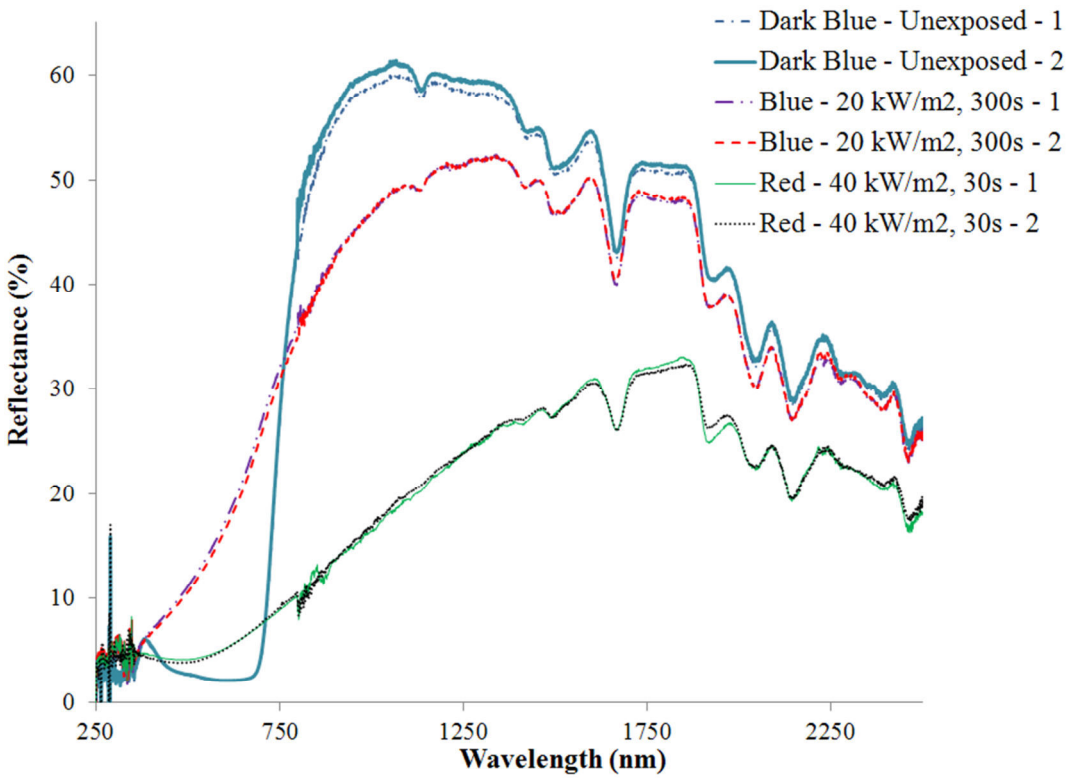

Figure 6.19: Repeatability of reflectance spectrum of specimens after different levels of thermal exposure

Several absorption bands of water are located in the infrared region. High level of moisture content in specimens can significantly change the shape of reflectance spectrum. From a

practical point of view, it is important to know whether there will be a need to condition firefighters' protective clothing before using infrared spectroscopy since there was a concern that the absorbed water could influence the reflectance spectra. Unexposed yellow outer shell specimens were conditioned in a similar procedure to section 2.2 at 20%, 50%, and 65% relative humidity and 22±2°C for 24 hr. Then, reflectance spectrum of specimens was measured immediately after taking them out of a conditioning chamber. Figure 6.20 presents reflectance spectra of unexposed yellow specimens conditioned under different levels of relative humidity. The figure illustrates minimal change in reflectance spectrum of new yellow outer shell specimens. This insignificant change implies that moisture absorption in specimen fabrics did not influence the reflectance spectrum.

This minimal change could be explained by the low moisture regain of the Nomex® fabric. Table 6.1 represents weight percentage of moisture regain for unexposed yellow specimens. A specimen, the weight of which was around 7 g, was heated in an oven at a temperature of 100°C for 1 hr. It was weighed immediately and then, conditioned under two circumstances, dry (20%) and semi humid (50%), in the conditioning chamber used in section 2.2 at 22±2°C. Relative humidity of the chamber and duration of conditioning are described in the table. The results support low moisture regain in the fabric, which is in agreement with the manufacturer's technical information [80]. Hence, conditioning of firefighters' protective clothing before conducting infrared spectroscopy is not necessary if the moisture regain of clothing fabric is low.

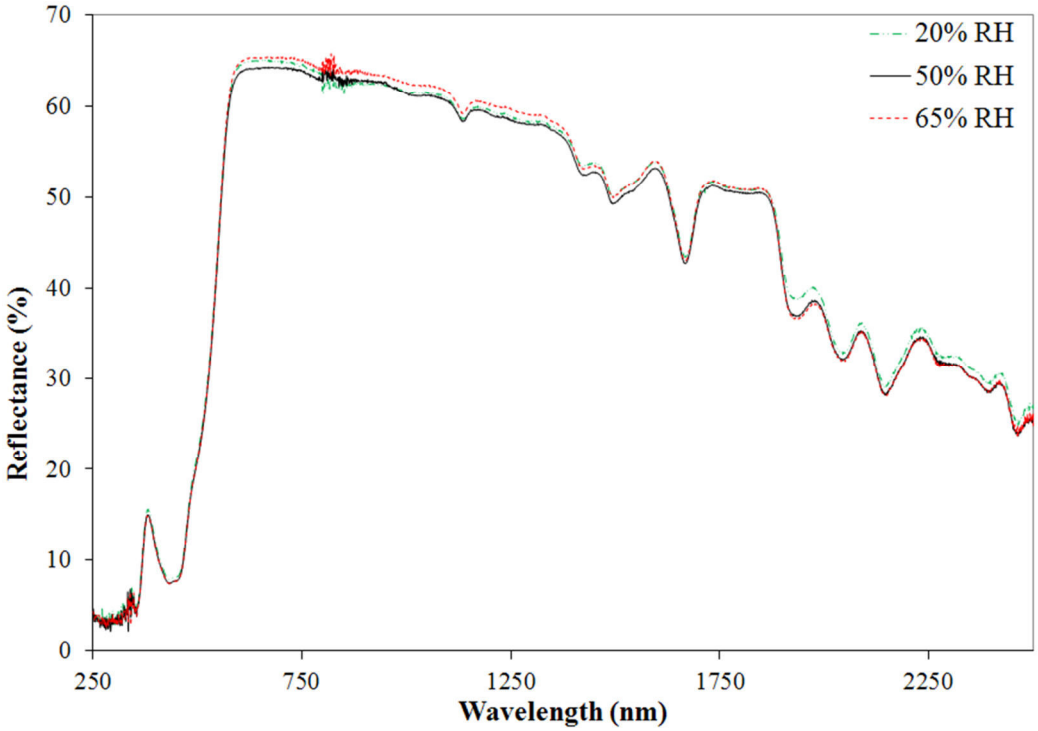

Figure 6.20: Effect of moisture on reflectance spectrum of yellow Nomex® unexposed specimens

Table 6.1: Mass moisture regain of unexposed yellow Nomex® outer shell specimens

Conditioning specification		Moisture regain,
Relative humidity (%)	Duration (hr)	weight percentage (%)
20	24	4.1
50	24	5.1
65	24	6.4

Reflectance spectrum of brown and black specimens changed similarly. The specimens were exposed to 20 kW/m^2 for durations ranging from 15 s to 300 s. The reflectance spectra of brown Kevlar®/PBI specimens exposed for 60 s and shorter were essentially the same. In addition, the reflectance spectra of specimens exposed for 90 s and longer were almost the same. Because of overlapping, reflectance spectra for only unexposed and thermally exposed specimens for 60 s and 90 s are shown in Figure 6.21. Specimens reached 414°C after 90 s exposure to 20 kW/m^2 as shown in Table 3.2 and Table 5.3. It was explained in section 5.3 that around this point, specimens experienced a temperature drop in the first stage of exposure, which was not observed

in the second and third stages. It implied that the specimen underwent a considerable level of degradation. This could be the reason for the noticeable change in reflectance spectra of specimens exposed for 90 s and longer in comparison with those of specimens exposed for 60 s or shorter. However, this change in reflectance of specimens after thermal exposure was not consistent within the full wavelength region. Even though it decreased with exposure duration within the wavelength region of 1500 – 1900 nm, it increased within the range of 1900 – 2500 nm. In addition, reflectance remained almost constant for thermally exposed specimens regardless of exposure duration within the wavelength region of 1900 – 2500 nm in comparison with the reflectance spectrum of unexposed specimens. This could be related to changes in chemical structure during degradation of specimen fabrics after short (15 s) thermal exposure to 20 kW/m^2.

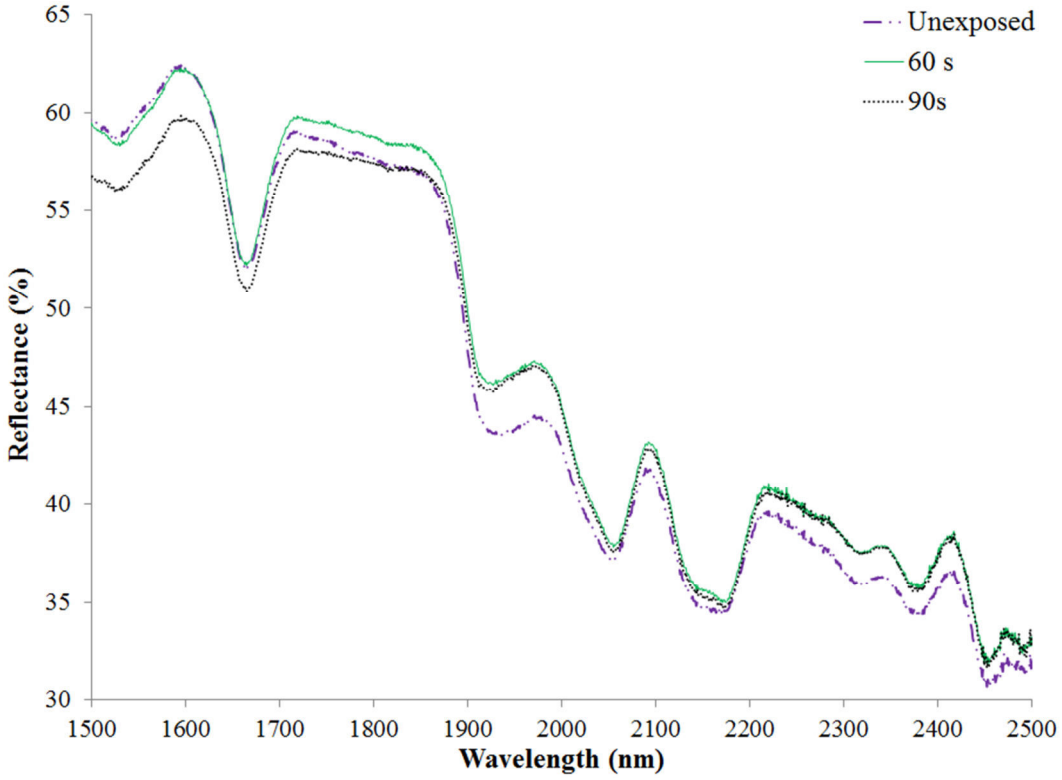

Figure 6.21: Reflectance spectrum for brown Kevlar®/PBI specimens after thermal exposure to 20 kW/m^2

Figure 6.22 depicts the reflectance spectra for black Kevlar®/PBI specimens for unexposed and specimens that were thermally exposed for 60 s, 90 s, and 150 s. The trend of change in reflectance spectra of black Kevlar®/PBI specimens is very similar to the brown Kevlar®/PBI specimens. Reflectance decreased continuously with exposure duration within the wavelength region of 1500 – 1900 nm. However, this decrease was more significant after 90 s of exposure. Besides, although the reflectance increased within the range of 1900 – 2500 nm after a short duration (15 s) of thermal exposure, it did not increase further after longer durations of exposure. The reflectance of Kevlar®/PBI black specimens is around 5% higher than that of brown specimens, which may be related to higher surface density of black Kevlar®/PBI fabric.

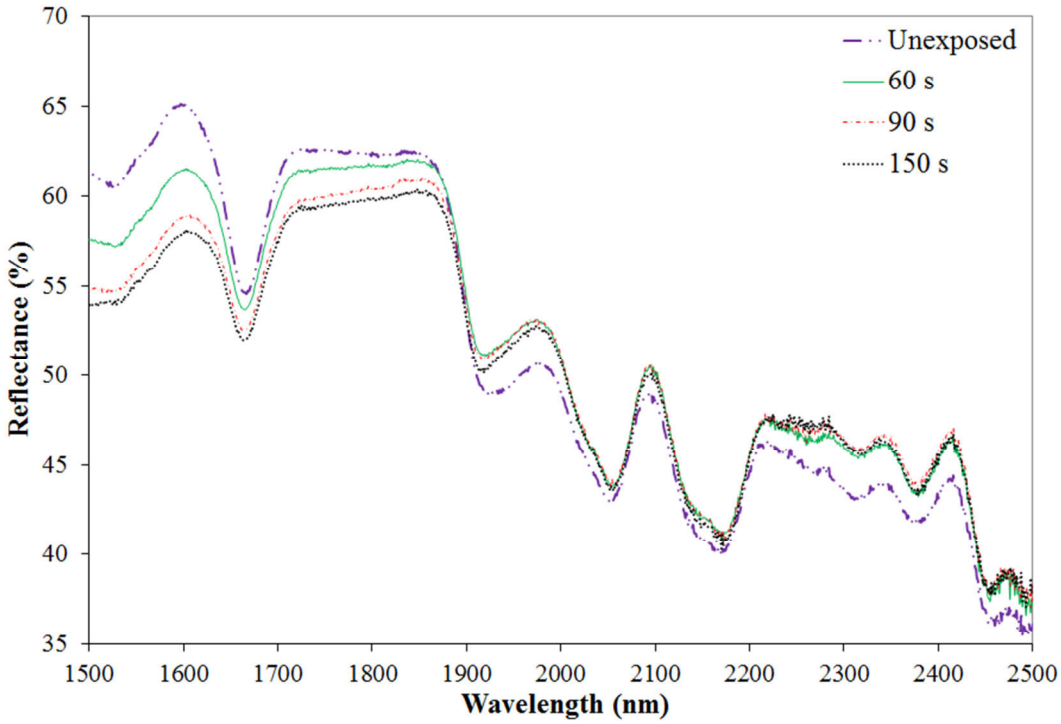

Figure 6.22: Reflectance spectrum for black Kevlar®/PBI specimens after thermal exposure to 20 kW/m^2

Figure 6.23 compares the effect of single-stage and multi-stage thermal exposures for total durations of 60 s and 300 s on reflectance spectrum of black Kevlar®/PBI specimens. Similar to Figures 6.20 and 6.21, changes in reflectance of thermally exposed specimens were limited to wavelength region of 1500 – 1900 nm. Reflectance of specimens exposed in multiple stages was

around 5% higher than that of specimens exposed in a single stage. This was related to more significant degradation in specimens after a single-stage exposure in comparison with multi-stage exposures. In a single-stage exposure of a given total duration, specimens reached higher temperature than in multiple 30 s exposures that produced the same total duration of exposure. In addition, the higher the number of stages of exposure, the bigger the difference was between reflectance of specimens after single-stage and multi-stage thermal exposures. This was associated with more severe degradation in fabrics after more stages of thermal exposure.

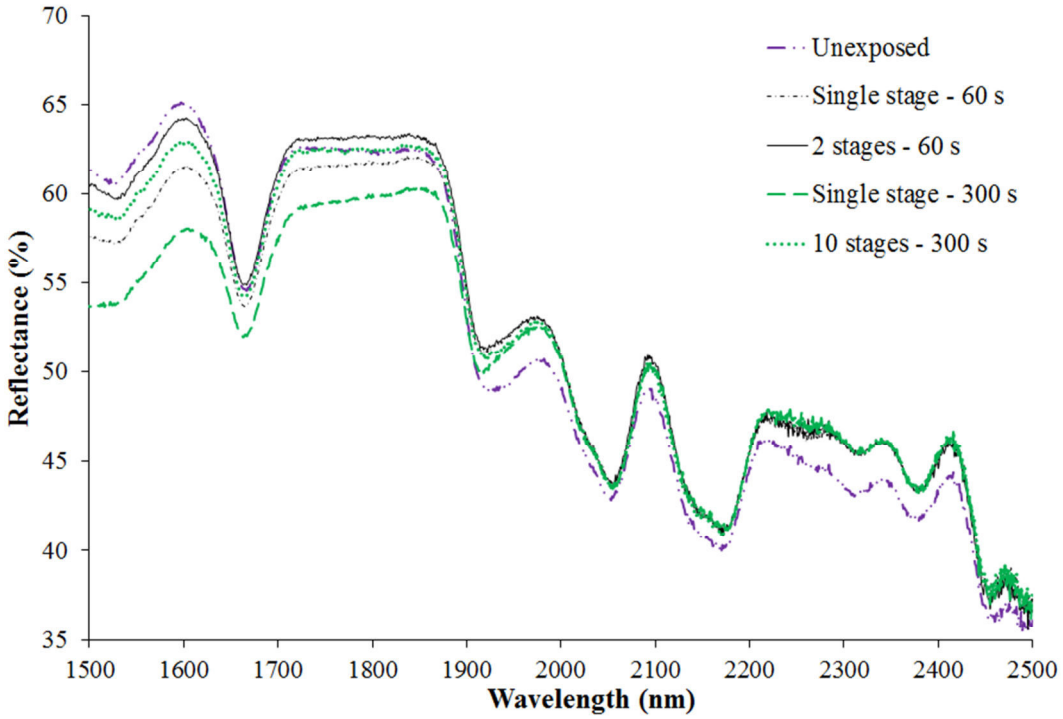

Figure 6.23: Effect of single-stage and multi-stage exposures on reflectance spectrum of black Kevlar®/PBI specimens

To summarize, outer shell specimens were evaluated using two non-destructive techniques in this chapter. The colour measurement technique showed that the trend in colour change in outer shell specimens after thermal exposure consists of two parts. In the first part, the dye gradually came out of the fabric during thermal exposure until the natural colour of the fabric was revealed. In this part, colour change increased. In the second part, the surface of the specimen charred and blackened. Depending on the difference between the initial colour of the dyed fabric

and black, colour change could increase or decrease. This trend of colour change will be correlated with tensile strength of specimens in chapter 7.

Reflectance spectra of thermally exposed specimens were recorded using NIR as the second non-destructive technique. It was observed that reflectance spectra were more sensitive to thermal exposure within the wavelength region of 1500-1900 nm. In this region, reflectance of specimens decreased more after more intense and longer thermal exposures. The change in reflectance spectra will be correlated with tensile strength of specimens in chapter 7.

7. PREDICTING TENSILE STRENGTH OF OUTER SHELL

It was discussed in section 1.6 that a comparison of changes in the main aspects of performance of outer shell and moisture barrier layers of firefighters' protective clothing showed that the most severe damage occurs in the outer shell. It is because the outer shell layer is the first line of defence against all types of destructive agents. Mechanical strength is an important aspect of performance of outer shell layer, which deteriorates significantly after harmful exposures. In addition, it is the outermost layer of firefighters' protective clothing and can easily be tested by non-destructive techniques. Hence, the focus of this research was on correlating the mechanical strength of outer shell with signal parameters of non-destructive tests.

Tensile strength of two groups of outer shell specimens made of Nomex® and Kevlar®/PBI were measured in chapters 3 and 5. Colour measurement and near infrared spectroscopy were implemented as two non-destructive techniques in chapter 6. In this chapter, tensile strength of outer shell specimens is correlated with colour difference and reflectance in the near infrared region as signal parameters of the non-destructive techniques.

7.1. Correlation between tensile strength and colour measurement

The purpose of this section is to identify qualitative correlation between tensile strength and colour measurement for Nomex® and Kevlar®/PBI outer shell specimens. Thorpe [14] initiated this work by correlating the changes in tensile strength with discoloration of 60% Kevlar®/40% Nomex® fabric after thermal exposure. In this research, Nomex® outer shell specimens in blue, red, dark blue, and yellow and Kevlar®/PBI outer shell specimens in brown and black were examined. This research extended Thorpe's initial research by looking at a wider range of fabric types and colour, after a wider range of thermal exposures.

Figures 7.1 to 7.4 illustrate the correlation between tensile strength and colour difference of Nomex® outer shell specimens after the thermal exposures listed in Table 3.1. Figures 7.5 and 7.6 depict similar information for brown and black Kevlar®/PBI specimens after the single-stage thermal exposures listed in Table 5.1. In general, two trends for colour difference of specimens can be observed, which depend on the initial colour of the fabric, the colour of the undyed fibres, and the colour of char. The trends in the figures are shown schematically by a solid line, which was fit by eye.

The first type of colour change was observed for blue, dark blue, and black colours in Figures 7.1, 7.2, and 7.3, respectively. For the purpose of comparison, Figure 7.4 illustrates the first type of colour change for all the three colour of specimens. The colour change first increased as the dye was removed from the fabric and continued to increase until a maximum value was reached, which was dependent on the initial colour of the specimen. The maximum point reached when the fabric dye came out to a large extent. Such a point could be reached after various intensities of thermal exposure or for different durations. For example, an exposure to 20 kW/m^2 for 30 s or 30 kW/m^2 for 15 s caused the maximum colour change in blue and dark blue specimens. Along with the degradation of the specimen fabric, tensile strength of specimens decreased. However, the rate of decrease was dependent on the type of the specimen fabric. By the time the maximum colour difference on the schematic line occurred for black Kevlar®/PBI fabrics, specimens had lost up to 40% of initial tensile strength (Figure 7.3).

Longer exposures to 30 kW/m^2 or exposures to higher intensities (40 kW/m^2) dropped the tensile strength of specimens approximately 60%. Then, discoloration started decreasing as a result of more severe degradation and char formation on the surface of specimens. This process turned the colour of the specimens darker. As the initial colour of fabrics (blue and dark blue) is close to black in RGB system, the resultant colour difference decreased. This trend is observed for specimens, the initial colour of which is close to black in RGB system.

A similar trend is observed for black specimens in Figure 7.3. Figure 7.3 illustrates the tensile strength of specimens in both fill and warp directions. After 30 s exposure to 20 kW/m^2, maximum discoloration occurred in the specimens. Tensile strength of specimens reduced quickly about 40% and fell below the minimum standard requirement of tensile strength for new fabrics. More severe degradation turned the colour of the specimens darker which was close to the initial colour of the specimen, black. In addition, the figure shows that data points after multi-stage exposure were along the schematic line drawn based on data points after single-stage exposure of specimens.

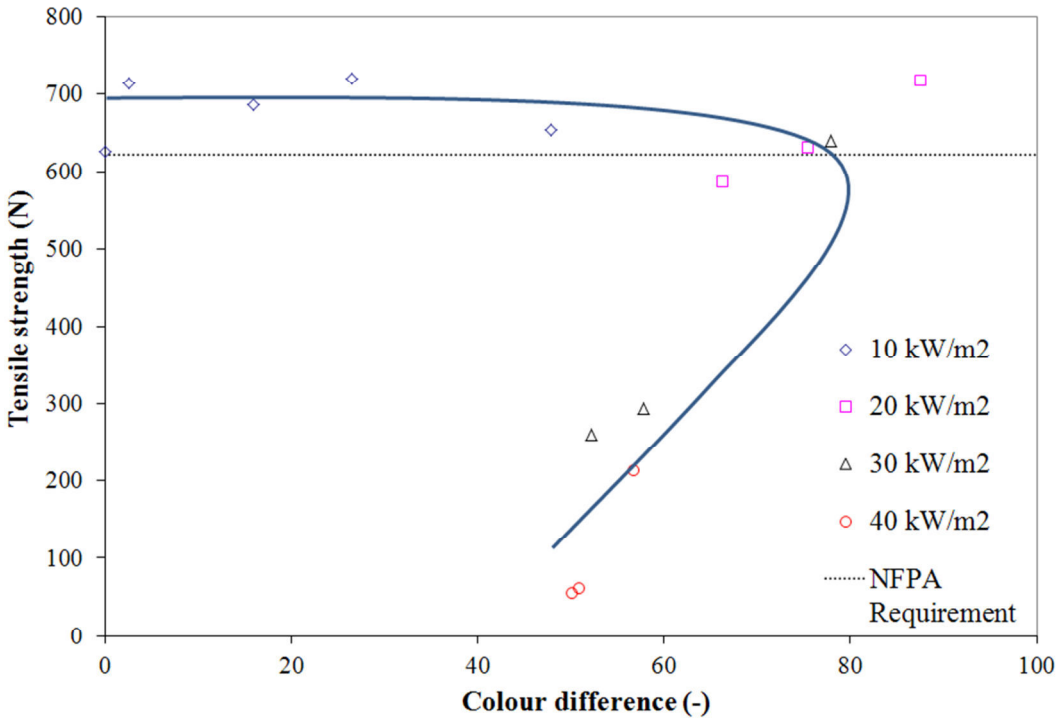

Figure 7.1: Correlation of tensile strength with colour difference for blue Nomex® specimens

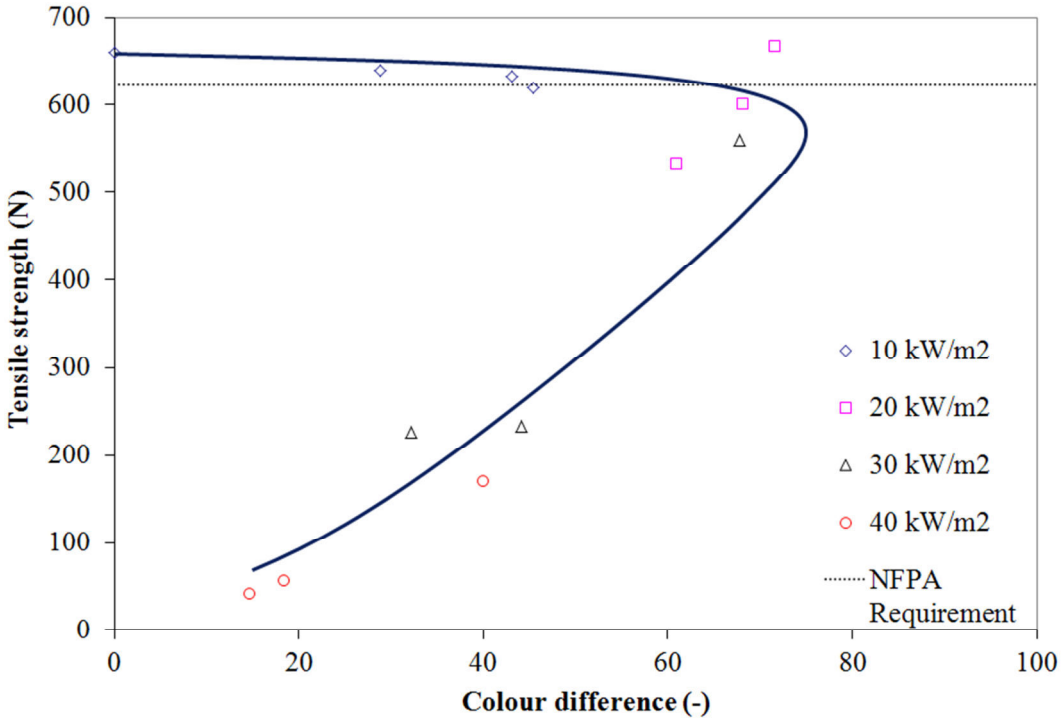

Figure 7.2: Correlation of tensile strength with colour difference for dark blue Nomex® specimens

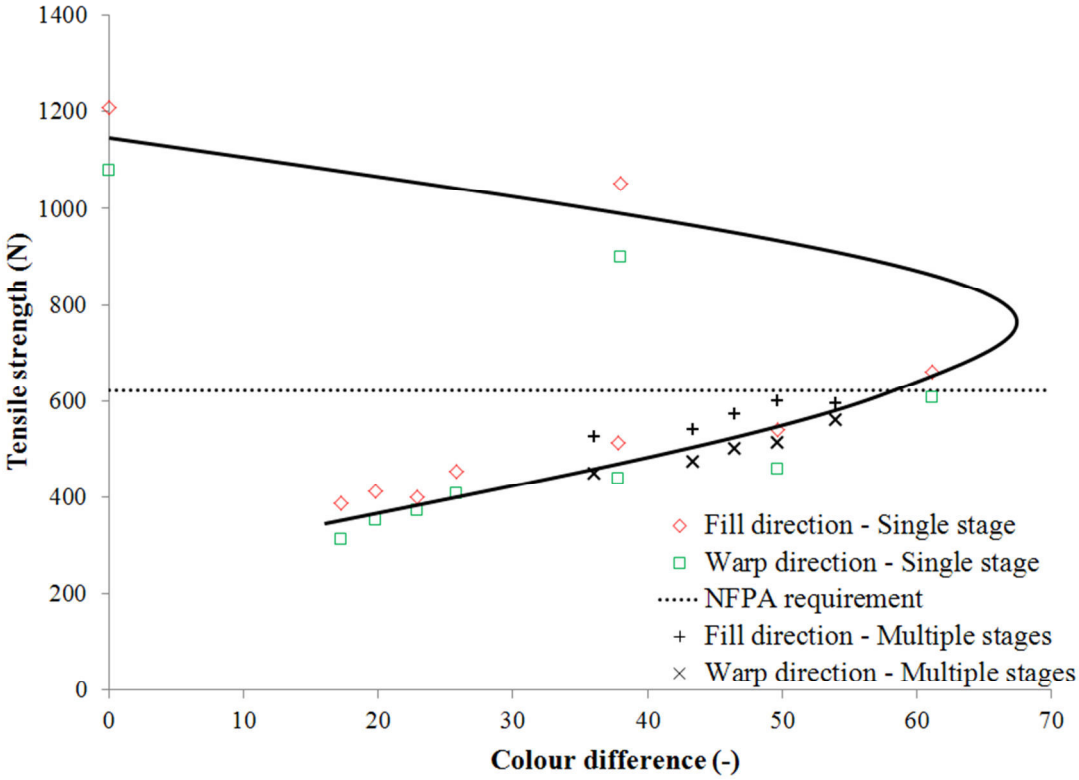

Figure 7.3: Correlation of tensile strength with colour difference for black Kevlar®/PBI specimens

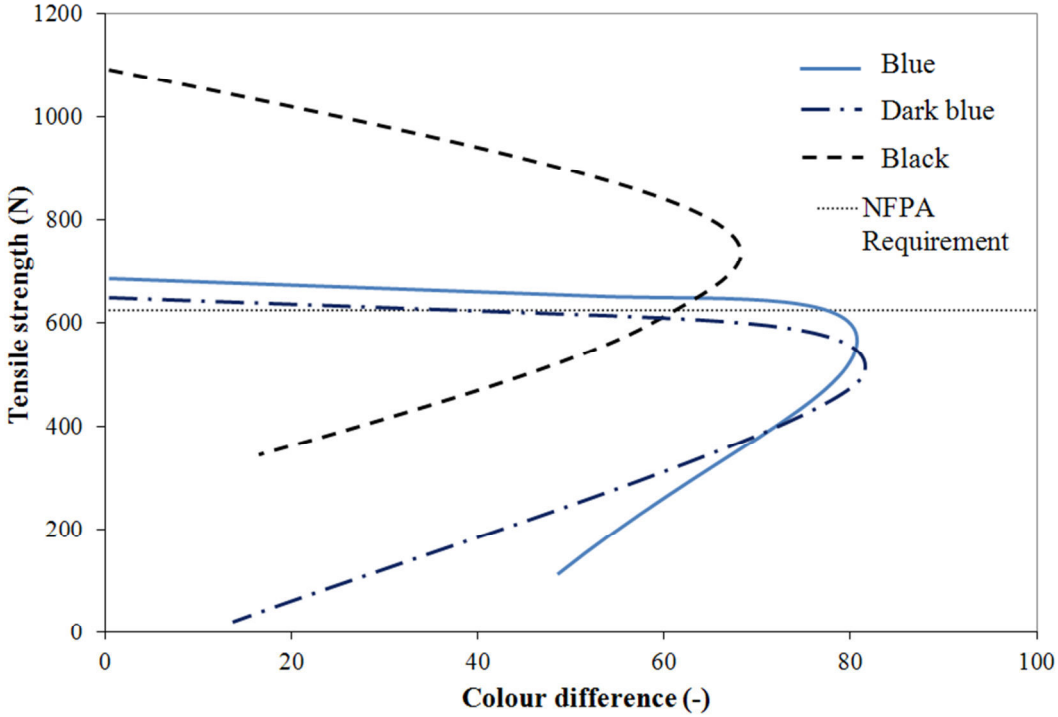

Figure 7.4: The first type of colour change and its correlation with tensile strength

The second type of colour change was observed for red, yellow, and brown fabrics in Figures 7.5, 7.6, and 7.7, respectively. Figure 7.8 illustrates the second type of colour change for fabrics in the three colours. The figure indicates that maximum colour difference depends on how different the initial colour of the fabric is from black.

In Figures 7.5 and 7.6, the colour difference continued to increase, and there was an inflection point in the curve. Similar to the first trend, progressive dye removal increased the difference between the initial colour and the colour of specimens after thermal exposure. Eventually, the colour difference reached a value corresponding to the colour difference between the initial colour and the natural colour of the fabric. This point seemed to be an inflection point for the trend. After this point, tensile strength of specimens reduced rapidly by around 50%.

The anomaly in the two trends started after this point. Unlike the first set of fabrics (blue, dark blue, and black) where, the colour difference started decreasing when the natural colour of the fabric was revealed, in the second set of fabrics, the colour change kept increasing, as the severe degradation and charring turned the specimen fabric colour darker and increased the difference from the initial colour in the RGB system. The colour change in brown specimens (Figure 7.7) followed only the second half of the trend after the inflection point since the specimen fabric was undyed and the initial colour was in fact the natural colour of the fabric. The first half of the colour change trend is a result of continuous dye removal, which does not apply to undyed fabrics. The figure illustrates the correlation between the colour change and the tensile strength for both fill and warp directions, which are essentially similar. The same as Figure 7.3, data points related to specimens after multi-stage thermal exposure also lie around the trend line drawn schematically based on single-stage exposure of specimens. This observation can imply ability of this non-destructive technique to predict tensile strength of fabrics after thermal exposure.

Two types of colour change were identified for a variety of colours of two fabrics of outer shell layer of firefighters' protective clothing. The main distinction between the two types is correspondence between the tensile strength and colour change. In the first type, there are two values of tensile strength for a single value of colour change. But, the second type creates one-to-one correspondence between tensile strength and colour change. The one-to-one correspondence is favourable for numerical modelling and would be easier to use. The advantages and disadvantages of this technique will be discussed at the end of this chapter.

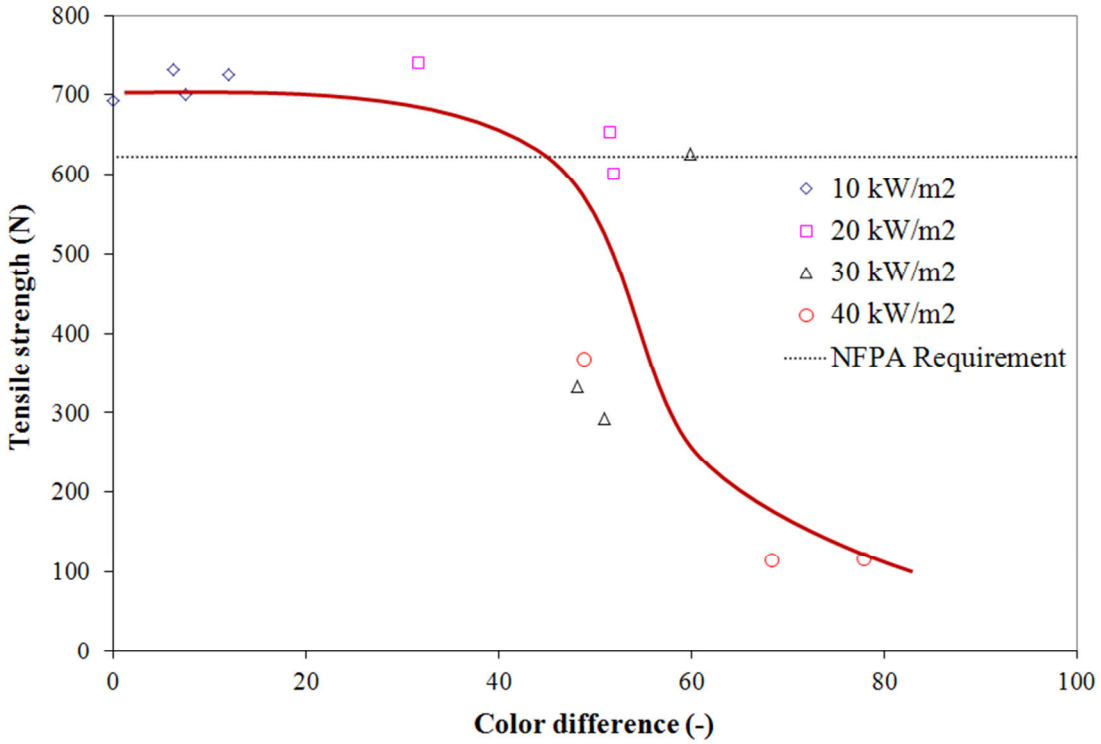

Figure 7.5: Correlation of tensile strength with colour difference for red Nomex® specimens

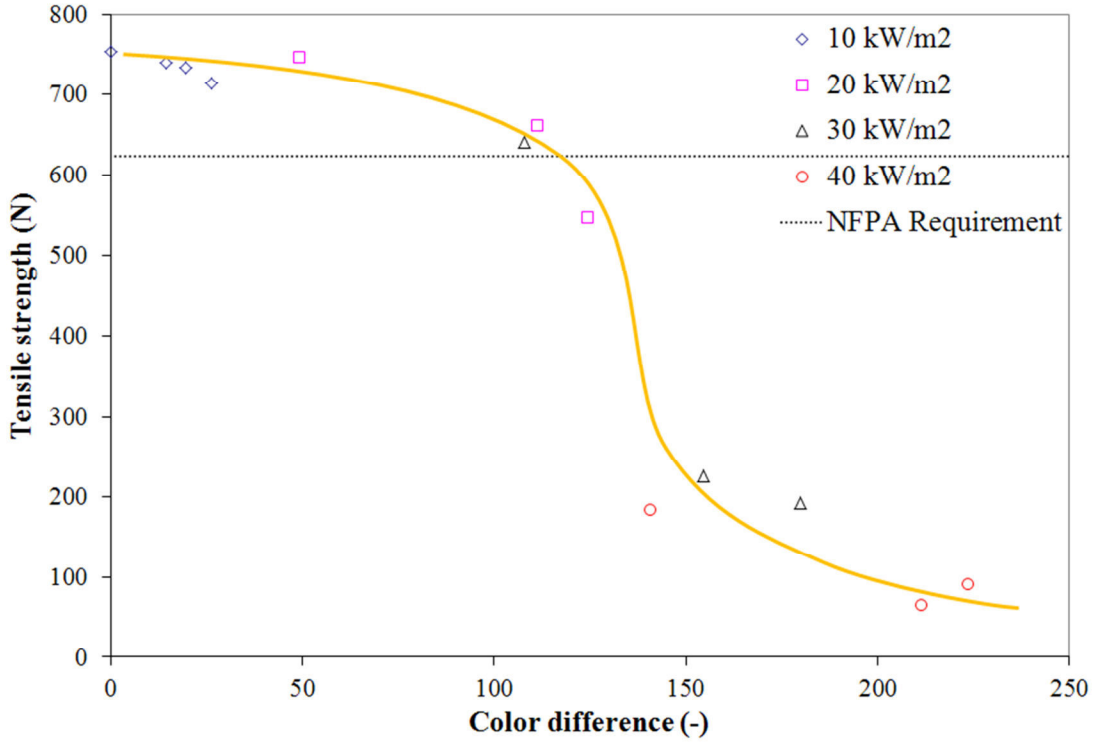

Figure 7.6: Correlation of tensile strength with colour difference for yellow Nomex® specimens

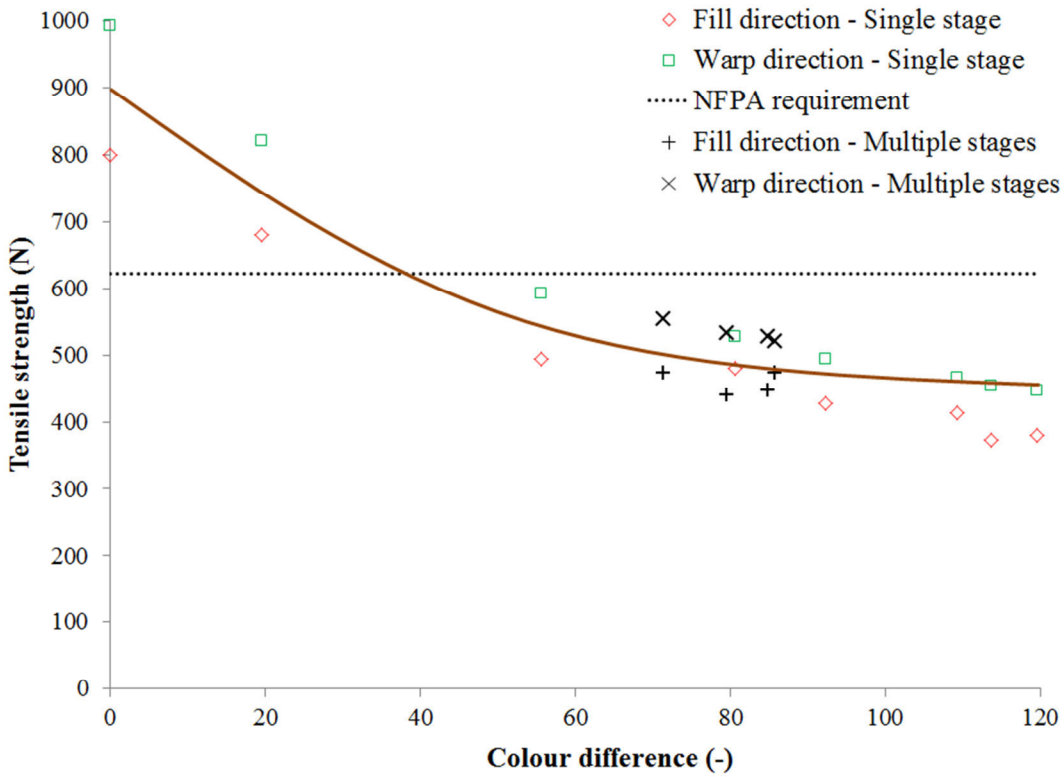

Figure 7.7: Correlation of tensile strength with colour difference for brown Kevlar®/PBI specimens

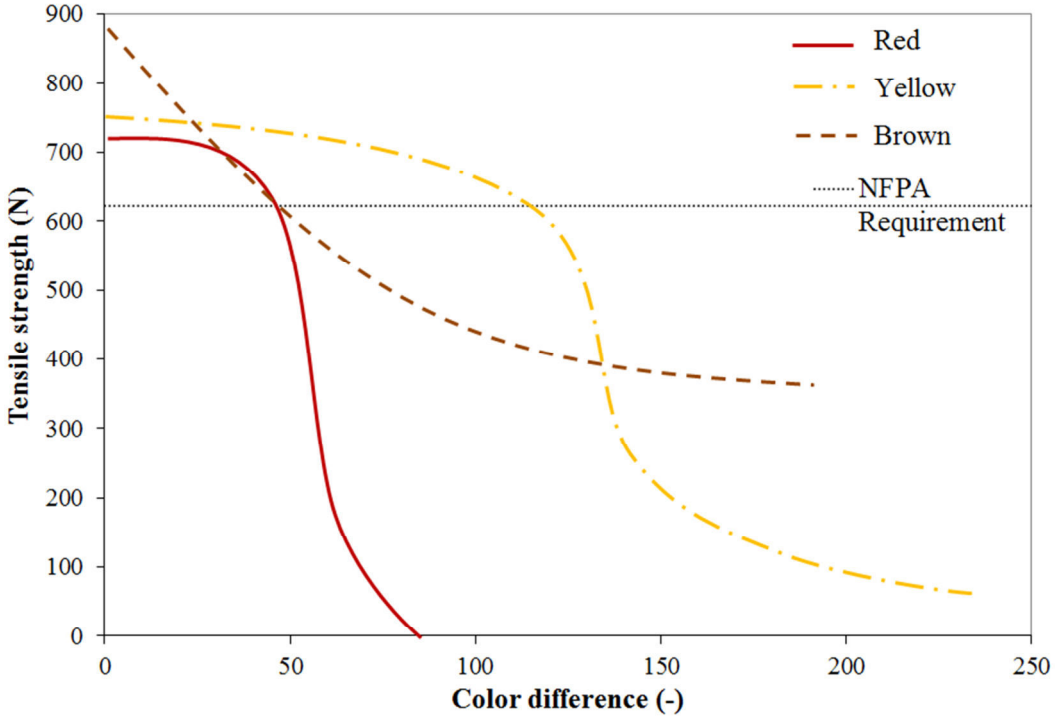

Figure 7.8: The second type of colour change and its correlation with tensile strength

7.2.Correlation between tensile strength and near infrared spectroscopy

In section 6.1.2, it was mentioned that reflectance spectrum of outer shell specimens would be analysed in the wavelength region of 1500 – 2500 nm. Since the reflectance spectrum was recorded at intervals of 1 nm, reflectance was measured at 1001 points within the wavelength region of 1500 – 2500 nm. From a mathematical point of view, it is feasible to develop a numerical model to correlate tensile strength with the reflectance at all of 1001 points. But, from practical point of view, it is expensive to purchase a spectrophotometer and to some extent, time-consuming to record the reflectance spectrum within the full wavelength region. In order to decrease the number of points for practical purposes, principal wavelengths should be recognized.

It was shown in section 6.3 that reflectance of specimens does not change uniformly within the wavelength region of 1500 – 2500 nm. For example, the reflectance spectrum of specimens within the wavelength region of 1900 – 2500 nm was not as sensitive as the region of 1500 - 1900 nm to the change in intensity or duration of thermal exposure. This observation indicates that some wavelength regions may be more useful and effective in order to correlate tensile strength with reflectance of specimens. If these important wavelengths were recognized, the numerical model (correlation) could be built only based on these wavelengths.

Designing a device to measure reflectance at several wavelengths costs just a few hundred dollars[5], depending on the region of wavelengths. In addition, such a device would be small and handy and can be used for in situ measurement. This can be a step forward in developing a practical and commercial procedure to predict tensile strength of outer shell using near infrared spectroscopy.

There are a variety of statistical methods to extract the main and the most influential factors from a mass of data. Regression analysis is a basic method to correlate a dependent variable to any number of independent variables. The mathematical equation that correlates a dependent variable to independent variables is called a regression equation [90].

[5]- Private conversation with Prof. Scott Noble, Department of Chemical and Biological Engineering, University of Saskatchewan in April 2013.

The simplest application of regression analysis is a first-order linear model. The most general form of a first-order linear model is shown by Equation 7.1

$$Y = \alpha_0 + \alpha_1 X_1 + \alpha_2 X_2 + \ldots + \alpha_n X_n + \varepsilon \tag{7.1}$$

where Y is a dependent variable, X denotes an independent variable, α signifies the coefficient of the independent variables, n indicates the number of the independent variables, and ε represents the deviation of the predicted response value from the real value. In the current application, tensile strength is the dependent variable and reflectance at a specific wavelength is an independent variable.

In order to predict a dependent variable in the simplest form, a first-order linear regression equation in terms of n independent variables should be established. On the one hand the equation should include as many independent variables as possible to ensure the accuracy and reliability of the prediction. On the other hand it should include as few independent variables as possible to keep the cost of monitoring, recording, and computing minimal. The compromise between these two conditions is found by statistical criteria such as R^2 and R^2_a (adjusted R^2) and obviously personal judgment to select the best subsets of the regression equations. R^2 and R^2_a are defined by Equations 7.2 and 7.3

$$R^2 = \frac{\sum_{i=1}^{m}(\hat{Y}_i - \bar{Y})^2}{\sum_{i=1}^{m}(Y_i - \bar{Y})^2} \tag{7.2}$$

$$R_a^2 = 1 - (1 - R^2)\left(\frac{n-1}{n-p}\right) \tag{7.3}$$

where, m is the number of observations of the dependent variable (Y), $\hat{Y}$ is the predicted value of the dependent variable, $\bar{Y}$ is the mean of the real values of the dependent variable in m observations, and p is the total number of coefficients including α_0. R^2_a is an adjusted form of R^2 which takes the number of coefficients (the number of parameters) used in developing the model into effect. This adjustment makes R^2_a a better statistic for comparison of models made of different numbers of parameters.

Most commercial statistical software packages carry out regression analyses. Their selection procedure is based on addition and subtraction of variables to and from a set of variables in order to minimize or maximize a particular statistical criterion. Such a selection procedure is dependent on the initial set of variables and therefore, the resultant equation is not unique. Furthermore, running these software packages often result in a single subset of variables, which has the highest rank in terms of a statistical criterion of interest, rather than a list of subsets. A single subset of variables is not enough to apply practical judgment since the cost of acquiring reflectance at different wavelengths may be quite different.

In order to respond to these issues, a numerical code based on linear regression analysis was written in MATLAB® to assess and order all possible subsets of regression equations according to statistical criterion of interest or the number of independent variables (wavelengths) in the regression equation. Selection of a regression equation can be made by personal judgment based on a compromise between a higher value of the statistical criterion, and a lower number of the independent variables (wavelengths), and the specific region of wavelengths.

One limitation of classical approaches to linear regression analysis is that the number of independent variables (as well as the constant term) should be less than the number of observations of dependent variables [90]. Otherwise, the matrix of equations would be singular and could not be solved. There are 13 observations for red, dark blue, and yellow outer shell specimens, which include an unexposed condition as well as 12 exposed conditions described in Table 3.1. There are 15 observations for blue specimens since two extra ageing conditions (exposure to 10 kW/m^2 for 15 s and 20 kw/m^2 for 60 s) were performed. Furthermore, there are 12 and 14 observations for brown and black specimens, respectively since a single-stage exposure for 300 s and correspondingly 10 stages of exposure were performed for black specimens only.

The maximum number of independent variables (wavelengths) is one less than the number of observations for each type of specimen. Depending on the number of observations for each type of specimen, maximum number of wavelengths in intervals of 100 nm starting from 2500 nm and backwards was selected. For instance, wavelengths of 2500, 2400, 2300, 2200, 2100, 2000, 1900, 1800, 1700, 1600, and 1500 nm were picked as 11 variables (training points) for analysis of red, dark blue, and yellow specimens. Figures 7.9 to 7.14 show the range of adjusted R^2 (R^2_a) as the statistical parameter of interest for all possible linear equations made of a particular

number of variables for blue, red, dark blue, yellow, brown, and black specimens, respectively. The dashed line in the figures is a schematic line which passes the maximum value of R^2_a and indicates the trend of change in R^2_a as the number of variables in equation increased.

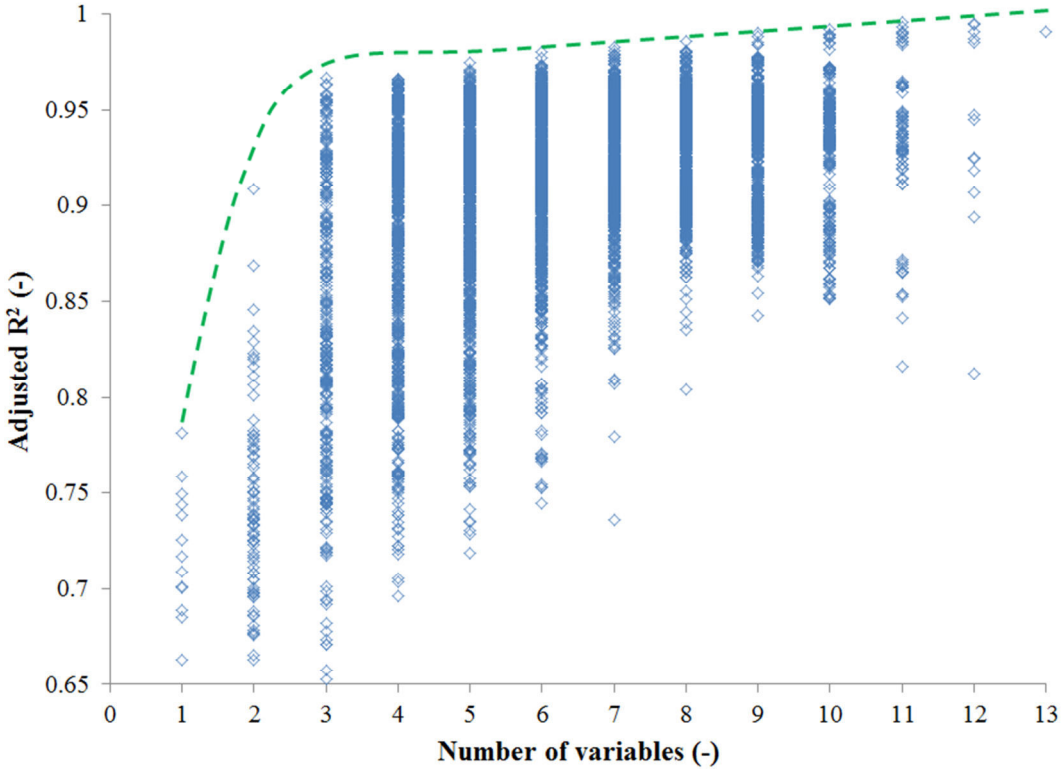

Figure 7.9: Range of adjusted R^2 values in equations made of a particular number of variables for blue Nomex® specimens

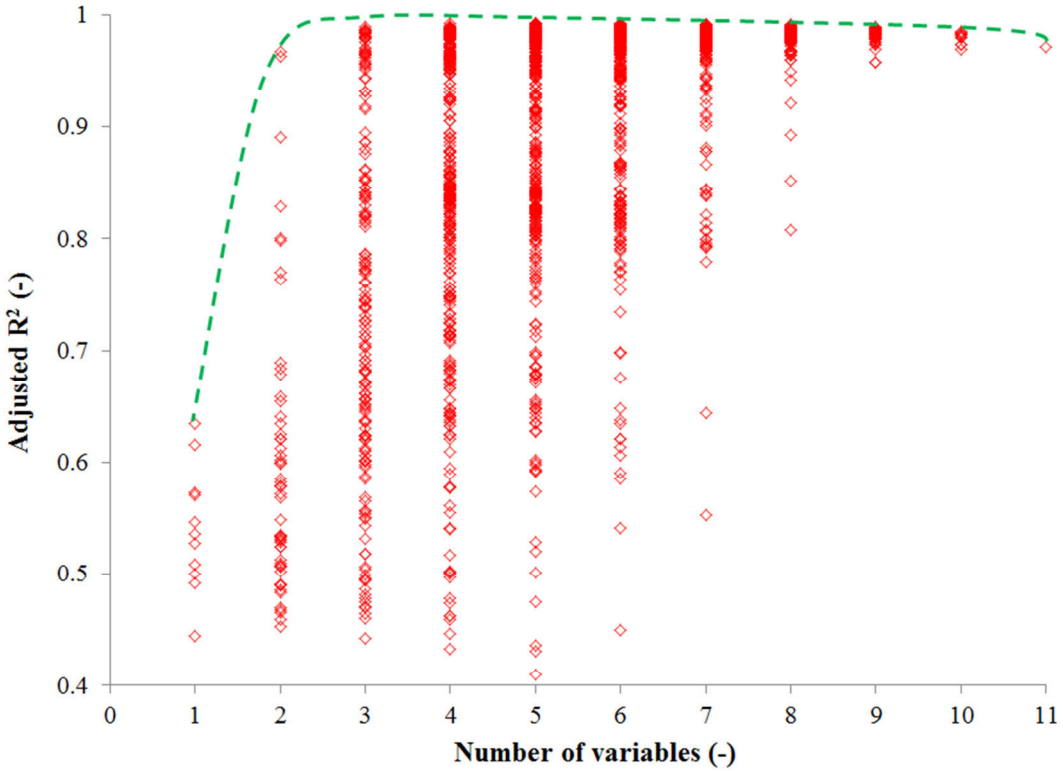

Figure 7.10: Range of adjusted R^2 values in equations made of a particular number of variables for red Nomex® specimens

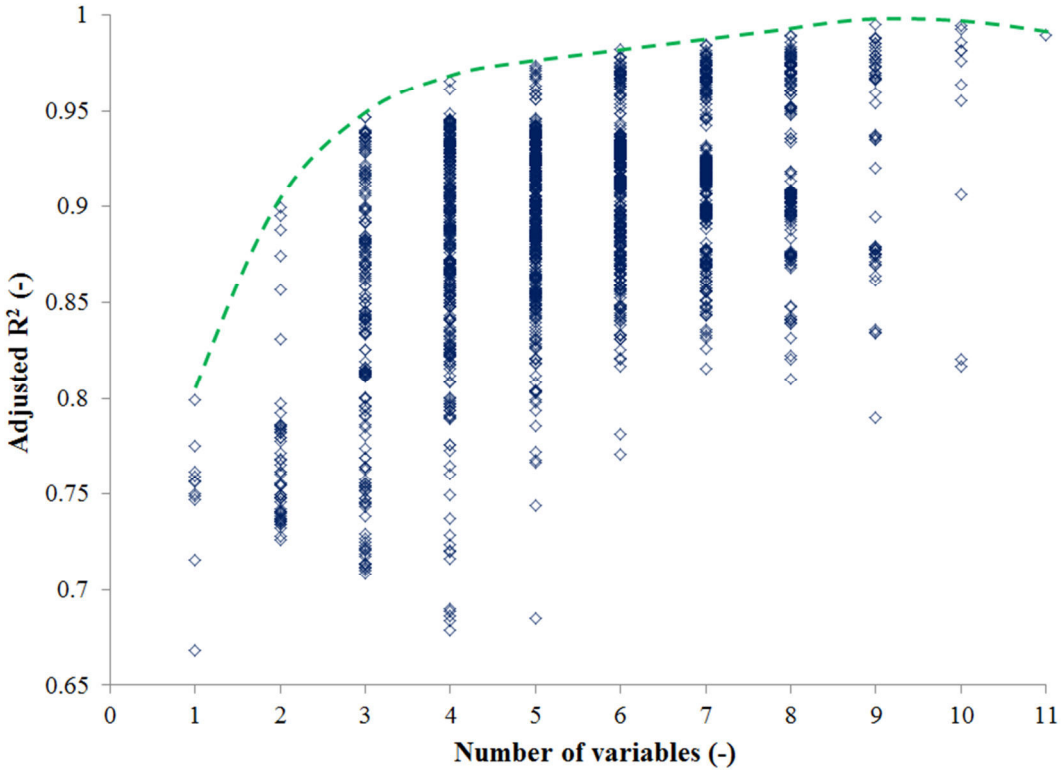

Figure 7.11: Range of adjusted R^2 values in equations made of a particular number of variables for dark blue Nomex® specimens

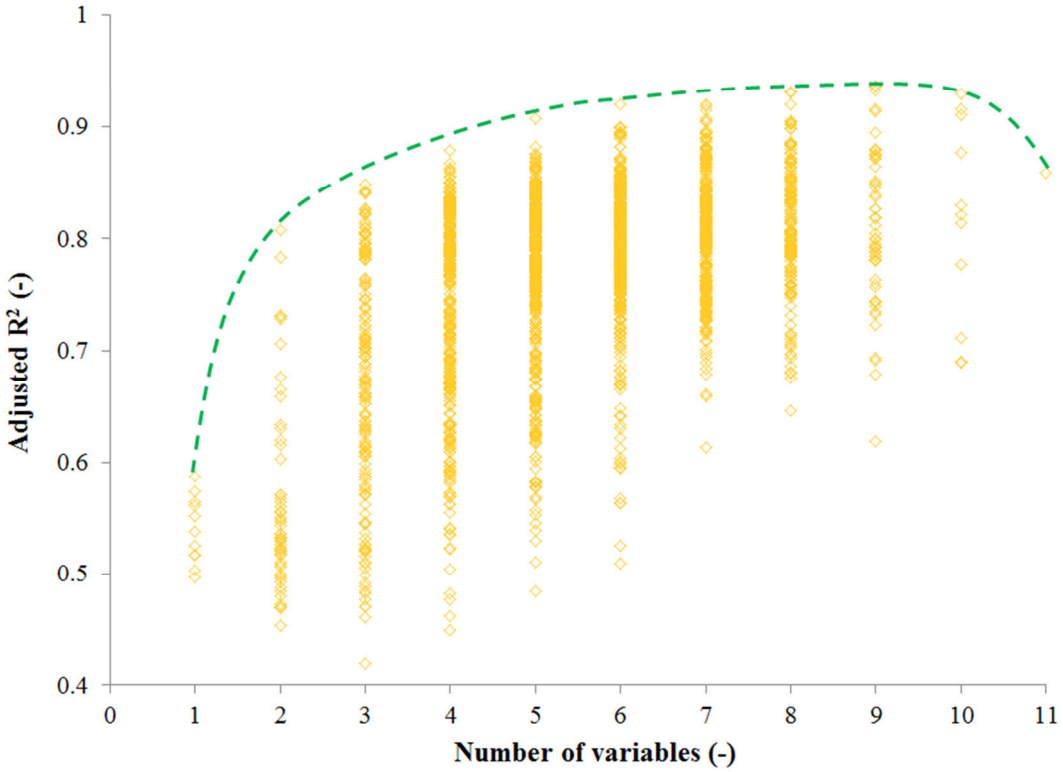

Figure 7.12: Range of adjusted R^2 values in equations made of a particular number of variables for yellow Nomex® specimens

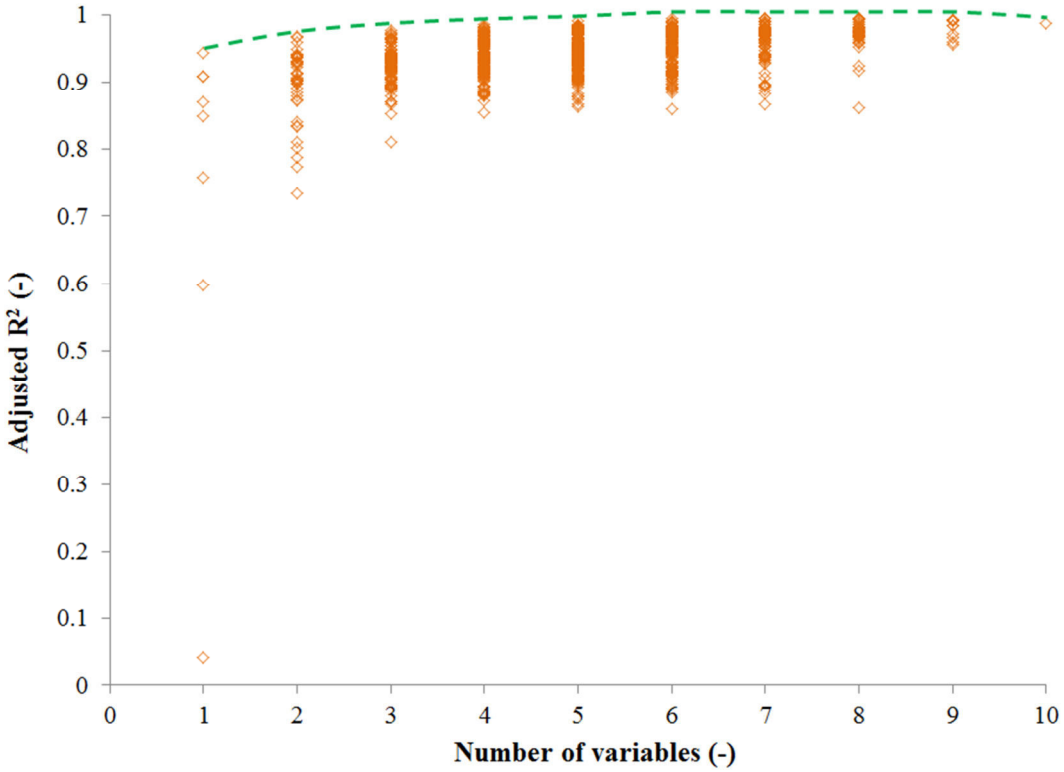

Figure 7.13: Range of adjusted R^2 values in equations made of a particular number of variables for brown Kevlar®/PBI specimens

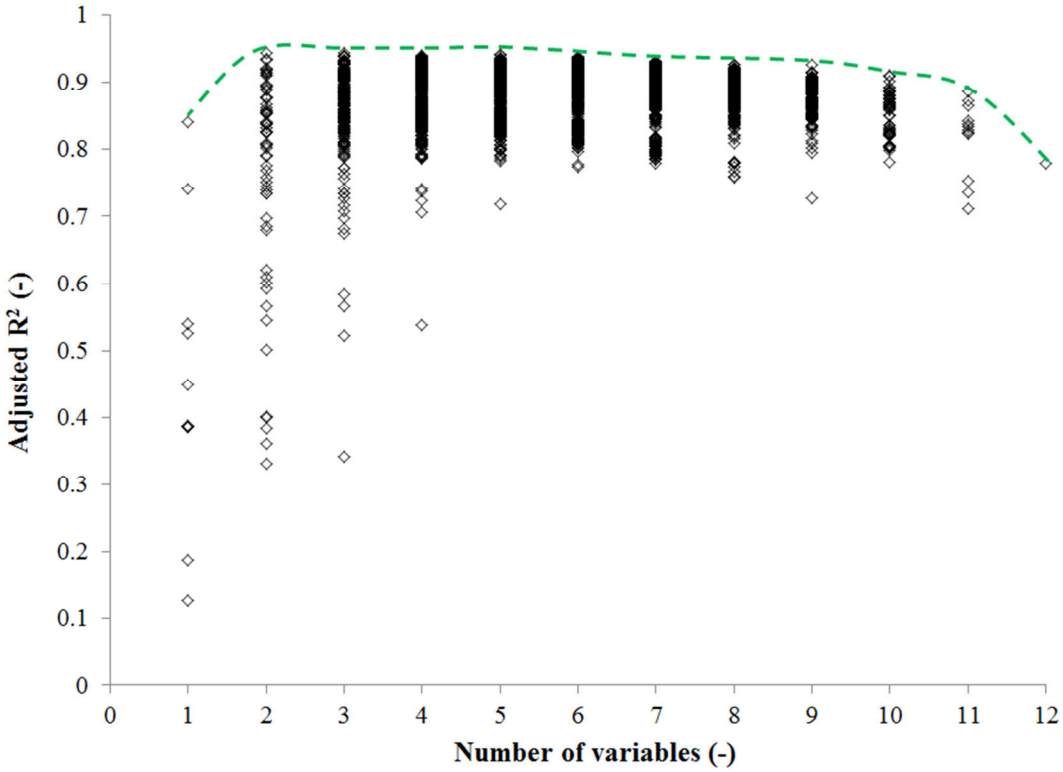

Figure 7.14: Range of adjusted R^2 values in equations made of a particular number of variables for black Kevlar®/PBI specimens

The figures indicate sensitivity of R^2_a to number of constituent variables (wavelengths). They illustrate that the deviation of training data points from a linear model for an equation made of two variables can be even less than for a 10-variable equation. It may be thought at the first glance that an equation constructed from maximum number of variables is the best linear model in terms of R^2_a. But, the figures depict that it is not always the case and models based on a much lower number of wavelengths could be a better linear fit and therefore, a better choice. This relates to the fact that reflectance spectra of specimens are not equally sensitive to thermal degradation at different wavelength regions, which originates from sensitivity of reflectance to specific molecular bonds and chemical structure. In addition, the figures may point out the role of colour since the predictive equations are more accurate for a colour like red than yellow.

The dashed schematic lines in the figures indicate that R^2_a for a three-variable equation is within almost 5% (10% for yellow specimens) of the value for the best linear equation. Developing a device to measure reflectance at three wavelengths is also quite simple and inexpensive. So, a three-variable equation may be an accurate enough model and predict tensile strength with sufficient accuracy. Table 7.1 shows the three wavelengths of the best predictive equation in terms of R^2_a for all types of outer shell specimens. The results indicate that the predictive models may work more accurately for some colours like red and brown than yellow in terms of R^2_a value.

A list of predictive equations was determined for each outer shell specimen using the numerical code. Specifications of an example of predictive equations constructed from three wavelengths are shown in Table 7.1. The table shows that a model based on even three wavelengths can be accurate enough in terms of R^2_a (>0.94 for all but the yellow fabric) for prediction of tensile strength of outer shell specimens. Besides, the table implies that wavelengths in the region 1500 – 2000 nm were used more frequently in making an accurate equation. This is in agreement with major absorption bands of functional groups (–CH, –OH, and –NH) of specimens fabrics in the wavelength region 1500 – 2000 nm, which were discussed in section 6.3.

Table 7.1: Wavelengths of the most accurate three-variable equation for each type of specimen

Specimen type	R^2_a (-)	Wavelengths (nm)		
		1	2	3
Blue	0.97	1500	1600	2000
Red	0.99	1600	1800	2300
Dark blue	0.95	1600	1800	2500
Yellow	0.85	1500	1600	1900
Brown	0.98	1600	1900	2000
Black	0.94	1400	1500	2500

Even though statistical parameters like R^2_a imply that a linear equation may fit training data points well within the test matrix, it does not give any information about how accurately a linear equation predicts tensile strength of fabrics that were not included in the training data (called interpolating points here). In order to investigate this issue, one specimen from blue, red, dark blue, and yellow fabrics was cut and was thermally aged using the same procedure in section 2.2. Then, reflectance spectrum and tensile strength of specimens were recorded. Table 7.2 shows tensile strength of these specimens after thermal exposure.

Table 7.2: Thermal exposure specification and tensile strength of blue, red, dark blue, and yellow Nomex® outer shell specimens for the purpose of interpolation

Intensity / Duration of thermal exposure	Tensile strength of specimens (N)			
	Blue	Red	Dark blue	Yellow
5 kW/m^2 / 3600 s	695	764	634	737
15 kW/m^2 / 1200 s	618	626	586	614
25 kW/m^2 / 180 s	324	325	302	291

Figures 7.15 to 7.20 illustrate the replication of data points by the predictive equations in Table 7.1 for all outer shell specimens. Figures 7.15 to 7.18 show also the error in predicting interpolating points for blue, red, dark blue, and yellow specimens, respectively. Predicted and actual values of tensile strength would lie on a 45-degree line if the model generated values exactly the same as actual values. This 45-degree line is presented by a solid line in the figures.

The figures show is a gap in the training data points within the range of 400 – 600 N. This could be improved in future work using a wider range of intensity and durations of thermal exposure to get wider range of degradation and deterioration in tensile strength.

The error percentage in predicting actual values of interpolating points are pointed out by labels beside each point. The models had varying degrees of success in predicting the interpolating points for different colours and exposures. Among the three interpolating points that were not part of the training points, the models predict lower than actual values for tensile strength of specimens which were moderately aged (exposure to 5 and 15 kW/m^2 which represent ordinary condition). For the more severe exposure to 25 kW/m^2 (which represents the lower portion of the emergency condition range), predicted tensile strength is higher than the actual value.

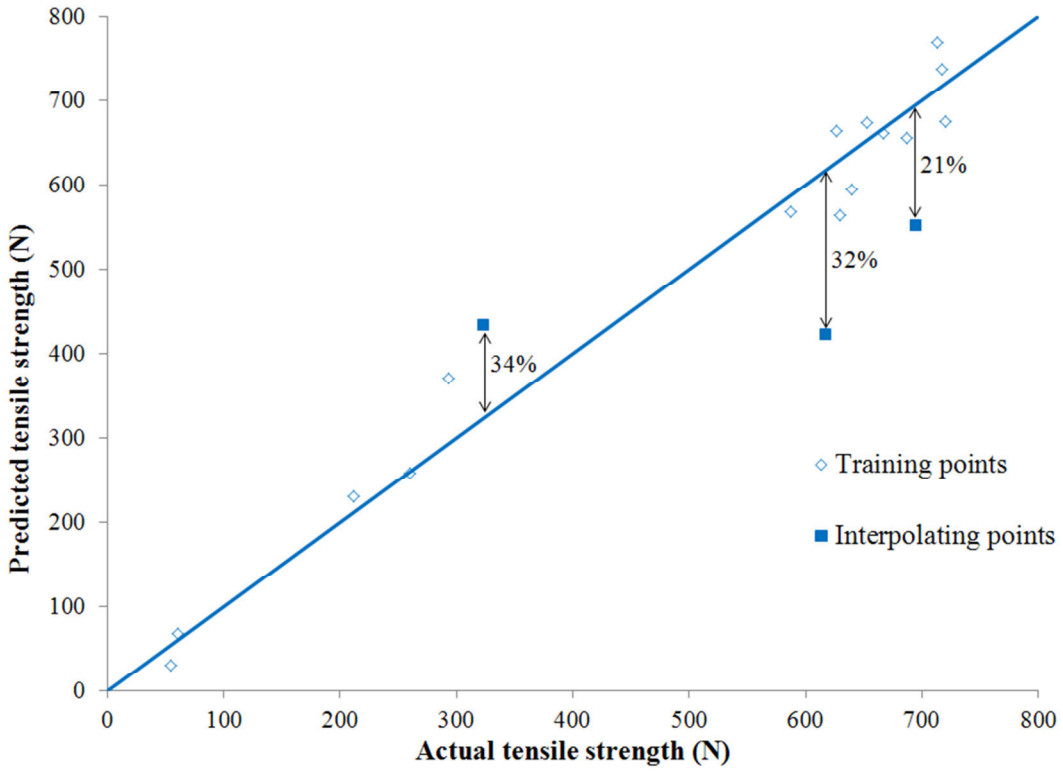

Figure 7.15: Accuracy of the three -variable model for blue Nomex® specimens to predict tensile strength of interpolating points

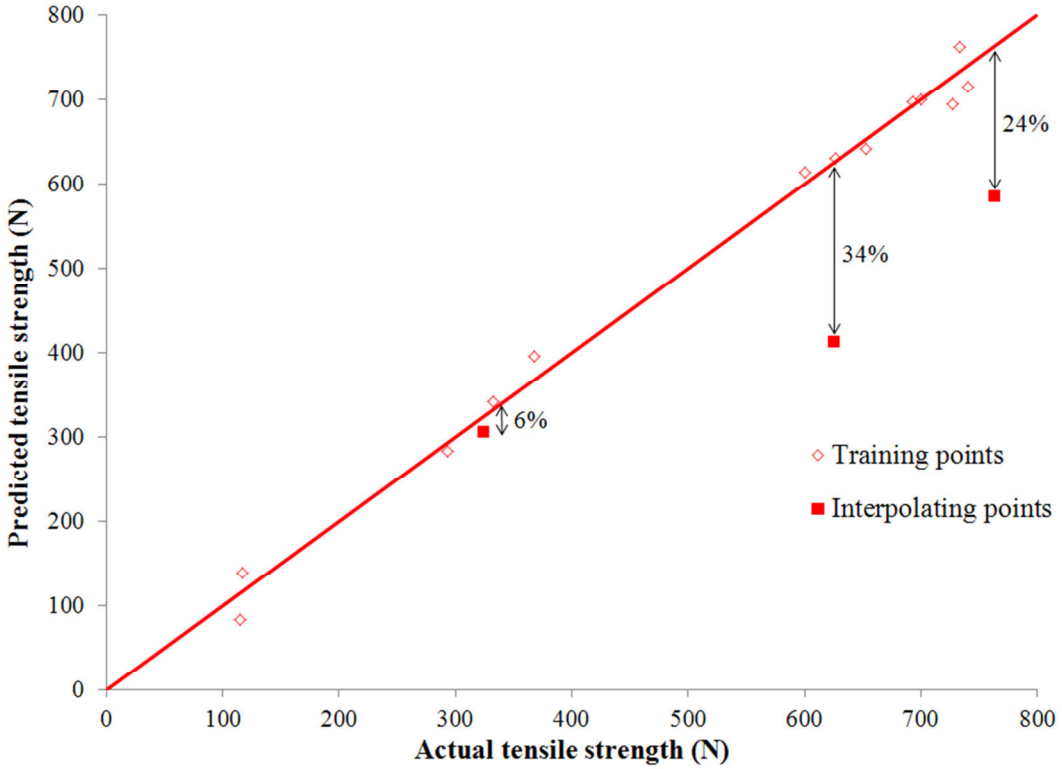

Figure 7.16: Accuracy of the three-variable model for red Nomex® specimens to predict tensile strength of interpolating points

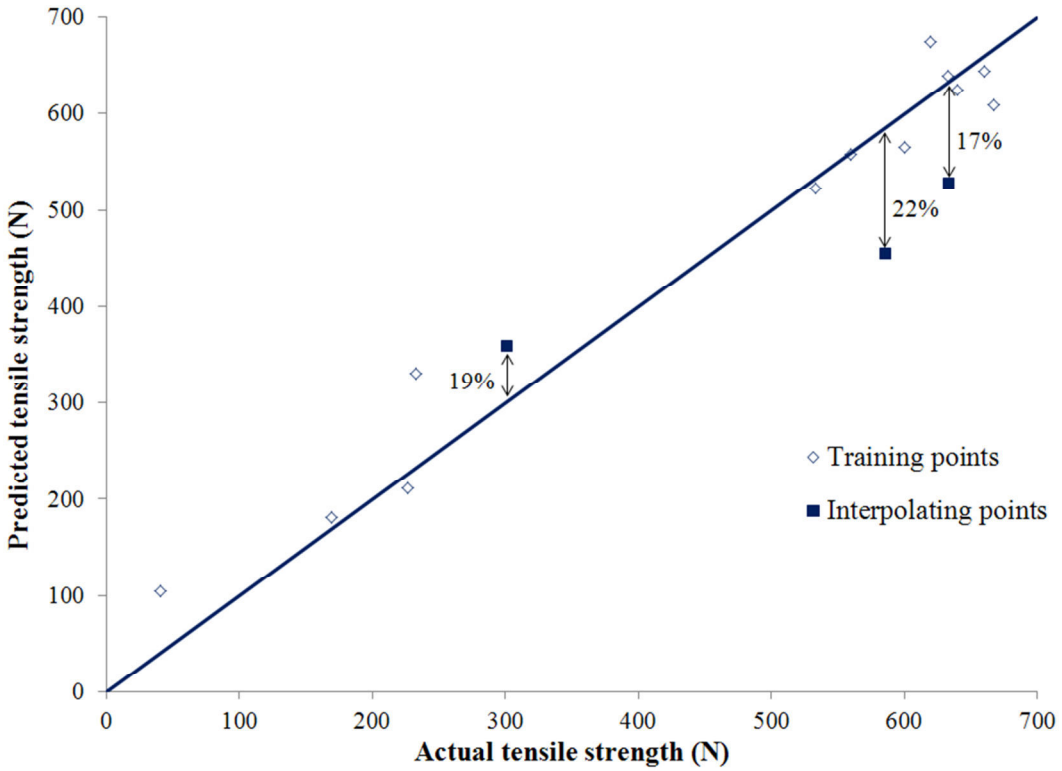

Figure 7.17: Accuracy of the three-variable model for dark blue Nomex® specimens to predict tensile strength of interpolating points

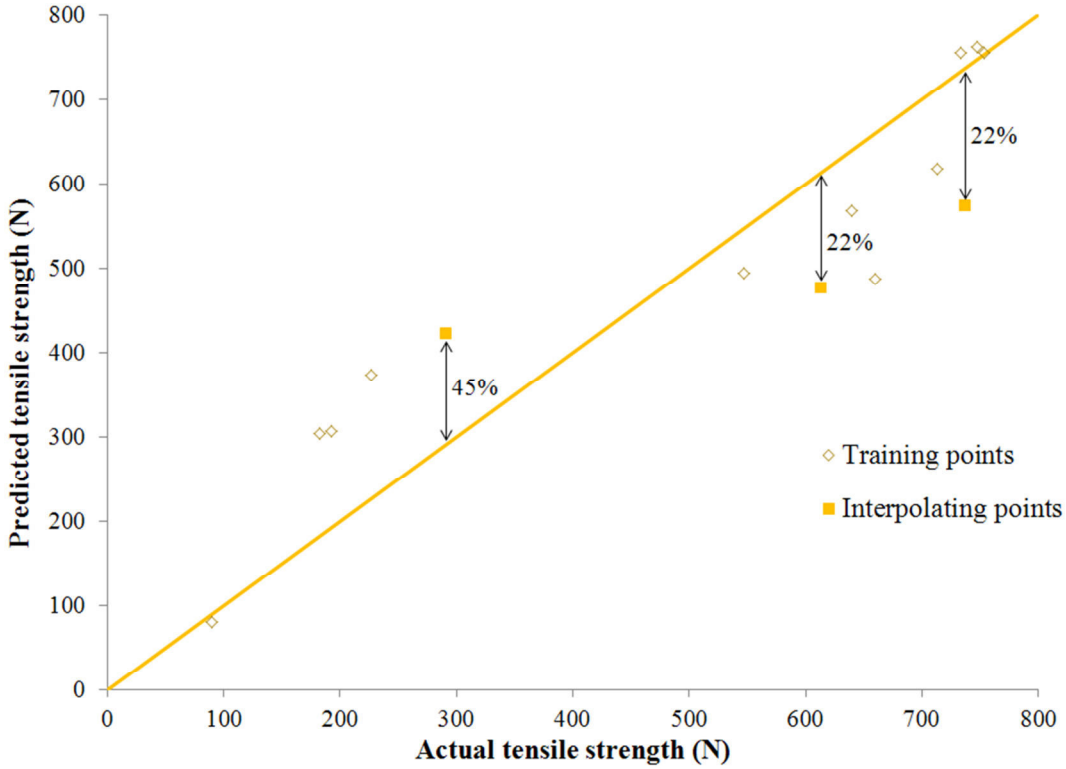

Figure 7.18: Accuracy of the three-variable model for yellow Nomex® specimens to predict tensile strength of interpolating points

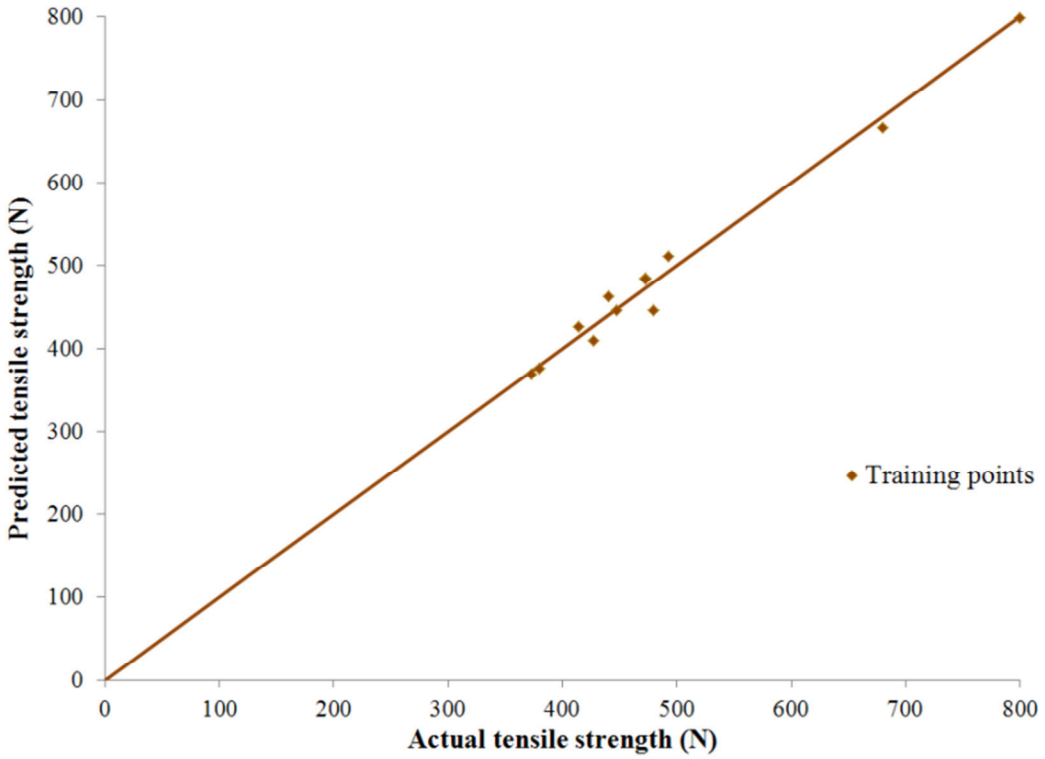

Figure 7.19: The three-variable model for brown Kevlar®/PBI specimens

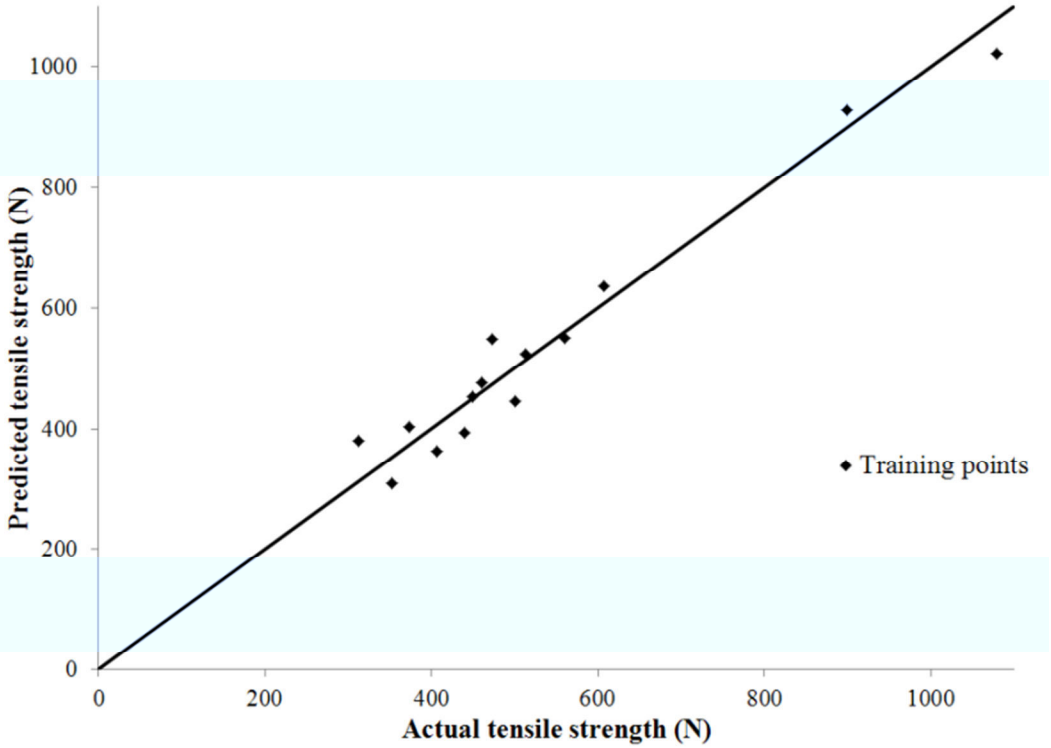

Figure 7.20: The three-variable model for black Kevlar®/PBI specimens

There are a number of potential ways to improve the prediction of data points using the models. The number of variables included in the model is one of these parameters. Figure 7.21 compares the effect of number of variables on the ability of the model to predict training data points using the equation with the highest value of R^2 for each number of variables for blue specimens. Appendix E shows the same figures for other outer shell specimens. Table 7.3 gives the numerical values of R^2 and R^2_a of the equations in Figure 7.21 and Appendix E for all outer shell specimens. Figure 7.21 illustrates that the percentage error decreased by increasing the number of wavelengths used in developing a model. Table 7.3 quantifies this change. Depending on the colour and material of outer shell specimens, R^2 increased by 1 to 10%. The increase in R^2 does not necessarily indicate an increase in R^2_a. R^2_a is an adjusted form of R^2, which takes the number of wavelengths into account according to Equation 7.3. For example, for brown Kevlar®/PBI specimens, increasing the number of wavelengths from 7 to 10 decreased R^2_a. The same decrease in R^2_a was observed for black Kevlar®/PBI specimens when the number of wavelengths increased to 7 and 10. Even though increasing the number of wavelengths increased R^2_a for some outer shell specimens in Table 7.3, it will increase the cost of a device to measure the reflectance at extra wavelengths. So, the decision to choose the number of wavelengths could be different depending on each application.

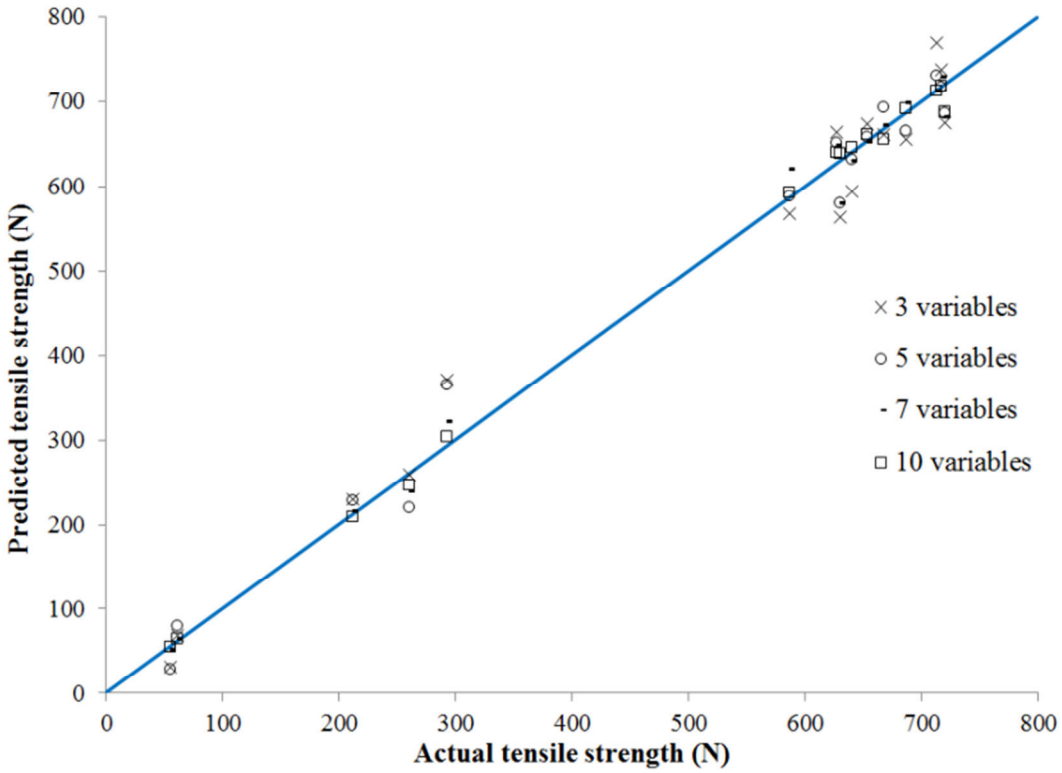

Figure 7.21: Replication of data points by the best equations made of 3, 5, 7, and 10 wavelengths for blue specimens

Table 7.3: R^2 and R^2_a for the equations made of 3, 5, 7, and 10 wavelengths

Number of wavelengths / Specimen type	3		5		7		10	
	R^2	R^2_a	R^2	R^2_a	R^2	R^2_a	R^2	R^2_a
Blue	0.974	0.967	0.984	0.975	0.991	0.983	0.998	0.992
Red	0.992	0.990	0.996	0.992	0.997	0.992	0.998	0.986
Dark blue	0.960	0.947	0.985	0.974	0.994	0.984	0.999	0.995
Yellow	0.886	0.849	0.946	0.908	0.966	0.920	0.988	0.929
Brown	0.984	0.977	0.995	0.990	0.998	0.995	0.999	0.988
Black	0.957	0.943	0.965	0.943	0.968	0.931	0.979	0.910

In order to consider the effect of wavelength regions on accuracy of predictive equations, the numerical code was run for three types of data input based on blue specimens training points. In

the first type, variables were selected from the wavelength region of 1500 – 1900 nm in intervals of 25 nm. Wavelengths in intervals of 50 nm in the region 1900 – 2500 nm were selected as the second input to the numerical code. For the third type of data input, wavelengths related to peaks and valleys in the reflectance spectrum of blue specimens (Figures 6.15-6.18) in the wavelength region 1500 – 2500 nm were determined and selected. The specifications of the three-variable equations which had the highest R^2_a are shown in Table 7.4. Among the three types of data input, the first type of data input limited to wavelengths in the region 1500 – 1900 nm resulted in the highest R^2_a for the predictive equation. The linear equation based on the second type of data input, the wavelengths of which were selected from the region 1900 – 2500 nm, had the lowest R^2_a. These observations are in agreement with the fact that reflectance spectrum was more sensitive to thermal exposure in the region 1500 – 1900 nm.

Table 7.4: Specifications of the three-variable equations with the highest R^2_a for blue specimens

Wavelength region (nm)	R^2_a (-)	Wavelengths (nm)		
		1	2	3
1500 – 1900	0.96	1500	1600	1700
1900 – 2500	0.88	2200	2450	2500
1500 – 2500*	0.93	1600	1750	2425

* Selected wavelengths based on peaks and valleys in NIR spectrum

Figures 7.22-7.24 compare the error percentages of the three linear equations in Table 7.4 in prediction of the interpolating points. Even though, the first equation in Table 7.4 had the highest R^2_a, it had the highest error in prediction of tensile strength for interpolating points. The second equation predicted the tensile strength for interpolating points with lower error. Although the first equation had higher error percentage in prediction of tensile strength of the interpolating points, it predicted the tensile strength of two specimens exposed to ordinary conditions conservatively. The prediction of tensile strength of the interpolating points using the second equation was higher than the actual values. As this application concerns safety of personnel wearing in-use protective clothing, a conservative model would be preferred since it provides an inherent margin of safety. A safety factor could also be included in the model used to predict tensile strength.

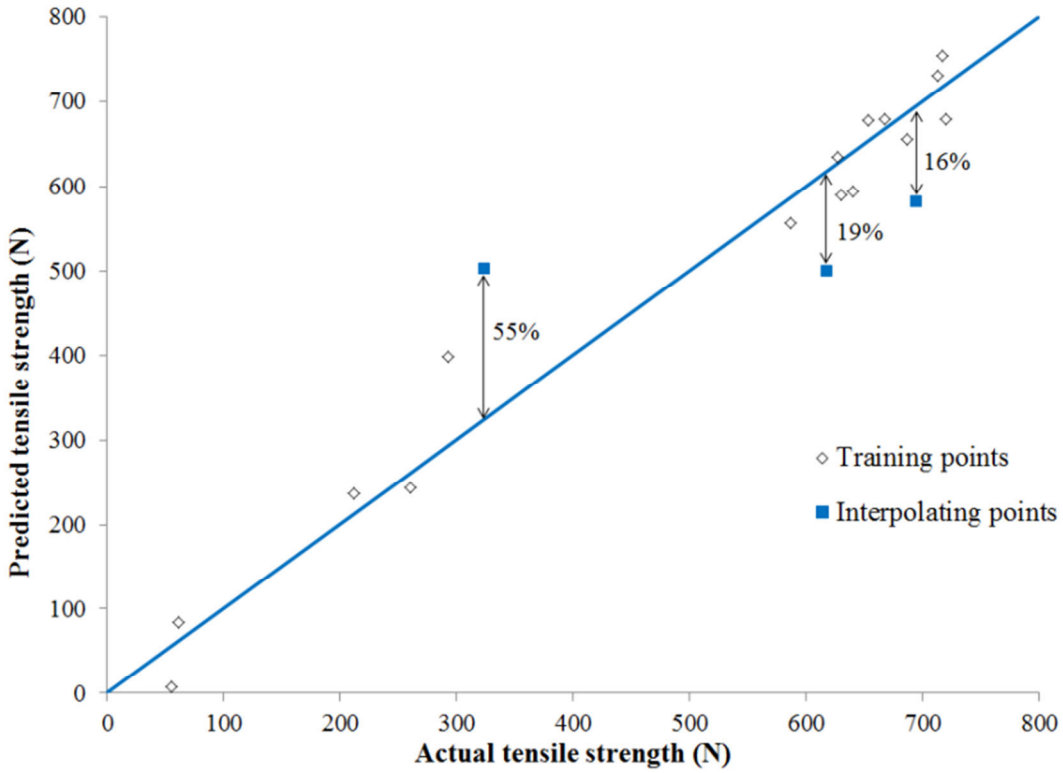

Figure 7.22: The three-variable model based on wavelengths in region 1500 – 1900 nm

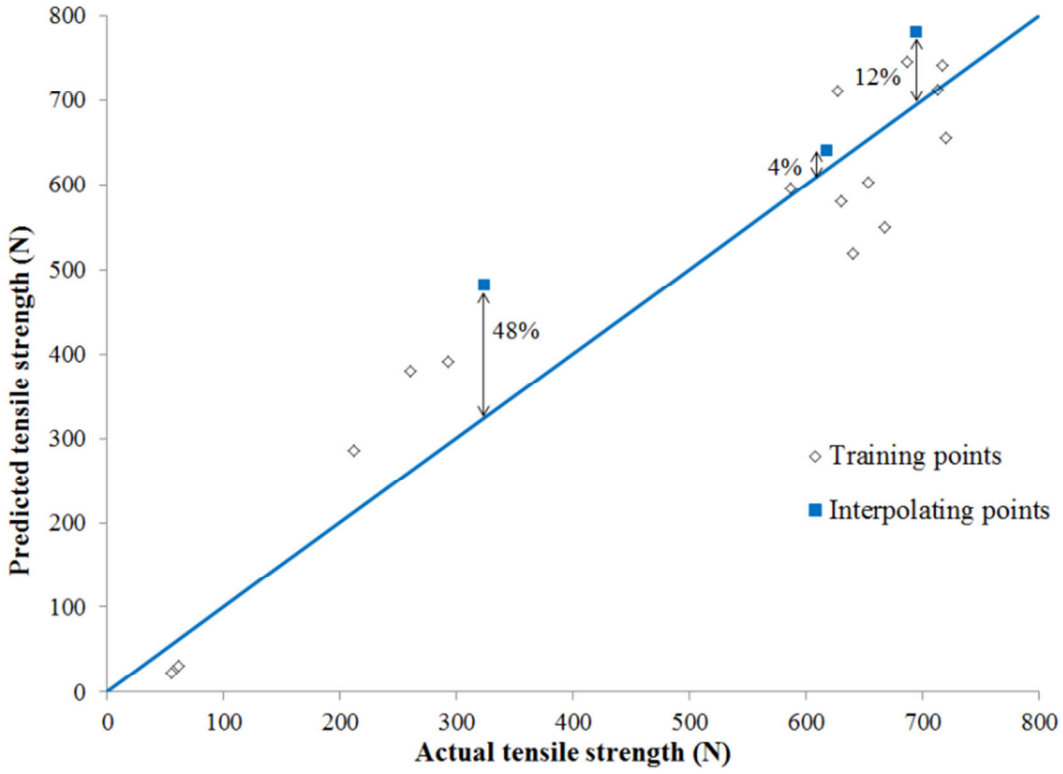

Figure 7.23: The three-variable model based on wavelengths in region 1900 – 2500 nm

Figure 7.24 depicts the three-variable equation based on wavelengths corresponding to maximum and minimum points in the reflectance spectrum of blue outer shell specimens. The selected wavelengths to develop the predictive equation were 1600, 1700, 1750, 1925, 1975, 2050, 2100, 2150. 2250, 2275, 2400, 2425, and 2475 nm. This is a more intelligent way of selection of wavelengths since it is based on important wavelengths in the reflectance spectrum of the specimen. Beside the fact that this model has high R^2_a (0.93), it predicted tensile strength of the two specimens exposed to ordinary conditions with an error percentage of less than 10% and conservatively. Based on these advantages, this model is the most favourable equation in prediction of tensile strength of outer shell specimens.

This model successfully predicted data points with an error of less than 10% for the interpolating points with tensile strengths of higher than 600 N. However, the percentage error for the interpolating point with a tensile strength of about 300 N is much higher. There is also a larger difference between the predicted and measured tensile strength for the training data point with an actual tensile strength of about 300 N. This may be because of the lack of training data for tensile strengths between 300 and 600 N for this fabric.

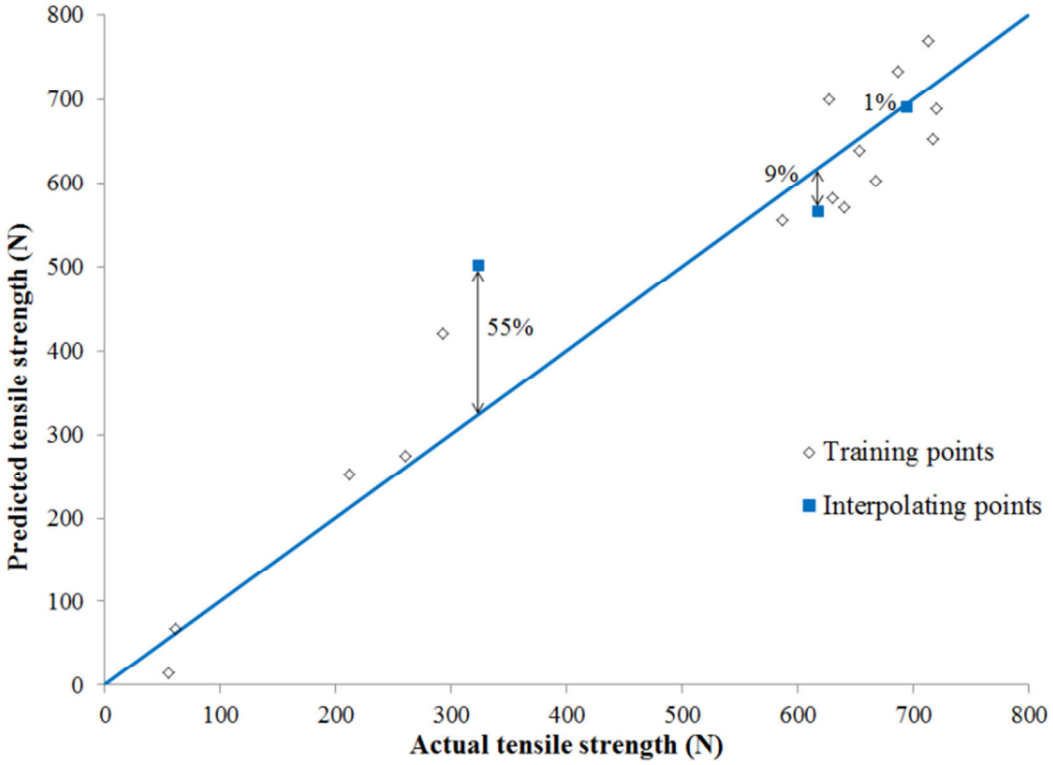

Figure 7.24: The three-variable model based on selective wavelengths

In summary, tensile strength of specimens was predicted using two selected non-destructive techniques. These non-destructive techniques showed promise and it is worth investing time and effort on additional work to refine these techniques. Colour measurement was implemented as the first technique. As a consequence of different levels of thermal ageing, the specimen's colour gradually changed to the natural colour of the fabric and then, turned into black as a result of char formation on the surface. This trend was translated into two types of colour difference in an RGB system. The difference in the two types of trends in colour difference originated from the differences between the initial colour of the specimen fabric relative to the natural colour of the specimen fabric and the colour of char (black). The two types of colour change were qualitatively illustrated in this chapter. The two types of colour change were also observed in discoloration of black and brown Kevlar®/PBI specimens.

As the second non-destructive technique, NIR was implemented to record reflectance spectrum of thermally aged specimens. The change in reflectance of specimens within the wavelength region of 1500 - 2500 nm was correlated with the tensile strength of specimens. It was demonstrated how models can be developed based on linear regression analysis. A numerical code was written to provide a list of equations constructed from different number of wavelengths. Such a list of predictive equations creates an opportunity to select equations based on criteria such as number of variables (wavelengths) and accuracy of prediction in terms of statistical parameters. The statistic for comparison of linear models was R^2_a which was greater than 0.94 for all but the yellow fabric for even models based on as few as three wavelengths. The models were tested by three interpolating points. These models could be practically implemented into a commercial device which can measure reflectance at several wavelengths.

The effect of wavelength selection on accuracy of models in prediction of tensile strength of interpolating points was discussed. Based on reflectance spectrum of specimens, the studied wavelength region was considered in two intervals of 1500 – 1900 nm and 1900 – 2500 nm. In addition, wavelengths corresponded to peaks and valleys in the reflectance spectrum were selected to develop a predictive equation. The results indicated that the model developed based on wavelengths representative of extreme points in the reflectance spectrum of the outer shell specimen more accurately predicted the tensile strength. One way to improve prediction of tensile strength could be developing higher order polynomials and non-linear numerical models.

Piecewise-defined functions could also be useful since the current models were more accurate for predicting the tensile strength of the Nomex® specimens when the tensile strength was greater than 600 N, than when the tensile strength was around 300 N.

Both colour measurement and NIR have comparative advantages and disadvantages. The colour measurement technique predicts tensile strength of specimens based on a single value which is a measure of discoloration. Furthermore, the required device could be as simple as an inexpensive office scanner. The NIR technique requires measurement of reflectance at several wavelengths which is time-consuming. In addition, the device to measure reflectance spectrum is to some extent more expensive. The colour measurement technique is highly dependent on the initial colour of fabrics, but the effect of colour could be minimized by selecting specific wavelength regions using the NIR technique. In this research, a qualitative correlation was identified between colour measurement and tensile strength. Numerical models should be developed to correlate the tensile strength and colour measurement quantitatively. In colour measurement technique, a single value of discoloration can correspond to two values of tensile strength, which is one challenge for numerical modelling. Linear regression models, which were developed in this research for correlation of tensile strength and NIR reflectance, could be improved by more training data points across the entire tensile strength range. Selection of appropriate wavelengths to develop an accurate model for the NIR technique is also a challenge and adds to the complexity of numerical analysis.

8. CONCLUSIONS AND FUTURE WORK

Coats and pants are important pieces of firefighters' protective clothing. Even though minimum requirements have been clearly set by national and international standards, there is no standard procedure on retirement of these pieces of firefighters' protective clothing. Late retirement of the clothing is a major concern for the safety of firefighters. The need to determine an appropriate time for retirement of firefighters' protective clothing has been discussed in literature and expressed by fire departments in Canada.

Aspects of performance of firefighters' protective clothing change differently as a consequence of exposure to a variety of detrimental ageing factors during services. One factor, thermal exposure, was selected in this research to age specimens made of common fabrics in construction of firefighters' protective clothing. Thermal exposure is an important factor since it can provide sufficient energy for physical and chemical changes in fabrics. Thermogravimetric analysis was carried out for outer shell and moisture barrier fabrics used as specimens in this research project. Thermal ageing of specimens was conducted using the conical heater of a cone calorimeter. The temperature profile of specimens was measured for each thermal exposure to help explain the changes in aspects of performance of specimens. Based on a comprehensive literature review, tensile strength of the outer shell layer and water vapour transmission rate, water penetration pressure, and tear strength of the moisture barrier layer were studied before and after a variety of thermal exposures.

8.1. Conclusions

The first set of outer shell specimens were cut from Nomex®. The Nomex® fabrics were blue, red, dark blue, and yellow in colour. Heat fluxes of 10, 20, 30, and 40 kW/m^2 were selected for thermal ageing of outer shell specimens. Major deterioration in tensile strength occurred in specimens after exposure to 30 and 40 kW/m^2 since specimens reached high enough temperatures for decomposition and chemical changes. However, changes did occur in exposure to 10 and 20 kW/m^2 especially after longer durations mainly due to oxidation, chain fracture, cross linking, and disorientation. The experiments showed that a longer duration of thermal exposure generally caused more damage in specimens and decreased tensile strength of specimens.

The first set of moisture barrier specimens were cut from Stedair® 4000, an ePTFE membrane laminated on Nomex®. The specimens were exposed to heat fluxes of 5, 10, 15, and 20 kW/m^2. The experimental results showed that tear strength of specimens after thermal exposure to 5, 10, and 15 kW/m^2 not only did not decrease, but increased. This was attributed to cross linking reactions. However, tear strength decreased substantially after a 5 min. exposure to 20 kW/m^2. Water vapour transmission rate did not change considerably after thermal exposure, most probably because of two mechanisms which acted in opposite directions. The results of these mechanisms were observed using images of specimens taken by a scanning electron microscope, which showed that pores were getting smaller while cracks and holes in the oleophobic layer of the membrane of the moisture barrier specimens formed. The required pressure for penetration of water decreased by up to 40% after thermal exposure. In summary, the aspects of performance for moisture barrier specimens exposed to ordinary and early stages of emergency conditions (heat fluxes of 5, 10, and 15 kW/m^2) considered in this research did not deteriorate as severely as tensile strength of outer shell specimens. In addition, the outer shell is the outermost layer of firefighters' protective clothing and can be easily inspected. So, tensile strength of the outer shell was selected to be correlated with signal parameters of non-destructive techniques.

As firefighters' protective clothing are worn many times over the entire service life, long single-stage thermal ageing may not accurately simulate the effect of thermal exposure on performance of firefighters' protective clothing. In order to study the effect of multi-stage exposure, exposures to 20 kW/m^2 was carried out in both single stage and multiple (up to five) 30-s stages but for the same total duration. Specimens included all three layers of firefighters' protective clothing. Outer shell layers of these specimens were cut from Kevlar®/PBI® fabric. The Kevlar®/PBI® fabrics were in brown and black. Moisture barrier layers of the specimens were cut from Stedair® 3000. Tensile strength of the outer shell layer and tear strength of the moisture barrier layer of the specimens were measured. In addition to these tests, single layer moisture barrier specimens made of Stedair® 4000 were exposed to a heat flux of 10 kW/m^2 both in single and multiple (up to 10) 30-s stages. Water vapour transmission rate and water penetration pressure were measured for these moisture barrier specimens.

The experimental results of both groups of tests demonstrated that multiple 30-s exposures were less destructive than a single exposure of the same total duration. All aspects of performance of outer shell and moisture barrier specimens did not change considerably even

after 10 stages of 30-s exposure. This minimal change in the studied aspects of performance was because specimens reached lower temperatures in multiple 30-s exposures than in longer single-stage exposures of the same total duration. Higher temperatures in single-stage exposures caused more severe physical and chemical changes in specimen fabrics. Hence, long single-stage exposure may not be representative of the level of damage to firefighters' protective clothing.

Based on the test results, tensile strength of outer shell specimens was regarded as more crucial than any other studied aspects of performance of outer shell and moisture barrier specimens in this research. Two non-destructive techniques were implemented to assess the change in tensile strength of outer shell specimens. The first technique was measurement of discoloration of specimens after thermal exposure. The variety of colours of outer shell fabrics was used to take the effect of colour into account and evaluate the potential of colour measurement technique. Discoloration of Nomex® and Kevlar®/PBI specimens was measured relative to the initial colour of the fabric in RGB system. Then, the colour difference was correlated with the tensile strength of specimens.

Two types of correlation were observed for different colours of specimens. The first type was observed for blue, dark blue, and black colours of specimens. The colour difference gradually increased as dye came out of specimens. The increasing trend of colour difference was reversed after the natural colour of specimens, brown for the fabrics used in this research, was revealed. Longer or more severe exposures charred the specimen fabric and changed the colour to black. This change decreased colour difference because of the relative difference of char colour (black) and natural colour (brown) with the initial colour of the specimens. The second type of correlation was seen for red, yellow, and brown specimens. The increasing trend continued after the natural colour of the fabric appeared since the colour difference between char colour (black) and the initial colour of the specimens increased in RGB system. These trends were also observed for brown and black outer shell fabrics and demonstrated the potential for colour measurement to be used to evaluate in-use protective clothing in future research.

Near infrared spectroscopy, the second non-destructive technique, was implemented to record reflectance spectra of specimens in wavelength region of 250-2500 nm. Reflectance spectra of specimens within the wavelength region of 1500-2500 nm were analysed before and after thermal exposure. Linear models were developed from three wavelengths using a numerical code written based on regression analysis to correlate tensile strength with reflectance of outer

shell specimens. The models were tested using three interpolating points for blue, red, dark blue, yellow Nomex® specimens, which were not included in the training data used to develop the models. Since designing a device to measure reflectance at a few wavelengths in near infrared region is inexpensive, there is commercial potential, and further research on developing models based on piecewise functions, higher order polynomials, and non-linear analysis would be useful to improve the accuracy of prediction using infrared spectroscopy. Appropriate selection of wavelengths and a relatively large set of training data points are crucial in developing a predictive model using NIR spectroscopy.

8.2. Future work

Although thermal exposure was used in ageing of specimens in this research, additional detrimental ageing factors after manufacturing of textiles and during service life include exposure to ultraviolet radiation such as sunlight, chemicals in the field and laundry, and abrasive and shear forces in laundry and intense physical activities during firefighting operations. The effects of these factors on the aspects of performance and also on the evaluation of the performance using non-destructive techniques should be taken into account in future studies. Heat fluxes and durations of thermal ageing were selected such that they represented thermal exposure on the fire ground. However, there is a need to expand the test matrix in terms of heat flux and duration for single-stage exposures and number and duration of stages in multi-stage exposure to make more general conclusions regarding the changes in performance of firefighters' protective clothing. In addition, the performance tests should be performed on more types of fabrics to validate the results. Combination of ageing factors should also be addressed in future studies.

Non-destructive techniques were used in assessment of deterioration level using signal parameters, colour measurement and reflectance, in this research. However, in real life not all the change in signal parameters originates from flaws and defect in the fabric. Change in signal parameters can be simply a result of exposure to non-harmful external agents such as soil. In addition, the correlations of tensile strength and signal parameters were established with limited data points. In order to improve the accuracy of the predictive models, non-linear regression analysis and more data points may be required. Testing actual used firefighters' protective

clothing using both destructive and non-destructive tests is another way to evaluate the potential of non-destructive techniques.

REFERENCES

1- Council of Canadian Fire Marshals and Fire Commissioners, 2007, "Fire losses in Canada", Annual Report, Ottawa, ON.

2- National Fire Protection Association, 2007, "NFPA 1971 standard on protective ensemble of structural firefighting", Quincy, MA.

3- National Fire Protection Association, 2011, "NFPA 1977 standard on protective clothing and equipment for wildland firefighting", Quincy, MA.

4- Lawson, J. R., 1996, "Firefighter's protective clothing and thermal environments of structural firefighting", NISTIR 5804, National Institute of Standards and Technology, Gaithersburg, MD.

5- Canadian General Standards Board, 2001, "Firefighter's protective clothing for protection against heat and flame", CAN/CGSB-155.1, Standard Council of Canada, Ottawa, ON.

6- Stoll, A. M., and Chianta, M. A., 1969, "Method and rating system for evaluation of thermal protection" Aerospace Medicine, 40(11), pp.1232–1238.

7- Globe Manufacturing Company, "Thermal Protection Performance (TPP)", Retrieved from http://www.globeturnoutgear.com/resources/nfpa-test-methods/thermal-protection-performance-tpp on Nov. 5, 2013.

8- Torvi, D. A., and Hadjisophocleous, G. V., 1999, "Research in protective clothing for firefighters: state of the art and future directions", Fire Technology, 35(2), pp.111-130.

9- Rezazadeh, M., and Torvi, D., 2010, "Assessment of factors affecting the continuing performance of firefighters' protective clothing: a literature review", Fire Technology, 47(3), pp.565-599.

10- National Fire Protection Association (NFPA), 2008, "NFPA 1851 Standard on selection, care, and maintenance of structural firefighting protective ensembles", Quincy, MA.

11- Lion Apparel, 2005, "User instruction, safety and training guide", Dayton, OH.

12- Slater, K., 1986, "The progressive deterioration of textile materials, part I: characteristics of degradation", Journal of The Textile Institute, 77(2), pp.76-87.

13- Davis, R., Chin, J., Lin, C., Petit, S., 2010, "Accelerated weathering of polyaramid and polybenzimidazole firefighter protective clothing fabrics", Polymer Degradation and Stability, 95(9), pp.1642-1654.

14- Thorpe, P., 2004, "Assessment of in-use firefighter's protective clothing", M.Sc. Dissertation, University of Saskatchewan, Saskatoon, SK.

15- Rossi, R. M., Bolli, W., Stampfli, R., 2008, "Performance of firefighter's protective clothing after heat exposure", International Journal of Occupational Safety and Ergonomics, 14(1), pp.55-60

16- Dolez, P.I., Vu-Khanh, T., 2009, "Recent developments and needs in materials used for personal protective equipment and their testing", International Journal of Occupational Safety and Ergonomics, 15(4), pp.347-362

17- Nazare, S., Davis, R. D., Peng, J. S., Chin, J., 2012, "Accelerated weathering of firefighter protective clothing: delineating the impact of thermal, moisture, and ultraviolet light exposures", NIST technical note 1746, National Institute of Standards and Technology, Gaithersburg, MD.

18- Timiras, P. L, Quay, W. B, Vernadakis, A., 1995, Hormones and aging, CRC Press, Boca Raton, FL, p.6.

19- Johnson, M. L, (ed.), 2005, The Cambridge handbook of age and ageing, 1st edn, The Cambridge University Press, Cambridge, p.48.

20- Slater, K., 1991, "Textile degradation", Textile Progress, 21(1), pp.1-150.

21- Federal Trade Commission, 2009, "Generic names and definitions for manufactured fibres", Title 16 CFR Part 303.7, National Archives and Records Administration, Washington, DC.

22- Day, M., Cooney, J. D., Suprunchuk, T., 1988, "Durability of firefighter's protective clothing to heat and light", Textile Research Journal, 58(3), pp.141-147.

23- Jain, A, Vijayan, K., 2002, "Thermally induced structural changes in Nomex fibres", Bulletin of Materials Science, 25(4), pp.341–346.

24- Iyer, R. V., Vijayan, K., 1999, "Decomposition behaviour of Kevlar 49 fibres: Part I. at T≈Td", Bulletin of Materials Science, 22(7), pp.1013–1023.

25- Iyer, R. V., Sudhakar, A., Vijayan, K., 2006, "Decomposition behaviour of Kevlar 49 fibres: Part II. At T values < Td", High Performance Polymers, 18(4), pp.495–517.

26- Iyer R. V., Vijayan, K., 1998, “Identification of a new parameter controlling the thermally induced effects on Kevlar® 49 fibres”, Current Science, 75(9), pp.946-951.

27- An, S. K., Barker, R. L., Stull, J. O, 1989, “Measurement of the flammability and thermal aging of chemical protective suit materials”. In: Perkins, J. L., Stull, J. O. (eds), Chemical Protective Clothing Performance in Chemical Emergency Response, ASTM STP 1037, American Society for Testing and Materials, West Conshohocken, PA, pp.86-101.

28- American Society for Testing and Materials, 1999, “ASTM F 1939-99a Standard test method for radiant heat resistance of flame resistant clothing materials with continuous heating”, West Conshohocken, PA.

29- International Organization for Standardization, 2002, “ISO 6942 Protective clothing - Protection against heat and fire - Method of test: Evaluation of materials and material assemblies when exposed to a source of radiant heat”, Geneva, Switzerland.

30- European Committee for Standardization, 1992, “EN 367 Protective clothing – Protection against heat and fire – Method of determining heat transmission on exposure to flame”, Brussels, Belgium.

31- European Committee for Standardization, 2005, “EN 469 Protective clothing for firefighters – Performance requirements for protective clothing for firefighting”, Brussels, Belgium.

32- Jain, A., Vijayan, K., 2002, “Thermally induced structural changes in Nomex fibres”, Bulletin of Materials Science, 25(4), pp.341–346.

33- Iyer R. V., Vijayan, K., 1999, “Decomposition behaviour of Kevlar 49 fibres: Part I. at T≈Td”, Bulletin of Materials Science, 22(7), pp.1013–1023.

34- Iyer, R. V., Sudhakar, A., Vijayan, K., 2006, “Decomposition behaviour of Kevlar 49 fibres: Part II. At T values < Td”, High Performance Polymers, 18(4), pp.495–517.

35- An, S. K., Barker, R. L., Stull, J. O., 1989, “Measurement of the flammability and thermal aging of chemical protective suit materials”, In: Perkins J. L., Stull, J. O. (eds), Chemical Protective Clothing Performance in Chemical Emergency Response, ASTM STP 1037, American Society for Testing and Materials, West Conshohocken, PA, pp.86-101.

36- Vogelpohl, T. L., 1996, “Post-use evaluation of firefighter’s turnout coats”, M.Sc. Thesis, University of Kentucky, Lexington, KY.

37- Stull, J. S., 2002, “Introduction to NDE”, In: Shull, J. S. (ed), Nondestructive evaluation: theory, techniques, and applications, Marcel Dekker Inc., New York, NY, pp.1-15.

38- Torvi, D. A., Hadjisophocleous, G. V., 2000, “Development of methods to evaluate the useful lifetime of firefighters’ protective clothing”, In: Nelson, C. N., Henry, N. W. (eds), Performance of Protective Clothing: Issues and Priorities for the 21st Century, ASTM STP 1386, American Society for Testing and Materials, West Conshohocken, PA, pp.117-129.

39- Galiotis, C., 1992, “Raman optomechanical studies on fibres, composites and fibre-matrix interfaces”, In: Paipetis, S., Papanicolaou, G. (eds), Phase interaction in composite materials, Omega Scientific, Wallingford, UK, pp.173-184.

40- Washer, G., Brooks, T., Saulsberry, R., 2009, “Characterization of Kevlar using Raman spectroscopy”, Journal of Materials in Civil Engineering, 21(5), pp.226-234.

41- Arrieta, C., David, E., Dolez, P., Vu-Khanh, T., 2011, “X-ray diffraction, Raman, and differential thermal analyses of the thermal aging of a Kevlar-PBI blend fabric”, Polymer Composites, 32(3), pp.362-367.

42- Bray, A. V., Stull, J. O., 1996, “A non-destructive inspection method to determine fatigue in chemical protective suit and shelter materials”, In: Johnson, J. S., Mansdorf , S. Z. (eds), Performance of Protective Clothing, ASTM STP 1237, American Society for Testing and Materials, West Conshohocken, PA, pp.281-295.

43- Gralewicz, G., Wiecek, B., 2009, “Active thermography in qualitative evaluation of protective materials”, International Journal of Occupational Safety and Ergonomics, 15(4), pp.363–371.

44- Frank, A. S., ed., 1997, Handbook of instrumental techniques for analytical chemistry, Prentice Hall, Upper Saddle River, NJ.

45- Arrieta, C., David, E., Dolez, P., Vu-Khanh, T., 2010, “Thermal aging of a blend of high-performance fibres”, Journal of Applied Polymer Science, 93(5), pp.3031-3039.

46- Gu, X., Dickens, B., Stanley, D., Byrd, W. E., Nguyen, T., Vaca-Trigo, I., Meeker, W. Q., Chin, J., Martin, J. W., 2008, “Linking accelerating laboratory test with outdoor performance results for a model epoxy coating system”, In: Martin, J. W., Ryntz, R. A., Chin, J., Dickie, R. (eds), Service Life Prediction of Polymeric Materials: Global Perspectives, Springer, Berlin, Germany, pp.3-28.

47- Cai, G. M., Yu, W. D., 2011, “Study on the thermal degradation of high performance fibres by TG/FTIR and Py-GC/MS”, Journal of Thermal Analysis and Calorimetry, 104 (2): 757-763.

48- Richardson, E., Martin, G., Wyeth, P., Zhang, X., 2008, “State of the art: non-invasive interrogation of textiles in museum collections”. Microchimica Acta. 162(2), pp.303-312.

49- Garside, P., Wyeth, P., Zhang, X., 2011, “Use of near IR spectroscopy and chemometrics to assess the tensile strength of historic silk”, e-PRESERVATIONScience, 8, pp.68-73.

50- Ghosh, S., Cannon, M. D., Roy, R. B., 1990, “Quantitative analysis of durable press resin on cotton fabrics using near-infrared reflectance spectroscopy”, Textile Research Journal, 60(3), pp.167-172.

51- Mora, C. R., 2009, “Rapid techniques for screening wood properties in forest plantations”, Ph.D. Dissertation, University of Georgia, Athens, GA.

52- Kludt, K. D., 2003, “Use of near infrared spectroscopy technology for predicting bending properties of clear wood specimens”, M.Sc. Thesis, Washington State University, Pullman, WA.

53- Kelley, S. S., 2003, Method of predicting mechanical properties of decayed wood, Patent No. US 6,593572 B2.

54- Hedrick, S. E., Bennett, R. M., Rials, T. G., Kelley, S. S., 2007, “Correlation of near-infrared spectroscopy measurements with the properties of treated wood”, Journal of Materials in Civil Engineering, 19(4), pp.279-285.

55- Smith, R. D., 1998, “Simulation article”, In: Encyclopedia of Computer Science, Reilly E. D., Ralston A., Hemmendinger D. (eds), Grove's Dictionaries, New York, NY.

56- Donnelly, M. K., Davis, W. D., Lawson, J. R, Selepak, M. J, 2006, “Thermal environment for electronic equipment used by first responders”, NIST Technical Note 1474, National Institute of Standards and Technology, Gaithersburg, MD.

57- United States Fire Administration, 1992, “Minimum standards on structural fire fighting protective clothing and equipment: a guide for fire service education and procurement”, FA-137, Federal Emergency Management Agency, Emmitsburg, MD.

58- Duffy, R. M., Sawicki, J. C., Beer A. R., 1985, “Project fires: firefighters integrated response equipment system – the final report, international association of firefighters”, Department of Occupational Health and Safety, Washington, D.C.

59- Foster, J. A., Roberts, G. V., 1994, Measurements of the firefighting environment – summary report, Report number 61, Central Fire Brigades Advisory Council Research, Home Office Fire Research and Development Group, London, UK.

60- Colletta, G. C., Arons, I. J., Ashley, L. E., Drennan, A. P., 1976, The development of criteria for firefighters’ gloves, Vol. I: glove requirements, National Institute for Occupational Safety and Health, Cincinnati, OH.

61- Abbott, N. J., Schulman, S., 1976, “Protection from fire: nonflammable fabrics and coatings”, Proceedings of International Symposium on Flammability and Fire Retardants, Toronto, ON.

62- Simms, D. L., Hinckley, P. L., 1960, “Protective clothing against flames and heat”, Fire Research Special Report No. 3, Joint Fire Research Organization, Her Majesty’s Stationery Office, London, UK.

63- Ordinanz, W., 1970, “Work in hot environments and protection against heat”, The Iron and Steel Institute, London, UK.

64- Utech, H. P., 1973, “High temperatures vs. fire equipment”, International Fire Chief, 39(1), pp.26-27.

65- Veghte, J. H., 1988, Firefighter’s protective clothing: design criteria, Lion Apparel, Dayton, OH.

66- Stull, J. O., 2008, “Significant injury investigative report”, Loudoun County Department of Fire, Rescue, and Emergency Management, Leesburg, VA.

67- National Fire Data Center, 2007, “Fire department overall run profile”, Topical Fire Report Series (TFRS), U.S. Fire Administration, Emmitsburg, MD, 7(4), pp.1-8.

68- Austin, C. C., Dussault, G., Ecobichon, D. J., 2001, “Municipal firefighter exposure groups, time spent at fires and use of self-contained-breathing-apparatus”, American Journal of Industrial Medicine, 40(6), pp.683-692.

69- American Society for Testing and Materials, 2007, “ASTM E 104 – 02 standard practice for maintaining constant relative humidity by means of aqueous solutions”, West Conshohocken, PA.

70- Robinson, J. W, Frame, E. M. S., Frame, G. M., 2005, Undergraduate instrumental analysis, Marcel Dekker Incorporated, New York, NY.

71- American Society for Testing and Materials, 2008, “ASTM F 2700–08 standard test method for unsteady-state heat transfer evaluation of flame resistant materials for clothing with continuous heating”, West Conshohocken, PA.

72- American Society for Testing and Materials, 2009, “ASTM D 5034 standard test method for breaking strength and elongation of textile fabrics (grab test)”, West Conshohocken, PA.

73- American Society for Testing and Materials, 2008, “ASTM D 5587 standard test method for tearing strength of fabrics by trapezoid procedure”, West Conshohocken, PA.

74- Stull, J. O., Duffy, R. M., 2000, “Field evaluation of protective clothing effects on firefighter physiology: predictive capability of total heat loss test”, In: Nelson, C. N., Henry, N. W. (eds), ASTM STP 1386: Performance of Protective Clothing: Issues and Priorities for the 21st Century, American Society for Testing and Materials, West Conshohocken, PA, pp.481-503.

75- American Society for Testing and Materials, 2001, “ASTM D 6701-01 standard test method for determining water vapor transmission rates through nonwoven and plastic barriers”, West Conshohocken, PA.

76- U.S. General Services Administration, 1978, “Federal standard for textile test methods no. 191a, method 5512, water resistance of coated cloth; high range, hydrostatic pressure method”, Washington, DC.

77- PPE Solutions, Outer Shells, Retrieved from https://www.ppes.ca/Outer-Shells_ep_77.html on July 19, 2013,

78- E.I. DuPont de Nemours and Company, 2000, Technical guide for Kevlar® aramid fibre, H-77848, Richmond, VA.

79- American Society for Testing and Materials, 2008, “ASTM Standard F1939 standard test method for radiant heat resistance of flame resistant clothing materials with continuous heating”, West Conshohocken, PA.

80- E.I. DuPont de Nemours and Company, 2001, Technical guide for Nomex® brand fibre, H-52720, Richmond, VA.

81- Zweben, C., 2002, Composite materials, In: Handbook of materials selection, Kutz, M., Ed., John Wiley, New York, NY, p.374.

82- Brown, J. R., Browne N. McM., 1976, "Environmental effects on the mechanical properties of high performance fibers", Report MRL-R-674, Materials Research Laboratories, Australian Defense Scientific Service, Maribyrnong, Victoria.

83- Lawson, J. R., 1998, "Thermal performance and limitations of bunker gear", Fire Engineering, 151(8), pp.37-46.

84- Fahy, R., LeBlanc, P., Molis, J., 2012, "Firefighter fatalities in the United States – 2011", National Fire Protection Association, Quincy, MA, p.20.

85- International Association of Fire Fighters, 1999, "Firefighters protective clothing: moisture barrier alert and recall", Retrieved from http://www.iaff.org/hs/alerts/alert06.asp on Nov. 5, 2013

86- Beyler, C. L. and Hirschler, M. M., 2001, "Thermal decomposition of polymers", In: SFPE handbook of fire protection engineering, DiNenno P.J. (ed.), pp.1-110-1-131, National Fire Protection Association, Quincy, MA.

87- Rezazadeh, M., and Torvi, D., 2012, "Non-destructive test methods to assess the level of damage to firefighters' protective clothing", STP 1544, Performance of Protective Clothing and Equipment, Emerging Issues and Technologies, American Society for Testing and Materials, West Conshohocken, PA, pp.202-226.

88- Wardman, R. H., 2006, Textiles, In: Kirk-Othmer Encyclopedia of Chemical Technology, John Wiley, New York, NY.

89- Schwanninger, M., Rodrigues, J. C., Fackler, K., 2011, "A review of band assignments in near infrared spectra of wood and wood components", Journal of Near Infrared Spectroscopy, 19(5), pp.287-308.

90- Draper, N. R., and Smith, H., 1981, Applied Regression Analysis, John Wiley & Sons, New York, NY, pp.1-20.

Appendix A: Photographs of Nomex® outer shell specimens

A.1.Blue outer shell specimens:

Figure A.1: Unexposed specimen

Figure A.2: After exposure to 10kW/m^2 for 600s

Figure A.3: After exposure to 10kW/m^2 for 1200s

Figure A.4: After exposure to 10kW/m^2 for 2400s

Figure A.5: After exposure to 20kW/m^2 for 30s

Figure A.6: After exposure to 20kW/m^2 for 150s

Figure A.7: After exposure to 20kW/m^2 for 300s

Figure A.8: After exposure to 30kW/m^2 for 15s

Figure A.9: After exposure to 30kW/m^2 for 30s

Figure A.10: After exposure to 30kW/m^2 for 60s

Figure A.11: After exposure to 40kW/m^2 for 10s

Figure A.12: After exposure to 40kW/m^2 for 20s

Figure A.13: After exposure to 40kW/m^2 for 30s

A.2.Red outer shell specimens:

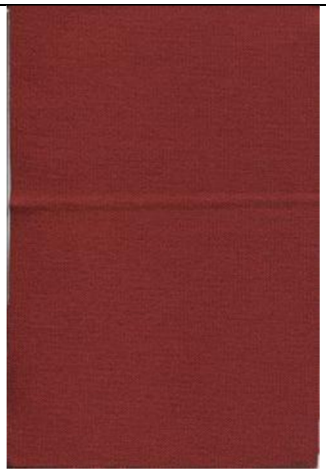

Figure A.14: Unexposed specimen

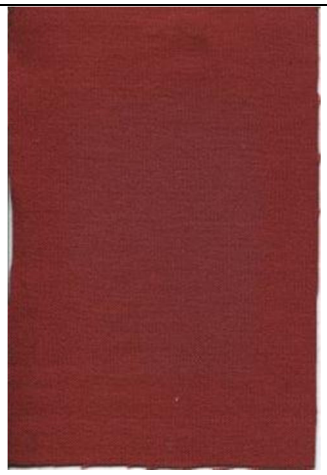

Figure A.15: After exposure to 10kW/m^2 for 600s

Figure A.16: After exposure to 10kW/m^2 for 1200s

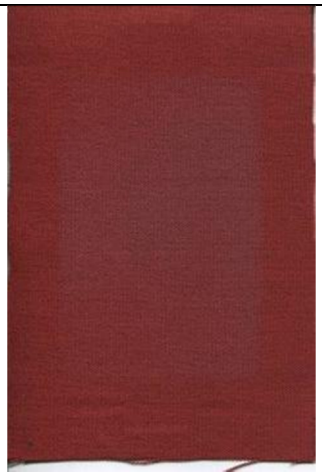

Figure A.17: After exposure to 10kW/m^2 for 2400s

Figure A.18: After exposure to 20kW/m^2 for 30s

Figure A.19: After exposure to 20kW/m^2 for 150s

Figure A.20: After exposure to 20kW/m^2 for 300s

Figure A.21: After exposure to 30kW/m^2 for 15s

Figure A.22: After exposure to 30kW/m^2 for 30s

Figure A.23: After exposure to 30kW/m^2 for 60s

Figure A.24: After exposure to 40kW/m^2 for 10s

Figure A.25: After exposure to 40kW/m^2 for 20s

Figure A.26: After exposure to 40kW/m^2 for 30s

A.3.Dark blue outer shell specimens:

Figure A.27: Unexposed specimen

Figure A.28: After exposure to 10kW/m^2 for 600s

Figure A.29: After exposure to 10kW/m^2 for 1200s

Figure A.30: After exposure to 10kW/m^2 for 2400s

Figure A.31: After exposure to 20kW/m^2 for 30s

Figure A.32: After exposure to 20kW/m^2 for 150s

Figure A.33: After exposure to 20kW/m^2 for 300s

Figure A.34: After exposure to 30kW/m^2 for 15s

Figure A.35: After exposure to 30kW/m^2 for 30s

Figure A.36: After exposure to 30kW/m^2 for 60s

Figure A.37: After exposure to 40kW/m^2 for 10s

Figure A.38: After exposure to 40kW/m^2 for 20s

Figure A.39: After exposure to 40kW/m^2 for 30s

A.4.Yellow outer shell specimens:

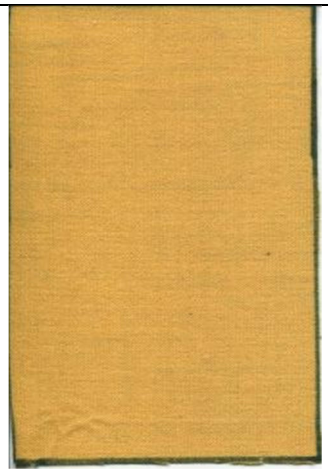

Figure A.40: Unexposed specimen

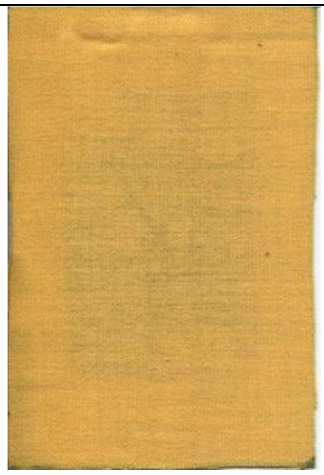

Figure A.41: After exposure to 10kW/m^2 for 600s

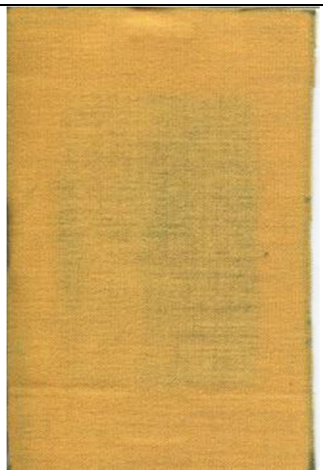

Figure A.42: After exposure to 10kW/m^2 for 1200s

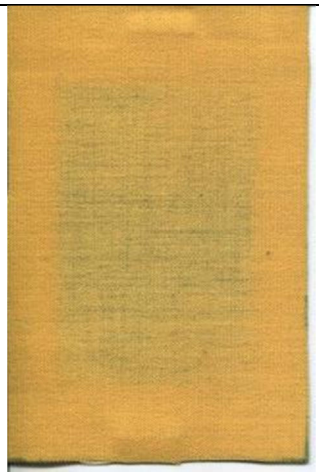

Figure A.43: After exposure to 10kW/m^2 for 2400s

Figure A.44: After exposure to 20kW/m^2 for 30s

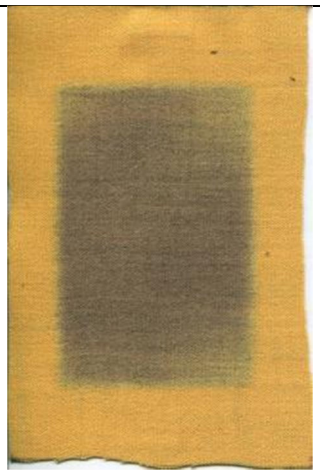

Figure A.45: After exposure to 20kW/m^2 for 150s

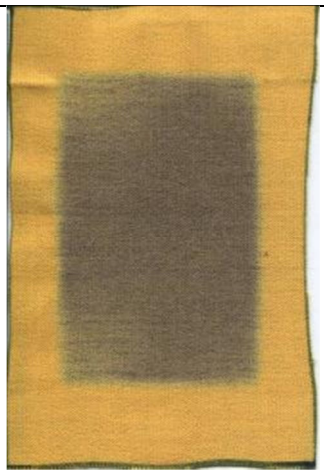

Figure A.46: After exposure to 20kW/m^2 for 300s

Figure A.47: After exposure to 30kW/m^2 for 15s

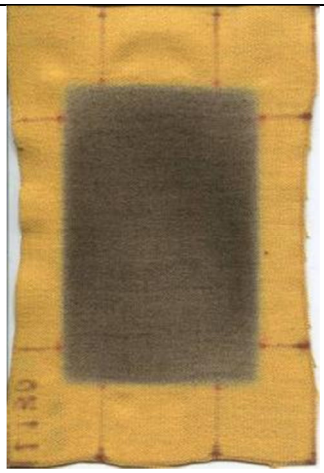

Figure A.48: After exposure to 30kW/m^2 for 30s

Figure A.49: After exposure to 30kW/m^2 for 60s

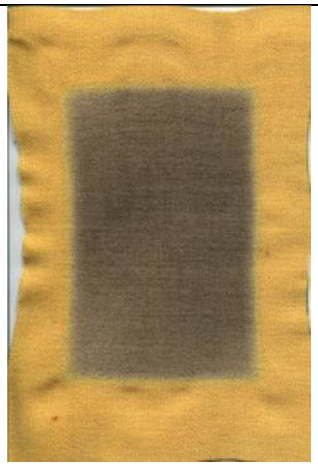

Figure A.50: After exposure to 40kW/m^2 for 10s

Figure A.51: After exposure to 40kW/m^2 for 20s

Figure A.52: After exposure to 40kW/m^2 for 30s

Appendix B: Images of ePTFE fibers of Stedair® 4000 moisture barrier specimens by scanning electron microscope

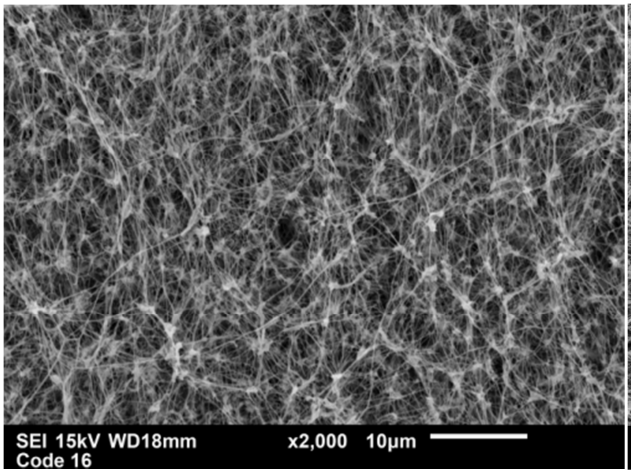

Figure B.1: unexposed specimen

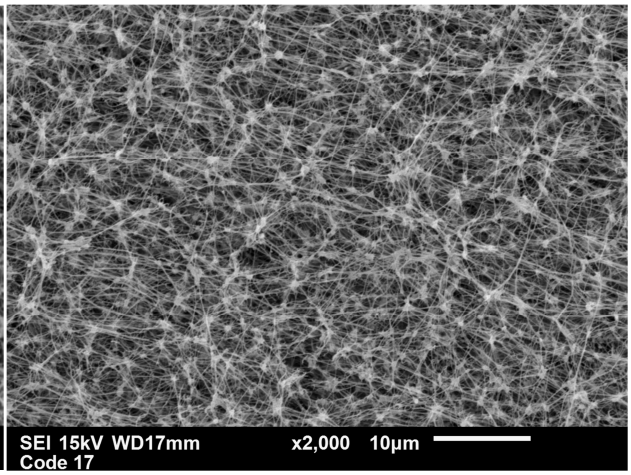

Figure B.2: After exposure to 5 kW/m^2 for 600 s

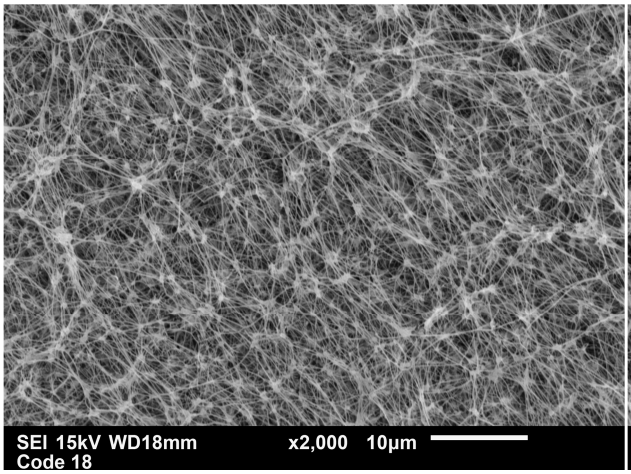

Figure B.3: After exposure to 5 kW/m^2 for 1200 s

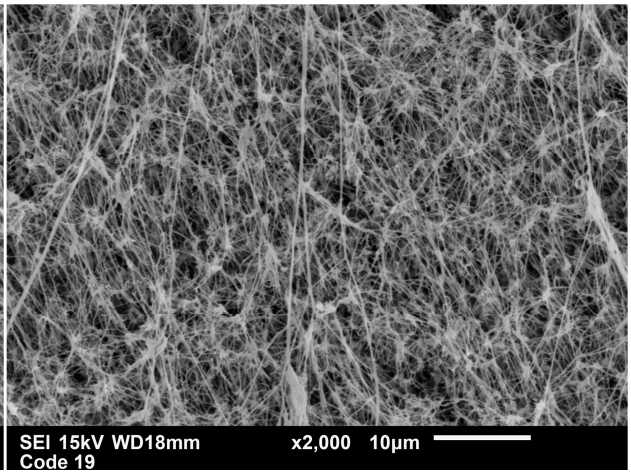

Figure B.4: After exposure to 5 kW/m^2 for 2400 s

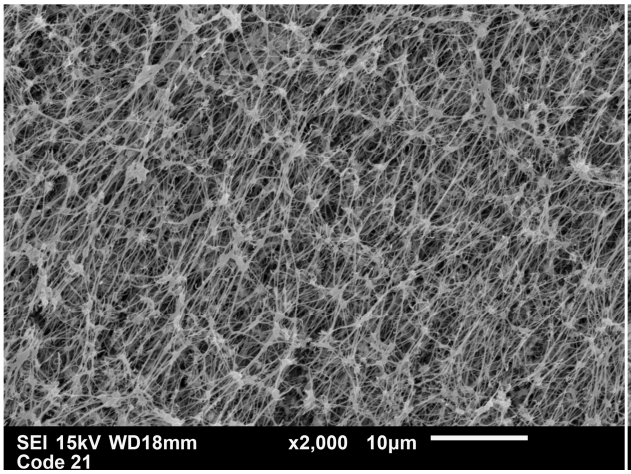

Figure B.5: After exposure to 10 kW/m^2 for 60 s

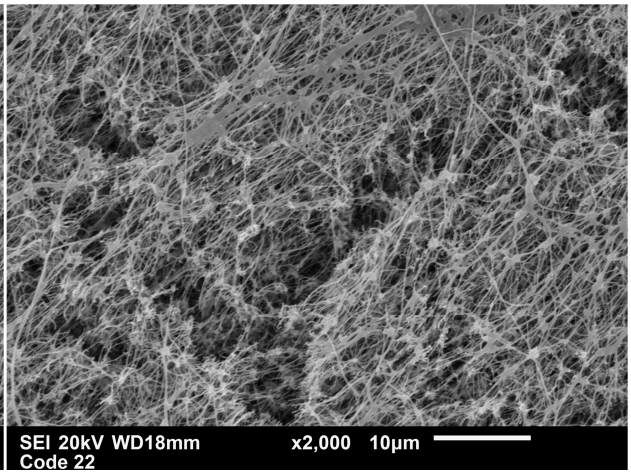

Figure B.6: After exposure to 10 kW/m^2 for 120 s

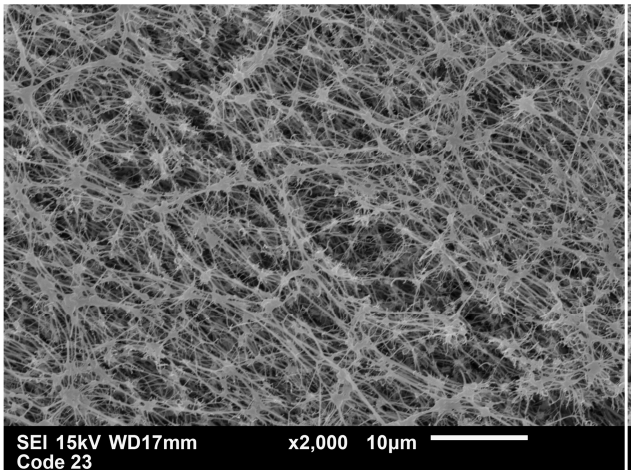

Figure B.7: After exposure to 10 kW/m^2 for 150 s

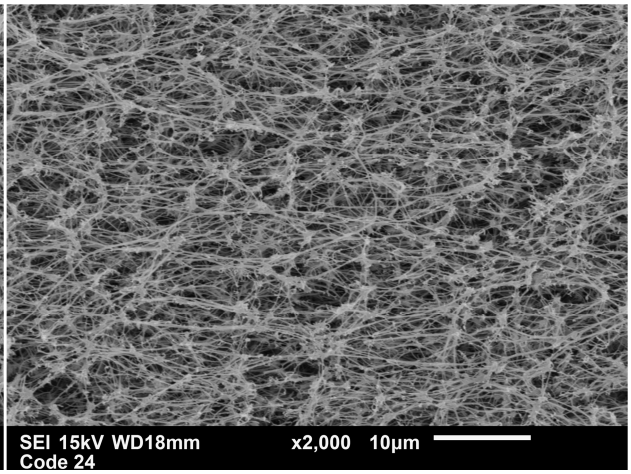

Figure B.8: After exposure to 10 kW/m^2 for 300 s

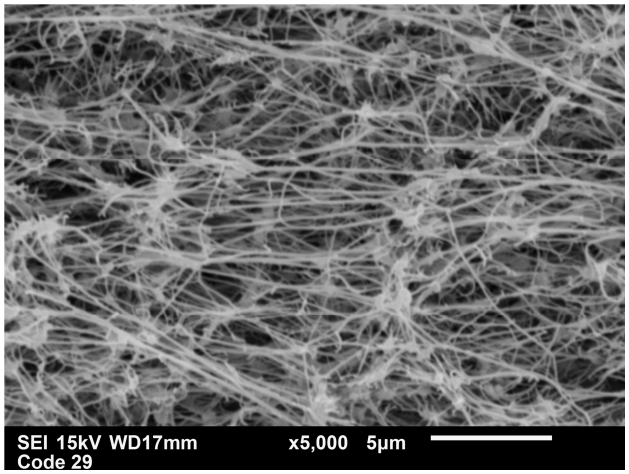

Figure B.9: After exposure to 15 kW/m^2 for 15 s

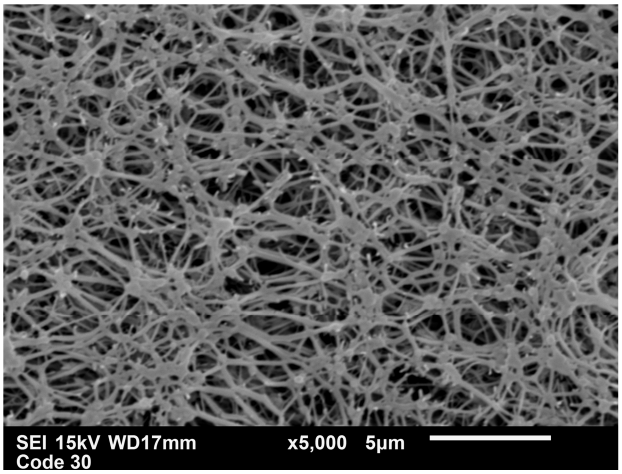

Figure B.10: After exposure to 15 kW/m^2 for 30 s

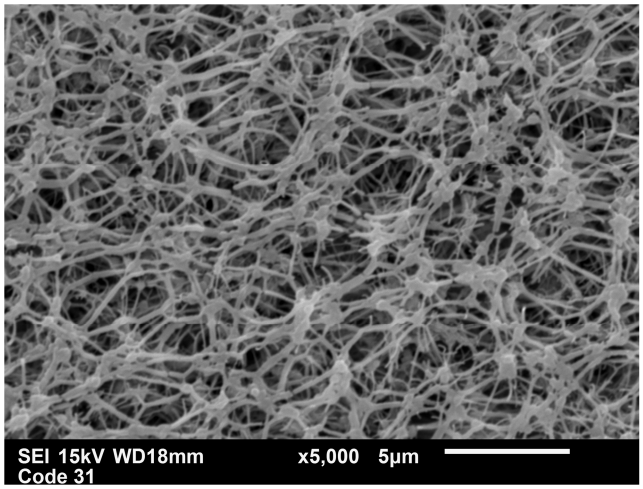

Figure B.11: After exposure to 15 kW/m^2 for 60 s

Appendix C: Photographs of Kevlar/PBI outer shell specimens – single and multiple exposures

C.1.Brown (undyed) outer shell specimens:

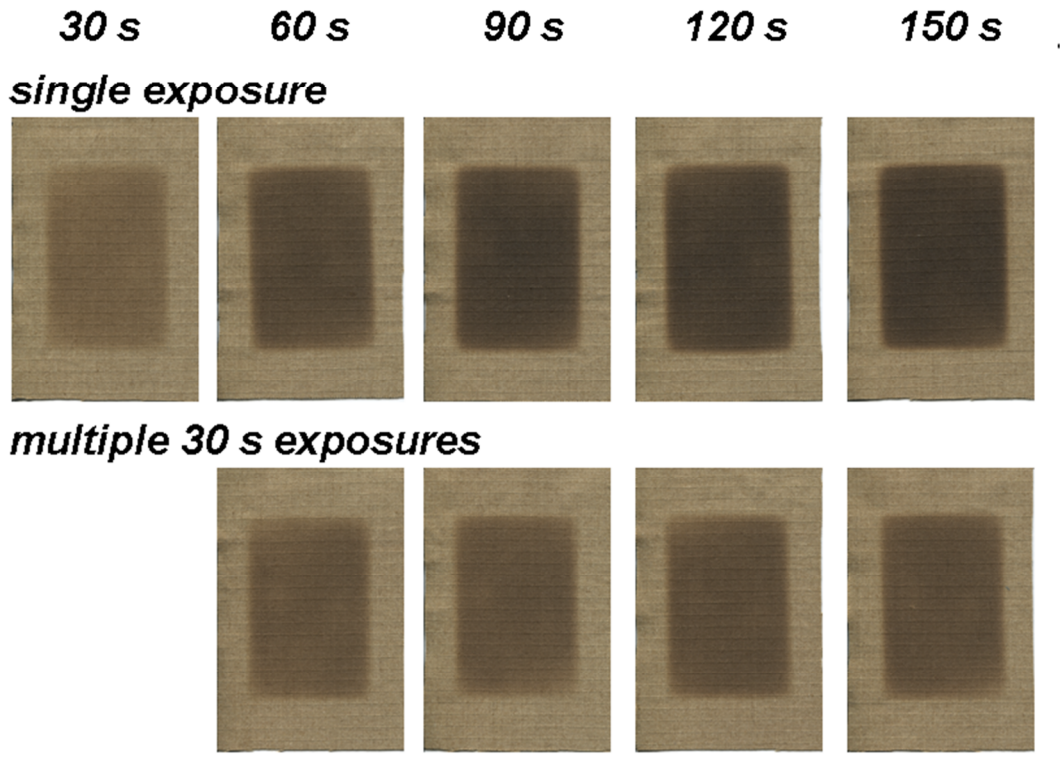

Figure C.1: Brown (undyed) Kevlar/PBI outer shell specimens after exposure to 20 kW/m^2 for particular duration in single-stage and multi-stage exposures

C.2.Black (dyed) outer shell specimens:

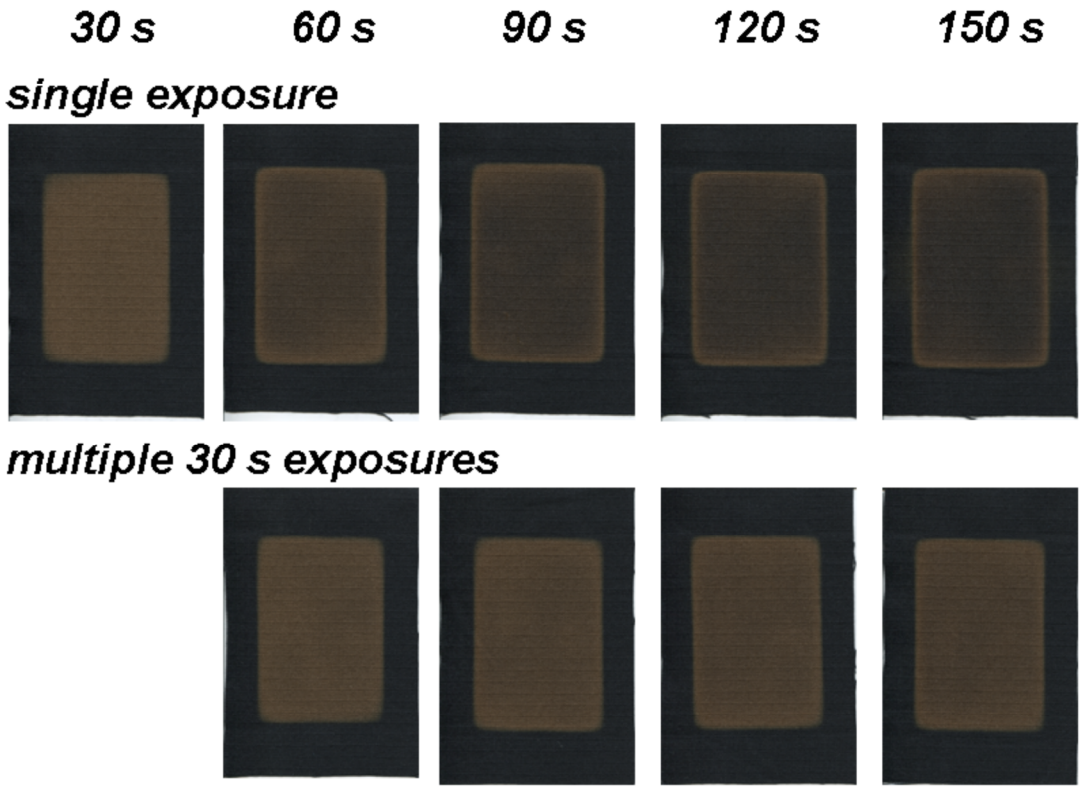

Figure C.2: Black (dyed) Kevlar/PBI outer shell specimens after exposure to 20 kW/m^2 for particular duration in single-stage and multi-stage exposures

Appendix D: Reflectance spectrum for Nomex® specimens

D.1.Red specimens:

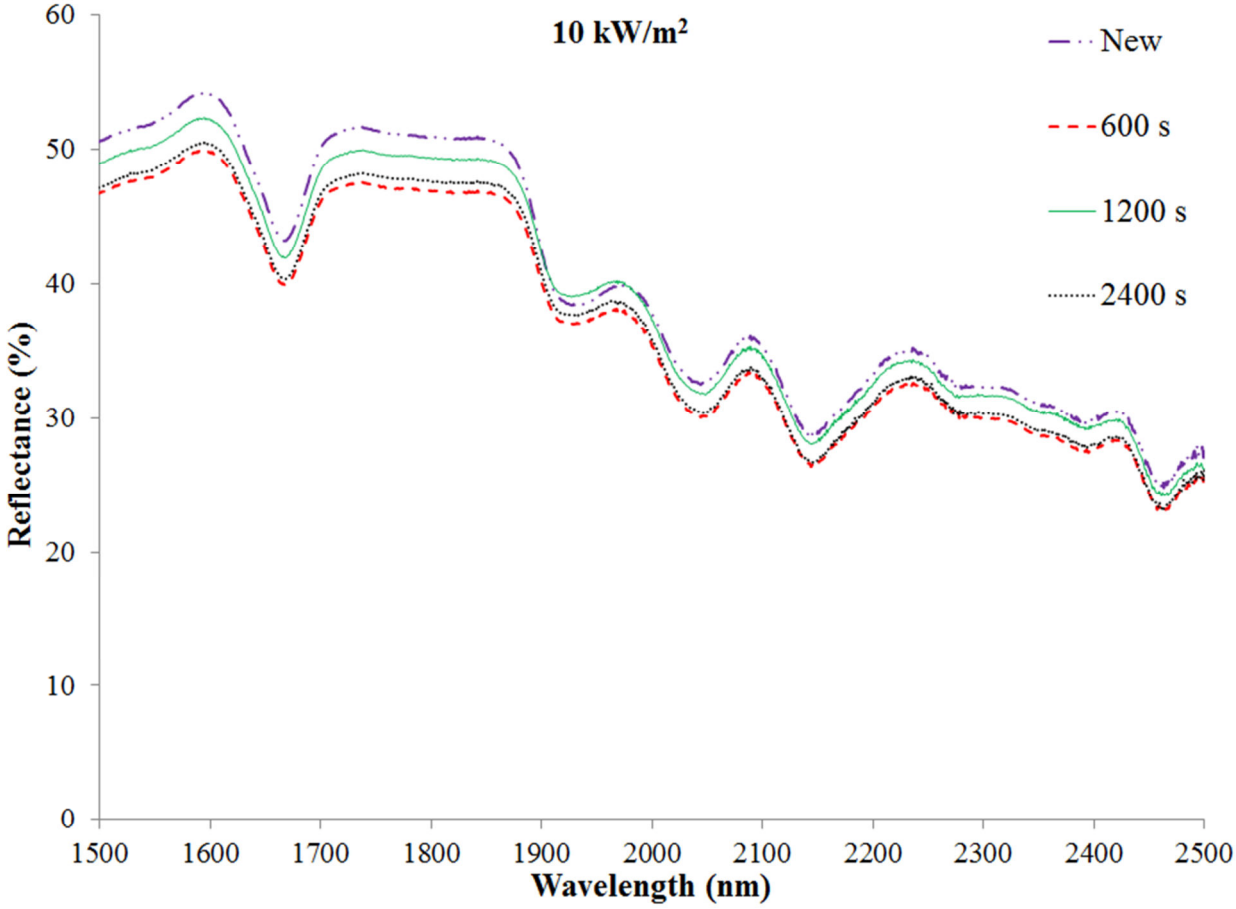

Figure D.1: Reflectance spectrum for red Nomex® specimens after thermal exposure to 10 kW/m^2

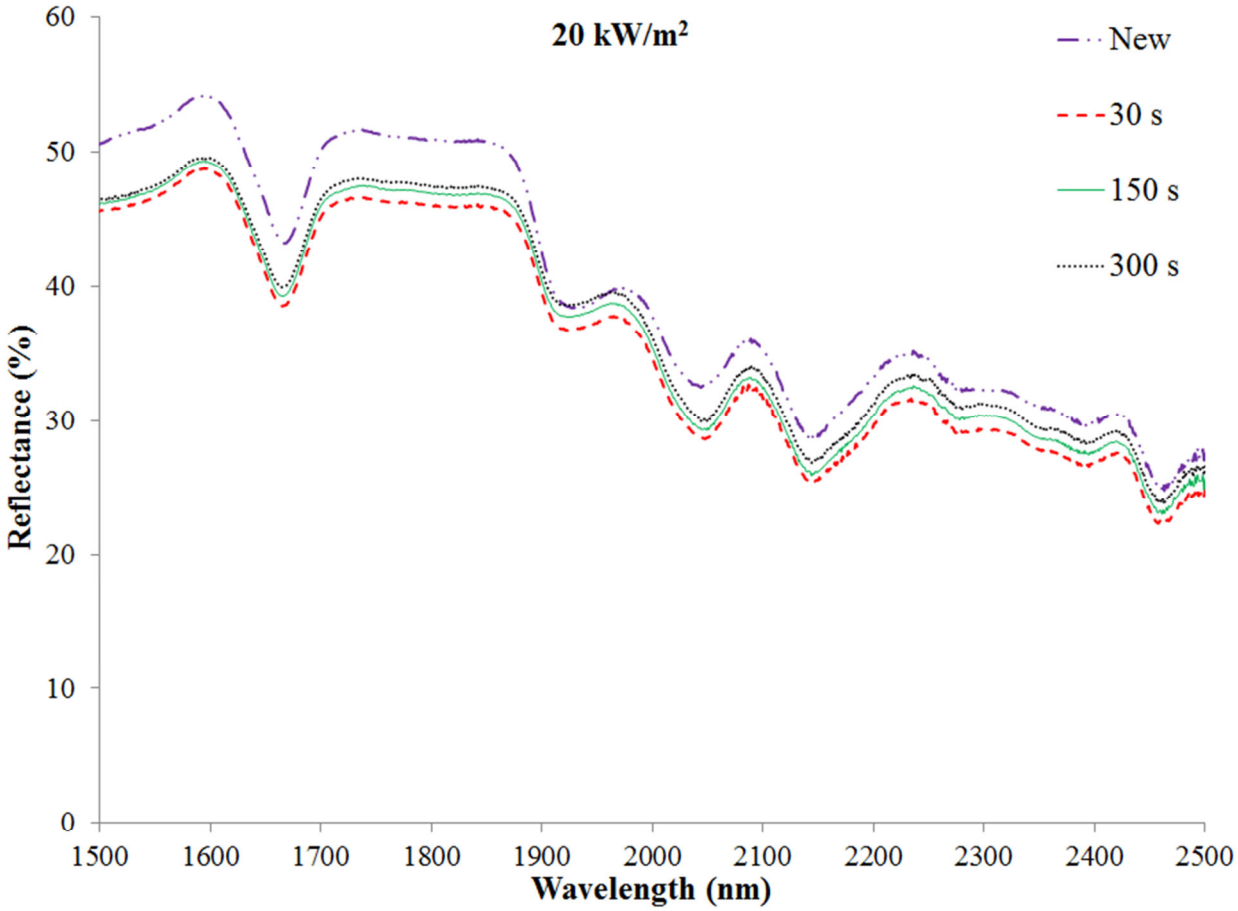

Figure D.2: Reflectance spectrum for red Nomex® specimens after thermal exposure to 20 kW/m^2

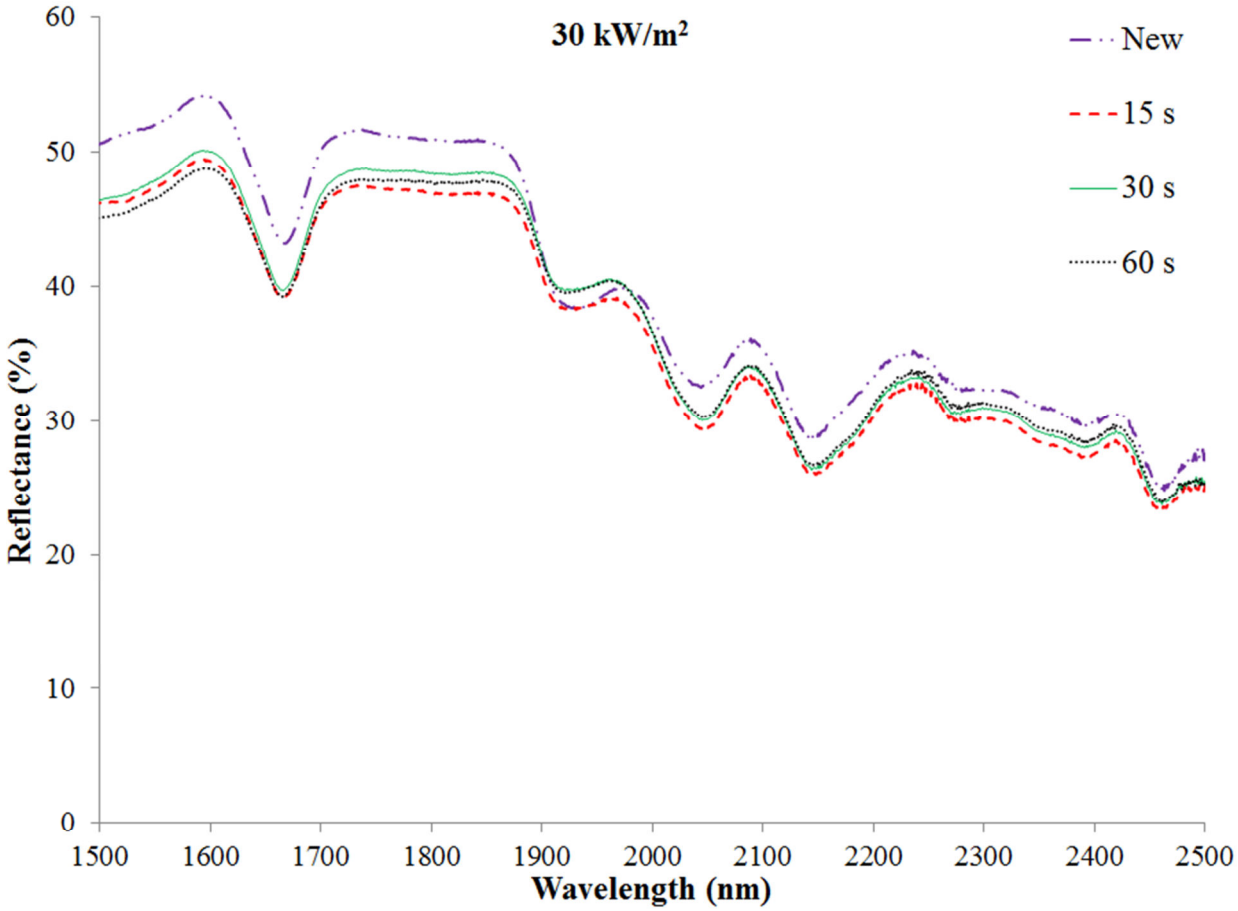

Figure D.3: Reflectance spectrum for red Nomex® specimens after thermal exposure to 30 kW/m^2

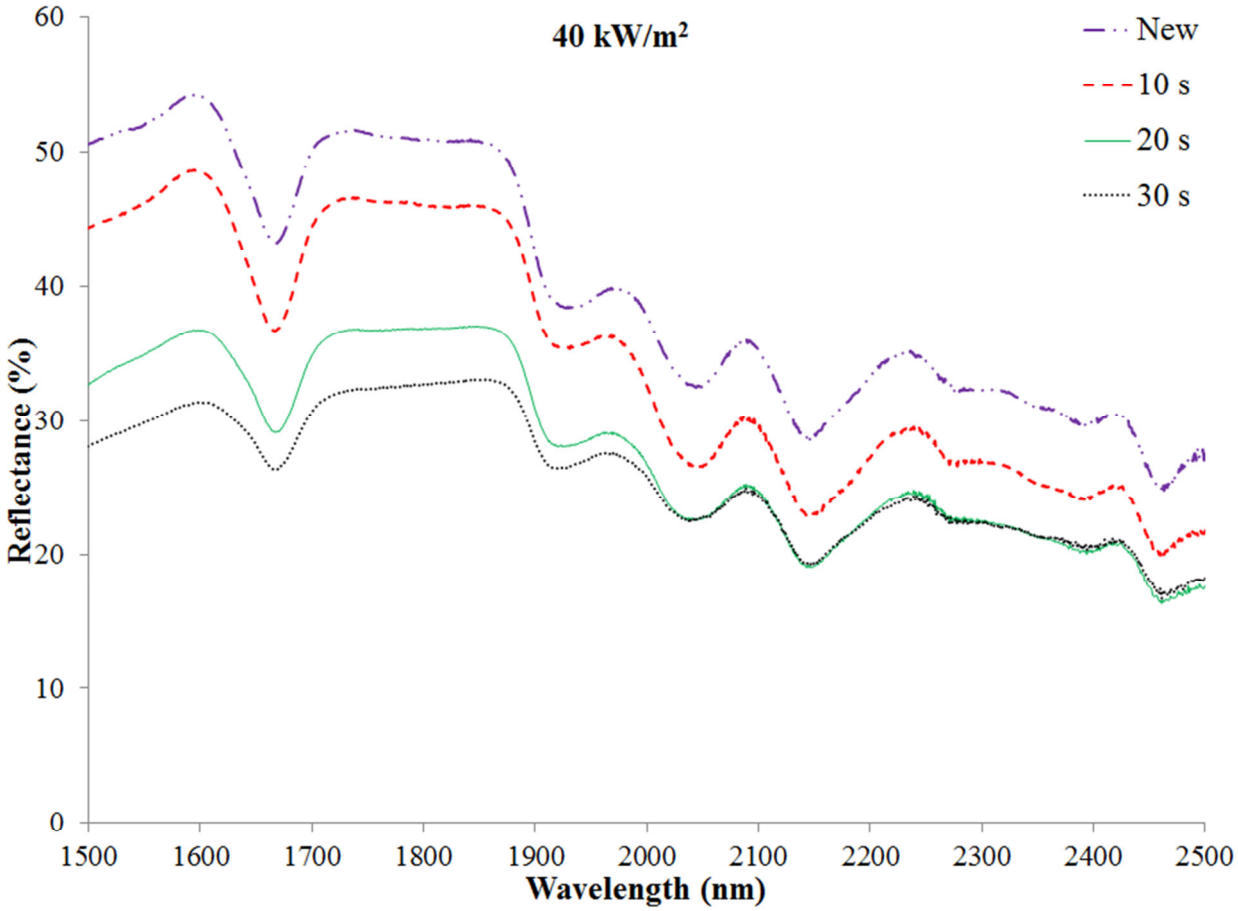

Figure D.4: Reflectance spectrum for red Nomex® specimens after thermal exposure to 40 kW/m^2

D.2.Dark blue specimens:

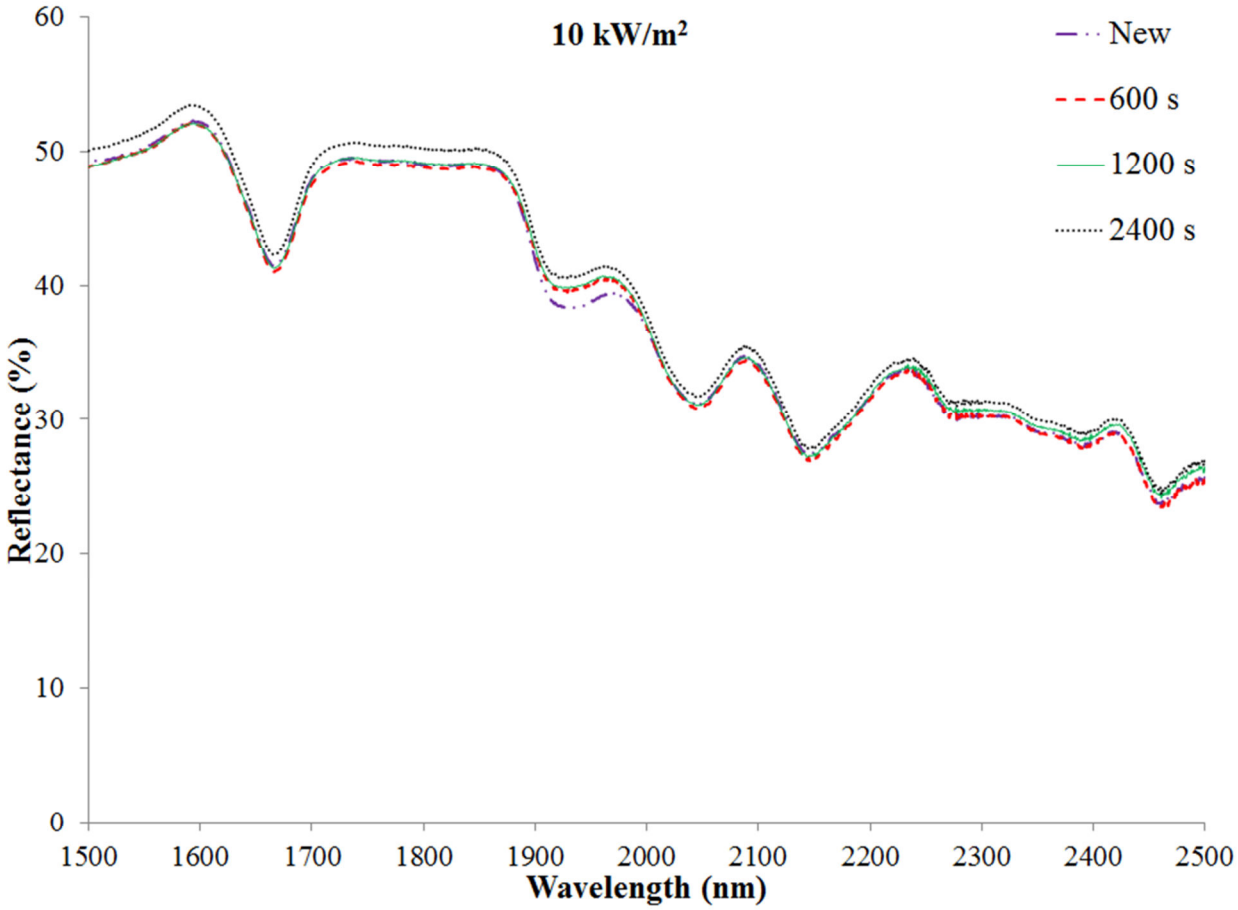

Figure D.5: Reflectance spectrum for dark blue Nomex® specimens after thermal exposure to 10 kW/m^2

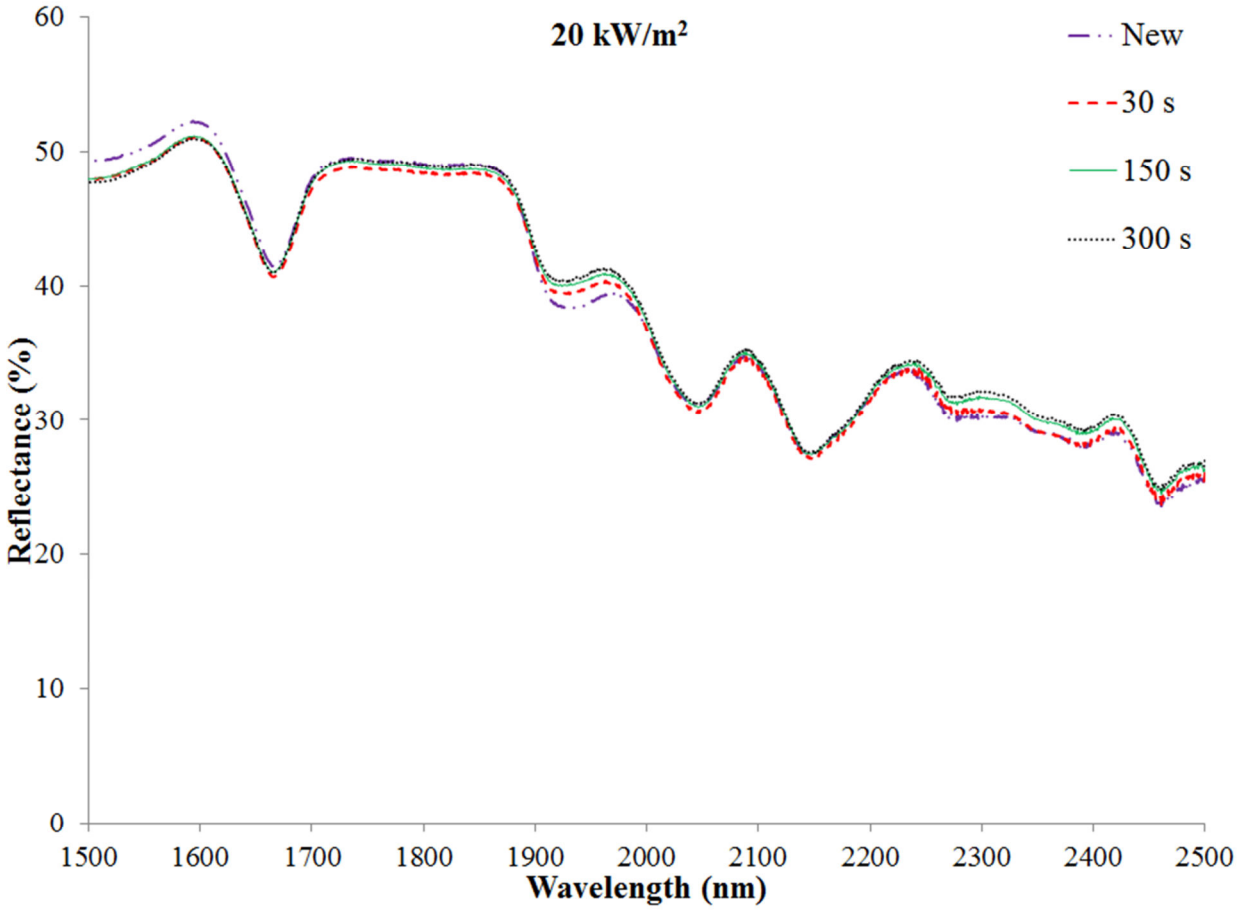

Figure D.6: Reflectance spectrum for dark blue Nomex® specimens after thermal exposure to 20 kW/m^2

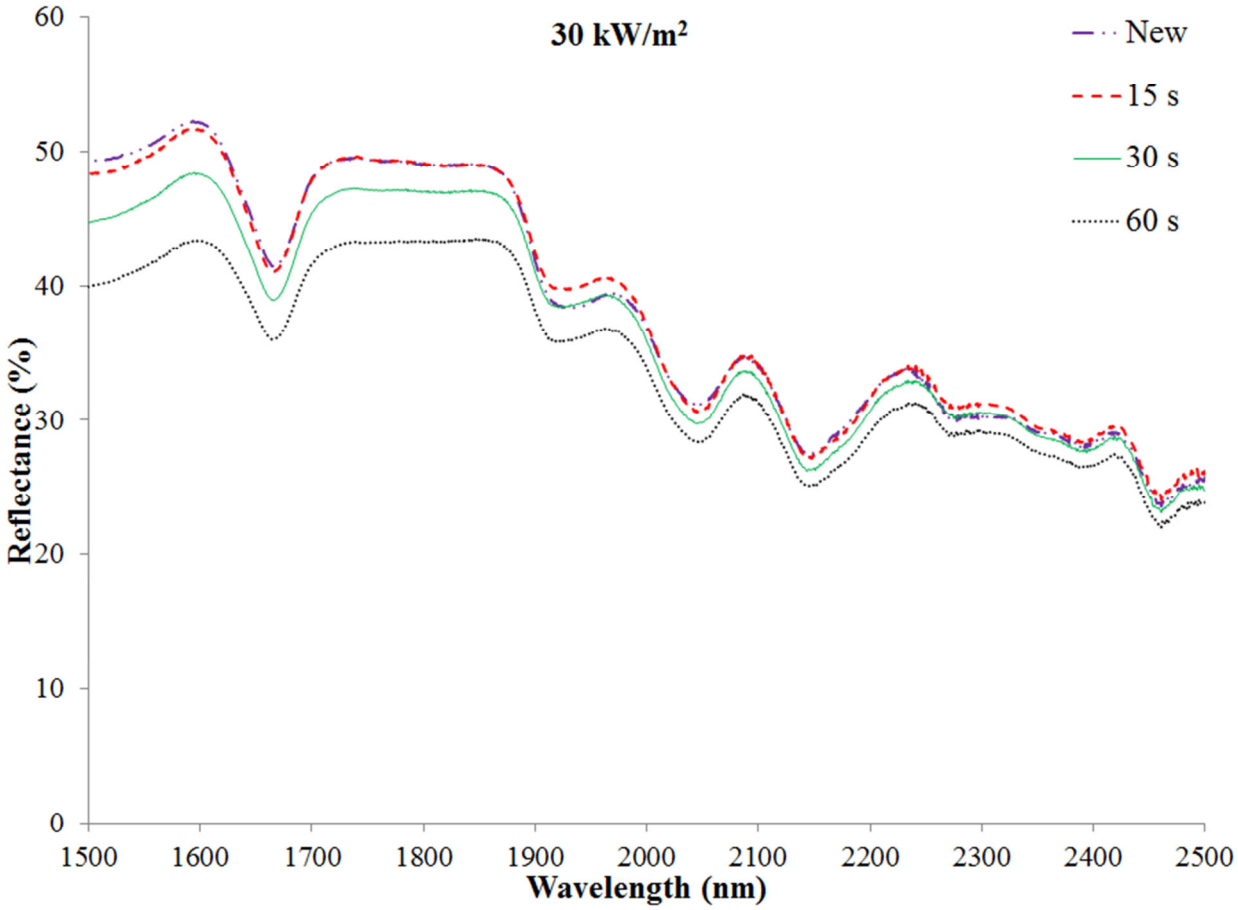

Figure D.7: Reflectance spectrum for dark blue Nomex® specimens after thermal exposure to 30 kW/m^2

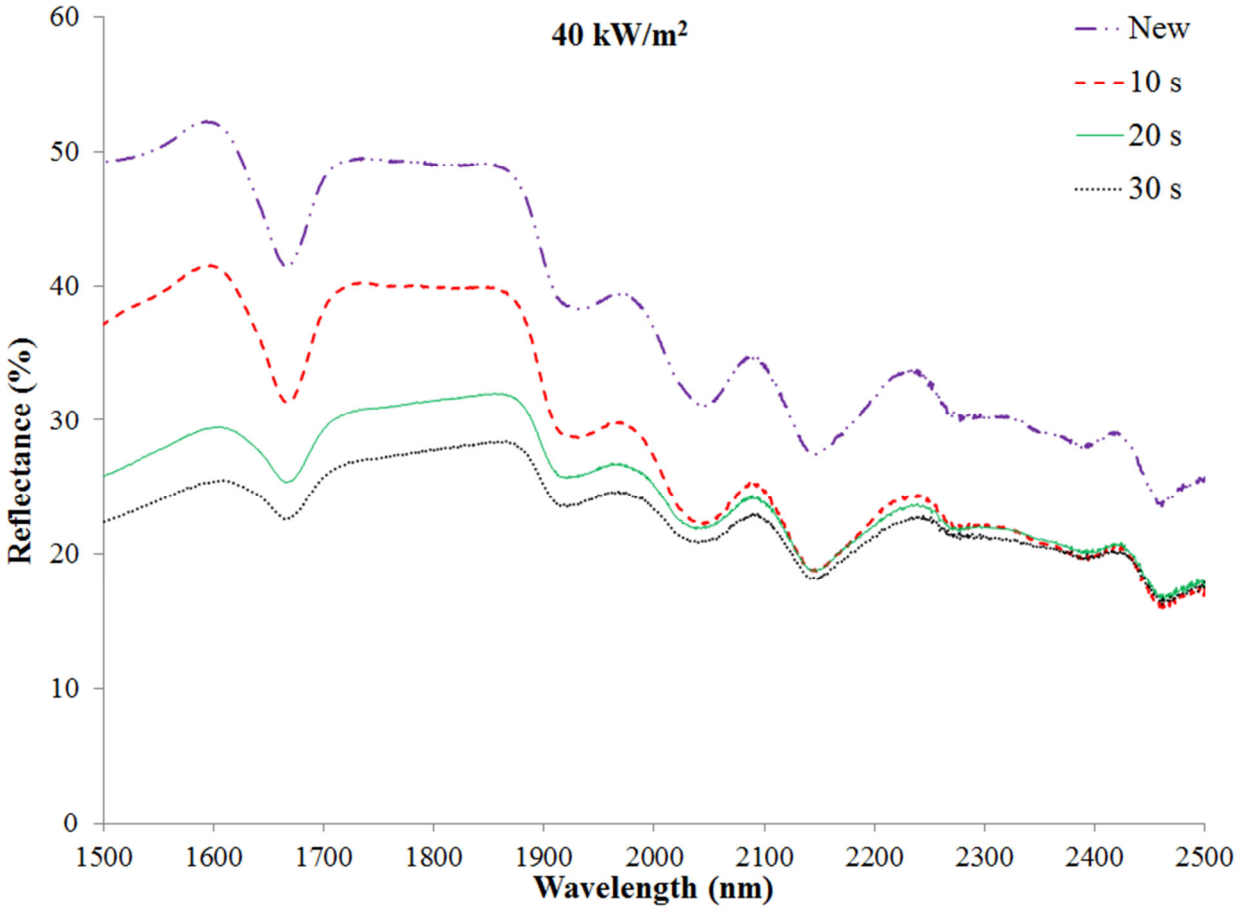

Figure D.8: Reflectance spectrum for dark blue Nomex® specimens after thermal exposure to 40 kW/m^2

D.3.Yellow specimens:

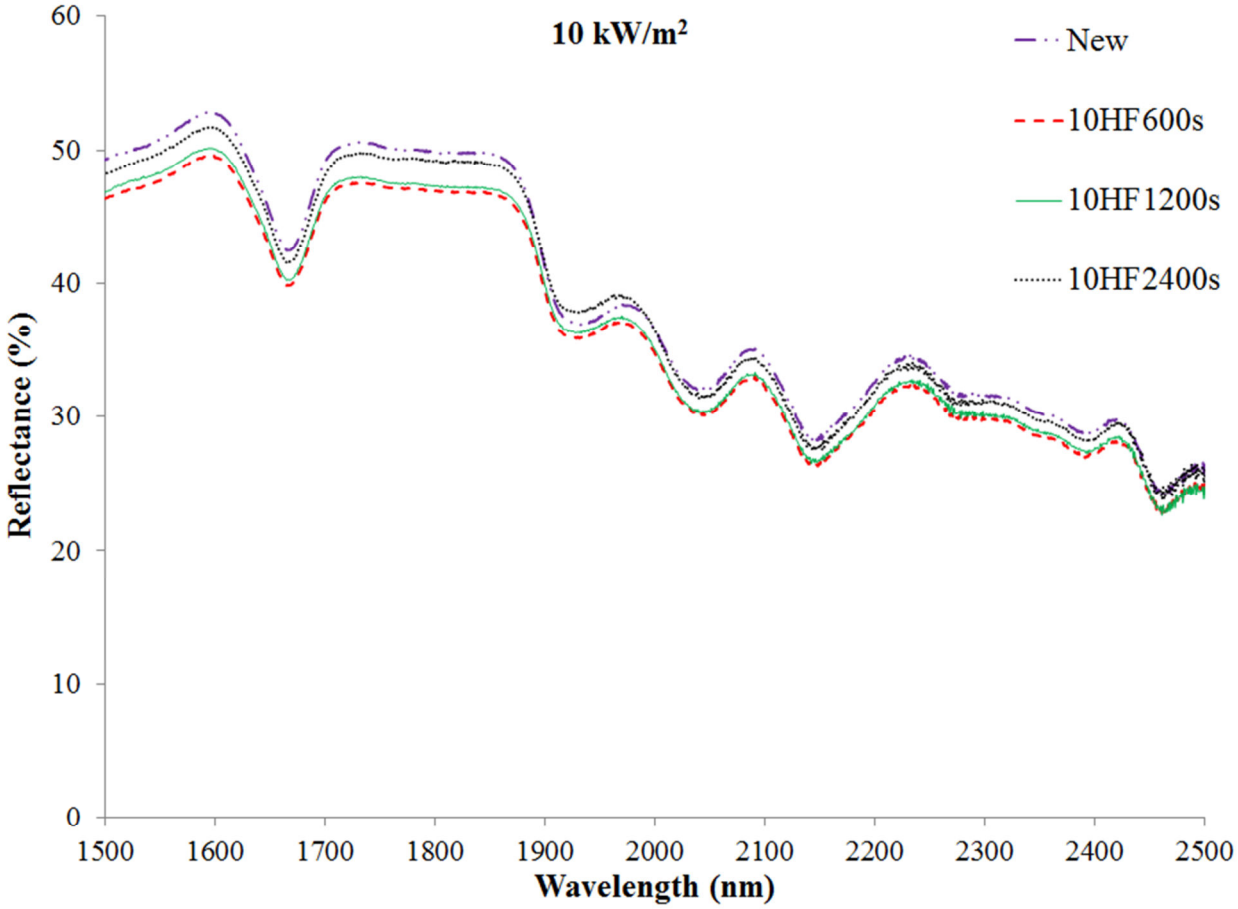

Figure D.9: Reflectance spectrum for yellow Nomex® specimens after thermal exposure to 10 kW/m^2

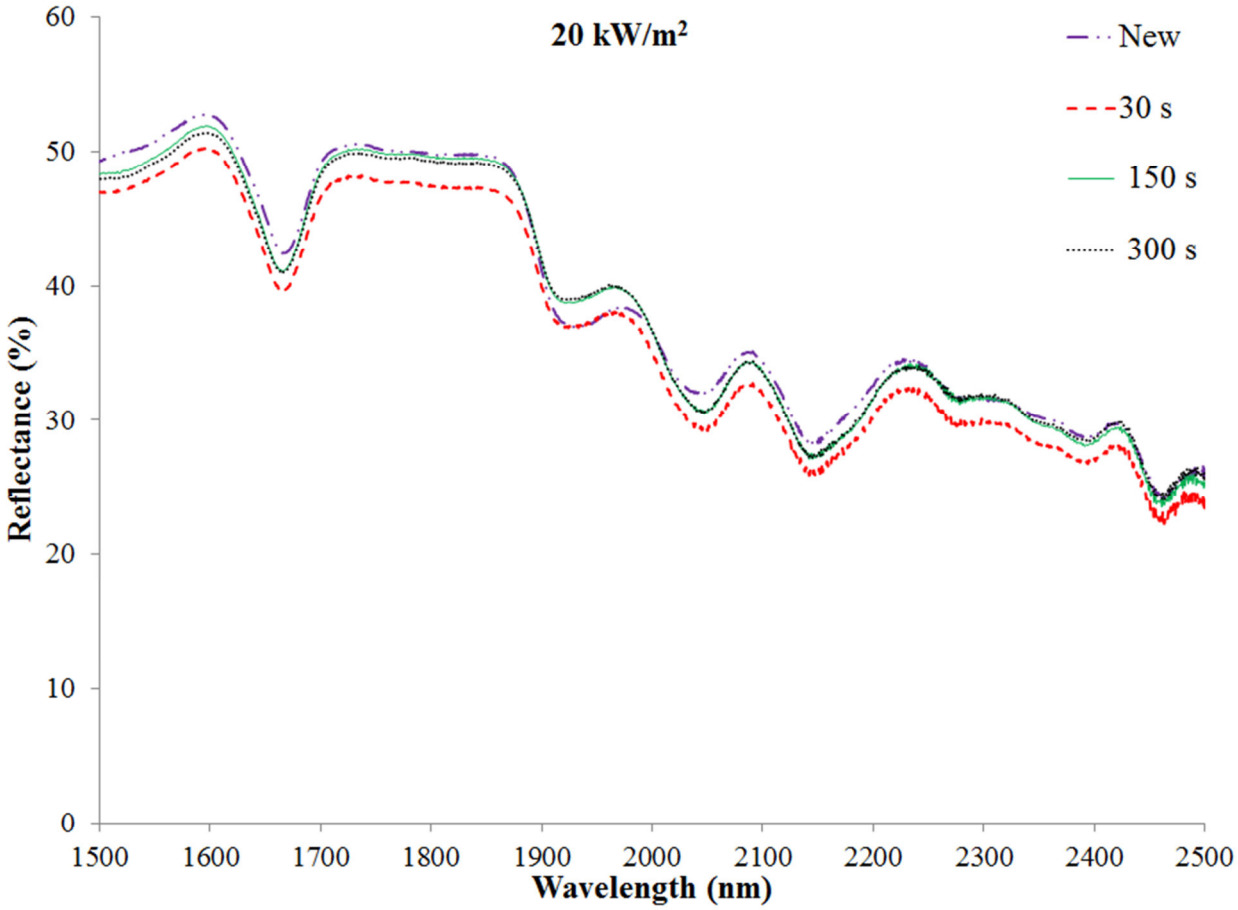

Figure D.10: Reflectance spectrum for yellow Nomex® specimens after thermal exposure to 20 kW/m^2

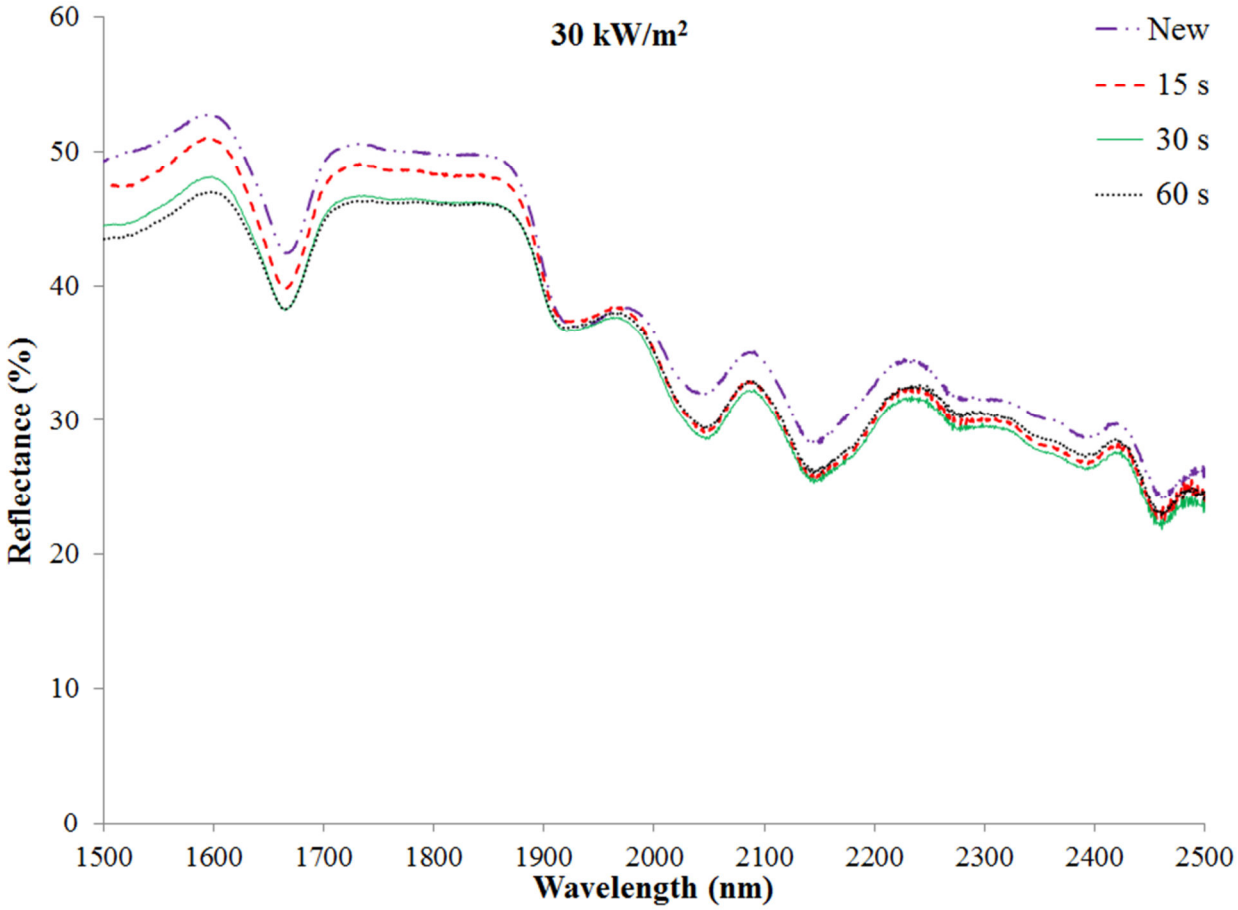

Figure D.11: Reflectance spectrum for yellow Nomex® specimens after thermal exposure to 30 kW/m^2

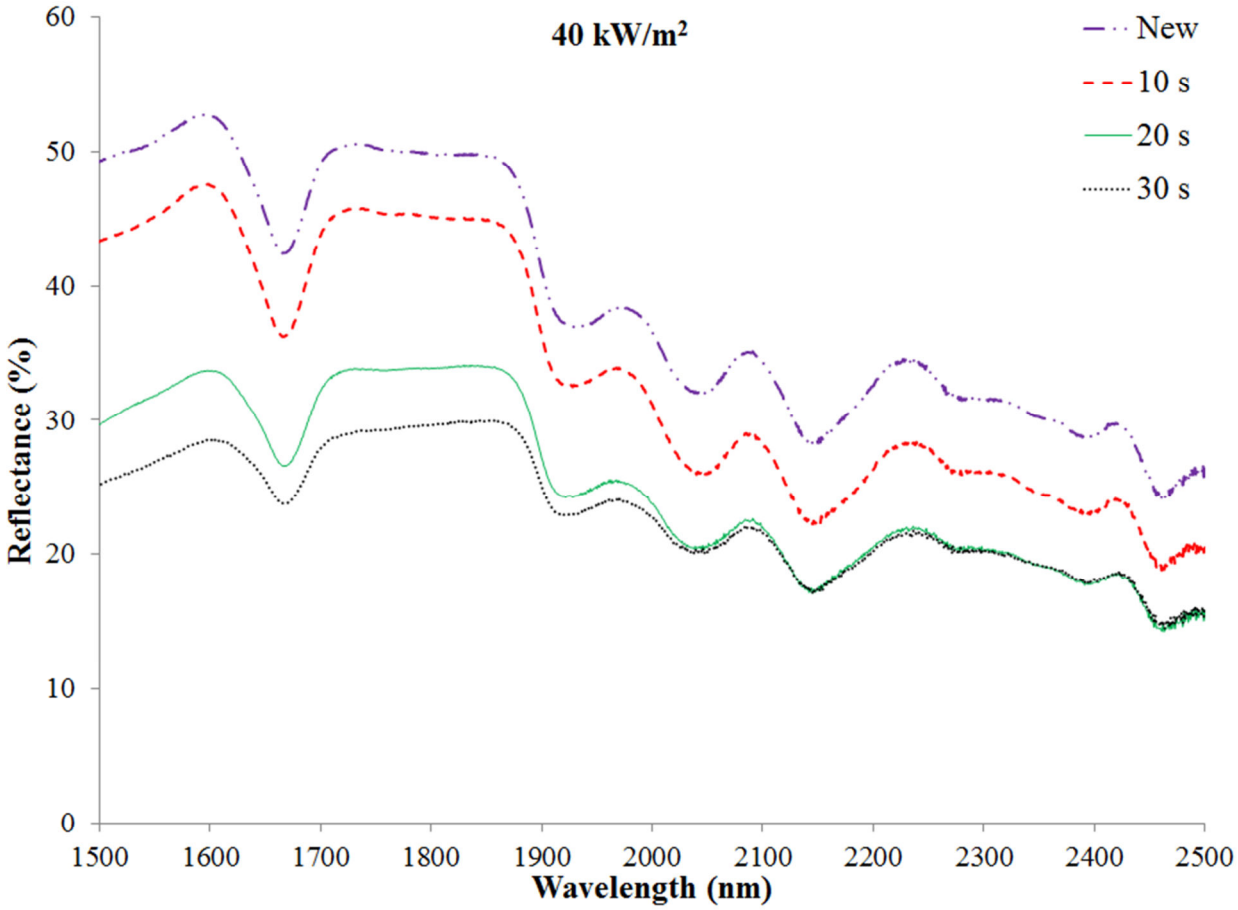

Figure D.12: Reflectance spectrum for yellow Nomex® specimens after thermal exposure to 40 kW/m^2

Appendix E: Replication of data points by the best equations made of 3, 5, 7, and 10 wavelengths for Nomex® outer shell specimens

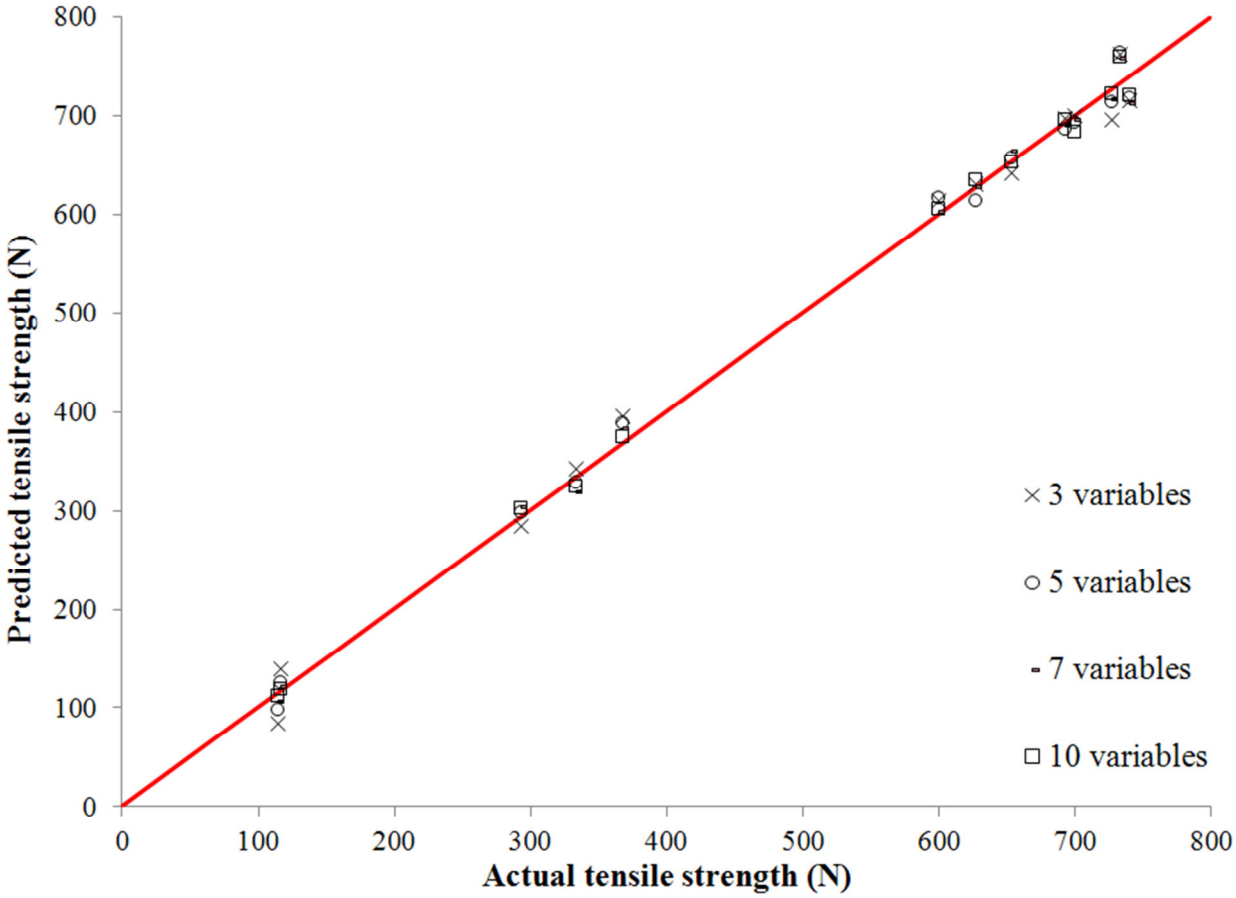

Figure E.1: Replication of data points by the best equations made of 3, 5, 7, and 10 wavelengths for red specimens

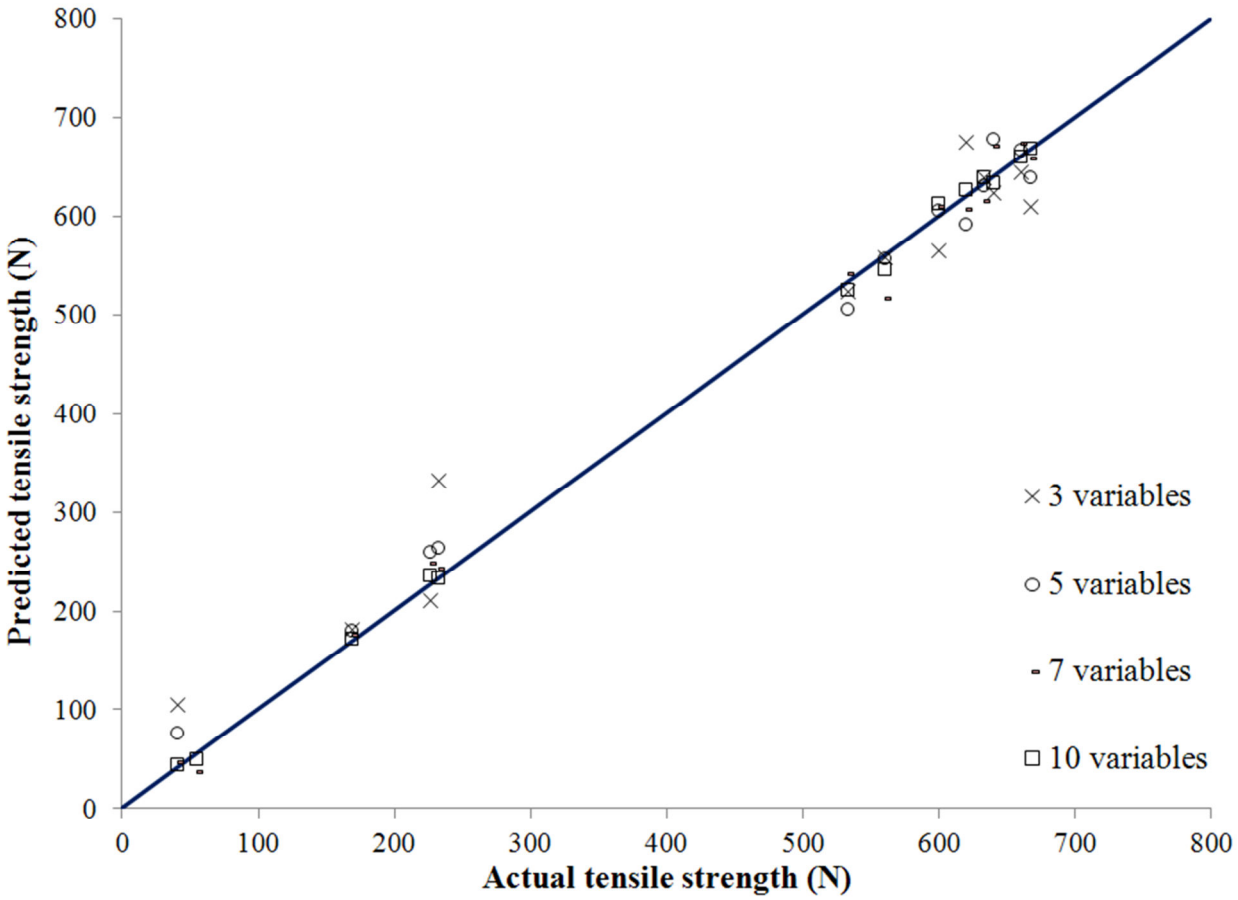

Figure E.3: Replication of data points by the best equations made of 3, 5, 7, and 10 wavelengths for dark blue specimens

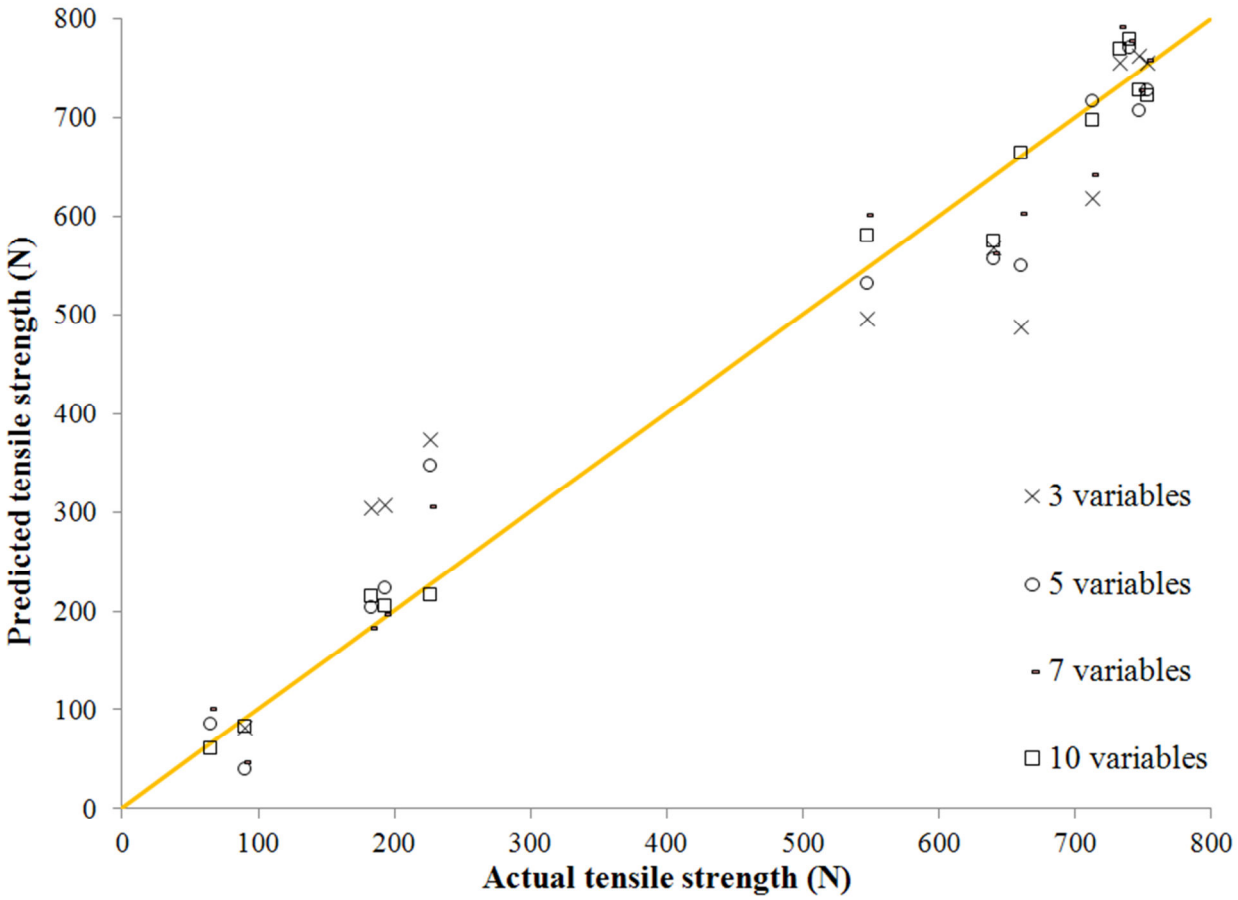

Figure E.3: Replication of data points by the best equations made of 3, 5, 7, and 10 wavelengths for yellow specimens